# ABSTRACT

| | |
|---|---|
| Title of Thesis: | VALIDATION OF RESIDENCE STRESS DISTRIBUTION METHODOLOGY USING 1-D COMPUTER SIMULATIONS |
| | Nitish Balakrishnan, Master of Science, 2017 |
| Thesis Directed By: | Associate Professor David I. Bigio<br>Department of Mechanical Engineering |

Residence Stress Distribution (RSD) Methodology was implemented as a tool to quantify the stress history (%BU) experienced by the polymer melt in the Twin Screw Extruder. This thesis focuses on using a computer simulation software called Ludovic, which is a 1-Dimensional twin screw simulation software, that models the co-rotating twin screw extruder. The goals of this research have been on identifying the relationship between the %BU and the physical properties that the polymer melt in the extruder is subjected to, such as the temperature, viscosity, shear rate and shear stress exhibited by the polymer melt. Another objective of this research has been to validate the experimental results obtained using RSD methodology as well as certain assumptions made with regards to the Residence Revolution Distribution (RRD). Computer Simulations are useful in understanding the internal behavior within the twin screw extruder and quantify parameters that are essential to understand the mixing behavior.

# VALIDATION OF RESIDENCE STRESS DISTRIBUTION METHODOLOGY USING 1-D COMPUTER SIMULATIONS

by

Nitish Balakrishnan

Thesis submitted to the Faculty of the Graduate School of the
University of Maryland, College Park, in partial fulfillment
of the requirements for the degree of
Master of Science
2017

Advisory Committee:
Professor David I. Bigio, Chair
Professor Hugh A. Bruck
Professor Amir Riaz

# Acknowledgements

Firstly, I take this opportunity to express my sincere gratitude to Dr. Bigio, my Graduate Advisor, who has been supportive right from the commencement of my Master's degree. I certainly have benefitted from being a research student under Dr. Bigio as I have been able to expand my knowledge and research qualities. Apart from academics, Dr. Bigio has been instrumental in helping me improve my interpersonal and communication skills. I am grateful for all the guidance that Dr. Bigio has provided me during my tenure as a Graduate Student. I would also like to thank Dr. Bruck and Dr. Riaz, for being a part of the advisory committee and providing me with valuable insights at a moment of need.

Secondly, I like to thank Jason Nixon and Benjamin Dryer, who had graduated in Spring 2016, who have helped me by providing inputs and help with MATLAB during the initial days of my graduate school life. I would also like to thank Aditya Sangli and Masuma Ema for their support and guidance as co-research students. During my tenure as a graduate student in the Advanced Manufacturing Laboratory, I have been fortunate to be helped by fellow undergraduates Connor Armstrong, Marcelo Arispe-Guzman and Thomas Carlacci, with my experiments.

I like to thank Mr. Laurent Ratte, Eric Chassognolle and David Philippe from SCC, who had trained me on using Ludovic Simulation software and patiently guiding me when I had questions while performing my experiments.

Lastly, I like to thank my family without whom this journey would not have been possible and I am grateful for all the support and kind wishes.

# Table of Contents

# List of Tables

# List of Figures

# Chapter 1 – Introduction and Fundamentals of Twin Screw Extrusion

This chapter of the thesis gives a background into extrusion and explains the different types of extruders that find use in the industry. The thesis focuses on experiments performed using the Twin Screw Extruder; a detailed study on the twin screw extruders, screw elements used in the extruder and the mixing behavior of the twin screw extruder has been performed and discussed in Chapter 1.

## 1.1 Extrusion

Extrusion is the process used to create products of a specific shape, by forcing the material through a shaped orifice [1]. The shaped orifice through which the material is forced out is referred to as a die [2]. The process of extrusion is performed using various methods and carried out on different machinery. The extruder is the most common machinery employed in the extrusion industry [2]. The material that passes through the extruder, which is referred to as the extrudate [2], acquires the shape of the die opening. A wide variety of materials is manufactured through the process of extrusion. These include polymers, pharmaceuticals, foods etc. [2]. This study focuses primarily on polymer processing.

Extruders used in the polymer industry, come in a variety of designs. The extruders are classified by the mode of operation i.e. continuous or discontinuous. Continuous extruders process materials until the feed supply is maintained, which is extremely helpful in generating significant outputs. Discontinuous Extruders have a reciprocating member while the continuous extruders have a rotating member. The different types of continuous screw extruders include Single Screw Extruders, Twin Screw, Triple Screw

Extruders, Drum Extruders [2]. Reciprocating extruders or Ram extruders are examples of discontinuous extruders [2].

The primary motive behind polymer processing is to convert raw polymer into a finished product, through a chain of chemical reactions and the inclusion of solid additives. The extruder is the machinery that facilitates the conversion of the raw polymeric material into the desired product. The extruder can be visualized as a set of screws in a heated barrel, that are rotated by an electric motor using a gear reducer [3]. The raw polymeric material, in the form of pellets or powder (solid form), is fed into the extruder gravimetrically through the feed hopper (Fig 1.1). The polymer is heated to its melting point and is conveyed forward along the screw. The polymer melt is subjected to pressure and homogenized to obtain a uniform polymer melt flow along the screw. The barrel that encompasses the screw is heated electrically or using a fluid heat exchanger system [3], and the temperature settings are monitored and controlled with the help of thermocouples placed in the metal barrel wall. To achieve the desired properties, a filler is added to the polymer melt through a secondary feed port, which is followed by the mixing section and the final product is extruded out of the die. The final product is allowed to cool; the process can be expedited using a chilled roller, which cools the final product as it is pushed out of the extruder die and is allowed to run over the surface of the chilled roller. The in-depth discussion about the extruders can be found in the following sections.

## 1.2 Screw Extruder

There are several types of extruders, of which, the screw extruder is the most commonly used extruder for polymer processing. Screw Extruders comprise of the single screw

extruders and the multiple screw extruders, which will be discussed in the following sections. Single Screw Extruder is defined as a continuous volumetric pump without an ability to facilitate back-mixing as well as positive conveying capacity; single screw extruders possess the capability to generate several thousands of pounds of pressure during melting and mixing [4]. Single screw extruders offer several advantages such as lower cost, simple design, reliability and relatively better performance/cost ratio [2]. Single Screw Extruders will not be discussed in detail since the focus of this thesis is on twin screw extrusion. Figure 1.1 provides an overview of the different zones in a screw extruder – conveying/feeding section, melting/transition section and melt pumping section.

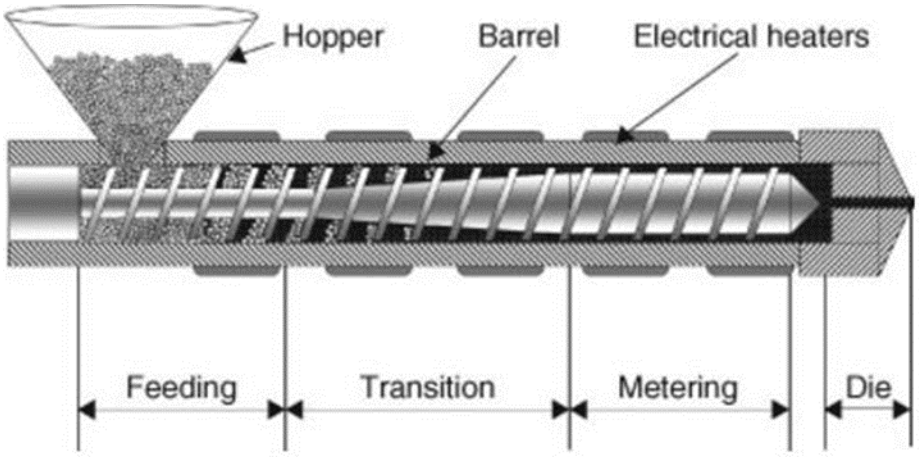


Figure 1.1: Different sections of Screw Extruder [5]

### 1.2.1 Twin Screw Extruder

Twin Screw Extruders are an advancement in the area of screw extrusion. It comprises of two screws rotating simultaneously inside a heated barrel. Twin Screw Extruders

give a higher flexibility when it comes to processing complex polymeric materials. Twin Screw Extruders can be classified based on the following types:

**Classification based on direction of screw rotation**

Based on the direction of screw rotation, Twin Screw Extruders are classified into Counter-Rotating and Co-Rotating Twin Screw Extruders. The counter-rotating twin screw extruders contain two screws that rotate in opposing directions and convey the feed forward. The Co-Rotating Twin Screw Extruders contain two screws that rotate in the same direction and convey the feed forward.

**Classification based on contact of screws**

Twin Screw Extruders are classified based on the contact between screws i.e. non-intermeshing and intermeshing screws. Intermeshing Twin Screw Extruders are further classified into Fully-Intermeshing and Partially Intermeshing. Fully Intermeshing Screws have a self-wiping ability.

**Classification based on Modularity of Design**

Twin Screw Extruders are classified based on the modularity of design i.e. if they contain uniformly machined screws or segmented screws. Segmented Screws comprise special elements for the purpose of mixing, such as kneading blocks, left handed screw elements which exert pressure in the direction opposite to the direction of feed conveying. Segmented Screw Extruders possess a combination of forward and reverse pumping screw elements for the purpose of increasing throughput and mixing abilities [7].

#### 1.2.1.1 Intermeshing Co-Rotating Twin Screw Extruders

Intermeshing Co-Rotating Twin Screw Extruders are a set of screws that rotate simultaneously in the same direction. The screw edges of one screw lies in between the screw edges of the second screw, hence, fully intermeshing. The polymer melt flows from one screw to the other or may continue its motion along the same screw. These extruders possess high mixing capability due to their ability to maintain the same interfacial interaction during the movement of the polymer melt. The self-wiping ability is also a key attribute of the Intermeshing Co-Rotating Twin Screw Extruders.

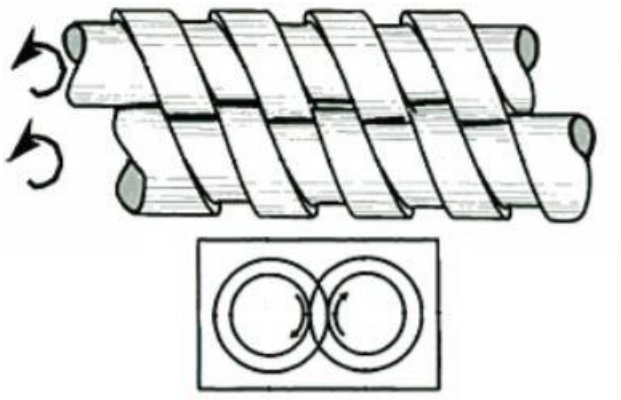

Figure 1.2: Intermeshing Co-Rotating Twin Screw Extruder [6]

#### 1.2.1.2 Non - Intermeshing Counter-Rotating Twin Screw Extruders

Non-intermeshing counter-rotating twin screw extruders comprise two screws, that rotate in opposing directions, and have screw edges aligned to each other (Figure 1.3), unlike the intermeshing screw extruders. The polymer melt from both screws is pushed into the gap between the screws, which causes the polymer melt to either flow along the same screw channel or along the other screw channel. These types of extruders possess high conveying and mixing capabilities. The only disadvantage is that they do not possess the ability to self-wipe, unlike the intermeshing twin screw extruders.

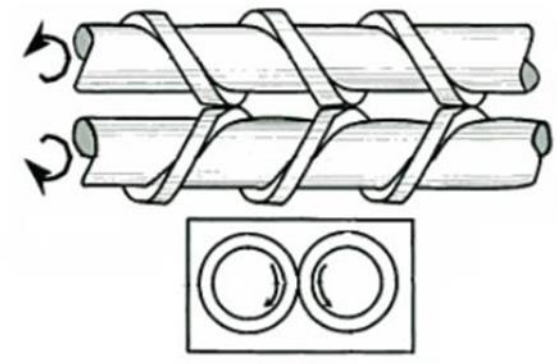

Figure 1.3: Non-Intermeshing Counter-Rotating Twin Screw Extruder [6]

*1.2.1.3 Intermeshing Counter-Rotating Twin Screw Extruders*

Intermeshing Counter-Rotating Twin Screw Extruders comprise two screws that rotate in opposing directions. The screw edges of one screw are positioned in between the screw edges of the other screw, hence intermeshed completely. Intermeshing Counter-Rotating Twin Screw Extruders have highly positive conveying capacity compared to the other types of twin screw extruders. The Intermeshing Counter-Rotating Twin Screw Extruders need to be operated at a lower speed in order to avoid high pressures developing in the intermeshing region. This can be avoided by designing screws with higher clearance (gap between the screws), which gives the flexibility to improve the screw speeds but ultimately results in the reduction of the conveying capacity [2].

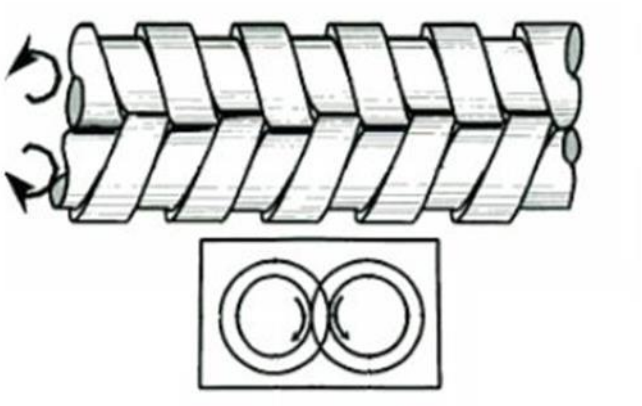

Figure 1.4: Intermeshing Counter-Rotating Twin Screw Extruder [6]

## 1.3 Screw Elements

This section discusses the different types of screw elements used in the twin screw extruder. For this study, the focus would be on the elements used in the Intermeshing Co-Rotating Twin Screw Extruder. The conveying and mixing screw elements will be explained in detail in the following pages.

The geometry of the screw system influences the conveying and mixing characteristics of the intermeshing co-rotating twin screw extruder. The axial mixing in the lengthwise direction of the screw, is facilitated by the presence of an open screw channel that runs in the axial direction from the inlet to the exit of the extruder [9].

The number of flights i.e. single, double, triple-flighted screw profile (explained in this section) and the width of the screw crest play a major role in conveying the material along the screw channel, by imposing a twist restraint on the material. Forced Conveyance is facilitated in the intermeshing region between the screws of the co-rotating twin screw extruder [9]. Increase in width of the screw crest, causes the material to alter its direction rapidly, that leads to an increase in the twist restraint.

Extruder Screws are classified based on the screw profile i.e. single-flighted, double-flighted and triple-flighted extruder screw.

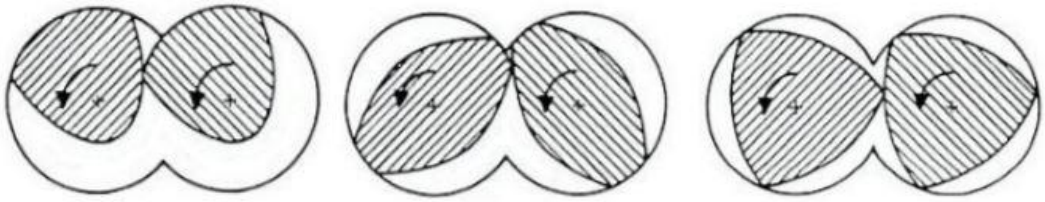

Figure 1.5: Cross-sections of co-rotating screws – Single flight (left), Two-flight (center), Three-flight (right) [2]

The different types of screw profiles used in screw extruders can be seen in Figure 1.5. Single-Flighted Screw Element comprises a single path along which the material travels, when fed into the extruder. This profile is ideal to maximize feed intake and convey maximum amount of feed, due to the presence of large channel. These screw profiles are used in situations where the intake ability limits the throughput and for materials with poor flow properties [9]. However, single-flighted screw elements exhibit extremely low shear and are poor agents for mixing. Double-Flighted Screw Elements comprise two paths along which the material can travel. They have high conveying capacity (lower than single-flight) but exhibit low shear (higher than single-flight), which makes it a better mixing agent compared to single-flight. These screw profiles are used in situations that require processing of materials with low bulk density or for shear-sensitive materials that require low shearing [9]. The triple-flighted screw element has the poorest conveying capacity amongst the three screw profiles but is extremely suitable for materials that require better mixing capability. The triple-flight screw profile is used in cases where high shearing forces are needed to break-up agglomerates [9]. The screw channels are shallower compared to double-flighted and

single-flighted screw elements, which acts as an excellent medium to facilitate heat transfer due to the presence of thin layers of material on the screw [9].

### 1.3.1 Conveying Elements

There are two kinds of conveying elements – right handed (forward) conveying element and left handed (reverse) conveying element. The right-handed conveying elements are used to convey polymer, which is fed through the hopper (Fig 1.1) and conveys it along the extruder length to the die (Fig 1.1). The amount of material conveyed forward is dependent on the pitch of the screw element. Large/Wide pitch forward conveying element increases the conveying capacity. The degree of fill, which is the ratio of volume occupied by the polymer to the free channel volume [9], is also dependent on the pitch of the right-handed screw element. Wider pitch reduces the degree of fill. Narrow pitch screw elements are used, in order to build up pressure and increase the degree of fill. In order to improve pumping efficiency in the regions of pressure-build up, element with narrow screw pitch is used [9].

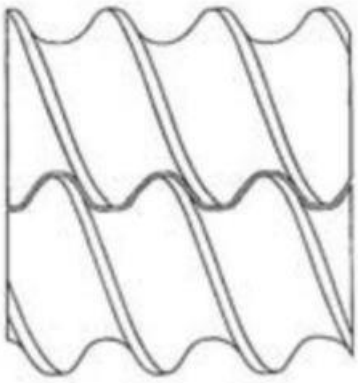

Figure 1.6: Conveying Screw Element [12]

Left-handed conveying element (Reverse conveying) is used to convey the polymer melt in the opposite direction i.e. from the die to the hopper. Left handed conveying

elements are commonly used in order to build up the pressure and increase the degree of fill to 100%. Left handed conveying elements are situated behind mixing elements such as kneading blocks (discussed in Sec 1.3.2), as it helps improving mixing [9]. Residence Time (discussed in Sec 1.5) and shear rate is increased when left-handed screw elements are used [9].

### 1.3.2 Mixing Elements

Mixing Elements are used to enhance the mixing process. Kneading Blocks perform this function in the Co-Rotating Twin Screw Extruder. Kneading Blocks comprise a set of staggering screw disks, that impart high shear stresses on the polymer melt [9]. The Kneading Blocks consist of a set of staggered disks (usually 5), oriented at different angles, and impart flow in the cross-channel direction. The staggering angle determines the degree to which the screw channel is open in the axial direction. The higher the staggering angle, the better the mixing performance. However, the conveying efficiency is affected when the staggering angle between the disks in the Kneading Block is increased. For instance, Kneading Block with screw disks having a staggering angle of $90^0$ has a better mixing efficiency compared to screw disks having a staggering angle of $60^0$. Kneading Blocks can be classified into three categories i.e. the forward-conveying kneading blocks, reverse-conveying kneading blocks and neutral kneading blocks. Neutral kneading blocks have no capacity to convey materials and are dependent on the forward conveying screw elements to push the material forward. Forward conveying kneading blocks convey materials forward; however, they allow back mixing of the material through the gap formed by the staggering angle [9]. Reverse conveying kneading blocks build up pressure, but of lower magnitude

compared to the reverse conveying screw elements, and increase the degree of fill upstream. The width of the kneading disks plays an important role in the mixing process. Narrow width kneading disks provide excellent mixing and conveying capabilities but induce very less amount of shear. Medium width kneading disks impart higher shear compared to narrow disks, however, they have lesser conveying and mixing capabilities. Wide Kneading disks impart the highest shear compared to the other types if kneading disks, and are suited to dispersive mixing (discussed in Sec 1.4.1.2). The effect of screw types on longitudinal mixing is explained by Peclet number [9]. The lower the Peclet number, the higher the magnitude of back mixing [9].

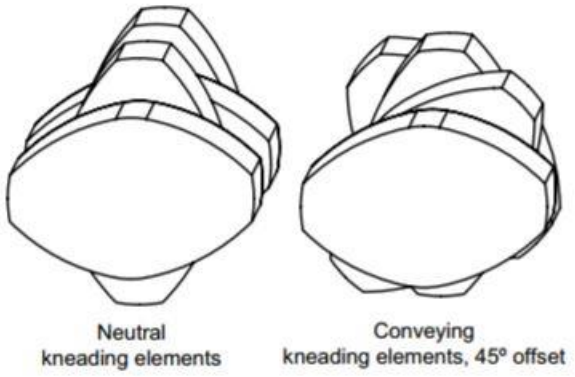


Figure 1.7: Kneading Block Representation

Sec 1.1 – 1.3 discusses the background of screw extruders – i.e. single screw, twin screw extruders and provides a detailed study on the Twin Screw Extruders. The screw geometry typically used in the Twin Screw Extruders were discussed in Sec 1.3 to provide a brief overview on the conveying and mixing characteristics of the individual screw elements. The configuration of screw elements is essential to understand the mixing behavior of the twin screw extruders. Twin screw extruders are widely known for their compounding behavior; the orientation of screw elements in the mixing section determines the mixing behavior of the extruder. Understanding mixing is vital in order

to improve the characteristics of the extrudate. The next section discusses the concept of mixing and the different types of mixing in the twin screw extruder.

## 1.4 Mixing

Mixing can be explained as the intermingling of two or more segregated components by mechanical action [9]. In the field of polymer processing, mixing plays a vital role in influencing the material properties, cost and accessibility. Laminar flow is the mechanism that influences mixing in polymers.

Spencer and Wiley [10] identified that better mixing is achieved through an increase in the interfacial surface area, which is a function of the magnitude of shear and initial orientation of the elements.

The ultimate goal behind mixing, is to reduce the concentration gradient to a minimum, which is achieved when random samples of the mixture extracted from the mixing system have similar composition [11].

Mixing can be performed by batch or continuous operations. Batch Mixing occurs within the closed volume of the mixer device. The efficiency of this process is deeply affected by the less amount of mixing time allocated towards achieving the desired uniformity in composition of the mixture [11]. The efficiency of batch mixers is compromised when processing large quantities of material, due to difficulties resulting from automating the process. Continuous Mixing, as the name suggests, is a continuous process that produces higher output, when the feed supply is maintained. The ability to maintain stability during the course of operation is an advantage of continuous mixing compared to batch mixing. Continuous mixing process consumes longer periods of mixing time, which can be adjusted by varying the intensity of the process i.e. adjusting

the screw speed, feed rate etc. However, this can be considered disadvantageous as there is an escalation in the mechanical energy dissipation as a result of varying the process intensity [11]. Twin Screw Extruders fall in the category of continuous mixers.

### 1.4.1 Types of Mixing

Mixing is classified into two categories, namely distributive and dispersive mixing.

#### 1.4.1.1 Distributive Mixing

Distributive Mixing is defined as the rearrangement of components along the entire cross section on a fine scale, during the process of mixing [12]. Mixing Quality in Distributive Mixing is measured by the type and number of rearrangement processes. Low magnitudes of shear are induced onto the polymer melt, resulting in the particles redistributing uniformly in the polymer melt. Narrow Kneading Blocks are used for distributive mixing, as they induce low magnitudes of shear. This is due to the fact that the narrow kneading blocks cause the polymer melt to flow around the paddles rather than in the gap between the barrel and the paddles. Due to the smaller width of the kneading paddles, high magnitudes of shear stress are not induced, to shatter the particles.

#### 1.4.1.2 Dispersive Mixing

Dispersive Mixing is defined as the rupture of agglomerates into tiny particles, as a result of the application of large magnitudes of flow forces [12]. Unlike distributive mixing, where low magnitudes of shear are sufficient to cause redistribution of particles, dispersive mixing requires large magnitudes of shear or extensional stresses, to overcome the critical stress limit that holds the particles together. Upon overcoming the critical stress limit, the agglomerate breaks down into smaller particles. In the Twin

Screw extruder, wide kneading blocks are used as dispersive mixers. Due to the presence of large width of paddles, the polymer melt is squeezed in the gap between the paddles and the barrel and due to high magnitudes of shear induced, the agglomerates rupture. For instance, dispersion of solid fillers into polymer melt, is an example of dispersive mixing.

## 1.5 Residence Time Distribution

Residence Time is defined as the total amount of time spent by a material element in the extruder, before exiting from the die. Residence time is not uniform for all the particles of the polymer melt, i.e. different particles spend different amount of time in the extruder as they travel using different paths. Residence Time Distribution provides a distribution of the residence time spent by all the particles in the extruder and provides information on the flow pattern as well as the mixing quality in the extruder [13]. RTD is calculated by injecting a tracer into the extruder and using an optical probe to measure the tracer concentration in the polymer melt at a particular location. A small amount of non-reactive tracer must be used for this purpose so that the flow field is not disturbed. RTD function can be denoted by the following equation:

$$e(t) = \frac{c(t)}{\int_0^\infty |c(t)| dt} \tag{1.2}$$

Where, e(t) is normalized RTD function and c(t) is the tracer concentration. Residence Time Distribution is dependent on the operating conditions, which run the extruder. An increase in the screw speed and feed rate results in a narrow RTD curve. A narrow RTD curve is an implication that the material did not have sufficient mixing time in the

extruder. When the RTD curve is broader, the particles tend to have a higher mixing time, which is an implication of the mixing quality.

RTD may not be important in studying the mixing behavior in applications where time is a less dependent parameter. In order to understand the mixing behavior, the number of screw revolutions or the volume of extrudate would be considered as a better tool, compared to time [14]. Each of these could be calculated by using the residence time and performing a simple transformation to obtain the Residence Revolution Distribution (RRD) and Residence Volume Distribution (RVD).

## 1.6 Residence Revolution Distribution

The RRD gives an estimate of the number of revolutions taken by the screw to push the material out of the extruder). The function for RRD can be seen in the expression below:

$$f(n) = \frac{c\left(\frac{n}{N}\right)}{\int_0^\infty \left|c\left(\frac{n}{N}\right)\right| dn} \tag{1.3}$$

Where, N = screw speed (in RPM) and n = number of revolutions

The relation between the residence time, t and (n/N) is given by

$$t = \frac{n}{N} \tag{1.4}$$

The transport behavior of the extruder is emphasized using RRD.

## 1.7 Residence Volume Distribution

The RVD provides a direct estimate of the tracer distribution within the extruder along the axial direction [14]. It can be used as a measure to understand the efficiency of the axial mixing process for particular extrusion conditions [14]. The function for RVD can be expressed as per the following equation:

$$g(v) = \frac{c\left(\frac{v}{Q}\right)}{\int_0^\infty \left|c\left(\frac{v}{Q}\right)\right| dv} \tag{1.5}$$

Where, v = volume of extrudate and Q = material throughput (L/min)

The relation between residence time, t and (v/Q) is given by:

$$t = \frac{v}{Q} \tag{1.6}$$

However, the scope is limited in understanding the mixing process using RVD, as there are several aspects of mixing, apart from axial mixing. The uniformity of distribution, size scale of phases and concentration gradient of the elements cannot be studied using RVD.

## 1.8 Residence Stress Distribution

The properties of extruded products can be improved by adding fillers to the base polymer. To maintain a uniform composition within the polymer matrix, there is a need to understand the process of mixing. In order to understand more about the intensity of mixing, there is a need to quantify the amount of material that undergoes a particular amount of stress within the twin screw extruder (TSE). The Residence Stress Distribution approach was implemented to quantify the amount of stress experienced by the polymer melt within the TSE. Using the RSD approach, stress beads of variable strength were dropped into the mixing section of the twin screw extruder and the stress history was recorded based on the rupture of the beads upon encountering stress greater than the critical stress limit value of the beads [21]. The percentage of beads that ruptured are denoted by the term percent break-up (%BU). Experiments have been conducted over the past few years in an attempt to understand the stress history experienced by different polymeric materials for different sizes of extruders.

## 1.9 Objective

My thesis focuses on using a 1- D computer simulation software which models the co-rotating twin screw extruder. The goals of my research have been on identifying the relationship between the %BU and the physical properties that the polymer melt in the extruder is subjected to, such as the temperature, viscosity, shear rate and shear stress exhibited by the polymer melt. The second goal of my research would be to validate the experimental results obtained from using the RSD approach. In continuation to that, the assumptions made using the RRD methodology will also be validated during the course of my research. The internal behavior of the twin screw extruder has been understood based on the computer simulations for different sets of screw configurations of the mixing section. The variations in the observed behavior for different choices of base polymers have been understood using the 1-D computer simulations.

# Chapter 2 - Literature Review

## 2.1 Residence Stress Distribution

The properties of base polymers can be improved by adding fillers to the base polymer and compounding it using the twin screw extruder. Mixing plays a vital role in determining the properties of the extrudate. In order to quantify mixing, Residence Time Distribution (RTD) was used. The RTD in the extruder can be found out by using a tracer and an optical probe. Experiments were conducted in order to use RTD as a tool to quantify mixing. Distributive mixing (explained in Sec 1.4.1.1) was measured by Shearer and Tzoganikis [15-16] through the use of polymer tracers. The polymer tracers were blended with Polypropylene (PP) at 25 weight% using a batch mixer and blended with a twin screw extruder at 5 weight%. The experiments were conducted for conveying elements as well as kneading elements, and RTD was used to evaluate the amount of mixing based on different operating conditions. It was observed that the amount of mixing increased with the average residence time in the conveying zone of the extruder. Higher flow rates influenced better mixing at similar residence times, suggesting that degree of fill plays a vital role in the mixing process. However, in the case of kneading blocks, it was observed that the effect of local residence time is independent of distributive mixing. Distributive mixing in the kneading blocks was seen as a function of the total number of screw revolutions taken by the polymer melt in the mixing section (product of local residence time and screw speed). Distributive mixing increased with the number of revolutions of polymer melt in the kneading blocks. Todd [17] and Tadmor et Al [18] used Peclet numbers to quantify the RTD mixing intensity. The higher the Peclet number, lower was the mixing intensity. In

order to increase the mixing intensity, the Peclet number had to be lower, which was facilitated by increasing the helical angle between the twin screws. Several experiments were performed by Cheng et al [19] and the others to correlate the mixing intensity with RTD. The inability of residence distributions to provide information on the stress history within the extruder, as it focused on the history of axial flow in the extruders, called for different methodologies that could be used to quantify stress.

Curry et Al [20] used hollow glass spheres of varying strengths to determine the stress distribution within the extruder. Two sets of experiments were performed on ZSK-40 twin screw extruders for two different geometries. In the first experiment, two different screw geometries were used to compare the stress distribution within the extruder, for the same polymer matrix. The first screw design consisted of numerous kneading blocks, which were predicted to generate high shear stress. The second screw design consisted of a series of forward conveying and reverse conveying screw elements. The glass beads used for the experiment were rated to fail at a pressure of 4.5kpsi for a 10% rupture. Polybutene (liquid form) was used to perform this experiment in order to prevent the rupture of glass beads during the melting phase. The glass beads were fed into the extruder separately as compared to polybutene. The glass beads were fed at 12.8 volume percentage concentration [20].

The experiment was performed for the two different screw geometries by running the extruder at a series of throughputs and screw speeds. Once the polybutene-glass sphere mixture was extruded, it was analyzed to quantify the percentage of broken glass beads. This was done using ASTM D792 method, which was used to estimate the density of the sample and count the number of broken glass spheres, after burning the polymer away from

the extrudate [20]. The experiment revealed that the second screw design, i.e. the series of forward and reverse conveying screw elements had resulted in the rupture of a greater percentage of glass spheres compared to the screw design comprising the numerous kneading blocks [20].

The second experiment was performed using the same screw geometries specified in the above section. However, the experiment was performed for two different grades of polybutene, namely H-300 and H-1500. The viscosities at room temperature i.e. $25^0$C was found to be 709 Pa-s for H-300 and 87 Pa-s for H-1500 (at $10s^{-1}$ $25^0$C). The experiment was conducted on three glass beads of varying strength. The glass beads were dropped into the extruder at 10% volume concentration. The extruder was run at a series of screw speeds i.e. 80, 150 and 350 RPM. However, the feed rate was kept constant at 50 lb/hr. Based on the data collected as a result of performing the experiment, it was observed that the rupture of glass beads was higher at an increased screw speed. The percentage rupture of beads was observed to be higher for the screw design #2 i.e. for a series of forward and reverse conveying screw elements compared to the kneading block screw geometry. The more viscous the material, the higher the breakage of the glass beads, as this result was observed from the experiment.

The experiment conducted by Curry et al. had quite a few limitations. Firstly, the process was time-consuming and the results were not obtained in real time as the extrudate had to be treated in order to burn off the polymer so that the glass beads could be counted. Secondly, each of the broken glass beads had to be counted manually, which was prone to human error and posed a challenge towards the accuracy of the results collected. Hence,

the experiment conducted was able to collect only a few samples due to the large-time consuming steps in the process.

Gao et al. [14] established the RRD and RVD methodology (explained in Sec 1.7 and 1.8) to interpret the quality of mixing based on operating conditions and screw geometries.

The Residence Stress Distribution (RSD) approach was developed by Bigio et al. [21], as a method to characterize dispersion, through stress quantification in the twin-screw extruder. The experiment was performed on a 28mm Coperion Co-Rotating Twin Screw Extruder, using HDPE Alathon H6018, as the base polymer. CAMES (Calibrated Micro Encapsulated Stress beads) are beads designed with a critical stress limit, which when exceeded, results in the rupture of the beads.

The experiment was performed for two screw geometries. The former geometry comprising wide kneading blocks in the mixing section, while the latter geometry comprising narrow kneading blocks in the mixing section. The experiments were performed for a set of nine operating conditions i.e. for a range of screw speeds and specific throughput (Q/N). The specific throughput is taken as a ratio of the feed rate (Q) to the screw speed (N). Reflective Optical probes were attached before the die section of the extruder as they transmit light through the polymer melt and the light reflected off the surface of the screw elements and the polymer melt was received by the fiber optic bundle. These were converted into voltage signals that were recorded and interpreted using LabVIEW. Due to the transparent nature of HDPE, $TiO_2$ pellets were added to the base polymer, by feeding through the vent at a constant rate. The presence of $TiO_2$ creates a white background for the optical probe, on the polymer melt. The reference shots provided the RTD curve along the twin screw extruder, while the CAMES beads provided the RSD

curve. The ratio of the areas under each of the RSD curve to the RTD curve provided the Percent Break-Up.

$$\%BU = \frac{A_C}{A_r} \tag{2.1}$$

Where, $A_C$ is the area under RSD curve and $A_r$ is the area under RTD curve.

This experiment was used to quantify the percentage of material that underwent a particular amount of stress within the twin screw extruder. The experiment was able to relate the stress data as a function of the residence distribution. The comparison between the mixing performances of two different screw geometries (narrow and wide kneading blocks) was explained using the Residence Stress Distribution approach.

As a continuation to the implemented RSD approach, Pappas et al [22] performed an experiment comparing the stress history developed by using the wide and narrow kneading block geometry using two different strength stress beads (92kPa and 119kPa). This experiment was used to validate that the stress beads did not rupture randomly but at a critical predetermined stress value. Secondly, this experiment reaffirmed the observations from the previous experiment, that the wider kneading blocks exhibited higher percent break-up values compared to narrow kneading blocks.

The experimental conditions were organized using a Central Composite Design (CCD) grid, where the horizontal axis represented the screw speed (in RPM) and the vertical axis represented the specific throughput (in mL/Rev). This approach helped visually represent an organized relationship between percent break-up (%BU) and the operating conditions (N and Q/N). Bigio et al [23] expanded the original CCD grid, by including an additional range of operating conditions to the original CCD grid, to provide a more robust design of experiment approach. The original CCD grid can be seen in Fig. 2.1.

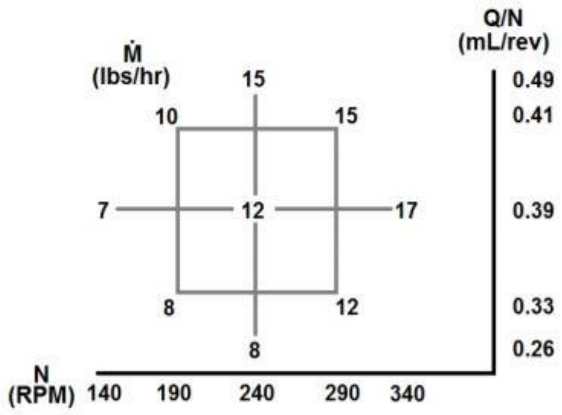


Figure 2.1: Original CCD grid [23]

The CCD grid seen in Fig. 2.1 was the base grid used to perform the experiment to obtain the percent break-up results. This grid was expanded by adding a range of operating conditions to the original CCD grid. There were two sets of modifications done to the original CCD grid, the first of which focuses on expanding the operating conditions along the cross in the original CCD grid, while the second comprises a CCD grid that was translated over the horizontal axis, i.e. starting with the rightmost condition in the original CCD grid followed by eight operating conditions spaced equally, similar to the original CCD grid.

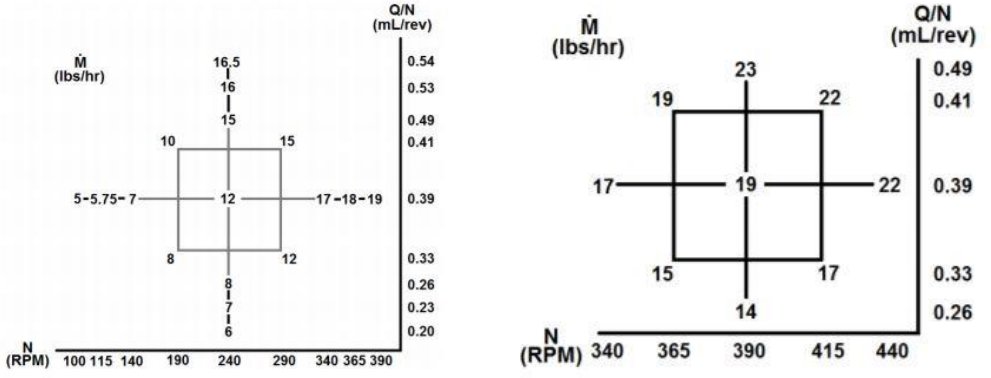


Figure 2.2: Expanded Cross Grid (left) and Translated DOE grid (right) [23]

From Fig. 2.2, the modifications to the original CCD grids can be identified. The CCD grid on the left-hand side is expanded along the cross i.e. additional operating conditions are added at the condition where Q/N is constant at 0.39 mL/Rev and when the screw speed is constant at 240 RPM. This modification lets expand the grid an additional half and full level. The DOE grid on the right-hand side translates the DOE grid over the horizontal axis. The rightmost condition from the original grid is considered as the starting point for this grid, which adds 8 operating conditions spaced in an equivalent manner, similar to the original CCD grid.

The goal of this experiment was to conduct a study on the percent break-up results in the mixing section of the extruder in greater detail, by experimenting with a wider range of operating conditions. The results provided by this experiment were consistent with the conclusions obtained from the previous experiments. The inclusion of additional operating conditions provided a more rigorous validation of the stress bead results that have been obtained from the conducted experiments.

Each of these experiments has shown the effects of N and Q/N on %BU, to be significant. The second order terms such as $N^2$, $(Q/N)^2$ and Q (interaction of N and Q/N) were found to be non-significant. The most recent experiment conducted using the RSD Methodology was the depiction of percent break-up as a three parameter residence distribution study. Dryer et al [24] performed an experiment to correlate the percent break-up of the polymer matrix with 3 operating conditions i.e. screw speed (N), specific throughput (Q/N) and barrel temperature ($T_b$). The experiment was conducted using Kollidon VA-64 as the base polymer. 9 operating conditions were chosen to perform this experiment which included a range of screw speed (N) and specific throughput (Q/N). Each of these 9 operating

conditions was run on the Twin Screw Extruder, at three different barrel temperatures ($170^0$C, $190^0$C and $220^0$C). The percent break-up results that were obtained for each of the experimental runs were statistically analyzed using JMP 11.0.0 in order to obtain predictive equations for percent break-up in terms of screw speed (N), specific throughput (Q/N) and barrel temperature ($T_b$). The results reflected on the fact that with an increase in barrel temperature, the percent break-up (%BU) decreases. This experiment was conducted to establish the fact that barrel temperature was an important variable along with screw speed (N) and throughput (Q/N) in the determination of a viable operating domain.

## 2.2 Computer Simulations

With the growing popularity of co-rotating twin screw extruders in the industry, there is a need to understand, control and optimize the extrusion parameters. The experimental results provided by the RSD Methodology do not explain the reasons behind the generated results i.e. the set of internal processes that trigger the obtained output. In order to validate the findings of the RSD, RRD and RVD experiments, computer simulations were performed.

Due to a large number of inter-related variables and complex flows developed in the Twin Screw Extruders, it has been an extremely difficult task to model flows. Prior efforts have been made in an attempt to model flow simulations along the TSE.

First attempts at modeling flows along a twin screw extruder, were performed by Booy et al. [25] and Meijer et al. [26]. As a first step towards modelling flow within a co-rotating twin screw extruder, an isothermal flow of incompressible Newtonian fluids was considered, similar to the modeling theory behind single screw extrusion. For this study, two flow scenarios were considered i.e. flow within a fully filled screw channel and flow

within a partially filled screw channel. The fully filled screw channel with liquid was considered similar to a single screw pump and the flow equations were modified accordingly for the twin screw extruder. The drag flow and backpressure flow equations were determined by solving Laplace and Poisson's differential equations. The shape factors for drag ($F_d$) and pressure flow ($F_p$) were computed. For partially filled screw channels, the liquid layers do not move for a longer duration during the cycle; however, they are pushed and smeared against the flight tips. By simplifying the shape of the flight tips and the cross-sectional area of the liquid region, the average axial velocity was computed. The degree of fill was calculated and expressed in terms of the flow rate, screw speed and the dimensions of the screw geometry. The mathematical model proposed by Booy seemed to be in agreement with the actual behavior, for highly viscous fluids and lower degree of fill. However, this approach paved way for the subsequent models proposed for the flow of Non-Newtonian fluids in the Twin Screw Extruder.

Tayeb et al. [27] developed a Twin Screw Extrusion model that predicts the product transformation (food extrusion in this case) based on thermomechanical history. The thermomechanical history (temperature, pressure and shear rate) was calculated based on internal conditions within the extruder, using physical laws. The model segregated the twin screw extruder into four zones namely the conveying, melt pumping, shearing and die zone. Temperature trends were calculated only in the conveying section as the rest of the zones were considered to have isothermal flow. The viscosity model was considered Newtonian; however, the viscosity values were computed based on the local shear rate and temperature within the element. In order to calculate the viscous flow, certain assumptions were put in place:

- Flow is steady, fully developed and isothermal.
- No slip at the barrel wall and the screw.
- Body forces and inertia were considered negligible.

The flow equations were modeled based on the assumption that the screw is stationary while the barrel moves over the stationary screw, similar to the single screw extruder model. The flow in the conveying section was modeled based on solving the thermal balance equations, while the solution of stokes equation was used to model flow equations for the remaining three sections. The flow equations will be discussed further in the theory section (Chapter 3). The computed thermomechanical results were compared to the actual results generated from performing the experiment on a Twin Screw Extruder, which consisted of a screw geometry with forward conveying elements and one reverse screw element located in front of the die zone. The extruder was run at 200 RPM and a feed rate of 30 Kg/Hr. The results obtained from the experiment seemed to agree with the computed results based on the model developed for the twin screw extruder. This was the first attempt at modeling the 1-Dimensional flow for a Non-Newtonian fluid along the twin screw extruder.

Denson & Hwang [28] analyzed the down channel Newtonian flow for a co-rotating Twin Screw Extruder and developed a computational model that relates the axial pressure gradient as a function of throughput rates for different screw geometries. Twin Screw Extruders with conveying elements having three tips were considered in this situation, and the effect of flow in the intermeshing region was neglected. The equation of motion for the down flow along the channel and the boundary conditions were non-dimensionalized using screw radius and velocity as the variables. This equation was solved using the finite

element method based on Galerkin's scheme [29]. The results generated depicted throughput rates as a function of parameters such as the number of screw tips, helix angles, ratio of the distance between center of the screw to the screw radius and the ratio of the clearance to the screw radius. An equation relating the axial pressure gradient to the throughput rate for a fully filled screw channel was developed using 2-D flow computations. Using the Flow Analysis Network (FAN) method, experiments were conducted by White et al. [30] to perform 2-D computations as well. Flow Analysis Method was developed by Tadmor et al. [31] to solve 2-D flow equations for complex screw geometries in the field of polymer processing. This method can be applied to a Non-Newtonian fluid that is incompressible, inelastic and time dependent. The flow field is divided into a mesh (Eulerian mesh) comprising nodes located at the center of each cell. Based on the flow analysis performed on each node, a set of algebraic equations with unknown pressure values are generated, which are solved to obtain the flow distribution. This process is done iteratively for Non-Newtonian fluids as opposed to Newtonian fluids where the solution is required to be obtained once.

Recently, 3-Dimensional flow models were developed both for Newtonian [32] and Non-Newtonian fluids. The study focused on developing a 3-Dimensional flow model for both conveying elements and kneading elements in a co-rotating twin screw extruder. Sepran, a Finite Element Software was used to solve the flow equations. The simulation model is based on the three-dimensional geometry of the screw elements along the twin screw extruder including the C-section as well as the intermeshing zone in between the screws. The flow patterns for a Newtonian fluid were simulated based on the 3-D model of a fully filled screw channel for conveying elements. However, each of these models concentrated

on isothermal flows as non-isothermal flows resulted in complex velocity fields and streamlines. When considering non-isothermal flows, either a full 3-Dimension Temperature field or a 1-Dimension Average Temperature flow model had to be considered. Chiruvella et al [33] used the former approach while White et al [34] preferred the latter approach. Chiruvella et al used the finite volume method to study the fluid flow and heat transfer within the co-rotating twin screw extruder. Since the flow in the translation region had already been mathematically modeled based on prior experiments conducted by Booy et al, this experiment focused on the intermeshing region, where the effects of mixing as well as diffusion of momentum and energy had to be considered. The governing equations (momentum, energy equations) were solved to obtain the velocity components in the 3 coordinate directions. Based on the velocity components, the shear rate was computed, which was used to calculate the temperature and viscosity along each point. The accuracy of the 3-D model developed was validated by performing the experiment on a ZSK-30 Twin Screw Extruder, with a L/D ratio of 29. The extruder was run at two sets of operating conditions (Q = 6 Kg/Hr, N = 30 RPM and Q = 7.5 Kg/Hr, N = 41 RPM). The velocity profile was measured using a Laser Doppler Anemometer. The experimental results obtained complied with the computational results obtained from the 3-D model. This section provides a background into the evolution of models, capable of simulating the flow within the co-rotating twin screw extruder using 1-D, 2-D and 3-D approach for Newtonian and Non-Newtonian Fluids.

Global Approach aims at creating a simple flow model of the entire operation performed by the extruder i.e. from the hopper to the die. It serves a link that simplifies and connects the local approach model developed for the individual screw elements. The first instance

of developing a global model for the flow in a co-rotating Twin Screw Extruder was performed by White et al [35] as well as Meijer et al [26]. A simple model was developed for a co-rotating intermeshing twin screw extruder, considering the non-isothermal flow for a Non-Newtonian fluid [27]. The main goal behind using such an approach was to develop a simplified model that could be used to describe the twin-screw extrusion process, which could ideally be used on personal computers and workstations to help understand the extrusion phenomenon. One such model which was developed based on the global approach was Ludovic. Different computer simulation models have been developed for the purpose of performing twin screw extrusion simulations are Akro-Co Twin Screw Extrusion Software developed by J.L. White, TXS developed by Polytech, Ludovic developed by SCC and Sigma developed by University of Paderborn [36]. The software offers a 1-Dimensional simulation approach, capable of modeling the twin screw extruder. Each of the above-mentioned software, work on an iterative method, perform thermomechanical calculations (pressure, fill ratio, temperature, viscosity) from the die until the hopper

Ludovic Simulation Software was the program chosen to perform simulations for operating conditions similar to those used to perform RSD experiments. It is used as a tool to understand the internal process parameters such as temperature, pressure, viscosity, shear rate etc. that affect the output (discussed in Chapter 3 in detail). The experimental results obtained from RSD can be validated using the results obtained from Ludovic and can help understand the physics behind the results obtained. A set of three base polymers i.e. Low Density Polyethylene (LDPE), High Density Polyethylene (HDPE) and Kollidon VA-64 are simulated using Ludovic for a range of operating conditions and different set of screw

configurations. The RRD and RVD methodology, which was explained in Section 1.7 and 1.8 had made certain assumptions based on the actual experiments performed. These assumptions could be ratified using Ludovic, as the quantitative results for the Fill Length, Number of Revolutions made by the screw in a particular element could be calculated and they can help explain the validity of the assumptions.

# Chapter 3 - Theoretical Calculations for Twin Screw Computer Simulations

The thesis focuses on some of the results generated as a result of the Ludovic simulations, which includes average shear rate, viscosity, temperature, pressure, degree of fill and residence time. This section provides an insight into the set of equations that are important towards the calculation of extrusion parameters. Vergnes et al. [37], had modeled the equations for polymer flows in co-rotating twin screw extruders. Flow equations for screw element i.e. conveying elements, kneading blocks etc. have been discussed in the following sections.

## 3.1 Modelling Flow in a Conveying Screw Element

While developing a flow model for the conveying screw elements, certain assumptions were put in place:

- The screw was considered stationary, while the barrel was considered to move over the top of the screw channel, as per the groove model [2].
- Cylindrical coordinates (seen in Fig. 3.1) are used to represent the screw channel, which is considered to be perpendicular to the screw flight [37]. Radial velocity component u is negligible, only longitudinal and transverse flow velocity components (v and w) considered.

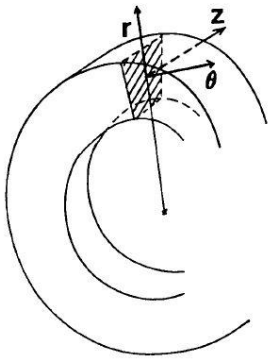


Figure 3.1: Configuration of Screw Element

- Screw channels are unwound and considered as simple rectangles with a constant width.
- The polymer flows along the screw channel in an eight-shaped pattern along consecutive C-shaped chambers, as well flows in the intermeshing zone in between the two screws [37].
- The flow is considered Newtonian and isothermal, which allows the use of Newtonian equations. However, instead of using constant viscosity term (Newtonian Flow), in this case, a specific viscosity term is used as a function of the shear rate and temperature along a particular point in the screw channel [37].

Based on these assumptions, the classical flow equation was developed as a sum of the drag flow and pressure flow term.

$$Q_c = F_d * W * R_e \left[1 - \frac{{R_i}^2}{{R_e}^2 - {R_i}^2} \ln\left(\frac{R_e}{R_i}\right)^2\right] * \left(\frac{N * R_e * \cos\varphi}{2}\right) - \frac{F_p}{8\eta}\left(\frac{\Delta P}{\Delta\theta_c}\right) * W * \left({R_e}^2 - {R_i}^2\right) *$$

$$[1 - (\frac{2R_iR_e}{{R_e}^2 - {R_i}^2} * \ln\left(\frac{R_e}{R_i}\right))^2] \quad (3.1)$$

Where, $Q_c$ is the Volumetric Flow Rate, $F_d$ and $F_p$ are shape factors, $R_e$ and $R_i$ are the external and internal radii of the screw channel, N is the screw speed, η is the viscosity, and $\Delta P/\Delta\theta$ is the pressure gradient.

$\dot{\gamma}$ is the average shear rate which is calculated based on the flow in the θ-direction and z-direction (See Fig. 3.1). The equation for average shear rate can be seen in Eq. 3.2.

$$\dot{\gamma} = \frac{2}{{R_e}^2 - {R_i}^2} \int_{R_i}^{R_e} r\left[\left(\frac{dv}{dr} - \frac{v}{r}\right)^2 + \left(\frac{dw}{dr}\right)^2\right]^{1/2} dr \tag{3.2}$$

Eq. 3.2 can be applied to Non-Newtonian Fluids, as per the assumption stated above i.e. the specific viscosity term could be used as a function of shear rate and temperature.

Using the average shear rate value, the specific viscosity value could be computed using any viscous law (Carreau-Yasuda, Power Law etc.). For instance, using power law, the viscosity of the melt could be calculated as per Eq. 3.3.

$$\eta = K\dot{\gamma}^{n-1} \tag{3.3}$$

Where, K and n are power law parameters. The computation for the K values is performed based on the Arrhenius Thermodependent Power Law, which can be seen in Eq. 3.4.

$$K = K_o \exp\left[\frac{E}{R}\left(\frac{1}{T} - \frac{1}{T_{ref}}\right)\right] \tag{3.4}$$

Using Eq 3.1-3.4, the calculations can be performed for both left handed and right handed conveying elements to calculate the pressure drop across the C-shaped chamber. The computation of temperature is discussed in detail in Sec 3.3.1.

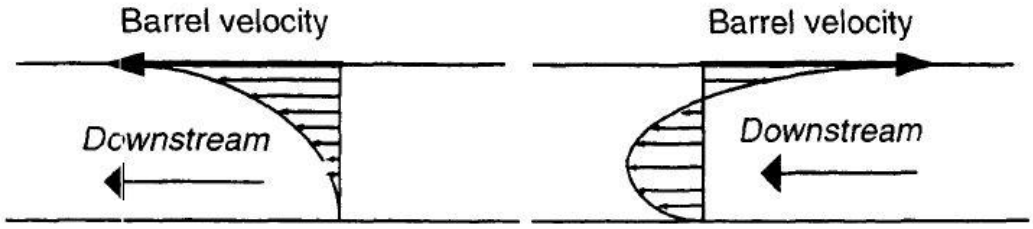


Figure 3.2: Flow across the screw channel for forward conveying (left) and reverse conveying (right) screw elements

The pressure drop values are calculated from Eq. 3.1, where, for forward conveying element, the barrel relative velocity is in the same direction as the downstream flow (Fig 3.2). In the case of reverse conveying elements, the relative barrel velocity is in a direction opposite to that of the downstream flow which results in a negative drag flow term. The pressure gradient term also becomes negative, which implies a pressure drop, in order to push the material downstream, which causes the pressure flow term to become positive. Eq. 3.1 changes sign convention for the reverse conveying elements. The calculations performed using the 1-D Global approach were compared to the 2-D computations, and the results seemed to agree, which implied that the 1-D approach could be utilized in comparison to complex techniques.

In the case of the intermeshing zone between the screws, the pressure flow term was only considered for the 1-D approach due to the complexity of kinematics and geometry [37]. The drag flow term was neglected in this situation, as the barrel velocity over the intermeshing zone was unknown [27]. To model the flow in the intermeshing zone, the actual geometry of the region had to be clearly specified. In the case of the 1-D model, an approximation of the mean cross section was performed, based on the characteristic parameters from the geometry/screw barrel [37]. The mean cross section was defined based on the following equations:

$$W^* = W - \alpha R_e sin\phi \tag{3.5}$$

$$\alpha = \frac{\pi}{m} - 2\psi \tag{3.6}$$

Where, α is the flight angle, m is the number of flights and ψ is the intermeshing angle

Booy [38] defined $\psi = \frac{C_l}{2R_e}$ (3.7)

Where, $C_l$ is the centerline distance between the screws.

Based on these geometrical changes, the equation for volumetric flow rate in the intermeshing zone can be seen in Eq. 3.8.

$$Q_c = \frac{F_p^*}{8\eta^*}\left(\frac{\Delta P^*}{\Delta \theta_c^*}\right) W^*\left({R_e}^2 - {R_i}^2\right)[1 - (\frac{2R_iR_e}{{R_e}^2-{R_i}^2}\ln\left(\frac{R_e}{R_i}\right))^2] \tag{3.8}$$

Eq. 3.8 is similar to Eq. 3.1 except that the drag flow term is neglected and the geometric dimensions are changed based on the local geometry (intermeshing zone).

## 3.2 Flow in Kneading Blocks

The simplified approach towards modeling flow in the Kneading Disks was performed based on the analysis carried out by Werner [39]. Fig 3.3 reveals the geometry of a bilobal kneading disk, and the flow in the peripheral direction (θ direction) is only considered.

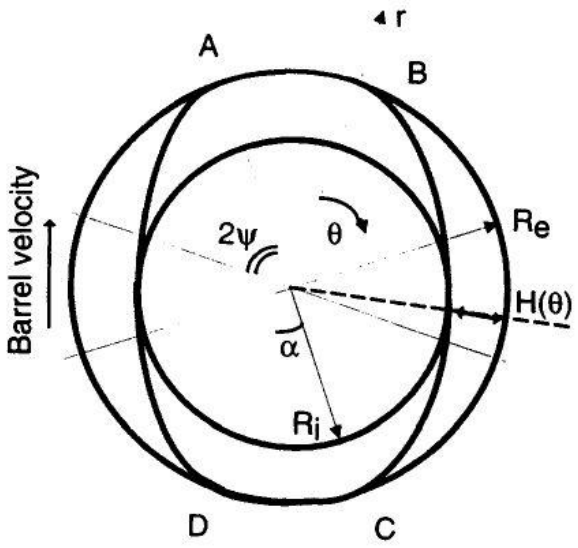


Figure 3.3: Bi-lobal Kneading disk

The pressure profile at point A is used to characterize the flow along the kneading disk, as a result of the barrel velocity and screw geometry. The material is pushed downstream as a consequence of the axial pressure gradient, generated by the staggering of the disks. Since the peripheral flow is only considered in this situation, the velocity component in the θ direction is considered. The velocity component is a function of r, which is the radial position. As a result, momentum equation (for isothermal Newtonian Fluid) is reduced to:

$$\frac{1}{\eta}\frac{dP}{d\theta} = r\frac{d}{dr}\left(\frac{1}{r}d\frac{rv}{dr}\right) \tag{3.9}$$

Applying boundary conditions to Eq. 3.9, i.e. no-slip condition on moving barrel and integrating the equation twice leads to Eq. 3.10

$$\frac{dP}{d\theta} = \frac{\frac{Q_\theta}{E}+\left(\Omega {R_e}^2\frac{(r(\theta)^2}{({R_e}^2-R(\theta)^2}\ln\frac{R_e}{R(\theta)}-\frac{1}{2}\right)}{\frac{1}{8\eta}\frac{4R(\theta)^2{R_e}^2}{{R_e}^2-R(\theta)^2}\ln\frac{R_e}{R(\theta)}^2-\left({R_e}^2-R(\theta)^2\right)} \tag{3.10}$$

Where, E = paddle thickness, $R_e$ is the external radius of the barrel and R(θ) is the internal radius. R(θ) can be obtained by Equation 3.11.

$$R(\theta) = R_e - H(\theta) \tag{3.11}$$

Based on Booy's analysis [38], the relation for H(θ) can be seen in Eq. 3.12

$$H(\theta) = R_e(1 + cos\theta) - \sqrt{{C_l}^2 - {R_e}^2 sin^2(\theta)} \tag{3.12}$$

Where, $C_l$ is the centerline distance.

Equation 3.10 showcases the relationship between pressure gradient in the peripheral direction dP/dθ and the peripheral flow rate $Q_\theta$. This equation can be used to calculate the pressure profile along the kneading disks as θ varies from 0 to π. Once dP/dθ is calculated, the axial pressure gradient (dP/dz) can be calculated along the staggered kneading disks and can be altered to match the axial flow rate (Q) [40]**.**

## 3.3 Calculations

### 3.3.1 Average Temperature Calculations

The polymer melt within the twin screw extruder is subject to non-isothermal conditions. This is difficult to model if a 1-Dimensional approach is considered, which prompts the calculation of average temperature over the channel depth as a solution. The temperature changes across the screw elements in the extruder [37], can be calculated using a thermal balance of the heat transfer between the screw and barrel and the average power dissipated, as seen in Eq.3.13

$$\rho C_p Q_c \overline{\Delta T} = h_{T_b}(T_b - \bar{T})S_b + h_{T_s}(T_s - \bar{T})S_s + \dot{W} \tag{3.13}$$

Where, ρ is the density of the polymer melt, $C_p$ is the specific heat, $h_{Tb}$ and $h_{Ts}$ are the barrel and screw heat transfer coefficients, $T_b$ and $T_s$ are the barrel temperature and screw temperature, $\bar{T}$ is the mean temperature, $\overline{\Delta T}$ is the change in the temperature between screw elements, $S_b$ and $S_s$ are the exchange surfaces for barrel and screw and finally $\dot{W}$ is the

power dissipated. The power dissipated can be calculated from Eq. 3.14 by integration over the volume of the element, V.

$$\dot{W} = \int_V \eta \bar{\gamma}^2 dV \tag{3.14}$$

Where, $\bar{\gamma}$ and η are calculated from Eq. 3.2 and 3.3.

The average temperature of the subsequent screw elements can be found from the $\overline{\Delta T}$ and the mean temperature of a given screw element, as can be seen in Eq. 3.15.

$$\bar{T}_{i+1} = \bar{T}_i + \overline{\Delta T} \tag{3.15}$$

The heat transfer coefficients mentioned in Eq. 3.13 are essential in calculating the temperature changes along the screw channel in the extruder. The heat transfer coefficient for the screw channel, $h_{Ts}$ is traditionally considered to be 0, i.e. adiabatic unless the screw is regulated thermally. In the case of the barrel, the heat transfer coefficient $h_{Tb}$ is calculated using Eq. 3.16, based on Todd's analysis [41]:

$$h_{T_b} = 0.69 \frac{k}{R_e} \frac{{R_e}^2 N\rho}{\eta}^{0.28} \frac{C_p\eta}{K}^{0.33} \frac{\eta}{\eta_P}^{0.14} \tag{3.16}$$

### 3.3.2 Residence Time Calculations

Residence time, which is the time that the polymer melt spends in the screw element can be calculated for the fully-filled screw elements as well as partially-filled screw elements. In the case of partially filled screw elements, there is no pressure flow as the polymer melt is conveyed by pure drag flow, as a result of the relative motion of the barrel. The mean velocity of the polymer melt being conveyed along the channel direction.

$$\bar{V} = \pi N R_e cos\phi \tag{3.17}$$

Where, N is the screw speed and $R_e$ is the external radius (barrel), $\phi$ is the pitch angle.

Residence Time can be calculated from the mean velocity and the length of the screw element using Eq. 3.18.

$$t_s = \frac{L}{\bar{V} sin\phi} \tag{3.18}$$

Where, $t_s$ is the residence time and L is the length of the partially filled screw element.

In the case of fully filled elements, the residence time is calculated using the following equation:

$$t_s = \frac{\rho V}{Q} \tag{3.19}$$

Where, ρ is the density of the polymer melt, V is the free volume within the screw element and Q is the flow rate.

The free volume, V is calculated based on the analysis conducted by Booy [38]

$$V = (A_b - 2A_s)L \tag{3.20}$$

Where, $A_b$ and $A_s$ are the barrel and screw cross-sections, L is the axial length of the screw element.

$$A_b = 2(\pi - \psi){R_e}^2 + C_l R_e sin\psi \tag{3.21}$$

$$A_s = m\left(\psi {C_l}^2 - C_l R_e sin\psi\right) + \frac{m\alpha}{2}({R_e}^2 + (C_l - R_e) \tag{3.22}$$

Eqs. 3.17-3.22 represent the equations that are used to calculate the residence time for the respective screw elements.

### 3.3.3 Degree of Fill Calculations

Degree of fill represents the ratio of the volume of screw channel filled with the polymer melt to the entire volume of the screw element, as it is a useful measure in understanding the mixing performance of the twin screw extruder. It is calculated using Eq. 3.23.

$$f_r = \frac{Q}{N} \frac{2L}{VBcos^2\phi} \tag{3.23}$$

Where, $f_r$ is the degree of fill, B is the pitch of the screw element, V is the free volume (calculated from Eq.3.20)

Eq. 3.23, used to calculate the degree of fill shows that it is a function of the specific throughput (Q/N).

## 3.4 Process of computing results using Twin Screw Simulation Software

This section of Chapter 3 provides an overview of the calculations performed by the twin screw simulation software [37]. Calculation of results is performed on an iterative basis. The properties of the base polymer and the screw design of the TSE are defined by the user. The thermomechanical properties i.e. pressure, temperature, residence time are calculated based on equations (3.1-3.24). However, a twin-screw extruder is starve fed, as a result of which the fill ratio of the screw channel is unknown; hence, the computations are made in the upstream direction from the die to the feeding section. The final temperature of the extrudate that exits the die is unknown; an arbitrary exit temperature is chosen. Based on the dimensions of the die, the shear rate and viscosity is calculated accordingly from Eq. 3.2 – 3.4. In this manner, the properties are calculated for each screw element from the Eq. 3.1 – 3.24 in the upstream direction. In the case of a forward conveying screw element, the pressure is zero (forward conveying screw elements convey the materials using drag flow as there is no back flow in these elements) and the software checks for the presence of a restrictive screw element (reverse screw element or kneading block) in the upstream direction; the pressure is computed as zero until the next restrictive element is encountered. When the first restrictive element is encountered i.e. only forward conveying screw elements are found in the upstream direction; the temperature is computed at this region. The computer simulation software assumes that the polymer feed melts

instantaneously upon reaching the first restrictive element; the temperature at this point is compared to the melting temperature of the polymer melt (this is specified by the user or can be retrieved from the software database). If the computed temperature corresponds to the actual melting temperature of the polymer melt, then the simulation is completed, and the results are obtained. However, if the computed temperature varies from the actual melting temperature of the polymer melt, the exit temperature from the die is altered, and the computations for each of the properties are performed on an iterative basis until the computed temperature at the first restrictive element corresponds to the melting temperature of the polymer melt.

# Chapter 4 - Experimental Setup

This section discusses the experimental setup that has been used to perform RSD experiment; the computer simulations are carried out using the same RSD experimental setup. The equipment, materials, and procedures used to perform the experiment have been discussed in the following pages. There are two parts to this chapter; the first phase being the description of Residence Stress Distribution (RSD) Methodology to calculate Percent Break-Up (%BU) and the second part being the description of simulation software setup that will be used to validate RSD results. The Percent Break-Up (%BU) has been used as a metric to evaluate the amount of stress that the polymer melt experiences within the twin screw extruder. The experimental procedure used to describe the Residence Stress Distribution (RSD) Methodology will be discussed in brief as the experimental procedures have been discussed in detail based on prior experiments conducted [21-24]. A table summarizing the experimental setup for this thesis can be seen in Table 4.1, which could help understand the layout of the experiment.

Table 4.1: Summary of the experimental setup

| Extruder Size | 18mm | | | | 26mm | | | | 16mm | | |
|---|---|---|---|---|---|---|---|---|---|---|---|
| Base Polymer | Mixing Section Config. | | | | Mixing Section Config. | | | | Barrel Temp. | | |
| | 24mm Narrow | 24mm Wide | 48mm Narrow | 48mm Wide | 24mm Narrow | 24mm Wide | 48mm Narrow | 48mm Wide | 170 $^0$C | 190 $^0$C | 220 $^0$C |
| LDPE | ✓ | ✓ | ✓ | ✓ | | | | | | | |
| HDPE | ✓ | ✓ | ✓ | ✓ | ✓ | ✓ | ✓ | ✓ | | | |
| Kollidon | | | | | | | | | ✓ | ✓ | ✓ |

## 4.1 Equipment

### 4.1.1 Twin Screw Extruder

#### 4.1.1.1 18-mm TSE

The RSD Experiments were conducted on a Coperion ZSK-18 Megalab Twin Screw Extruder (Fully-Intermeshing Co-Rotating TSE), situated at the Dupont Facility at Wilmington, DE. The base diameter for this TSE was 18mm, with an L/D ratio of 40. The screws were double-flighted (discussed in Sec 1.3), consisting of 10 barrels. The temperature profile used for the barrels can be seen in Table 4.2.

Table 4.2: Temperature profile for 18mm TSE

| Barrel | 1 | 2 | 3 | 4 | 5 | 6 | 7 | 8 | 9 | 10 | Die Zone |
|---|---|---|---|---|---|---|---|---|---|---|---|
| Temp ($^{o}$C) | 0 | 0 | 150 | 150 | 150 | 150 | 150 | 125 | 125 | 135 | 140 |

The temperature profile was maintained for each of the screw geometries (discussed in Sec 4.2**)** used to perform the experiment. The barrels were heated to a temperature of $150^{0}$C, until the mixing section, where the barrels were heated to a temperature of $125^{0}$C. The barrel between the mixing section and the die zone was heated to $135^{0}$C; the die zone was heated to $140^{0}$C. The optical light probe, part of the data acquisition system to receive the feed input from the CAMES bead break-up, is inserted into an opening after the mixing section of the extruder. The Data Acquisition Setup will be discussed in brief in Section 4.1.2.

#### 4.1.1.2 26-mm TSE

The second set of the RSD experiments were performed on the ZSK-26 MC fully intermeshing co-rotating Twin Screw Extruder. The experiments were performed at the Coperion Headquarters at Ramsey, NJ. The base diameter for this TSE was 26mm, with an L/D ratio of 37. The screws were double-flighted consisting of 9 barrels, which were heated uniformly to a temperature of $200^0$C, including the die. The optical light probe was injected into the opening slot, after the mixing section of the TSE.

#### 4.1.1.3 16-mm TSE

The final set of RSD experiments, relevant to this thesis, were conducted on a 16mm Thermo-Extruder with an L/D ratio of 40. The screws were double flighted, consisting of barrels, that were heated to varying barrel temperatures i.e. $170^0$C, $190^0$C and $220^0$C (discussed in detail in Sec 4.2.3).

### 4.1.2 Data Acquisition Setup

This section briefly discusses the data acquisition setup used to calibrate the percent break-up values using the RSD Methodology. The data acquisition setup used to perform the RSD experiment consists of an optical light probe, CPU, connector block and amplifier [21-22]. The optical probe is inserted into the extruder before the die via a probe slot. The light probe measures the intensity of the light reflected off the polymer melt. The light source is transmitted using a fiber optic cable towards a stainless-steel sheath that is mounted onto the extruder barrel. The scattered light, which is received by another fiber optic cable, is converted into voltage. The obtained voltage is amplified using an amplifier device. The voltage signals are transmitted to the connector block that is connected to the CPU. LabVIEW is the interface that helps visualize the obtained experimental data.

## 4.2 Screw Geometries

The configuration of screws in the extruder is vital to the process of mixing. Different screw elements have different mixing and conveying capabilities (discussed in Chapter 1), and the orientation of the screws helps determine the quality of mixing. The degree of fill (discussed in Chapter 3) is an important indicator of the mixing efficiency of the process. Degree of fill varies with the orientation of screw elements along the extruder length. To understand the influence of screw geometry in the process of mixing, only the mixing sections of the following screw geometries would be discussed. The mixing section comprises a series of kneading blocks (discussed in Chapter 1) which influence the mixing process based on their size and orientation. Preceding the mixing section is the melting zone, where the polymer pellets are melted into a molten state. The polymer melt is conveyed towards the mixing section using conveying elements. Following the mixing section, the polymer melt is 'pumped' towards the die, from where the extrudate is obtained. A brief overview regarding the melting and the melt pumping section has already been discussed in Chapter 1. The Screw Geometries used to perform the experiment for the 18, 26 and 16mm extruder will be discussed in this section.

### 4.2.1 18mm TSE

The 18mm TSE used for this experiment consists of four screw geometries. The conveying zone and the melting zone remains the same for each of the four screw geometries. The difference between the screw geometries is in the mixing section.

#### 4.2.1.1 Narrow 24mm Mixing Section

The first screw geometry can be seen in Fig 4.1. The extruder consists of 10 barrels as seen in Fig 4.1. The different screw elements used for the screw geometry have been labeled in

Fig 4.1, from the feeding zone (left) to the die (right), for a better understanding. The melting region consists of a forward kneading block ($45^0$ stagger angle, 5 paddles of 2.4 cm length) followed by two left-handed conveying elements, each 0.8 cm in length with an axial pitch of 1.6 cm. The conveying zone consists of right-handed conveying element of 2.4 cm length with an axial pitch of 2.4 cm. The different screw elements used for the screw geometry have been labeled in Fig 4.1, for a better understanding. These zones remain similar for each of the 4 geometries used to perform the experiment. The mixing section consists of 3 narrow forward kneading blocks (5 paddles), with an axial length of 0.8 cm staggered at $45^0$. The kneading block is followed by a left handed conveying screw element of 0.8 cm length having an axial pitch of 1.6 cm.

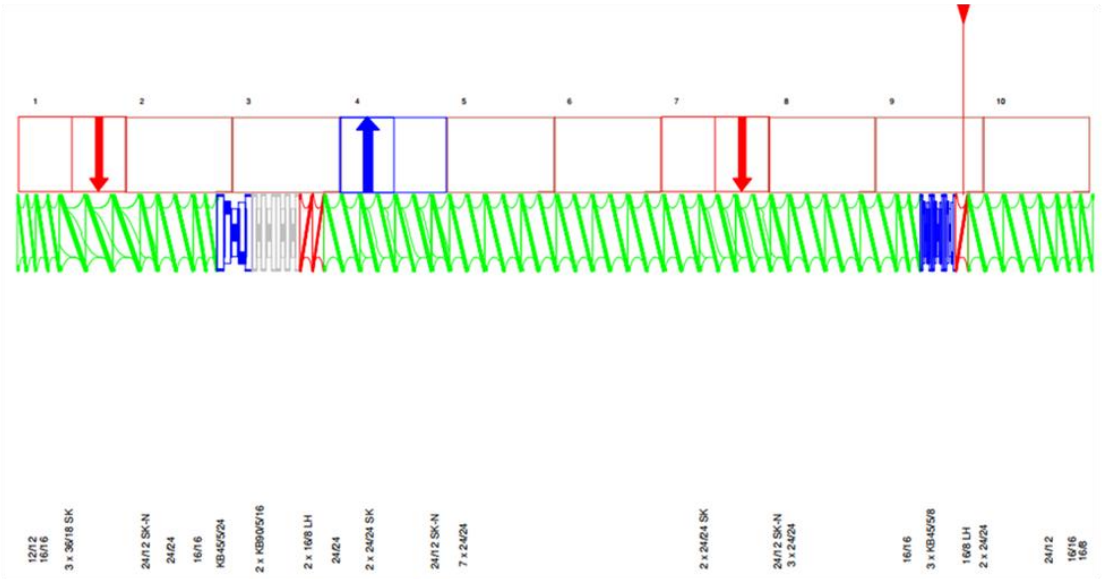

Figure 4.1: Narrow 24mm Mixing Section Screw Geometry

#### 4.2.1.2 Wide 24mm Mixing Section

This screw configuration is similar to the previous screw configuration, except for the mixing section. The mixing section consists of a wider forward kneading block (2.4 cm length, 5 paddles staggered at $45^0$) in comparison to the Narrow 24mm Mixing section,

which has 3 narrow kneading disks. The kneading block is followed by a left handed conveying element

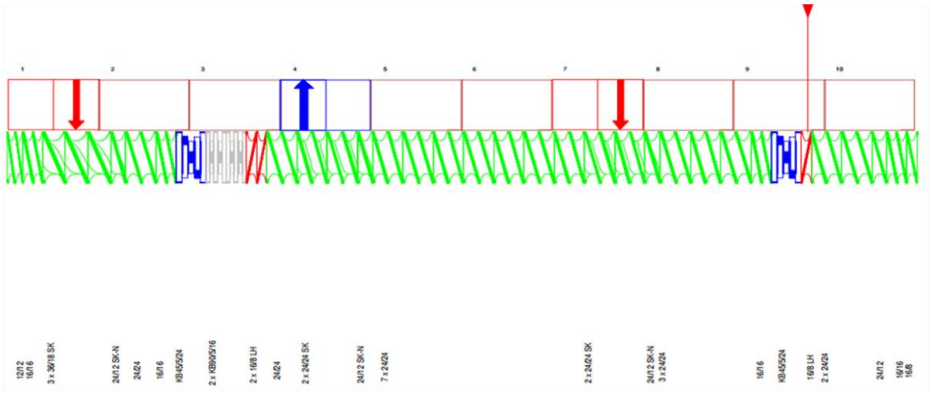

Figure 4.2:24 mm Wide Mixing Section Screw Configuration

#### 4.2.1.3 Narrow 48 Mixing Section

The third screw configuration used for the 18mm TSE is similar to the first and second screw configuration in terms of the melting and conveying sections. The mixing section differs in the sense that the length of the mixing section is doubled. The first and second screw geometries consist of kneading blocks to a length of 24mm, while the third screw configuration consists of narrow kneading blocks (each kneading block 0.8 cm) for a total length of 48mm as seen in Fig. 4.3.

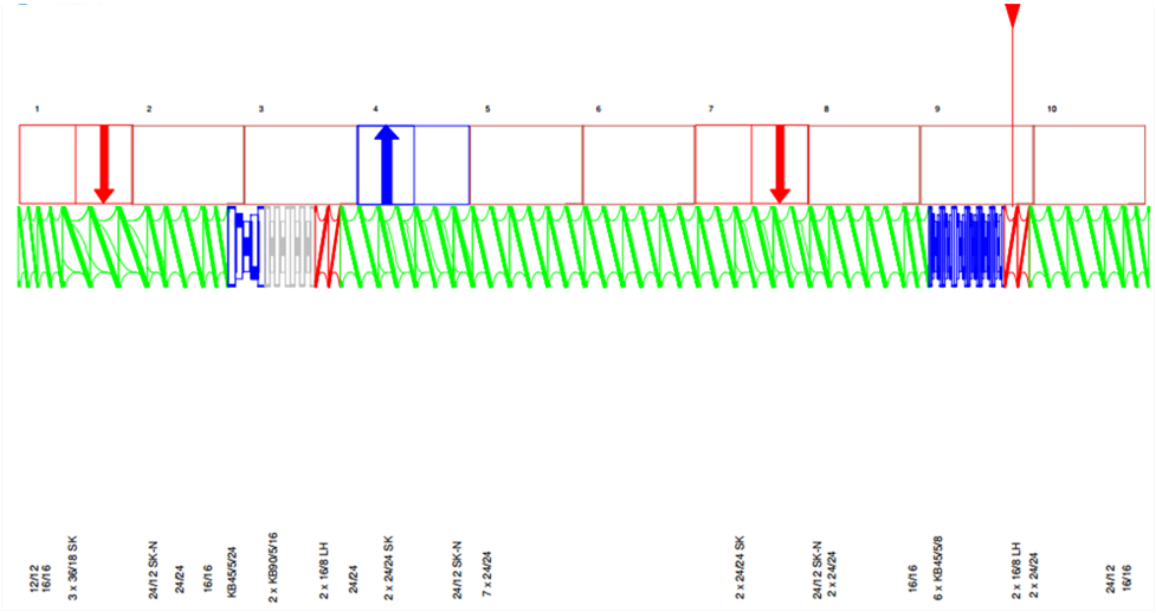


Figure 4.3: Narrow 48 Mixing Section Screw Configuration

#### 4.2.1.4 Wide 48 Mixing Section

The fourth screw configuration used for the 18mm TSE, is similar to the Narrow 48 Mixing Section Screw Geometry, except that the mixing section is replaced with wider kneading blocks (2.4 cm length each) for a total length of 4.8 cm. This screw geometry consists of forward kneading blocks (2.4 cm each, 5 paddles staggered at $45^0$). The mixing section is followed by a left handed conveying screw element to build back pressure, ensuring that the kneading blocks are fully filled.

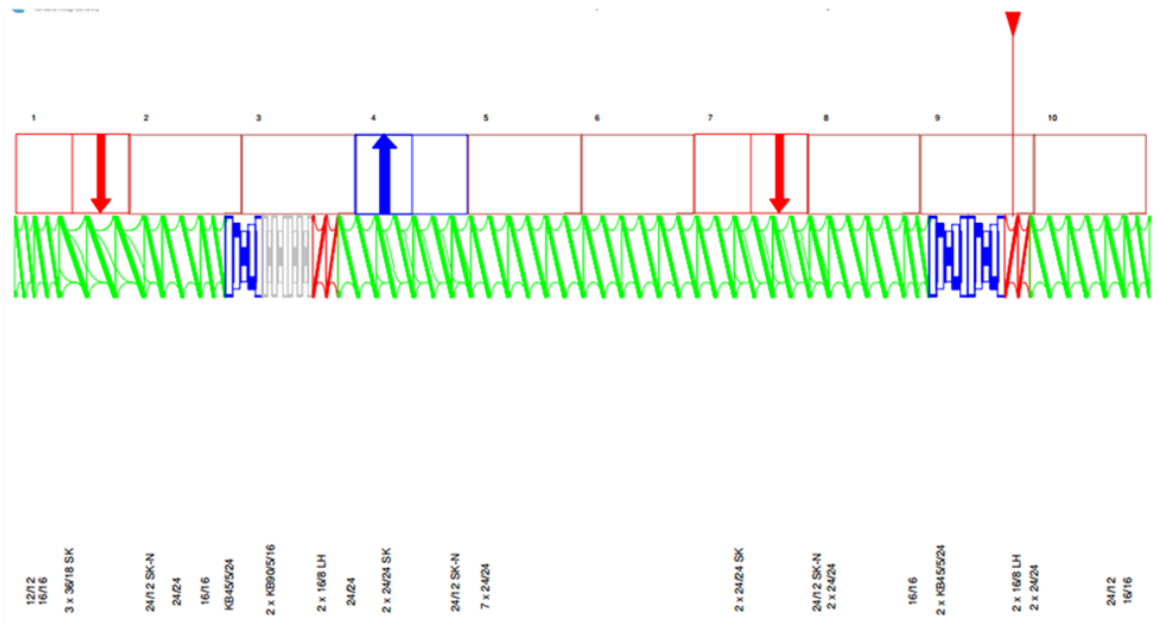


Figure 4.4: Wide 48 Mixing Section Screw Configuration

The 4 screw geometries listed above are used for the ZSK-18mm Twin Screw Extruder. The experiments were conducted in order to understand the impact of changing the mixing section geometry on the RSD results and the computer simulations (Ludovic). The operating conditions used for the 18mm TSE will be discussed later in the chapter after explaining the screw geometry used for the 26mm TSE and 16mm TSE.

### 4.2.2 26mm TSE

The 26mm TSE for this experiment considers two screw geometries. The first screw geometry uses a Narrow Mixing Section screw configuration and the second screw geometry uses a Wide Mixing Section screw configuration.

#### 4.2.2.1 Narrow 72mm Mixing Section


Figure 4.5: Narrow Mixing Section 26mm

Figure 4.5 provides the screw configuration of the 26mm TSE with narrow kneading blocks in the mixing section. The screw configuration seen in Fig 4.5 is input into Ludovic in order to perform the simulations accordingly. The orientation of screw elements is similar to that of 18mm Extruder – 48mm Mixing Section with Narrow Kneading blocks. The melting region consists of a kneading block of length 3.6cm (5 disks staggered at $45^0$) followed by two kneading blocks of length 2.4cm each (10 disks staggered at $90^0$). The kneading blocks are followed by reverse conveying elements (2 left handed screw elements of pitch 2.4cm and length 1.2cm each). The melting section is followed by a series of forward conveying elements of pitch 3.6 cm and length 3.6cm each. The mixing section comprises narrow kneading blocks (kneading blocks to a total length of 7.2 cm, 5 disks each staggered at $45^0$). The kneading blocks are followed by 2 left handed screw elements (axial pitch 2.4cm and length 1.2 cm each).

#### 4.2.2.2 Wide 72mm Mixing Section


Figure 4.6: Wide Mixing Section 26mm

Fig 4.6 discusses the wide mixing section. The screw configuration is similar to the narrow mixing section (Sec 4.2.2.2) except that the mixing section comprises wider kneading block instead of narrow kneading blocks to a length of 7.2cm.

### 4.2.3 16mm TSE

The last equipment considered for this experiment is the 16mm Thermoextruder, used at the Merck facility. A single screw geometry was considered for the 16mm TSE. This screw configuration consists of a series of conveying elements with kneading blocks of varying staggering angles. The melting section was relatively small. The kneading blocks comprise paddles with the same thickness i.e. 0.4 cm. The mixing section began with forward conveying kneading blocks consisting of 5 paddles staggered at $30^0$, followed by 5 more paddles staggered at $60^0$. Reverse conveying kneading blocks consisting of 10 paddles staggered at $90^0$ were used at the end of the mixing section. The stagger angles between the paddles were varied from $30^0$ to $60^0$ to $90^0$ to alter the mixing behavior [24]. The barrel temperatures were varied for the same screw configuration to understand the impact of barrel temperature on the experimental results obtained.

## 4.3 Materials

The thesis focuses on three base polymers which were used to perform the experiments.

### 4.3.1 Low Density Polyethylene (LDPE)

Low Density Polyethylene (LDPE), Petrothene NA 206, which was supplied in pellet form by Equistar Chemicals. LDPE has a density of 0.918 g/cc and melt flow index of 13.5 g/10 min. This grade of polymer is used in blow molding, injection molding, extrusion coating

etc. ZSK-18 TSE was used to process LDPE to obtain the experimental results (RSD and Ludovic Simulations).

### 4.3.2 High Density Polyethylene (HDPE)

High Density Polyethylene (HDPE), Alathon H6018 supplied in pellet form by Equistar Chemicals, Houston, TX [21]. The HDPE has a density of 0.960 /cc and melt flow index of 18.0 g/10 min. The melt temperature of HDPE is $199^0$C. ZSK-18 and ZSK-26 MC TSE were the equipment used to process HDPE to obtain the experimental results required for the thesis.

### 4.3.3 Kollidon VA-64

Kollidon VA-64 is the third base polymer considered for the experiment. It is also referred to as Copovidone. Kollidon VA-64 has a glass transition temperature of $101^0$ C. MK-A, which is an Active Pharmaceutical Index (API) of Merck, was also used along with the base polymer. MK-A has a melting temperature of $180^0$ C. A 72/23/5 weight percentage of Kollidon VA-64, MK-A and a surfactant were used for the experiments [24].

### 4.3.4 CAMES Beads

To perform the RSD experiments, stress beads were dropped into the polymer melt before the mixing section. CAMES (Calibrated Micro Encapsulated Beads) are stress beads with a critical stress limit which, when exceeded causes the beads to rupture and release an encapsulated dye into the polymer melt. The CAMES beads were encapsulated with Red B Disazo dye. The stress beads were dropped into the extruder, before the mixing section and upon reaching the critical stress limit, the beads ruptured releasing the encapsulated dye into the polymer matrix. Prior to dropping the CAMES beads into the polymer matrix,

reference shots were used to serve as a reference point. Reference shots were prepared by dissolving polystyrene pellets into xylene and adding Red B Disazo dye to the mixture [21]. The prepared solution was cooled down and a batch sample equivalent to the total weight of the CAMES beads was removed from the solidified mixture.

The CAMES beads are manufactured by Mach 1 Inc, King of Prussia, PA. The stress history in the twin screw extruders is measured with the help of the CAMES beads, which are designed to rupture, based on their wall thickness and diameter, upon encountering critical stress in the mixing section of the extruder. AUTOMATE Blue 8A, manufactured by Rohm & Haas Co., is the dye used in the CAMES beads. Reference shots, which comprise the same dye used in the CAMES beads, are used to provide RTD, as it represents all the path travelled, a situation similar to when every stress bead is broken (100% break up of CAMES beads). The critical stress limit for the CAMES beads used for the 18mm TSE was 158 ± 21 kPa and 92 ± 14 kPa for the 26mm Coperion TSE.

## 4.4 Operating Conditions

This section discusses the operating conditions chosen to perform the experiment. The operating conditions were chosen based on the capabilities of the extruder. A Central Composite Design (CCD) grid was used to depict the relationship between the operating conditions and the results, due to the non-linear relationship between the operating conditions. The purpose behind using a CCD grid was to visualize the relationship between the operating conditions and the results (both RSD experiment and Ludovic simulation results). Statistical analysis was easier to be performed on the obtained experimental data and it was possible to correlate the results as a function of the operating conditions. This was facilitated using JMP 12.2 Statistical Analysis Software. The important operating

conditions considered for the experiments were the rotational screw speed N (RPM), feed rate Q (g/min) and specific throughput Q/N (mL/rev). The vertical axis for the CCD grid consisted of a range of specific throughput (Q/N) values, while the horizontal axis of the CCD grid consisted of a range of screw speed (N) values. Specific throughput was chosen because it was a key parameter in determining the characteristics of RVD and RRDs. Gao's study [14] on RTD analysis showed that Q/N is an important variable in the extrusion process. For each of the 18mm, 26mm and 16mm TSE, a different set of operating conditions were chosen.

### 4.4.1 18mm TSE

For the 18mm TSE, the same CCD grid was chosen for each of the four screw geometries.

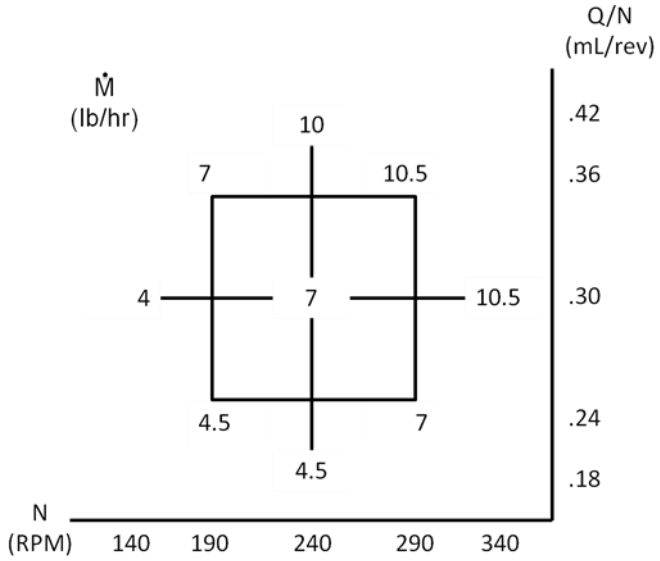


Figure 4.7: Operating Conditions for 18mm TSE

Fig 4.7 reveals the operating conditions for the experiment performed on the 18mm TSE for each of the four screw geometries. The screw speed N ranges from 140 RPM to 340 RPM at an interval of 50 RPM, while the specific throughput Q/N ranges from 0.18 mL/rev

to 0.42 mL/Rev at an interval of 0.06 mL/rev. Along the downward diagonals from left to right, the feed rate is almost constant for each of the three diagonals.

### 4.4.2 26mm TSE

For the 26mm TSE, two sets of operating conditions can be seen in Fig 4.8 and Fig 4.9. The experiment performed on the 26mm extruder was to understand the process of scale-up in extrusion. The two CCD grids correspond to grid points obtained as a result of using Volumetric Scale Up approach and Percent Drag Flow Scale Up approach [Discussed in Chapter 5].

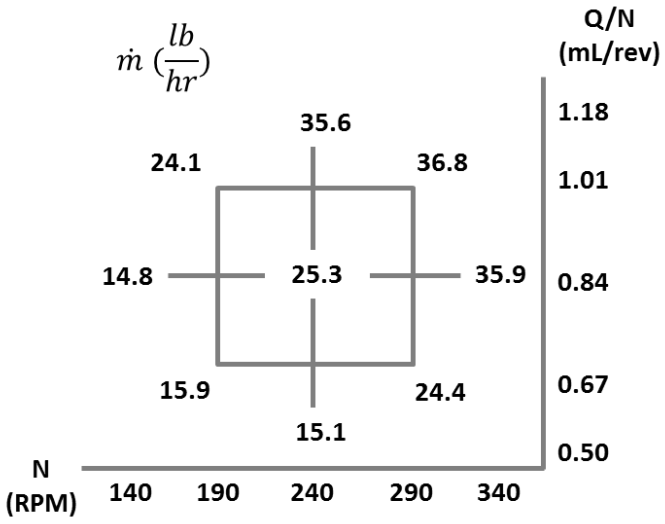


Figure 4.8: Operating Conditions for 26mm TSE (Volumetric Grid)

Fig 4.12 corresponds to the CCD grid used for the 26mm TSE. The screw speed range remains constant to the 18mm TSE, but the specific throughput range changes based on the Volumetric Scale-up method. The specific throughput values range from 0.5 mL/rev to 1.18 mL/rev at an interval of 0.17 mL/rev. Along the downward diagonals from left to right, the feed rate is almost constant as in the case of CCD grid for 18mm TSE.

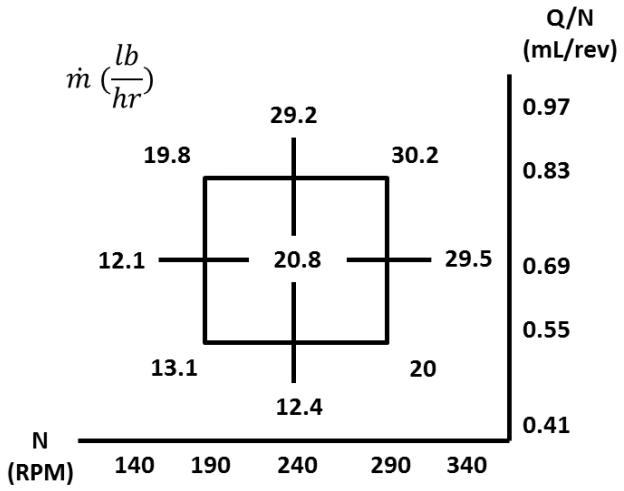


Figure 4.9: Operating Conditions for 26mm TSE (Percent Drag Flow)

Figure 4.13 corresponds to the second set of operating conditions for the 26mm TSE. The screw speed N values are similar to the 18mm TSE, but the specific throughput values (Q/N) vary based on the Percent Drag Flow Scale Up Methodology. The specific throughput values range from 0.41 mL/rev to 0.97 mL/rev at an interval of 0.14 mL/rev. Along the downward diagonals from left to right, the feed rate values remain almost similar along the 3 diagonals. The experimental results obtained from each of the CCD grids used for 26mm TSE is compared to understand the more efficient scale-up method which could be used in large-scale extruders in the industries.

### 4.4.3 16mm TSE

For the 16mm TSE, a single CCD grid with specific operating conditions was used. The screw speed (N) values range from 50 RPM to 250 RPM at an interval of 50 RPM. The specific throughput (Q/N) ranges from 0.1 to 0.5 mL/rev at an interval of 0.1 mL/rev. The feed rate (lb/hr) remains constant along the downward diagonal from left to right for each of the 3 diagonals. The 9 operating conditions seen in Fig 4.10 were used to extrude

Kollidon VA-64 at three different barrel temperatures – $170^0$C, $190^0$C and $220^0$C in order to understand the influence of barrel temperatures on Percent Break-Up and Ludovic results.

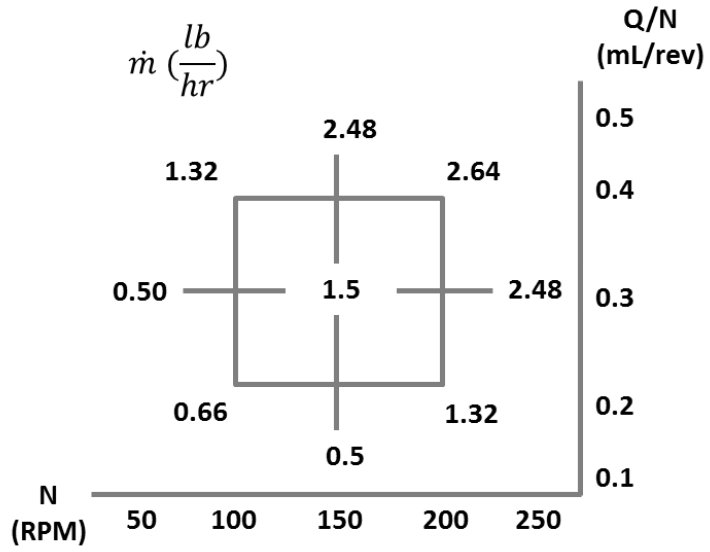


Figure 4.10: Operating Conditions for 16mm TSE

The Percent Break-up results calculated based on RSD Methodology have been explained in detail by Pappas et al [22]**.** The Simulation results obtained from Ludovic for each of the screw geometry and operating conditions discussed above, have been statistically analyzed in order to correlate the obtained results with the operating conditions.

## 4.5 Statistical Analysis

The results that were obtained from the RSD experiment and Ludovic Simulations were statistically analyzed using JMP software. The JMP 12.2 is the statistical software, created by SAS, that has been used to generate predictive equations for each of the below-mentioned results as a function of the operating conditions. The statistically significant parameters ($p<0.05$) on the 95% confidence interval, were used in the predictive equations.

The software was used to determine the best model in order to evaluate and predict trends for the input data. JMP 12.2 was useful in providing a detailed report on the statistical significance of the variables as well as predict an equation correlating the operating conditions with the experimental results.

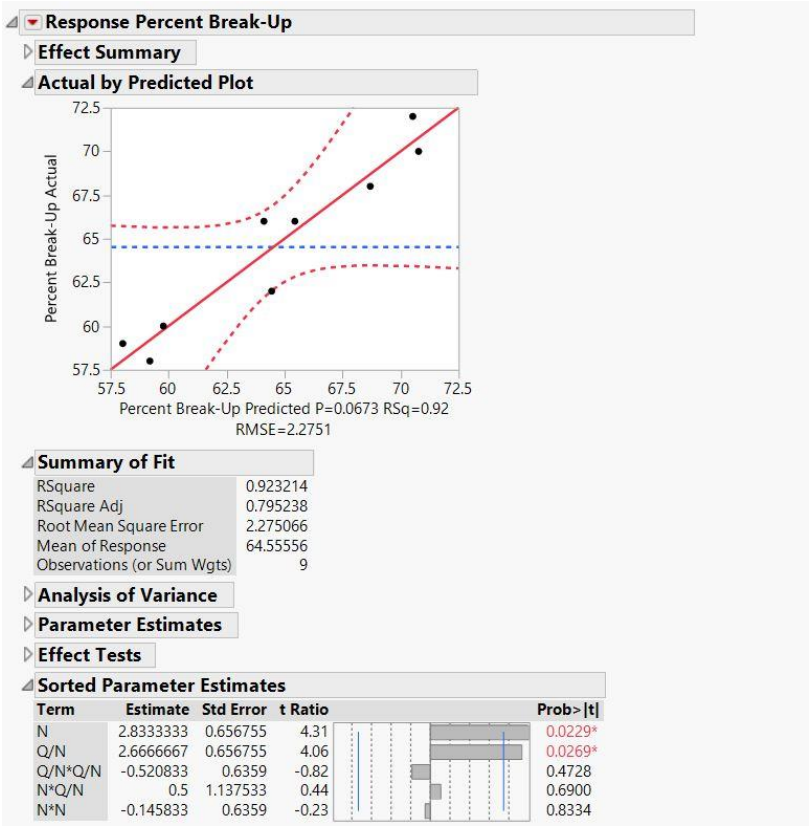


Figure 4.11: Statistical Analysis using JMP 12.2

## 4.6 Computer Simulations Setup

The RSD Methodology experimental setup had been discussed earlier in this chapter. The next phase of the experiment is to use Ludovic to perform simulations for the same operating conditions (discussed in Sec 4.4) that had been used to perform RSD experiments. This section discusses the different steps required to setup the experiment using Ludovic. Ludovic is a 1-Dimensional Twin Screw Simulation (Co-Rotating TSE)

Software developed by Sciences Computer Consultants (Discussed in Chapter 2). Based on the screw design and operating conditions defined by the user, Ludovic performs simulations and generates output. The following section discusses in detail about the process of setting up Ludovic and the results that are generated by the software.

### 4.6.1 Extruder Screw Design

The first phase of the process is to define the screw design that needs to be used to perform simulations. The base diameter of the extruder is specified along with the screw/barrel leakage (mm). The different screw elements from the feed zone to the die are specified. The length of the screw element along with the axial pitch is specified (conveying elements) as well as the staggering angle and number of disks (kneading block). The type of screw elements i.e. forward conveying, reverse conveying, neutral kneading block, forward kneading block, reverse kneading block etc. can be selected based on the required screw design. Fig 4.12 depicts the process of setting up the screw design on Ludovic.

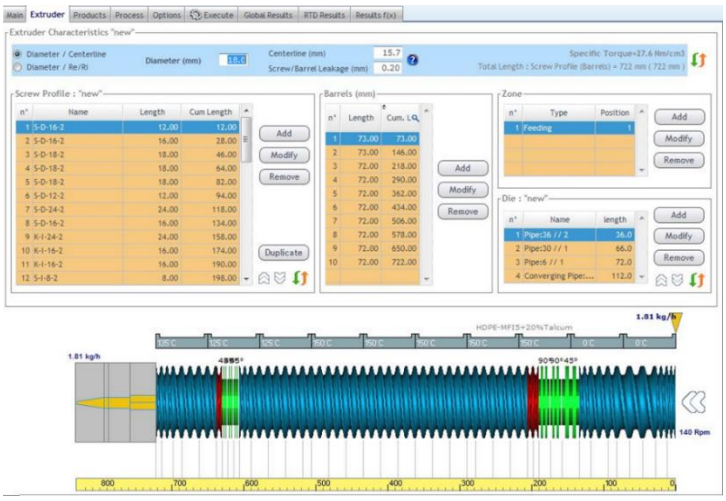


Figure 4.12: Screw Design Setup using Ludovic

The extruder barrels are also setup in this stage, where the total number of barrels and the required length of each barrel are specified. The number of feed inlets can be specified as

different extrusion processes require different feed inlets to add fillers etc. The final step of the screw design process is to define the die design, i.e. the length and shape of the die desired for the final extrudate.

### 4.6.2 Selection of Base Polymer

After configuring the screw design for the extruder, the base polymer must be selected in order to proceed with the subsequent stages of the simulation process. Ludovic offers the flexibility to select the base polymer by either inputting custom values for the thermal characteristics of the polymer melt or by making the selection from the Ludovic library which contains the database for a wide variety of polymers.

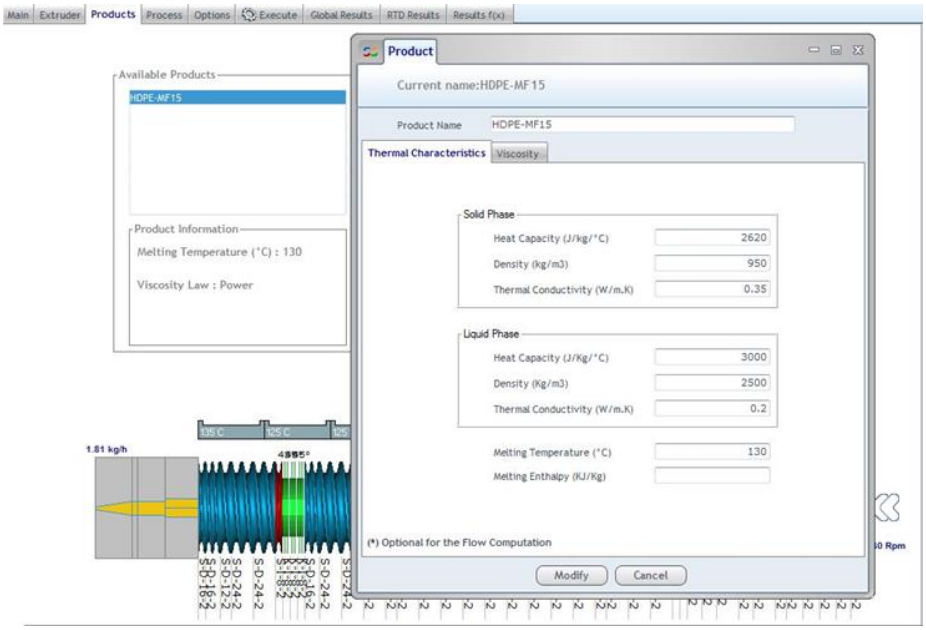


Figure 4.13: Selection of Base Polymer

Fig 4.9 reveals the process of selecting the base polymer to perform the simulation.

### 4.6.3 Specification of Operating Conditions

The final stage of the process required to set up the software to perform simulations is to specify the operating conditions. In this case, the required operating conditions include the rotation speed (RPM), feed rate (Kg/Hr) and the barrel temperature, as seen in Fig 4.14. The thermal exchange coefficients are also specified in order to perform the simulations. The results provided based on the simulations vary depending on the thermal exchange coefficients i.e. at higher values of thermal exchange coefficients, the temperature that the polymer melt would be subjected to in the extruder would be lesser.

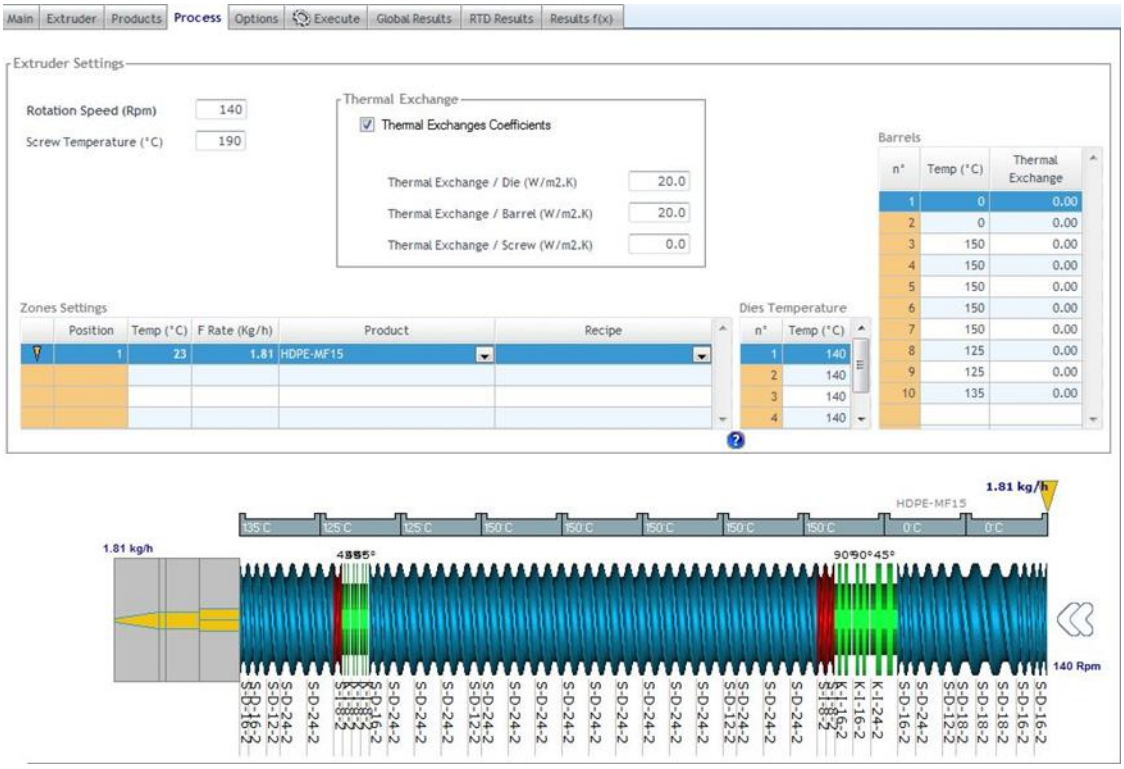


Figure 4.14: Specification of Operating Conditions

The steps mentioned above are required to setup the operating conditions to perform the simulations. These simulations are setup based on the operating conditions that were used to perform the RSD experiments on each of the 18mm, 26mm and 16mm TSE.

# Chapter 5 - Results Analysis

The RSD Methodology was used to generate Percent Break-Up results as a metric to quantify the stress that a polymer melt experiences when processed in a Twin Screw Extruder. To validate the findings of the RSD Methodology, 1-D Computer Simulation software called Ludovic is used. Based on the experimental setup discussed in Chapter 4, this section presents the results obtained from the RSD experiments and the Ludovic Simulations. The results presented in this chapter will be discussed in four sections

- Based on changes to the mixing section screw configuration
- Based on Different Base Polymers
- Based on Scale-Up
- Based on Influence of Barrel Temperature

The RSD experiments generate the Percent Break-Up (%BU) results which will be explained in the form of CCD grids to provide a better understanding of the relationship between %BU and the Operating Conditions.

The output generated from Ludovic Simulations focuses on the thermo-mechanical properties of the polymer melt being extruded. The Ludovic results which we would be discussing in this section include:

- Maximum Shear Rate in the Mixing Section
- Temperature of the Polymer Melt in the Mixing Section
- Viscosity of the Polymer Melt in the Mixing Section
- Shear Stress exerted on the polymer melt in the Mixing Section
- Maximum Pressure in the Mixing Section
- Residence Time in the Mixing Section

- Number of Revolutions taken by polymer melt in the Mixing Section

The results generated using Ludovic will help provide an understanding of the internal behavior within the extruder when run at different operating conditions and different screw configurations. The trends obtained in the percent break-up results obtained via the RSD methodology could be explained based on the Ludovic simulations. The results will be displayed using the CCD grids and the data obtained will be presented in the form of equations correlating the operating conditions and the results, based on statistical analysis using JMP 12.2.

## 5.1 Experimental data and Ludovic Validation of 18mm TSE using LDPE– for different mixing section screw configurations

This section focuses on the experiments performed on the ZSK-18 Twin Screw Extruder, whose operating conditions and screw geometry had been explained in Chapter 4 (Sec 4.2.1). Four different mixing section screw configurations had been discussed in Chapter 4 and the results corresponding to the screw geometries will be discussed in this section. Low Density Polyethylene (LDPE) is the base polymer that was used to perform the experiments on ZSK-18. The results will be presented in the order as shown in the above section.

### 5.1.1 Percent Break-Up Results

The %BU results for each of the four screw geometries can be seen using the four CCD grids, as shown in Figure 5.1-5.2. Each coordinate point shows the average %BU value at that point. The average was taken from 2 to 3 data points at each set of operating conditions.

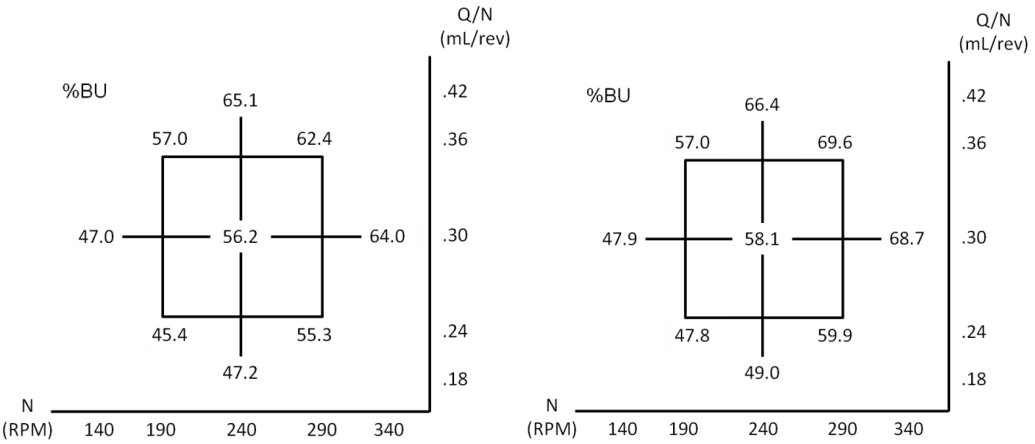


Figure 5.1: Narrow (Left) and Wide (Right) 24mm Mixing Section

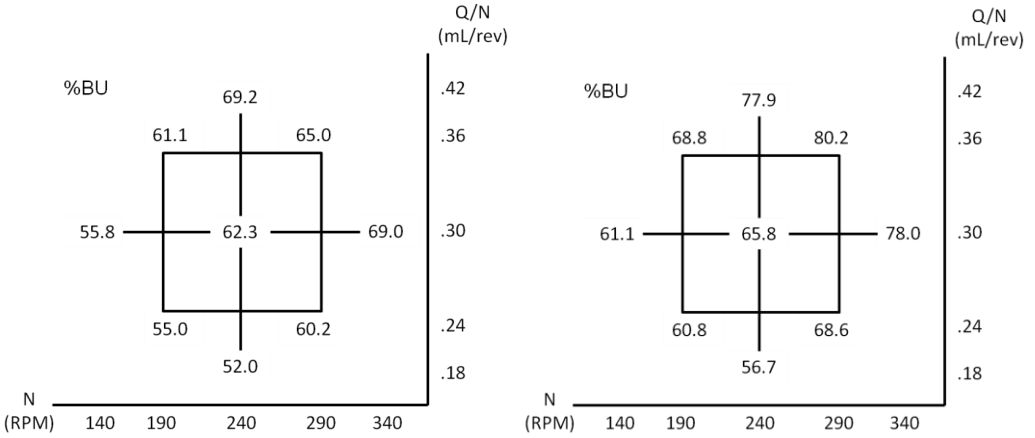


Figure 5.2: Narrow (Left) and Wide (Right) 48mm Mixing Section

The percent break-up results for the 18mm TSE for different screw configurations of the mixing section can be seen from Fig 5.1-5.2. A general trend observed across each of the CCD grids; at a constant screw speed (N), an increase in specific throughput (Q/N) results in an increase in the %BU results. Similarly, at a constant specific throughput (Q/N), an increase in screw speed (N) results in an increase in the %BU results. As the screw configuration of the mixing section changes, the %BU values change implying that mixing section screw configuration is an important parameter in determining the stress experienced by the polymer melt in the mixing section. In Fig 5.1, it can be seen that when narrow kneading blocks are replaced with wide kneading block, the %BU increases. Wider

kneading blocks are better dispersive mixers, and the wider paddles squeeze the polymer melt to a greater extent inducing higher magnitudes of extensional stress; causing the percent break-up to increase. Comparing Fig 5.1 to 5.2, it can be seen that doubling the length of the mixing section increases the percent break-up results to a greater extent. To understand the influence of the operating conditions and screw configuration on the %BU results, the obtained data was input into JMP 12.2 in order to obtain the relationship between %BU and the operating conditions.

Table 5.1: Predictive Equation Coefficients for %BU

| Screw Geometry (18mm) | COEFFICIENTS | | |
|---|---|---|---|
| | Intercept | $X_N$ | $X_{Q/N}$ |
| Narrow 24 Mixing Section | 55.3 | 4.11 | 4.54 |
| Wide 24 Mixing Section | 58.5 | 5.53 | 4.48 |
| Narrow 48 Mixing Section | 61.1 | 2.95 | 3.86 |
| Wide 48 Mixing Section | 68.0 | 4.42 | 5.18 |

Table 5.1 reveals the intercept value of %BU and the corresponding coefficients for screw speed (N) and specific throughput (Q/N) for the four different screw geometries. The intercept value is an average of the %BU values obtained across the 9 grid points on the CCD grid. From Table 1, it can be seen that the average %BU value increases as the narrow kneading blocks are replaced by the wider kneading blocks. Similarly, when the length of mixing section is doubled (from 24mm to 48mm), the intercept values increase to a greater extent. Interestingly when the narrow screw configurations are considered, the screw speed seems to have a lesser influence on %BU compared to specific throughput, while in the case of wider screw configurations, %BU seems to be more dependent on the screw speed compared to the specific throughput. Similarly, the coefficients of N and Q/N for the wider

geometry seems to be larger compared to the narrow screw geometry, which implies that a change in the operating conditions would have a greater change in the %BU values.

**Ludovic Results**

### 5.1.2 Maximum Shear Rate in the Mixing Section

The maximum shear rate that the polymer melt is being subjected to, is simulated by Ludovic. Each of the CCD grid points in Fig 5.5-5.8 represents the maximum value of shear rate ($s^{-1}$). The shear rate values for each corresponding screw geometry can be seen in the following figures.

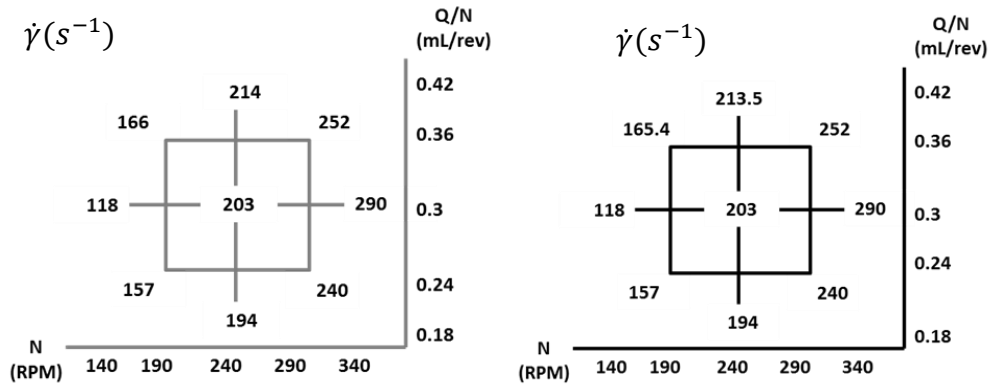


Figure 5.3: Narrow (Left) and Wide (Right) 24mm Mixing Section

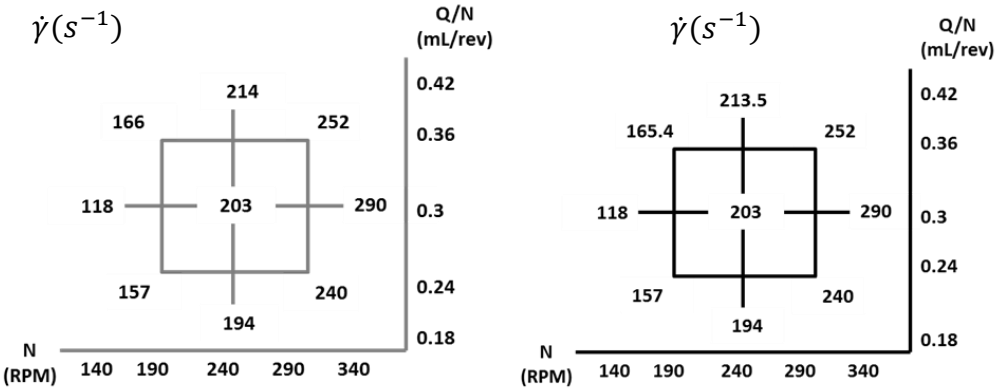


Figure 5.4: Narrow (Left) and Wide (Right) 48mm Mixing Section

Fig 5.3-5.4 displays the maximum shear rate attained by the polymer melt in the mixing section. Across all the 4 CCD grids, a general trend has been observed: at constant Q/N, shear rate increases with screw speed (N). Similarly, at constant N, shear rate increases slightly as specific throughput (Q/N) increases. Interestingly, across each of the 4 screw geometries from Fig 5.3-5.4, the maximum shear rate values are almost identical for each corresponding CCD grid point, implying that change in screw configuration in the mixing section for a particular extruder base diameter (18mm in this case), does not impact the maximum shear rate that a polymer melt is being subjected to. However, each of the values represented in the CCD grid represents the maximum shear rate and based on the graph plotted using Ludovic simulation data (Fig 5.5), it can be seen that the maximum shear rate is subjected for a longer length of the mixing section in a wide kneading block compared to a narrow kneading block; this implies that despite having identical maximum shear rate values the wider kneading block subjects the polymer melt to the higher shear rate for a longer duration compared to the narrow kneading block. Similarly, upon doubling the length of the mixing section, the maximum shear rate is being subjected to a longer length of the kneading block compared to 24mm long mixing section. Statistical analysis of the Ludovic results on JMP displays the following results:

Table 5.1: Predictive Coefficient equations for shear rate

| Screw Geometry (18mm) | COEFFICIENTS | | |
|---|---|---|---|
| | Intercept | $X_N$ | $X_{Q/N}$ |
| Narrow 24 | 203.22 | 42.75 | 5.1 |
| Wide 24 | 203.1 | 42.8 | 4.95 |
| Narrow 48 | 203.22 | 42.75 | 5.1 |
| Wide 48 | 203.1 | 42.8 | 4.95 |

Based on JMP analysis, it can be seen that the intercept value for maximum shear rate across all the 9 CCD grid points for each of the 4 screw geometries remains almost identical. The coefficient values suggest that screw speed is the dominating term that influences the shear rate compared to specific throughput. Fig 5.5 shows a comparison between Narrow 48 and Narrow 24 mixing section shear rate values that had been plotted based on the Ludovic Simulations. The graph has been plotted from feeder (right) to die (left) along the length of the twin screw extruder.

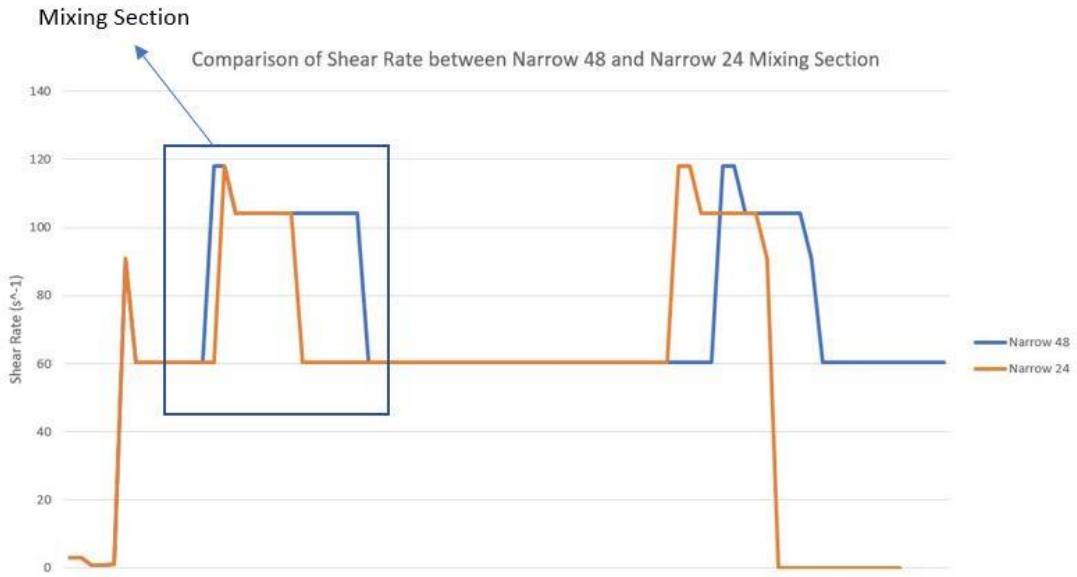


Figure 5.5: Comparison of shear rate between Narrow 24 and Narrow 48

### 5.1.3 Maximum Temperature in the Mixing Section

The temperature that the polymer melt is subjected to in the mixing section is a critical parameter in determining the polymer melt viscosity, shear stress and the residence time. Ludovic Software was used to calibrate the highest temperature reached in the mixing section for each coordinate point on the CCD grid, for every screw geometry.

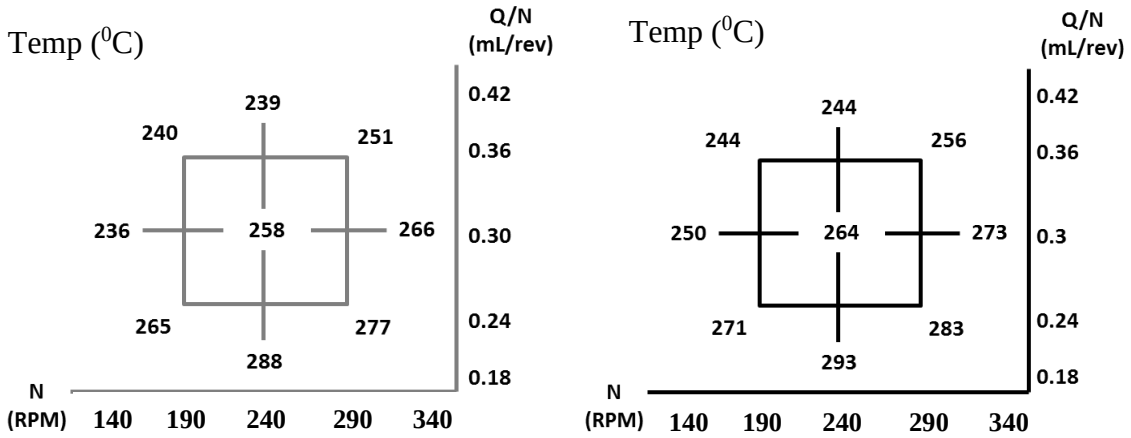


Figure 5.6: Narrow (Left) and Wide (Right) 24mm Mixing Section

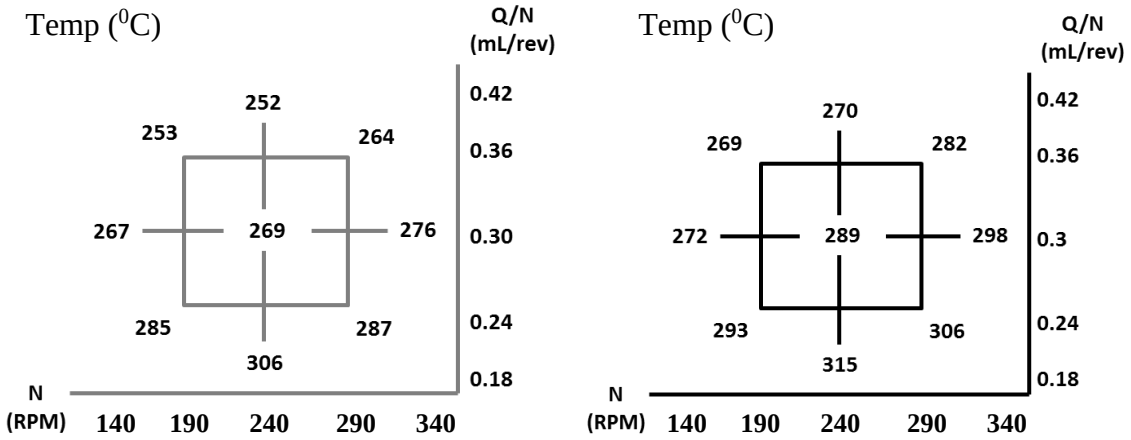


Figure 5.7: Narrow (Left) and Wide (Right) 48mm Mixing Section

Fig 5.6-5.7 show the maximum temperature in the mixing section for every corresponding point on the CCD grid for the 4 screw geometries. From the Figure, it can be seen that at a constant (Q/N), the temperature increases with increase in screw speed. This is due to the fact that higher shear rate leads to more viscous dissipation heating. The torque supplied to rotate the screw becomes heat, which is induced into the polymer melt causing an increase in the temperature of the polymer melt. At constant N, when the (Q/N) is increased, the temperature decreases. An increase in Q/N at a constant screw speed implies that the mass flow increases and the amount of heat conducted through an increased mass flow is less;

thereby causing a decrease in the temperature of the polymer melt. When the narrow KBs are replaced by wider KBs, the temperature of the polymer melt is seen to increase; this is due to the fact that wider kneading blocks generate higher cumulative shear on the polymer melt and the heat transfer coefficient is lower compared to narrow kneading blocks. When the length of mixing section is doubled from 24mm to 48mm, the temperature in the mixing section increases by an average of about 10%. The polymer melt is being subjected to a higher shear in the 48mm Mixing Section compared to the 24mm Mixing Section as seen in Maximum Shear Rate results.

In order to get a better understanding of the influence of the operating conditions on the temperature of the polymer melt in the mixing section, the results obtained from Ludovic were input into JMP software.

Table 5.3: Predictive Coefficient Equations for Temperature

| Screw Geometry (18mm) | COEFFICIENTS | | |
|---|---|---|---|
| | Intercept | $X_N$ | $X_{Q/N}$ |
| Narrow 24 | 258.5 | 6.91 | -12.41 |
| Wide 24 | 263.1 | 5.83 | -12.67 |
| Narrow 48 | 269.1 | 2.58 | -13.58 |
| Wide 48 | 287.7 | 6.5 | -11.5 |

From Table 5.3, the predictive equation coefficient for the different screw geometries can be seen. As with RSD and %BU, the only two predominant parameters are screw speed

(N) and specific Throughput (Q/N)! The intercept value for temperature increases as narrow kneading blocks in the mixing section are replaced by wider kneading blocks; the temperature of the polymer melt increases as the length of mixing section is doubled. Screw speed has a positive coefficient value which implies that temperature of the polymer melt increases with screw speed. Specific throughput has a negative coefficient value which implies that temperature of the polymer melt decreases with increase in Q/N. Based on the coefficient values for each of the screw configuration, Q/N has a higher impact on the temperature of polymer melt compared to N.

### 5.1.4 Viscosity in the Mixing Section

Viscosity of the polymer melt is an important characteristic that determines the stress, residence time and other extrusion parameters. Ludovic simulates the viscosity of the polymer melt over the entire length of the extruder channel. The focus is on the mixing section of the TSE; the viscosity of the polymer melt at the maximum shear rate is taken into account for the results displayed below. The viscosity values provided in the CCD grids below are in units of Pa-s.

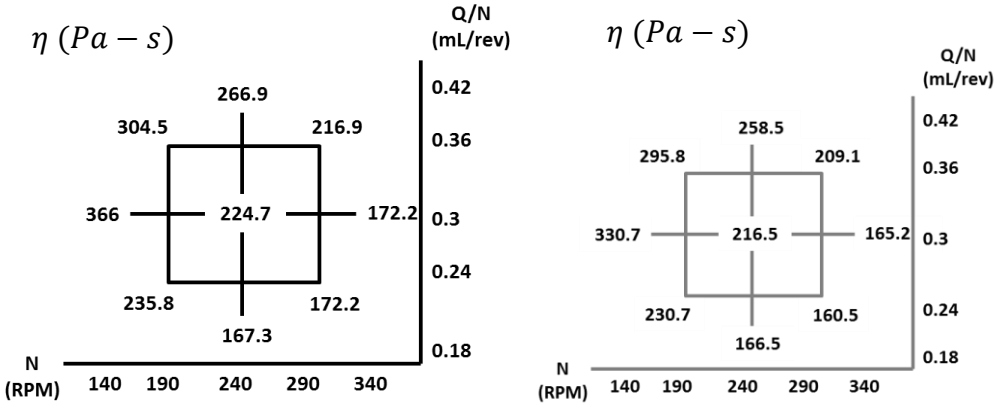


Figure 5.8: Viscosity in the Mixing Section 24mm Narrow - Left and Wide – Right

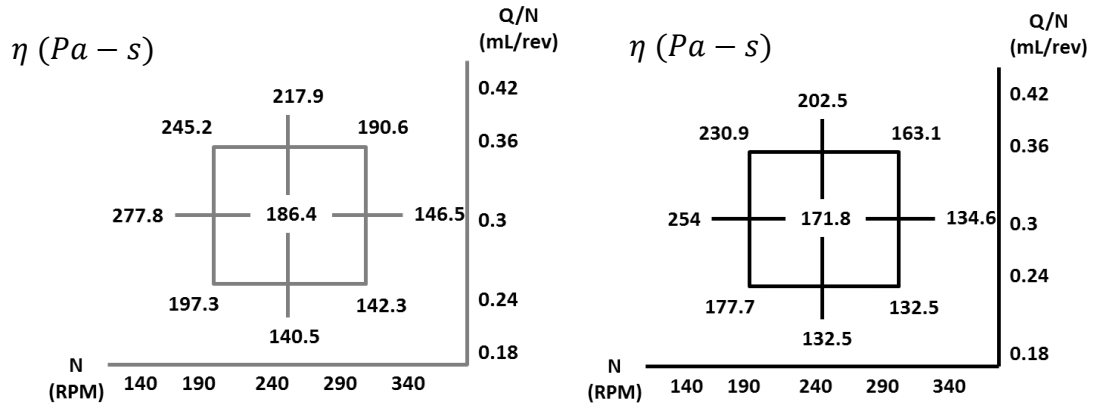


Figure 5.9: Viscosity in the Mixing Section 48mm Narrow - Left and Wide – Right

Fig 5.8 and Fig 5.9 compare the viscosity of the polymer melt in the mixing section when the screw configuration of the mixing section is changed. CCD grids comprising the 9 grid points for each of the screw geometry can be seen in Fig 5.8 and 5.9. A general trend observed across each of the CCD grids; at constant Q/N, the viscosity decreases with increase in screw speed, which can be explained by the behavior of temperature and shear rate values that were explained in the previous section. An increase in screw speed leads to an increase in shear rate and temperature of the polymer melt, which leads to a decrease in the viscosity values. Eq. 9 and Eq. 10 from Chapter 3, explain the relationship between shear rate, viscosity and temperature based on the power law model. The theory behind computer simulations for polymer flows has been explained in Chapter 3. At constant N, the viscosity increases with specific throughput (Q/N), because temperature decreases when mass flow increases at a constant screw speed. Despite the slight increase in shear rate, the reduction of temperature leads to an overall reduction in the viscosity values. As the feed increases at a constant screw speed, there is higher restriction towards the flow of molten polymer due to higher viscosity. As the narrow kneading blocks are replaced by wider kneading blocks, the viscosity of the polymer melt at the corresponding CCD grid points decreases. Similarly, when the length of the mixing section is doubled, the viscosity

of the polymer melt decreases as the polymer melt is subjected to more shear and higher temperature. The influence of the operating conditions on the viscosity of the polymer melt has been analyzed using JMP, the results of which can be seen below in Table 4.

Table 5.4: Predictive Equation Coefficient for Viscosity

| Screw Geometry (18mm) | COEFFICIENTS | | |
|---|---|---|---|
| | Intercept | $X_N$ | $X_{Q/N}$ |
| Narrow 24 | 223.3 | -44.9 | 26.1 |
| Wide 24 | 217.1 | -40.7 | 24.8 |
| Narrow 48 | 188.9 | -31 | 20.9 |
| Wide 48 | 171.5 | -29.31 | 18.65 |

Table 5.4 shows that screw speed is a dominant factor in influencing the viscosity of the polymer melt compared to the specific throughput. Within the 24mm mixing section, as the narrow kneading blocks are replaced by wide kneading blocks, the intercept value of viscosity decreases; the coefficient of N and Q/N decrease as well. The influence of the operating conditions on viscosity of the polymer melt decreases as the length of the mixing section is doubled. The coefficient of screw speed (N) is higher compared to specific throughput, which implies that screw speed has a greater influence on the viscosity values compared to the specific throughput. The narrow screw geometry seems to be having a higher N coefficient relative to the wide screw geometry; similarly, there is a small magnitude of change in the coefficient values for specific throughput when switching from the narrow to the wide screw geometry. In the case of the longer mixing section, the magnitude of changes in the viscosity on switching from narrow to wide would be lesser as the difference in the coefficient values for both N and Q/N seems to be small.

### 5.1.5 Shear Stress in the Mixing Section

Shear Stress values are vital in understanding the percent break-up behavior exhibited by the different screw configurations of TSE. Based on the shear rate and the viscosity values provided by Ludovic, shear stress values have been calculated using Eq. 30

$$\tau = \eta\dot{\gamma} \tag{5.1}$$

The shear stress values have been calculated in kPa and can be seen in the CCD grids corresponding to each screw geometry for the 18mm TSE.

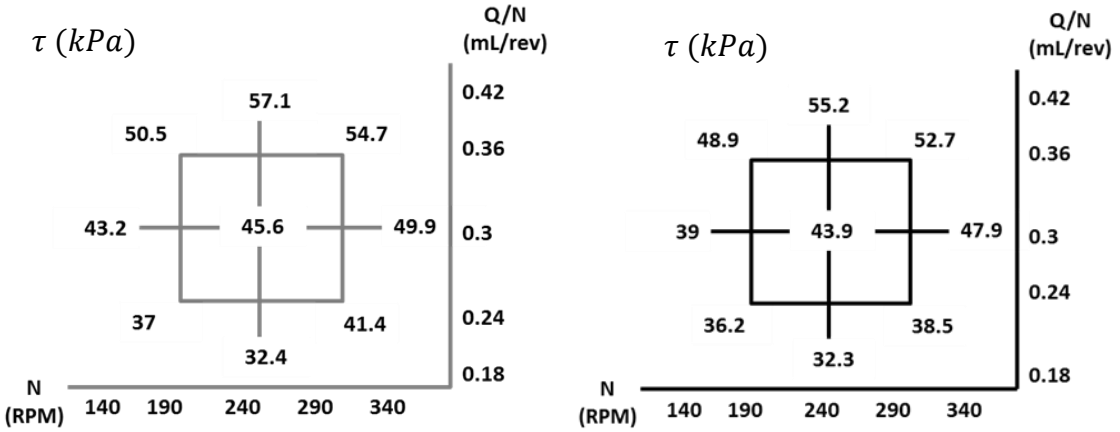


Figure 5.10: Shear Stress in the Mixing Section - 24mm Narrow - Left and 24mm Wide - Right

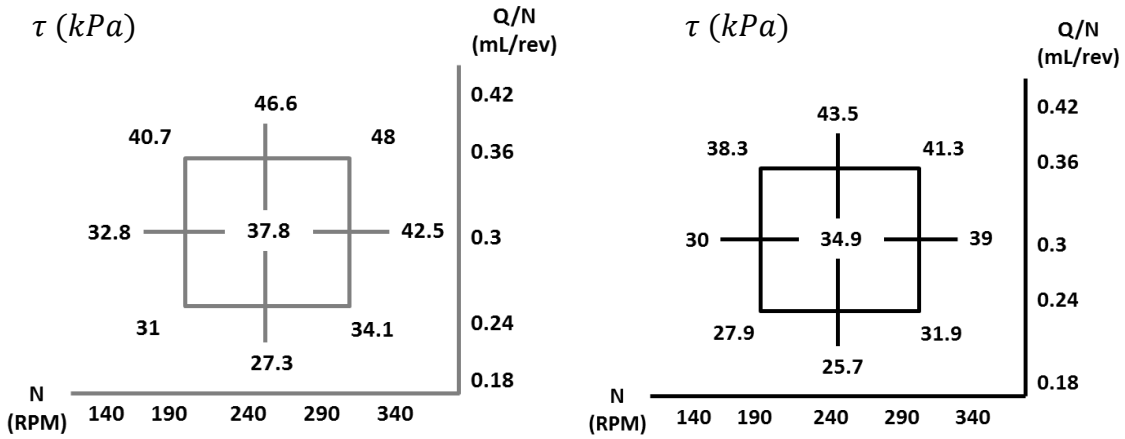


Figure 5.11: Shear Stress in the Mixing Section 48mm Narrow - Left and Wide – Right

Fig 5.10 and 5.11 reveals the data on the shear stress values calculated using Ludovic results for the 4 different screw configurations of the mixing section. A general trend

observed across each of the 4 CCD grids is that shear stress increases with increase in screw speed (N) at a constant specific throughput (Q/N). Similarly, the shear stress increases with specific throughput (Q/N) as the screw speed (N) is kept constant. However, the shear stress values across each of the 9 CCD grid points decreases as the narrow kneading blocks are replaced by the wide kneading blocks. Similarly, the shear stress values are seen to be on the decreasing trend as the length of the mixing section is doubled. This observation is not consistent with the %BU trends (Sec 5.1.1), although for a particular screw geometry the trends in shear stress values seem to align with the %BU trends. This calls for the fact that shear stress is not the only contributor towards the percent break-up of the CAMES beads in the RSD experiments as the magnitude of shear stress is lesser to cause significant rupture of the beads.

The shear stress values obtained based on the performed calculations were statistically analyzed using JMP 12.2 in order to understand the influence of the operating conditions on the shear stress values.

Table 5.5: Predictive Coefficients for Shear Stress

| Screw Geometry (18mm) | COEFFICIENTS | | |
|---|---|---|---|
| | Intercept | $X_N$ | $X_{Q/N}$ |
| Narrow 24 | 45.84 | 1.83 | 6.35 |
| Wide 24 | 44.2 | 1.99 | 6.05 |
| Narrow 48 | 38.6 | 2.48 | 5.18 |
| Wide 48 | 35 | 2.08 | 4.61 |

Table 5.5 reveals the intercept values as well as the coefficients of the operating conditions (N, Q/N) to understand the influence of operating conditions on shear stress. The intercept values of shear stress decrease as the narrow kneading blocks in the mixing section are replaced by wide kneading blocks as well as when the length of the mixing section is

doubled. Based on the coefficient values determined from the data, specific throughput (Q/N) has a higher influence on shear stress compared to screw speed (N). As the narrow kneading block is replaced by the wider kneading block, the coefficient of N increases while the coefficient of Q/N decreases. Similarly, when the length of the mixing section is doubled, the coefficient on N increases further while the coefficient of Q/N reduces in magnitude implying that the change in Q/N will have a lesser impact on the shear stress values compared to the change in N values.

### 5.1.6 Maximum Pressure generated in the Mixing Section

The pressure generated in the mixing section is computed by Ludovic based on the model equations (Eq. 7) relating drag flow and pressure flow. The pressure flow is generated due to the back flow of a reverse conveying screw element as the polymer is conveyed forward by the forward conveying screw elements purely based on drag. Pressure can be used as a metric to understand the degree of fill [9]; at regions of higher pressure, the degree of fill is higher because when a screw channel is fully filled, the material can be pushed forward when the pressure gradient is higher. For each of the 4 screw configurations, the maximum pressure recorded in the mixing section can be seen in the CCD grids displayed below.

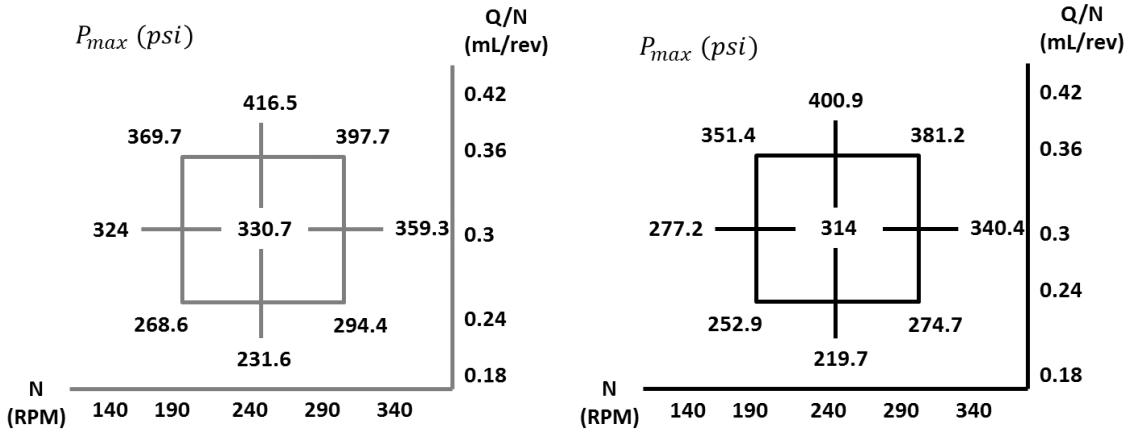


Figure 5.12: Maximum Pressure in the Mixing Section 24mm Narrow - Left and Wide - Right

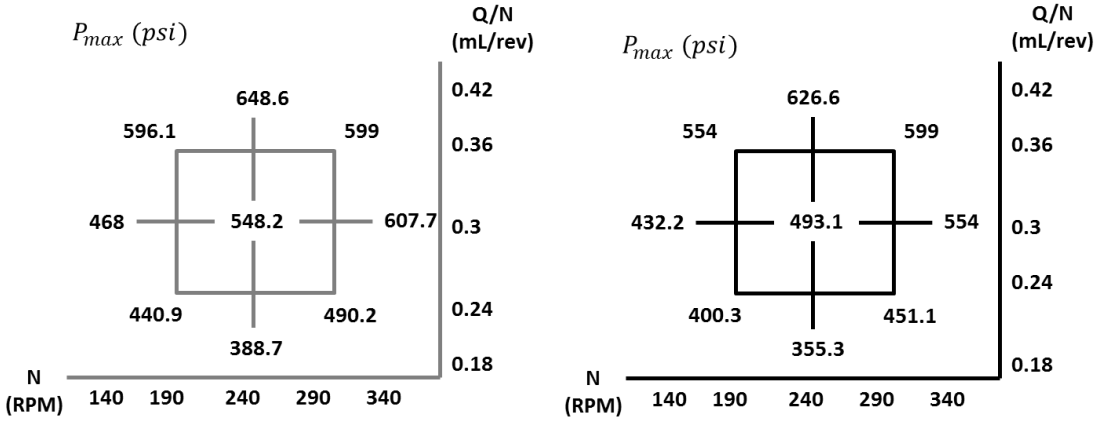


Figure 5.13: Maximum Pressure in the Mixing Section 48mm Narrow - Left and Wide – Right

Fig 5.12 and Fig 5.13 reveal the maximum pressure generated in the mixing section for the four screw configurations. A general trend observed across all the 4 CCD grids; at constant Q/N, the pressure in the mixing section increases with screw speed. Similarly, at constant N, the pressure in the mixing section increases with Q/N. This trend could be explained using the classical drag flow equation:

$$Q_c = K_d N - \frac{K_p \Delta P}{\eta L_f} \quad (5.2)$$

Where, N is the screw speed (RPM), $\frac{\Delta P}{L}$ is the pressure gradient, η is the viscosity of the polymer melt.

Eq. 5.2 is the abbreviated form of the actual drag flow equation, where only the dimensions that change with operating conditions are taken into account and the rest of the terms belonging to the equation are considered as a constant $K_d$ and $K_p$. Eq.5.2 is the equation for a forward conveying screw element and since the focus is on the mixing section, the equation has been written for a reverse conveying element as per Eq. 5.3.

$$Q_c = -K_d N + \frac{K_p \Delta P}{\mu L_r} \quad (5.3)$$

In case of the reverse conveying element, the flow is in the upstream direction and the sign conventions are changed from Eq. 5.2. As per Eq. 5.3, when specific throughput (Q/N) is increased at constant N, which implies Q increases when N is kept constant, the viscosity also increases as seen from previous section. Since a reverse element is fully filled, $L_r$ is always a constant for all the operating conditions. In order to accommodate the increase in viscosity, the pressure term increases which explains the results mathematically. At constant Q/N, when N increases, implies that Q and N increase at a constant ratio. In this case, the viscosity of the polymer melt decreases as discussed in the previous section. In order to accommodate this change, the pressure term increases slightly. To understand the influence of the operating conditions on pressure generated in the mixing section, the results were statistically analyzed using JMP.

Table 5.6: Prediction of Coefficients of Pressure in the Mixing Section

| Screw Geometry (18mm) | COEFFICIENTS | | |
|---|---|---|---|
| | Intercept | $X_N$ | $X_{Q/N}$ |
| Narrow 24 | 331.4 | 10.3 | 47.8 |
| Wide 24 | 316.9 | 14.8 | 47.2 |
| Narrow 48 | 542.3 | 27.6 | 65.3 |
| Wide 48 | 500.6 | 28.3 | 70.2 |

Table 5.6 reveals the intercept and coefficient values for the operating conditions post statistical analysis. As seen in the CCD grids from Fig 5.12 and 5.13, the intercept values of the pressure generated in the mixing section decrease as the narrow kneading blocks in the mixing section are replaced by wide kneading blocks. However, as the length of mixing section is doubled, intercept values of pressure increase to a greater extent, implying that the longer the duration that the polymer melt experiences in the extruder, the more pressure it is being subjected to. Secondly, specific throughput is the more significant operating condition that influences the pressure in the mixing section to a greater extent compared to the screw speed. As the narrow kneading blocks are replaced by the wide kneading blocks, the coefficient of N increases for both the 24mm as well as 48mm long mixing section. However, the coefficient of Q/N decreases slightly for the 24mm mixing section but increases for the 48mm mixing section, as the narrow kneading blocks are replaced by the wide kneading blocks.

### 5.1.7 Residence Time in Mixing Section

Residence Time is the amount of time that a polymer spends in the extruder, before exiting the die. It is an extremely important parameter to understand the mixing behavior of the twin screw extruder. Using Ludovic, Residence time was computed for each of the 4 screw geometries for the 18mm TSE. Fig 5.14 and Fig 5.15 show the residence time values computed for each of the 9 CCD grid points for each screw configuration. The Residence time values in the mixing section were computed in order to understand the behavior of the mixing section of the TSE as the screw configuration is changed.

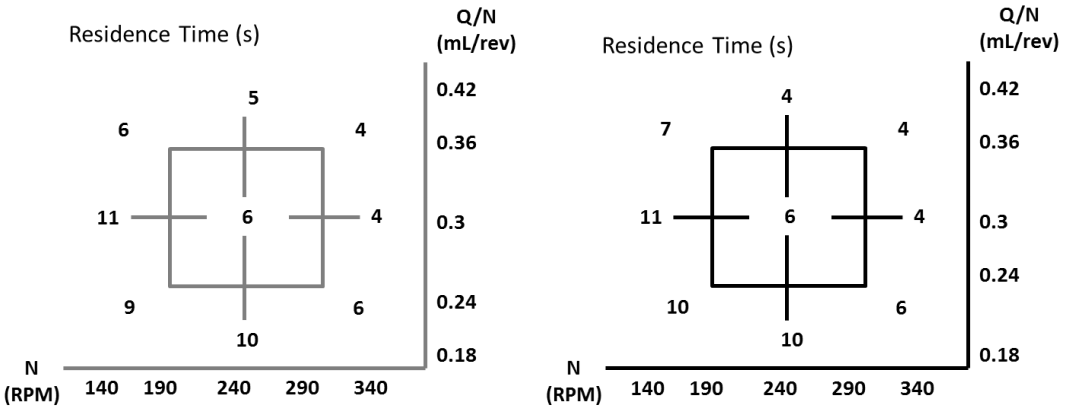


Figure 5.14: Residence Time in the Mixing Section 24mm Narrow - Left and Wide – Right

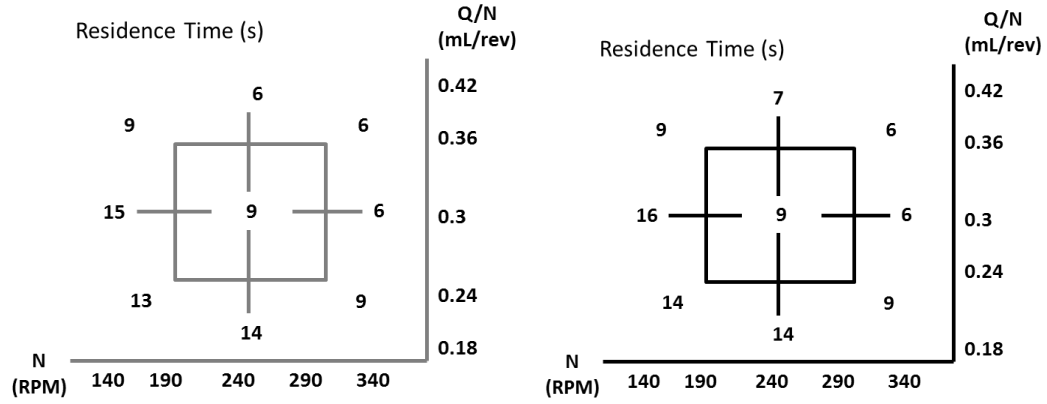


Figure 5.15: Maximum Pressure in the Mixing Section 48mm Narrow - Left and Wide – Right

Fig 5.14 and 5.15 display the residence time values obtained in the mixing section of the TSE. A general trend observed across all the screw configurations; at constant Q/N, when the screw speed increases the residence time decreases. Similarly, at constant N, when the specific throughout is increased, the residence time decreases as well. This implies that the residence time decreases when either the feed rate increases or when the screw is rotated at a higher RPM, as material is conveyed quickly through the length of the extruder channel. Along the lower diagonals from left to right, it can be seen that residence time is a constant. From Chapter 4, in the section that discusses the operating conditions chosen for the experiments, it was stated that the mass flow rate (Q) was kept almost constant

along the lower diagonals from left to right. This could imply that when Q is kept a constant, the residence time in the mixing section remains constant. To have a better understanding of the influence of operating conditions on the residence time, the data was statistically analyzed using JMP.

Table 5.7: Prediction of Coefficients of Residence Time in the Mixing Section

| Screw Geometry (18mm) | COEFFICIENTS | | |
|---|---|---|---|
| | Intercept | $X_N$ | $X_{Q/N}$ |
| Narrow 24 | 5.5 | -1.6 | -1.25 |
| Wide 24 | 6.1 | -1.75 | -1.42 |
| Narrow 48 | 8.7 | -2.1 | -1.92 |
| Wide 48 | 8.7 | -2.3 | -1.85 |

Based on Table 5.7, it can be seen that intercept values for residence time in the mixing section, increases as the narrow kneading block in the mixing section is replaced by wide kneading block. Similarly, as the 24mm mixing section is replaced by a 48mm long mixing section, the residence time in the mixing section increases to a greater extent. The negative value of the coefficients of operating conditions imply that when the magnitude of operating conditions increase, the residence time in the mixing section decreases. The influence of the operating conditions on residence time increases as the narrow kneading blocks in the mixing section is replaced with wide kneading blocks as well as when the length of the mixing section is doubled.

### 5.1.8 Maximum Number of Revolutions in the Mixing Section

The final result that will be discussed in this section is regarding the number of revolutions that the polymer melt takes as it moves from the mixing section towards the die. The

number of revolutions in the mixing section is calculated based on the Ludovic results simulated for residence time in the mixing section as per Eq. 5.4.

$$Rev_{mix} = t_{mix}N \tag{5.4}$$

Where, $Rev_{mix}$ is the number of revolutions in the mixing section, $t_{mix}$ is the residence time in the mixing section and N is the screw speed (RPM)

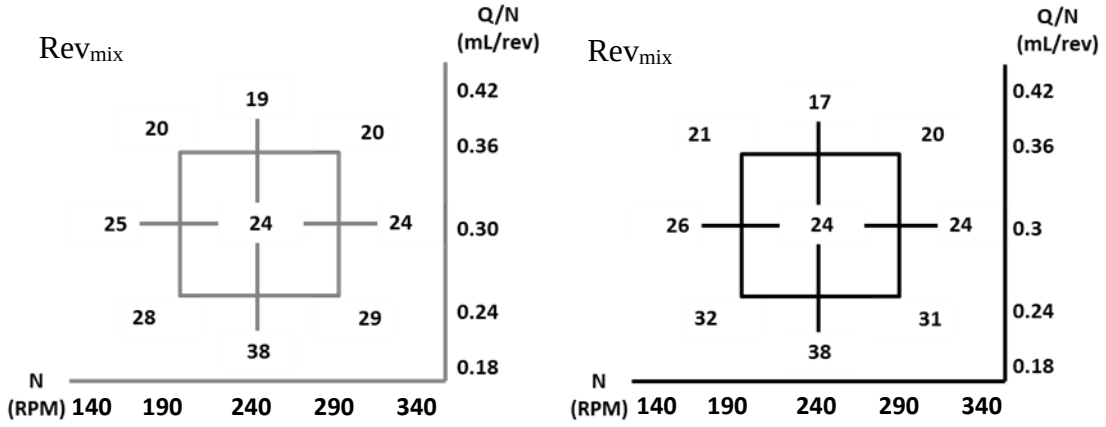


Figure 5.16: Number of Revolutions in 24mm Mixing Section Narrow- Left and Wide - Right

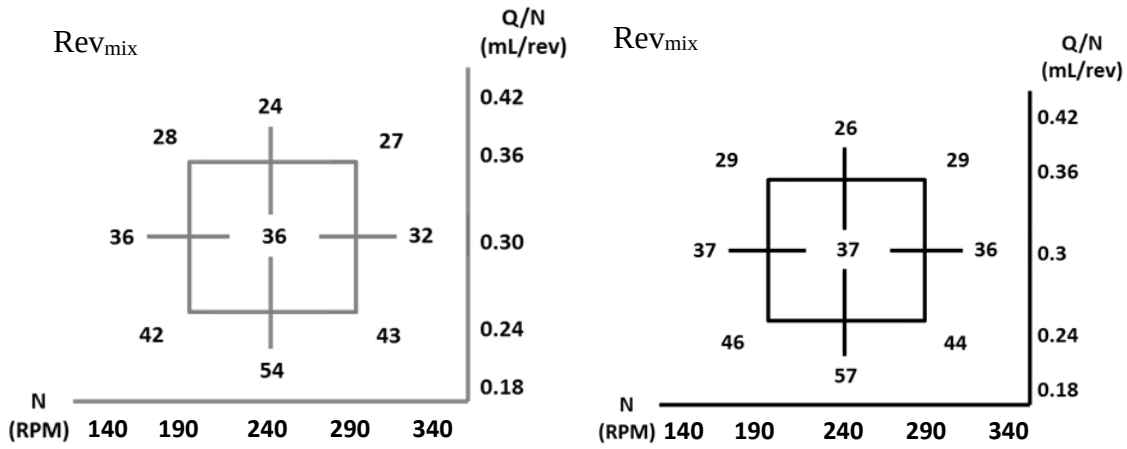


Figure 5.17: Number of Revolutions in 48mm Mixing Section Narrow - Left and Wide – Right

Fig 5.16 and Fig 5.17 reveal the data on the number of revolutions in the mixing section across the 4 screw geometries used for the 18mm TSE. A general trend observed across all the 4 CCD grids; at constant Q/N as screw speed increases the number of revolutions in

the mixing section almost remains constant. Similarly, at constant N, when the specific throughput increases, the number of revolutions in the mixing section decreases. This implies that number of revolutions in the mixing section are dependent on the specific throughput which confirms the assumption made for RRD (Sec 1.7) which implies that at a constant specific throughput, the polymer melt follows the same path along the extruder channel. When the narrow kneading blocks in the mixing section are replaced by the wide kneading blocks, the number of revolutions in the mixing section increase slightly. Similarly, when the length of the mixing section is doubled, the number of revolutions taken by the polymer melt to travel along the mixing section also increases. In order to understand the influence of the operating conditions on the number of revolutions in the mixing section, the data was statistically analyzed using JMP.

Table 5.8: Prediction of coefficients for the number of revolutions in the mixing section

| Screw Geometry (18mm) | COEFFICIENTS | | |
|---|---|---|---|
| | Intercept | $X_N$ | $X_{Q/N}$ |
| Narrow 24 | 23.11 | - 0.08 (NS) | - 4.58 |
| Wide 24 | 24.8 | - 0.5 (NS) | - 5.33 |
| Narrow 48 | 34.9 | - 0.67 (NS) | - 7.5 |
| Wide 48 | 36.1 | - 0.33 (NS) | - 7.8 |

Based on Table 5.8, it can be seen that the intercept values for the number of revolutions in the mixing section increase as the screw configuration of the mixing section changes. When the narrow kneading blocks in the mixing section is replaced by wider kneading block, the intercept value of $Rev_{mix}$ increases. Similarly, $Rev_{mix}$ increases as the length of the mixing section is doubled. The coefficient of screw speed is non-significant which implies that changes in screw speed at constant Q/N are unlikely to impact the number of revolutions. Specific throughput is the dominant operating condition that influences the

number of revolutions in the mixing section. The higher the specific throughput, the lesser is the number of revolutions in the mixing section. The influence of specific throughput increases as wide kneading block geometry is used in the mixing section as well as when the length of the mixing section is doubled.

Section 5.1 discusses the results collected based on the conducted RSD experiments and the simulations performed using Ludovic for 4 corresponding screw geometries of the 18mm Twin Screw Extruder. The experiment was performed using Low Density Polyethylene (LDPE).

## 5.2 LDPE vs HDPE for 18mm TSE Screw Configurations

The experiments were conducted on the 18mm Twin Screw Extruder for the 4 screw configurations for both Low Density Polyethylene (LDPE) and High Density Polyethylene (HDPE). This section compares the results generated when using different base polymers and helps get an insight into the RSD and Ludovic Simulations. The results will be discussed in the same order as they had been presented in Section 5.1.

Table 5.9: Thermal Characteristics of HDPE and LDPE

| **Thermal Characteristics** | **HDPE** | **LDPE** |
|---|---|---|
| Heat Capacity (J/kg/$^0$C) | 2620 | 2200 |
| Density (kg/m$^3$) | 920 | 740 |
| Heat Capacity (J/kg/$^0$C) | 3000 | 3000 |
| Density (kg/m$^3$) | 2500 | 1300 |
| Thermal Conductivity (W/m.K) | 0.5 | 0.3 |
| Melting Temperature ($^0$C) | 130 | 117 |

The table compares the thermal characteristics of HDPE and LDPE which will be useful in interpreting the results provided based on the RSD experiment as well as the Ludovic Simulations.

### 5.2.1 Percent Break-Up

The results in this section will be provided similar to Section 5.1. The results obtained from the experiments will be compared for each base polymer for every corresponding screw configuration. JMP has been used to statistically analyze the experimental data and the predictive equations will be displayed under each CCD grid. A surface plot has been created using Matlab R2016A, codes used for generating the plots can be found in Appendix A. The same set of operating conditions had been used to collect data on both HDPE and LDPE, so that the %BU results can be correlated with the Ludovic simulations and can help us understand the behavior exhibited. Fig 5.18-5.25 provide the CCD grid comprising the %BU values and the surface plots generated using MATLAB based on the predictive equations generated using JMP 12.2, for each of the 4 screw configurations.

Screw Configuration – 24mm Mixing Section (Narrow)

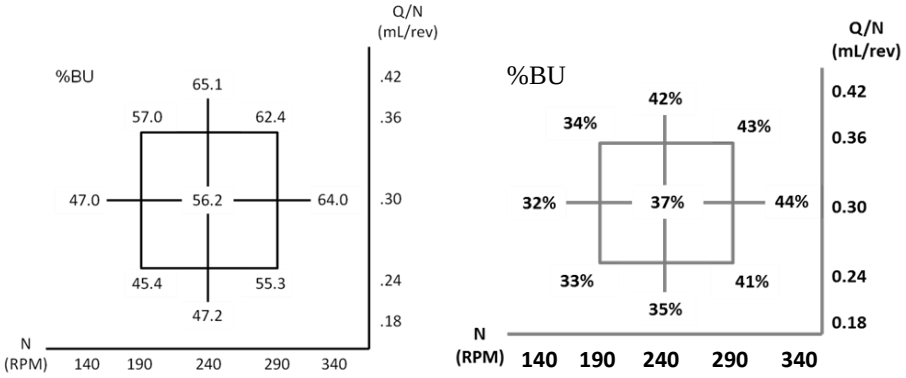


Figure 5.18: %BU comparison for 24mm Narrow Mixing Section LDPE (left) vs HDPE (right)

$$\%BU_{LDPE} = 55.3 + 4.11\,N + 4.45\frac{Q}{N} \tag{5.5}$$

$$\%BU_{HDPE} = 38.2 + 3.42\,N + 1.42\frac{Q}{N} \tag{5.6}$$

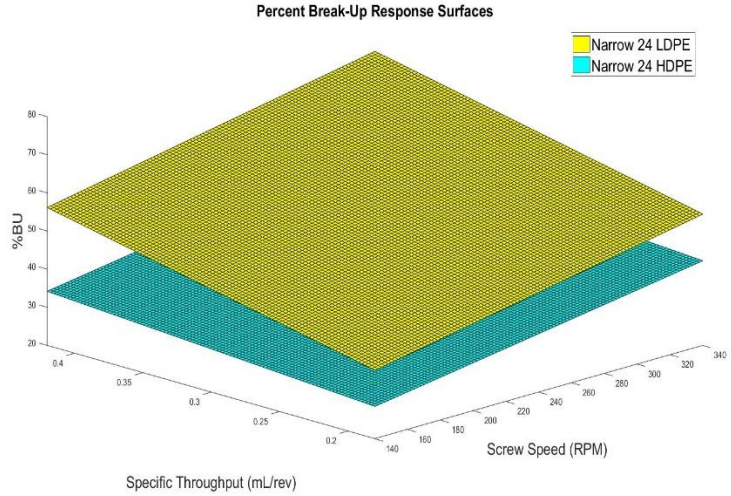


Figure 5.19: Surface Plot Comparison between %BU values for 24mm Narrow Mixing Section

Screw Configuration – 24mm Mixing Section (Wide)

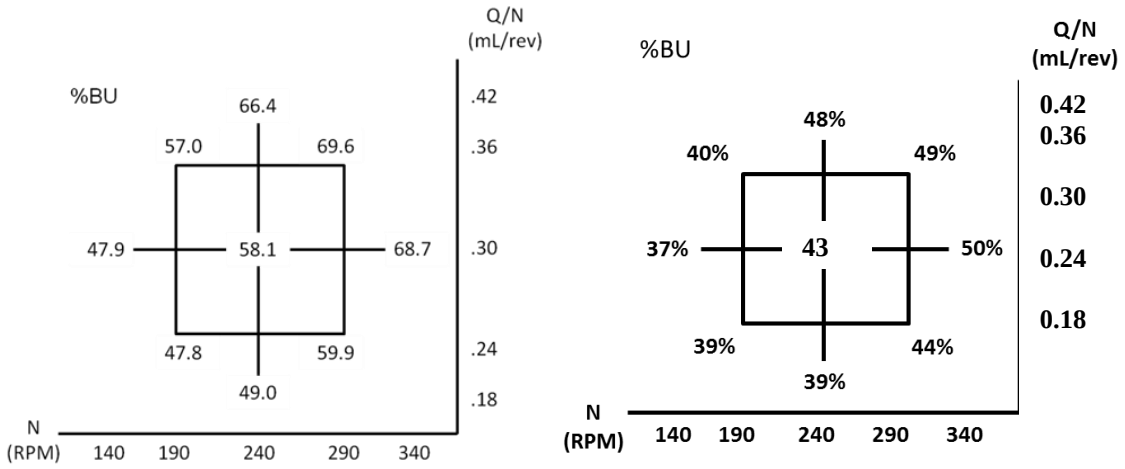


Figure 5.20: %BU comparison for 24mm Wide Mixing Section LDPE (left) vs HDPE (right)

$$\%BU_{LDPE} = 58.5 + 5.53\,N + 4.48\frac{Q}{N} \tag{5.7}$$

$$\%BU_{HDPE} = 41.7 + 3.08\,N + 2.25\frac{Q}{N} \tag{5.8}$$

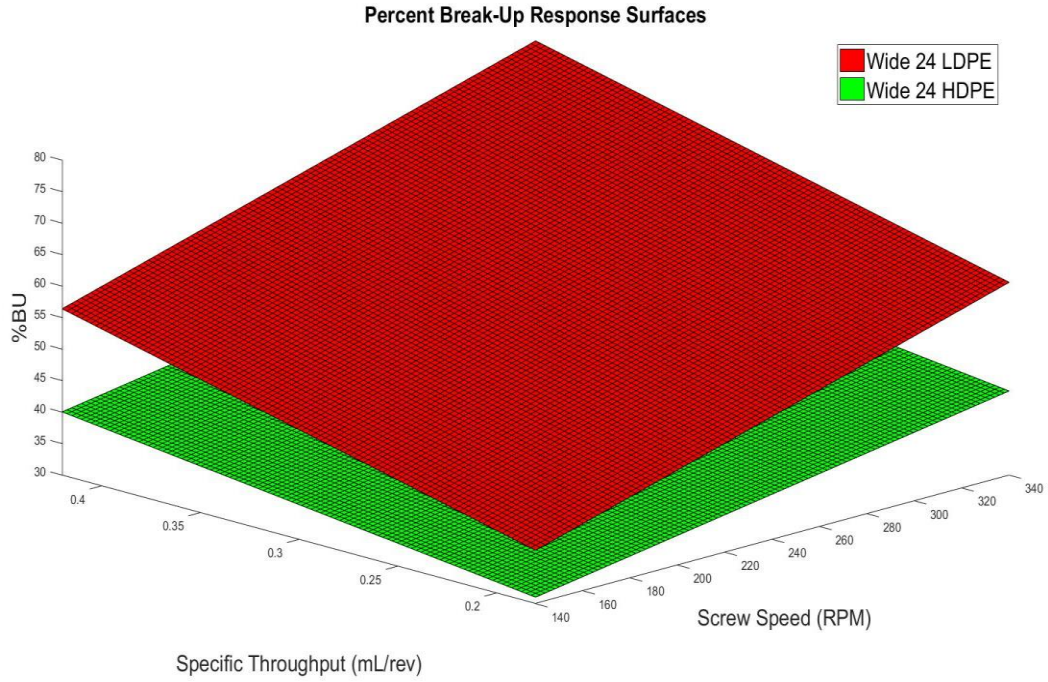


Figure 5.21: Surface Plot Comparison between %BU values for 24mm Wide Mixing Section

Screw Configuration – 48mm Mixing Section (Narrow)

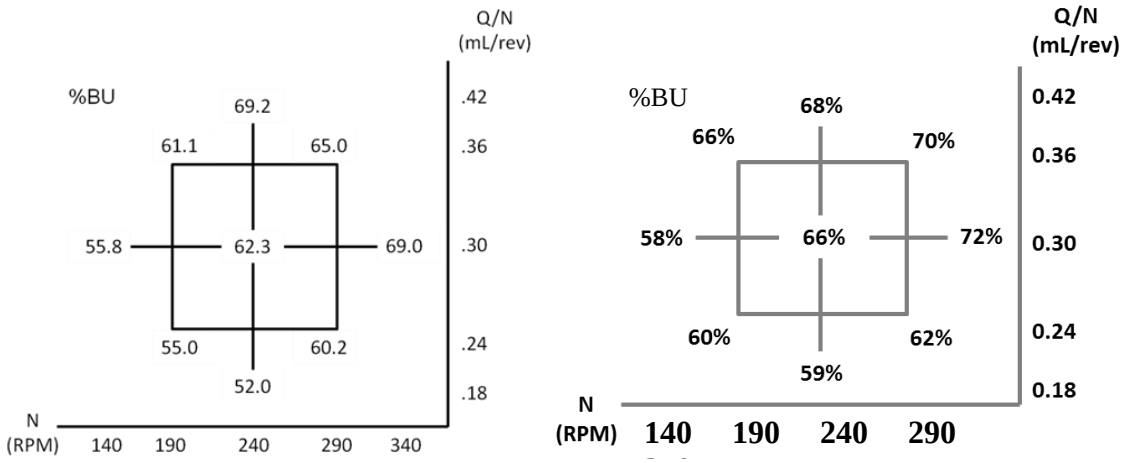


Figure 5.22: %BU comparison for 48mm Narrow Mixing Section LDPE (left) vs HDPE (right)

$$\%BU_{LDPE} = 61.1 + 2.95\,N + 3.86\frac{Q}{N} \tag{5.9}$$

$$\%BU_{HDPE} = 65.4 + 2.83\,N + 2.67\frac{Q}{N} \tag{5.10}$$

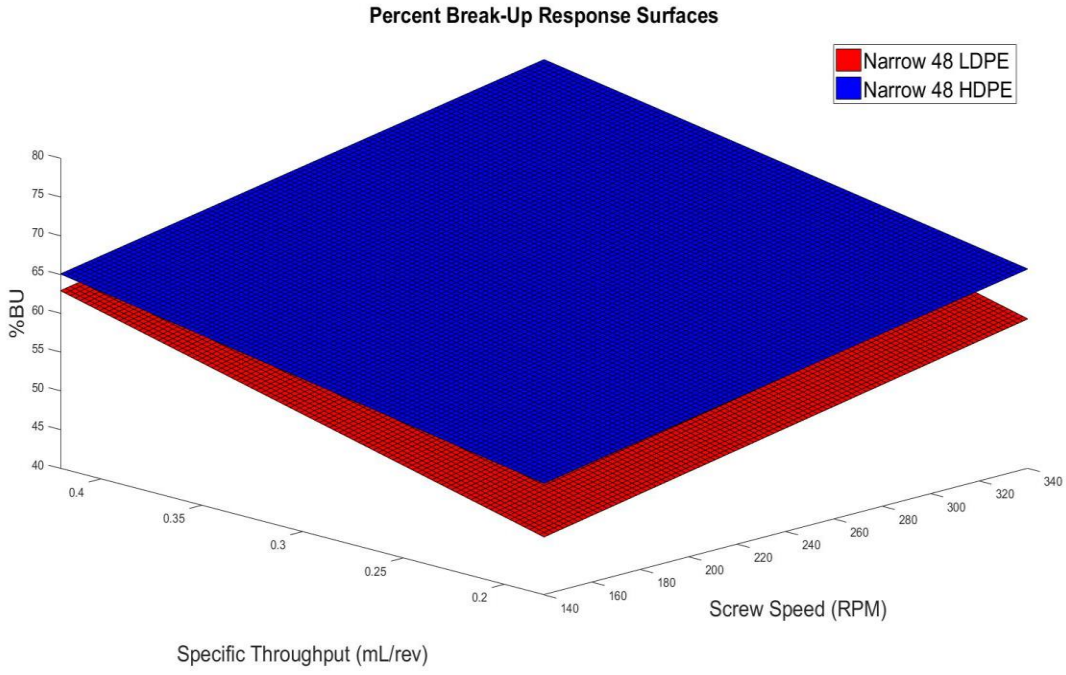


Figure 5.23: Surface Plot Comparison between %BU values for 48mm Narrow Mixing Section

Screw Configuration – 48mm Mixing Section (Wide)

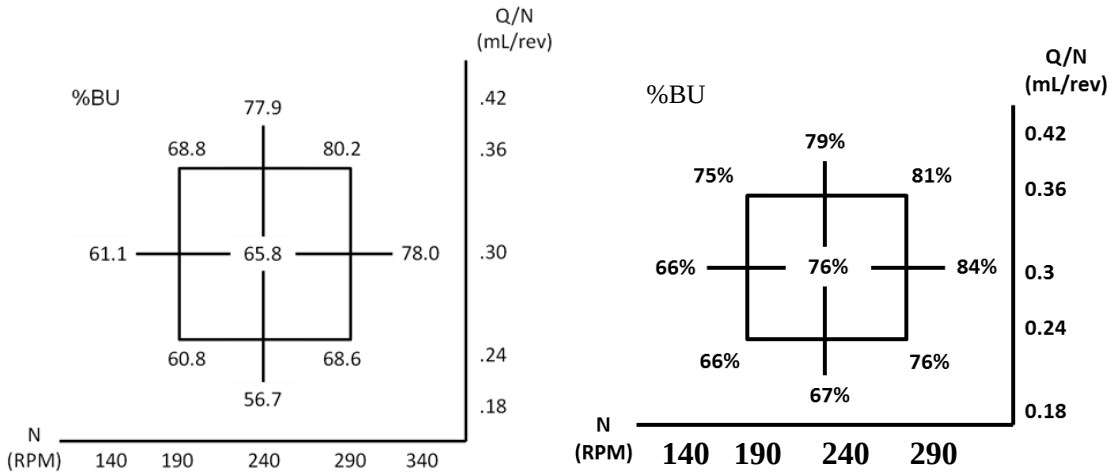


Figure 5.24: %BU comparison for 48mm Narrow Mixing Section LDPE (left) vs HDPE (right)

$$\%BU_{LDPE} = 68 + 4.42\,N + 5.18\,\frac{Q}{N} \tag{5.11}$$

$$\%BU_{HDPE} = 65.4 + 3.83\,N + 3.17\,\frac{Q}{N} \tag{5.12}$$

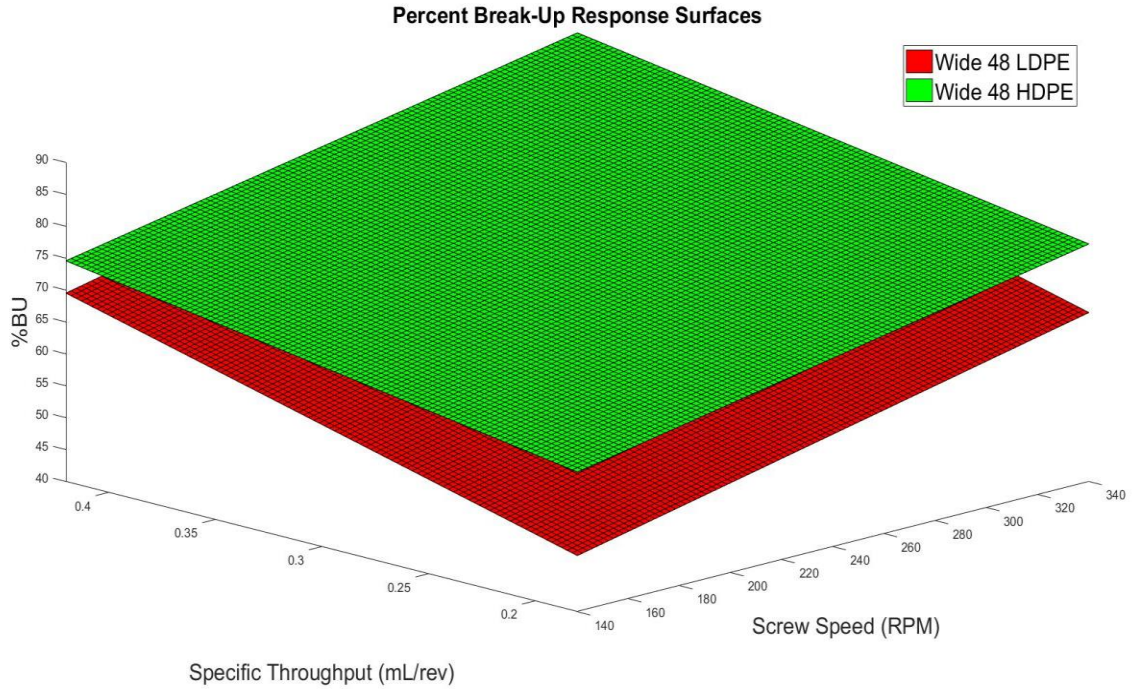


Figure 5.25: Surface Plot Comparison between %BU values for 48mm Narrow Mixing Section

Fig 5.18-5.25 provide data on the %BU results obtained upon performing experiments using both LDPE and HDPE. Based on the comparison, the %BU is higher for LDPE compared to HDPE for the 24mm long mixing sections – both narrow and wide. However, %BU for HDPE is slightly higher than LDPE, when the mixing section lengths are doubled. The intercept values obtained for %BU is higher for LDPE in every screw geometry configuration except for the 48mm long Narrow Mixing Section. HDPE being a densely packed base polymer requires higher amount of stress to break-up. For a specific screw geometry, the shear stress that the polymer melt could be subjected to was seen in Section 5.1.5. When the same amount of stress is being subjected to both HDPE and LDPE, HDPE being a densely-packed polymer would break-up at a lower rate compared to LDPE which was seen for the mixing section of length 24mm. However, in the case of 48mm long mixing section, the stress values are higher (due to shear stress and extensional stress). The magnitudes of stress are higher which causes higher % BU for LDPE and HDPE. For 48mm mixing section, the magnitudes of difference in %BU values between HDPE and LDPE is lesser.

**Ludovic Results**

### 5.2.2 Maximum Shear Rate in the Mixing Section

The results to be compared in this section include the maximum shear rate that the polymer melt experiences in the mixing section of a TSE. The results have been displayed in the CCD grids and have been created as surface plots using MATLAB.

Screw Configuration – 24mm Mixing Section (Narrow)

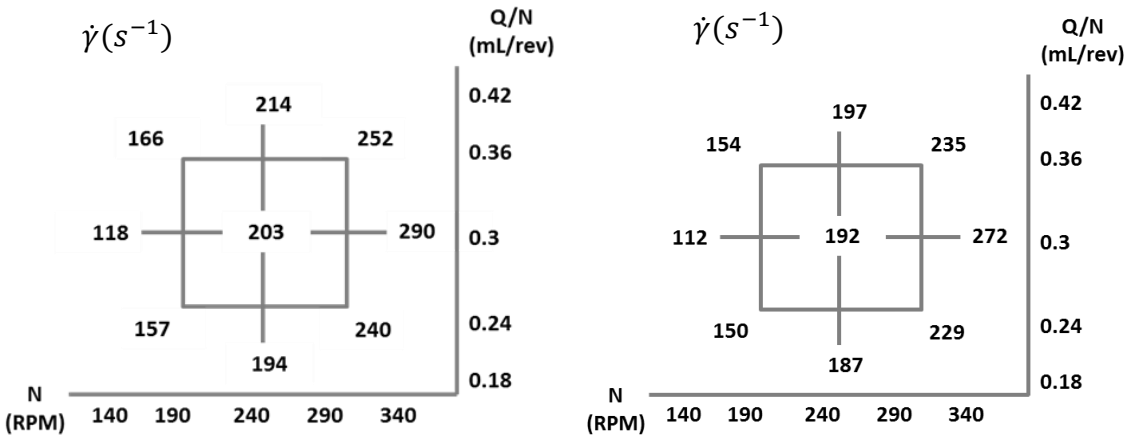


Figure 5.26: Shear Rate for 24mm Narrow Mixing Section LDPE (left) vs HDPE (right)

$$\dot{\gamma}_{LDPE} = 203.2 + 42.75\,N + 5.1\frac{Q}{N} \tag{5.13}$$

$$\dot{\gamma}_{HDPE} = 192 + 40\,N + 2.5\frac{Q}{N} \tag{5.14}$$

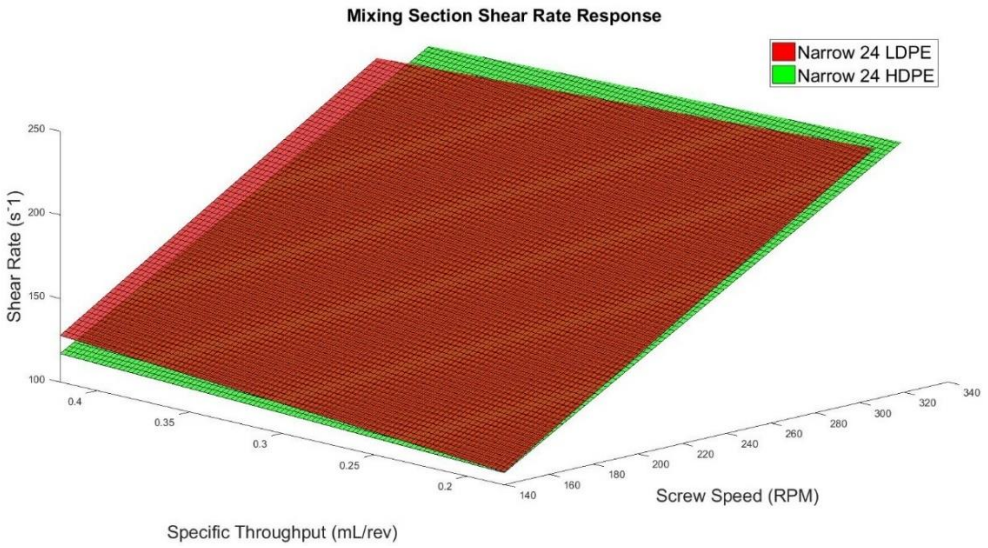


Figure 5.27: Surface Plot Comparison between shear rate for 24mm Narrow Mixing Section

Screw Configuration – 24mm Mixing Section (Wide)

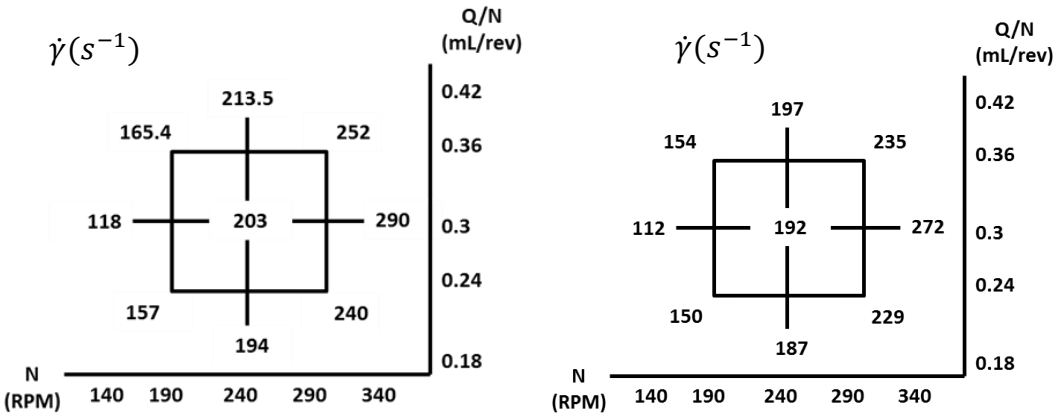


Figure 5.28: Shear Rate for 24mm Wide Mixing Section LDPE (left) vs HDPE (right)

$$\dot{\gamma}_{LDPE} = 203.1 + 42.8\,N + 4.95\frac{Q}{N} \tag{5.15}$$

$$\dot{\gamma}_{HDPE} = 192 + 40\,N + 2.5\frac{Q}{N} \tag{5.16}$$

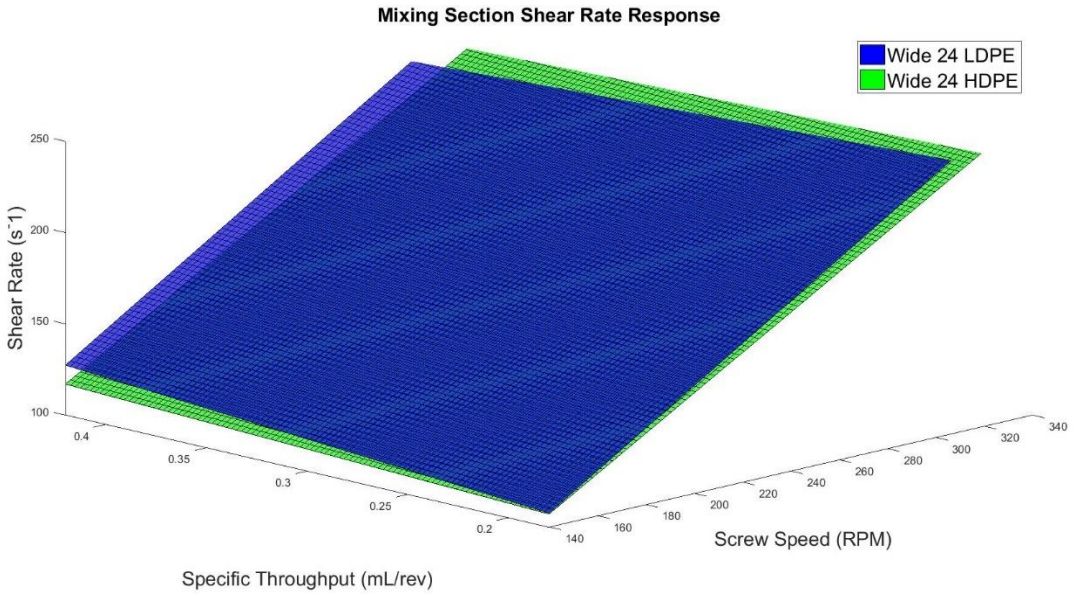


Figure 5.29: Surface Plot Comparison between shear rate for 24mm Wide Mixing Section

Screw Configuration – 48mm Mixing Section (Narrow)

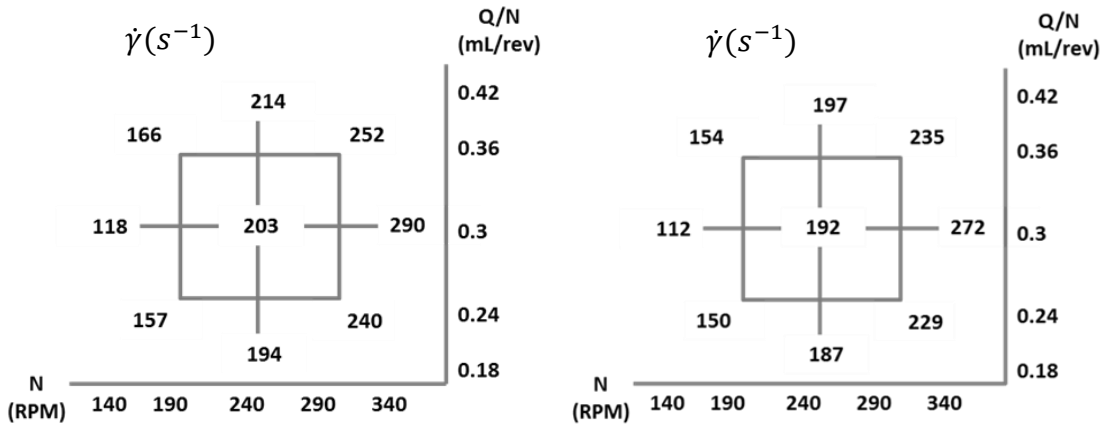


Figure 5.30: Shear Rate for 48mm Narrow Mixing Section LDPE (left) vs HDPE (right)

$$\dot{\gamma}_{LDPE} = 203.2 + 42.75\,N + 5.1\frac{Q}{N} \tag{5.17}$$

$$\dot{\gamma}_{HDPE} = 192 + 40\,N + 2.5\frac{Q}{N} \tag{5.18}$$

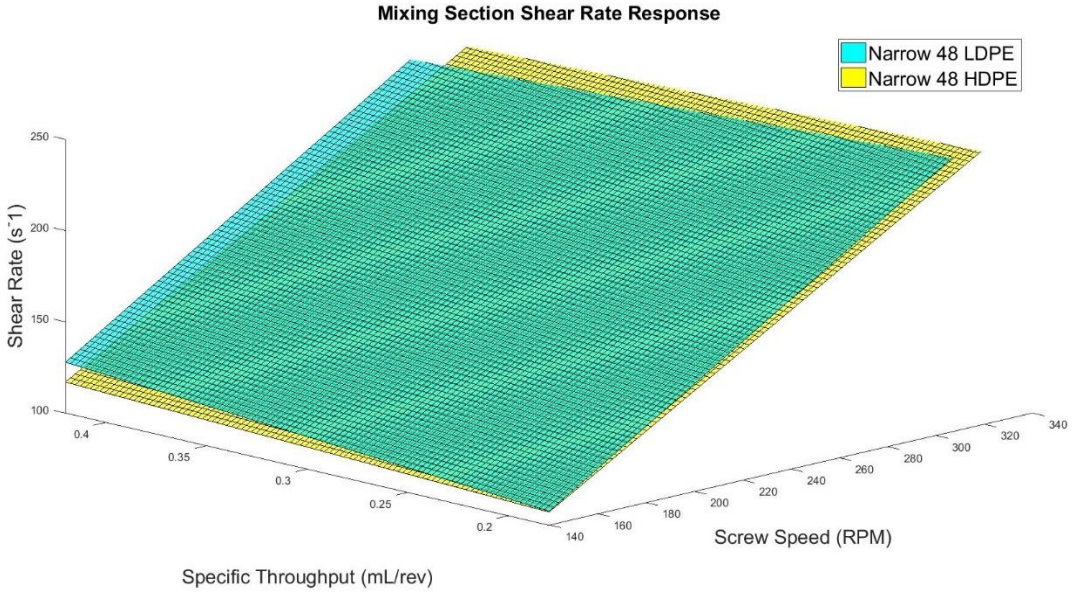


Figure 5.31: Surface Plot Comparison between shear rate for 48mm Narrow Mixing Section

Screw Configuration – 48mm Mixing Section (Wide)

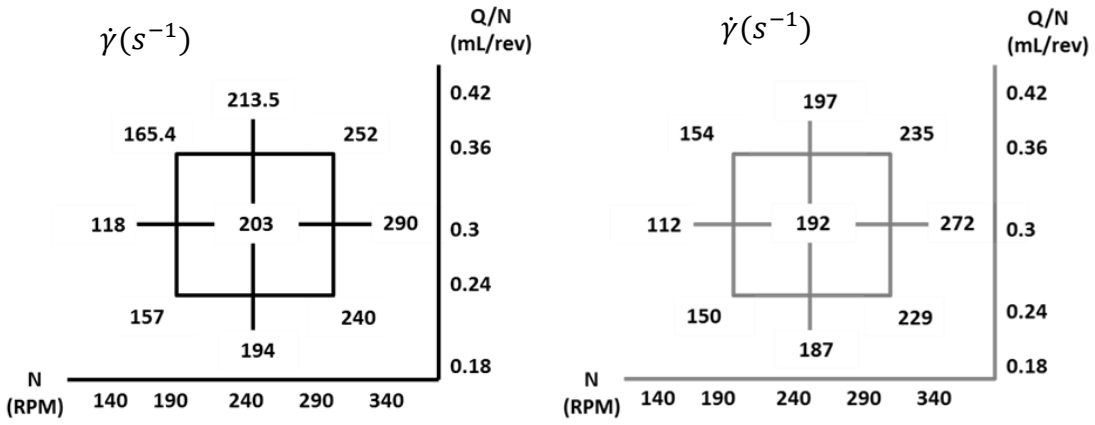


Figure 5.32: Shear Rate for 48mm Wide Mixing Section LDPE (left) vs HDPE (right)

$$\dot{\gamma}_{LDPE} = 203.1 + 42.8\,N + 4.95\frac{Q}{N} \tag{5.19}$$

$$\dot{\gamma}_{HDPE} = 192 + 40\,N + 2.5\frac{Q}{N} \tag{5.20}$$

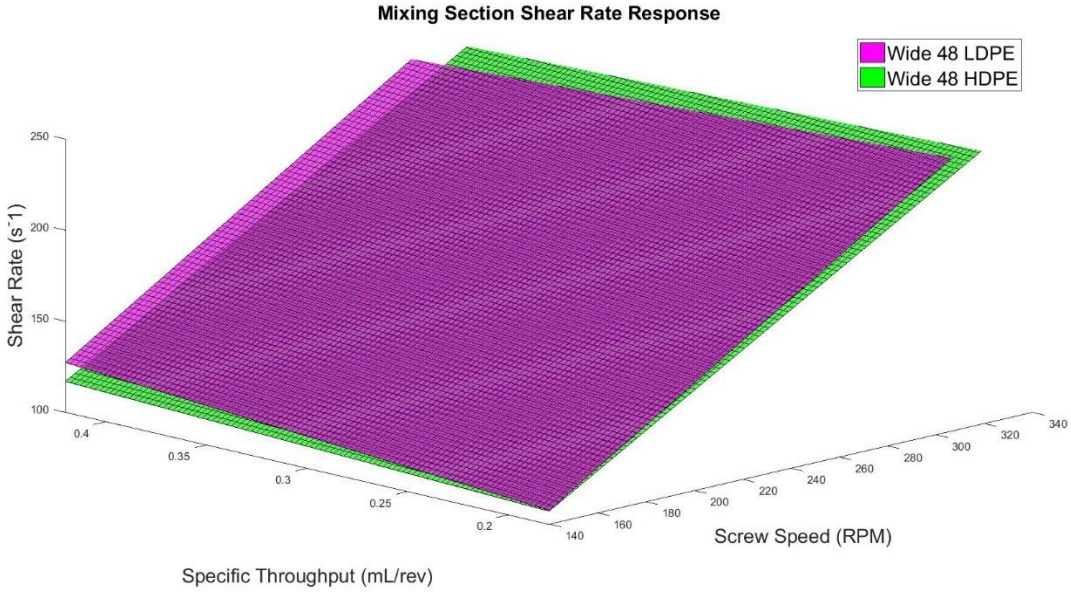


Figure 5.33: Surface Plot Comparison between shear rate for 48mm Wide Mixing Section

Fig 5.26-5.33 shows the data on the maximum shear rate comparison between LDPE and HDPE for four screw configurations of the mixing section. For each of the four screw

configurations, the shear rate generated by LDPE is higher compared to HDPE. The intercept value for shear rate i.e. mean value of shear rate across all the 9 grid points is higher for LDPE compared to HDPE. The coefficient of N is higher for LDPE compared to HDPE implying that change in screw speed has a greater change in the shear rate values for LDPE compared to HDPE. HDPE being a high-density polymer due to smaller branching is extremely rigid compared to LDPE. Due to the morphology of HDPE, the untangling of polymer chains is difficult. This is the reason for the slight change in the shear rate values for HDPE and LDPE.

### 5.2.3 Maximum Temperature in the Mixing Section

The maximum temperature attained by the polymer melt in the mixing section when processing HDPE and LDPE has been simulated using Ludovic. The results have been displayed in the CCD grids and have been created as surface plots using MATLAB.

**Screw Configuration – 24mm Mixing Section (Narrow)**

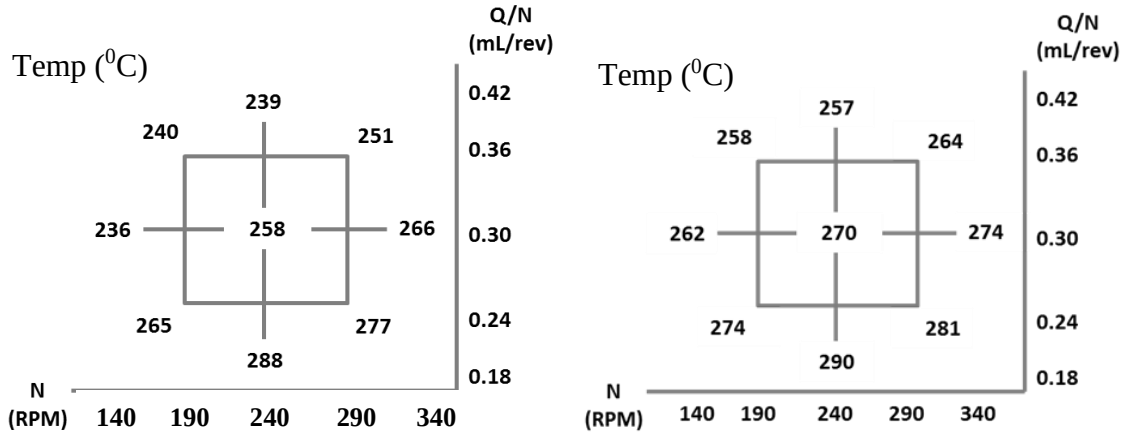


Figure 5.34: Max. Temperature for 24mm Narrow Mixing Section LDPE (left) vs HDPE (right)

$$T_{max-LDPE} = 258.5 + 6.92\,N - 12.67\frac{Q}{N} \tag{5.21}$$

$$T_{max-HDPE} = 273.7 + 2.92N - 8.4\frac{Q}{N} \tag{5.22}$$

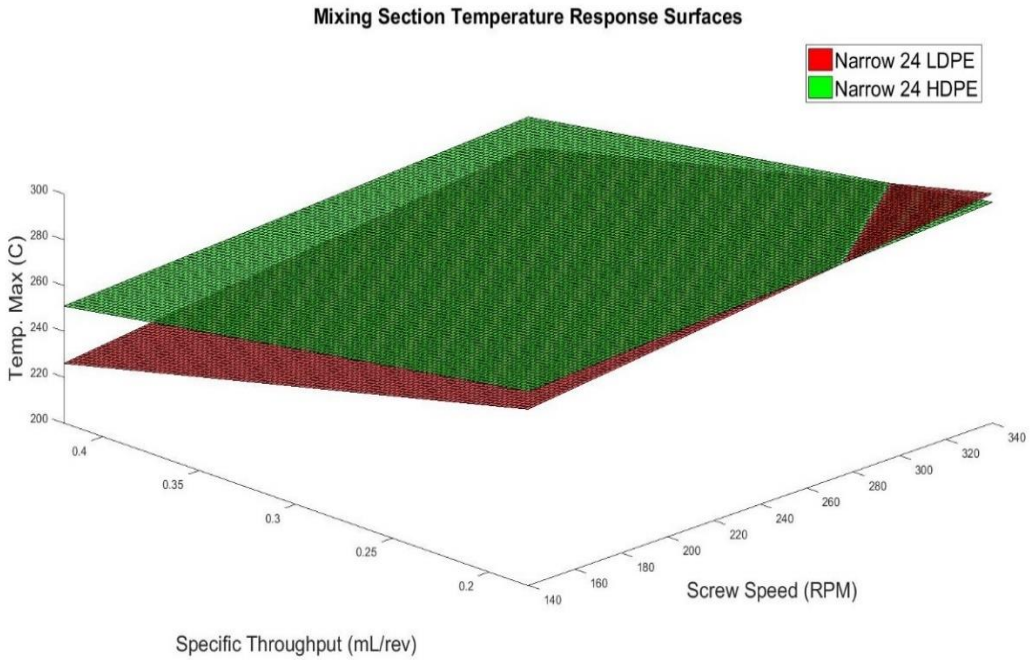


Figure 5.35: Surface Plot Comparison between Max. temperature for 24mm Narrow Mixing Section

**Screw Configuration – 24mm Mixing Section (Wide)**

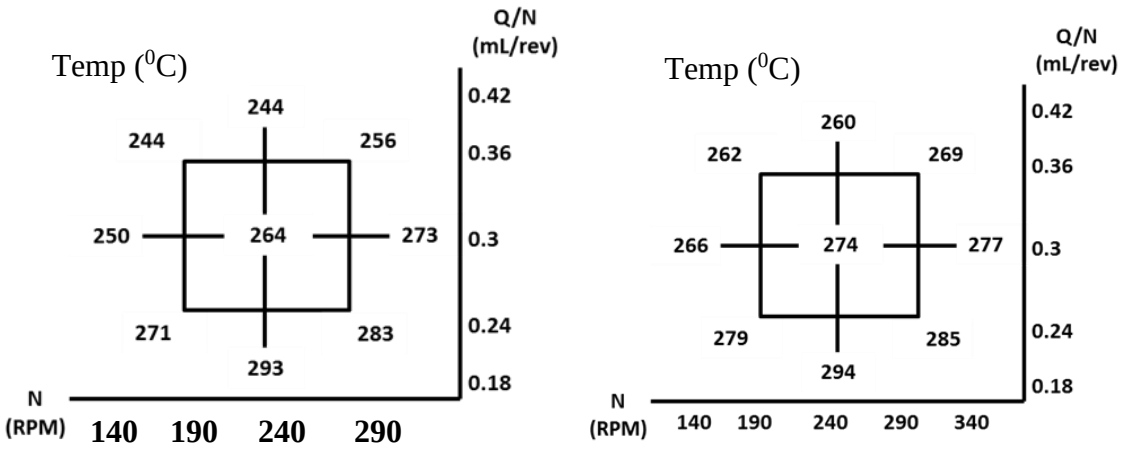


Figure 5.36: Max. Temperature for 24mm Wide Mixing Section LDPE (left) vs HDPE (right)

$$T_{max-LDPE} = 263.1 + 5.83\,N - 12.67\frac{Q}{N} \tag{5.23}$$

$$T_{max-HDPE} = 273.7 + 2.92N - 8.4\frac{Q}{N} \tag{5.24}$$

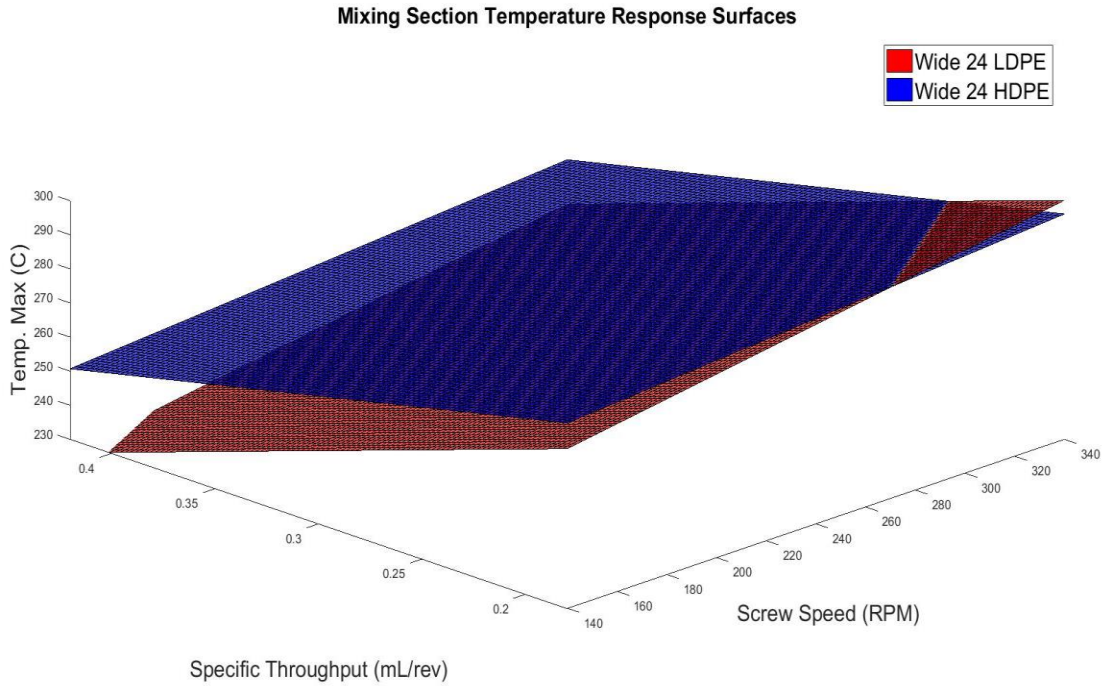


Figure 5.37: Surface Plot Comparison between Max. temperature for 24mm Wide Mixing Section

**Screw Configuration – 48mm Mixing Section (Narrow)**

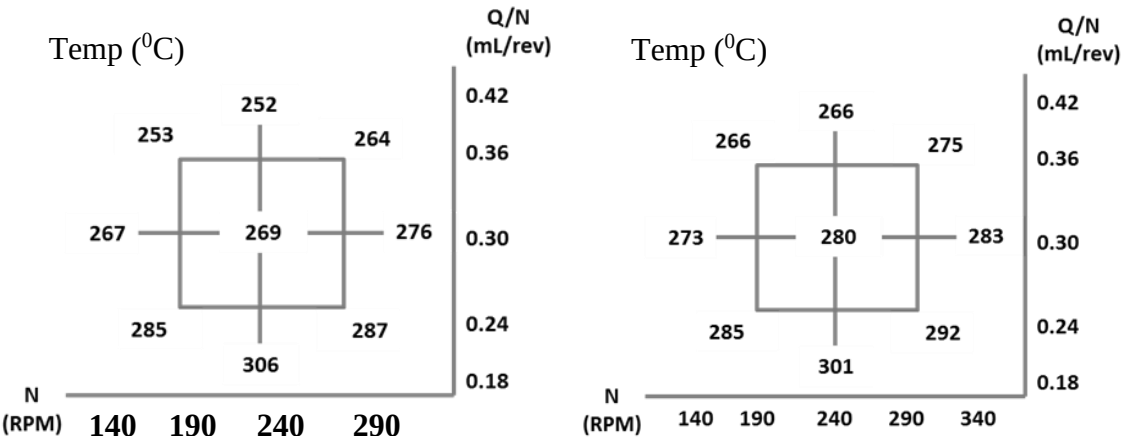


Figure 5.38: Max. Temperature for 48mm Narrow Mixing Section LDPE (left) vs HDPE (right)

$$T_{max-LDPE} = 269.1 + 2.58\,N - 12.41\,\frac{Q}{N} \tag{5.25}$$

$$T_{max-HDPE} = 279.2 + 3\,N - 8.8\,\frac{Q}{N} \tag{5.26}$$

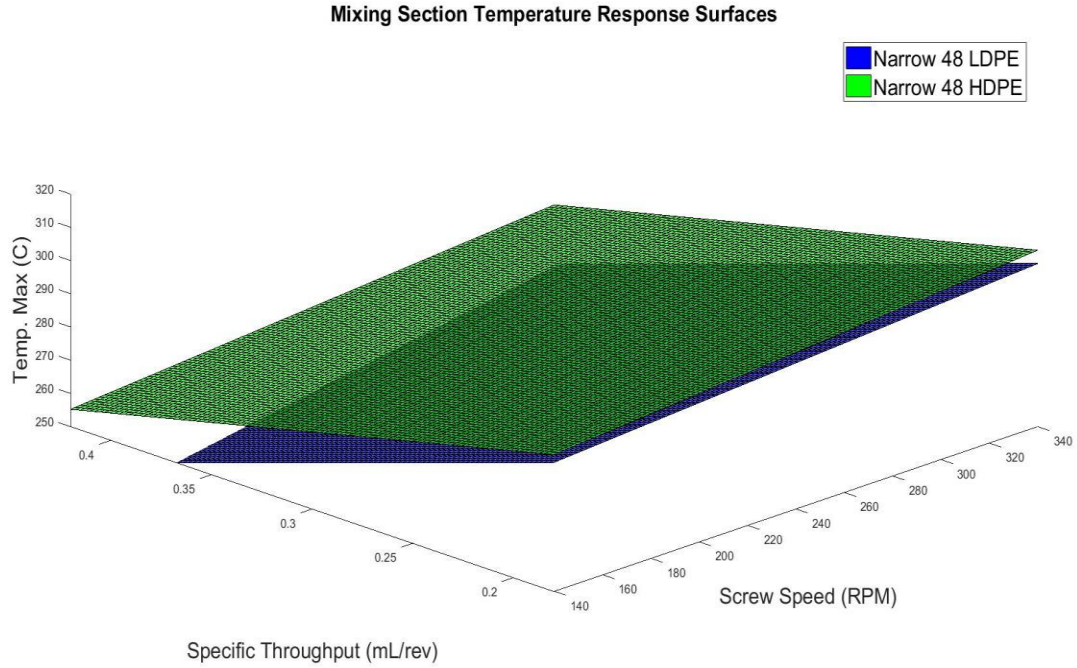


Figure 5.39: Surface Plot Comparison between Max. temperature for 48mm Wide Mixing Section

**Screw Configuration – 48mm Mixing Section (Wide)**

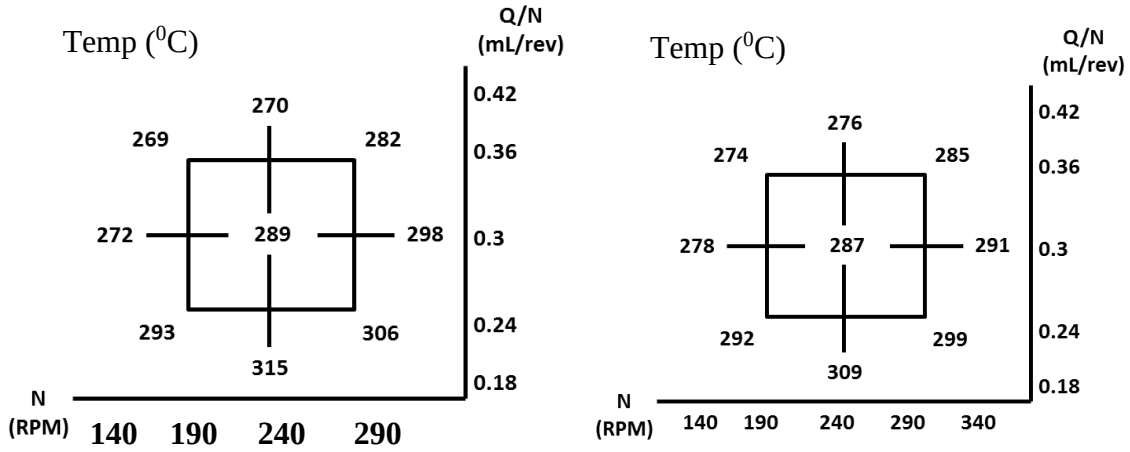


Figure 5.40: Max. Temperature for 48mm Wide Mixing Section LDPE (left) vs HDPE (right)

$$T_{max-LDPE} = 287.8 + 6.5\,N - 11.5\,\frac{Q}{N} \quad (5.27)$$

$$T_{max-HDPE} = 286 + 3.67\,N + 1.42\,\frac{Q}{N} \quad (5.28)$$

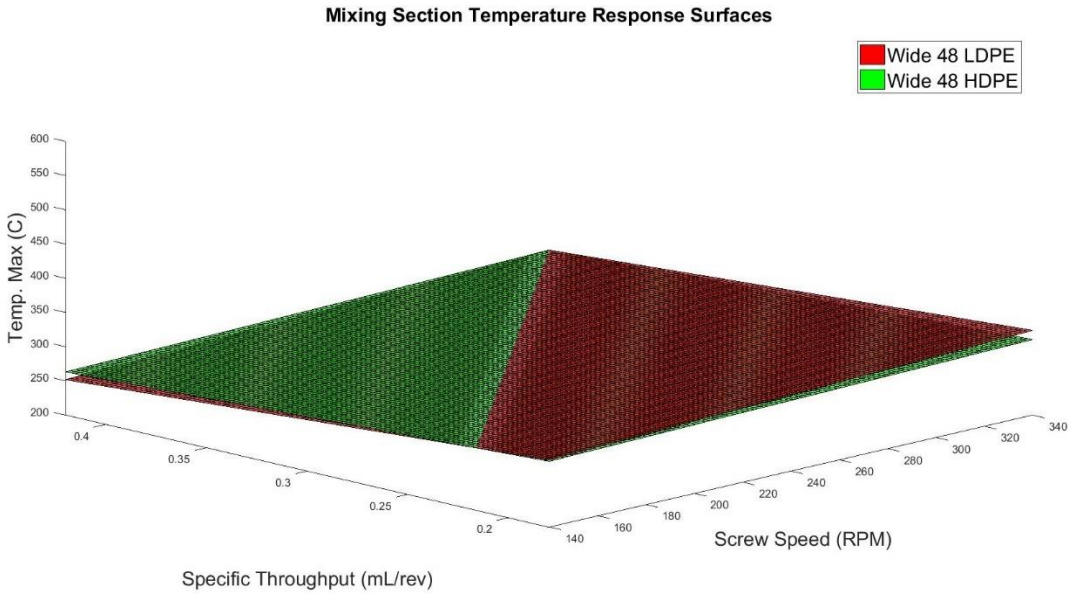


Figure 5.41: Surface Plot Comparison between Max. temperature for 48mm Wide Mixing Section

Fig 5.34-5.41 provide the comparison between the maximum temperature attained by the polymer melt for the same screw configuration for two base polymers – LDPE and HDPE.

Across the four screw configurations, the temperature of HDPE is higher compared to LDPE. The coefficient of N is higher for LDPE compared to HDPE for almost all the screw configurations implying that change in screw speed affects the temperature of LDPE in the mixing section to a greater extent compared to HDPE. Similarly, the coefficient of Q/N is higher for LDPE compared to HDPE for all the screw configurations. The intercept values of $T_{max}$ is higher for HDPE compared to LDPE. For narrow screw configurations, the difference in temperature values between HDPE and LDPE, for the corresponding CCD grid points is higher. For wider screw configurations, the difference in temperature values between HDPE and LDPE is lower and at certain CCD grid points LDPE has higher temperature value compared to HDPE. Despite a few anomalies, the general trend is that HDPE generates higher temperature compared to LDPE for similar screw configurations. Despite having a lower shear rate compared to LDPE, HDPE exhibits higher temperature due to higher thermal conductivity compared to LDPE (Table 5.9).

### 5.2.4 Viscosity in the Mixing Section

The viscosity of the polymer melts for four different screw configurations of the mixing section are being compared in this section. The viscosity values (Pa-s) are simulated by Ludovic based on the inputs specified by the user regarding the screw geometry and the operating conditions. The viscosity values provided in the CCD grids are created as surface plots using MATLAB based on the predictive equations generated for each base polymer (LDPE, HDPE) for every screw configuration.

Screw Configuration – 24mm Mixing Section (Narrow)

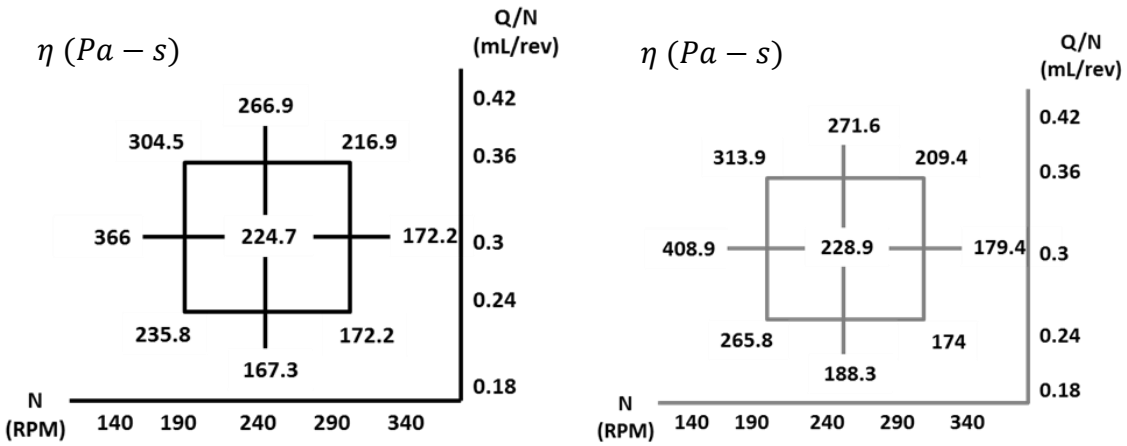


Figure 5.42: Viscosity for 24mm Narrow Mixing Section LDPE (left) vs HDPE (right)

$$\eta_{LDPE} = 223.3 - 44.9\,N + 26.1\,\frac{Q}{N} \tag{5.29}$$

$$\eta_{HDPE} = 224.7 - 54.6\,N + 20.8\,\frac{Q}{N} \tag{5.30}$$

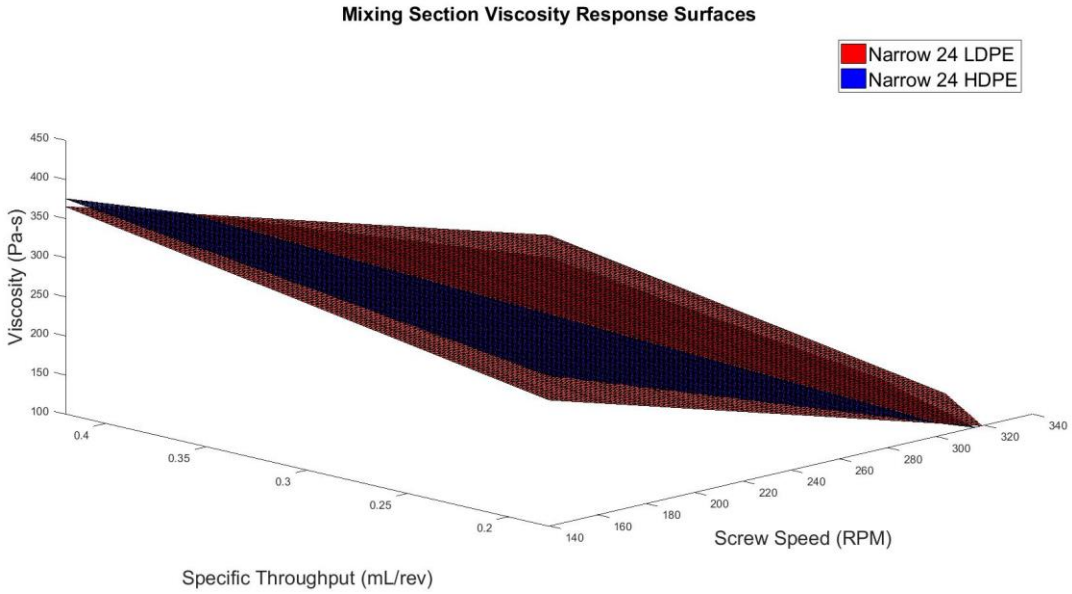


Figure 5.43: Surface Plot Comparison between Viscosity for 24mm Narrow Mixing Section

Screw Configuration – 24mm Mixing Section (Wide)

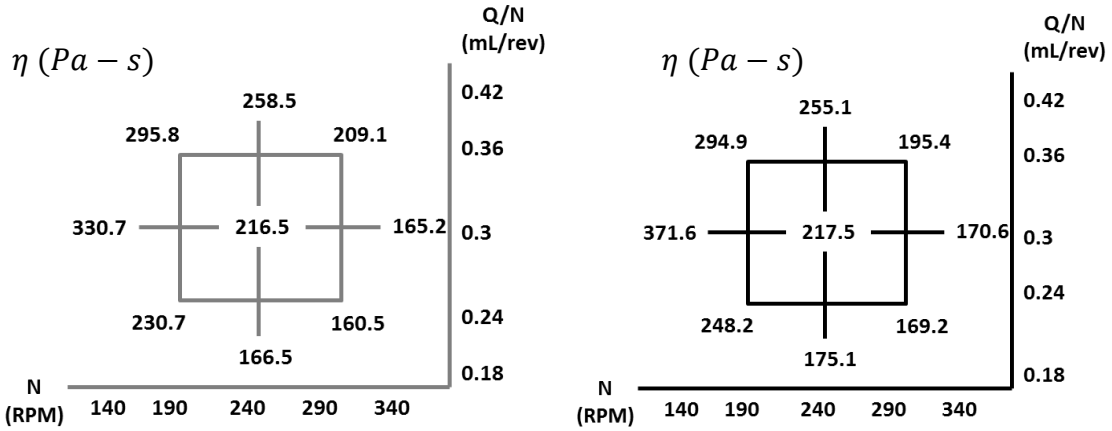


Figure 5.44: Viscosity for 24mm Wide Mixing Section LDPE (left) vs HDPE (right)

$$\eta_{LDPE} = 217.1 - 40.65\,N + 24.8\,\frac{Q}{N} \quad (5.31)$$

$$\eta_{HDPE} = 214.5 - 48.4\,N + 19.4\,\frac{Q}{N} \quad (5.32)$$

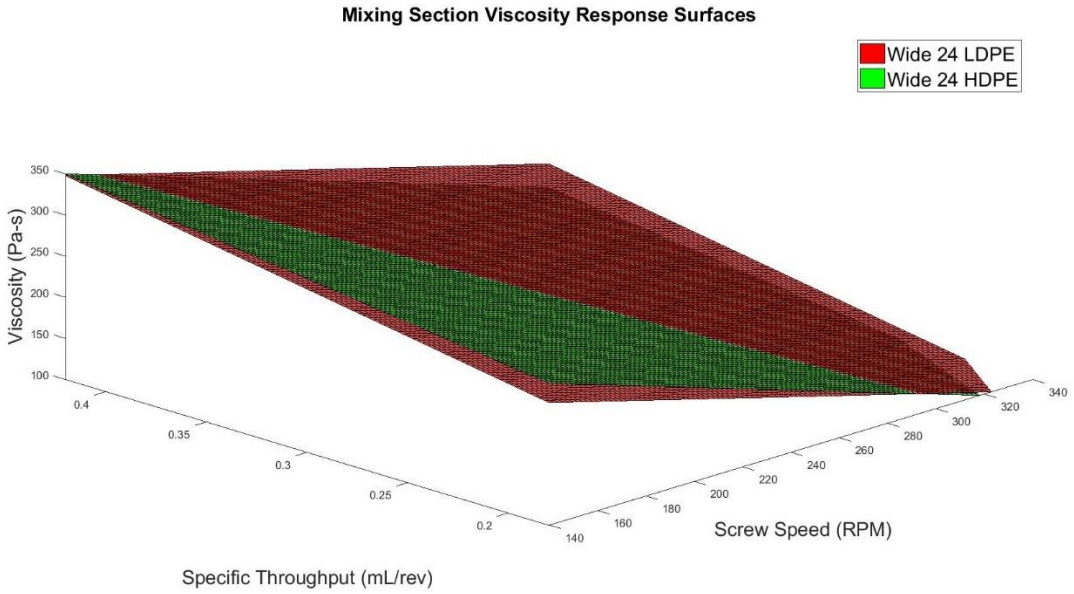


Figure 5.45: Surface Plot Comparison between Viscosity for 24mm Wide Mixing Section

Screw Configuration – 48mm Mixing Section (Narrow)

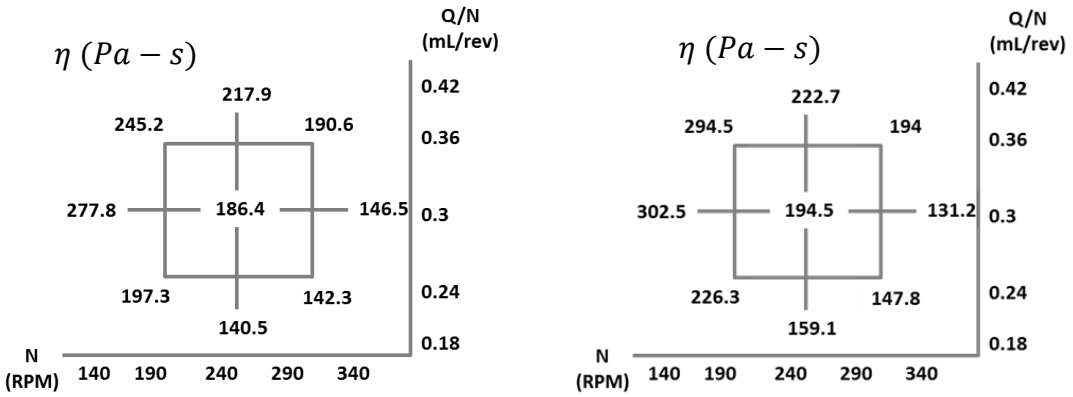


Figure 5.46: Viscosity for 48mm Narrow Mixing Section LDPE (left) vs HDPE (right)

$$\eta_{LDPE} = 188.9 - 31\,N + 20.9\,\frac{Q}{N} \tag{5.33}$$

$$\eta_{HDPE} = 209.1 - 43.4\,N + 19.4\,\frac{Q}{N} \tag{5.34}$$

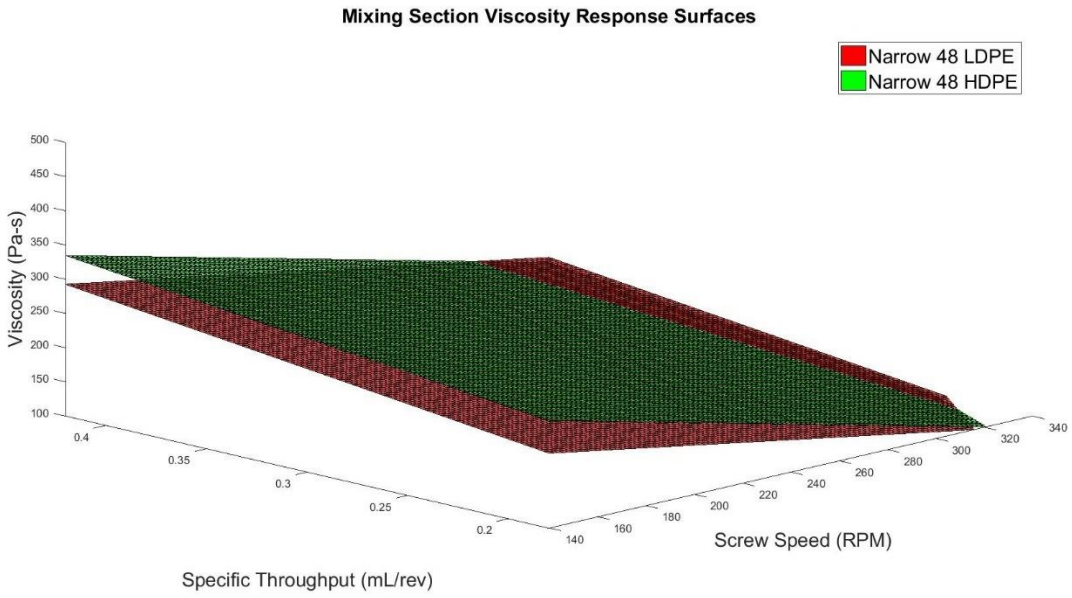


Figure 5.47: Surface Plot Comparison between Viscosity for 48mm Narrow Mixing Section

Screw Configuration – 48mm Mixing Section (Wide)

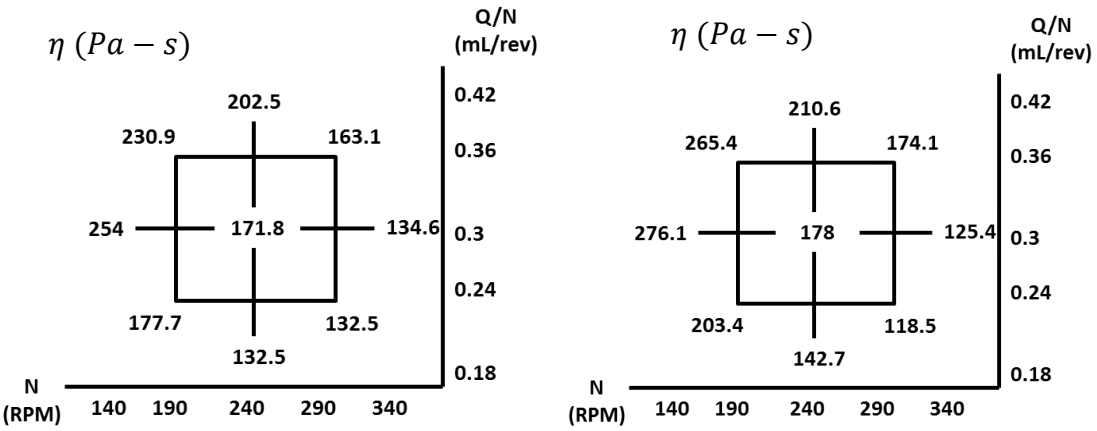


Figure 5.48: Viscosity for 48mm Wide Mixing Section LDPE (left) vs HDPE (right)

$$\eta_{LDPE} = 171.5 - 29.3\,N + 18.6\,\frac{Q}{N} \tag{5.35}$$

$$\eta_{HDPE} = 184.2 - 39.8\,N + 21.1\,\frac{Q}{N} \tag{5.36}$$

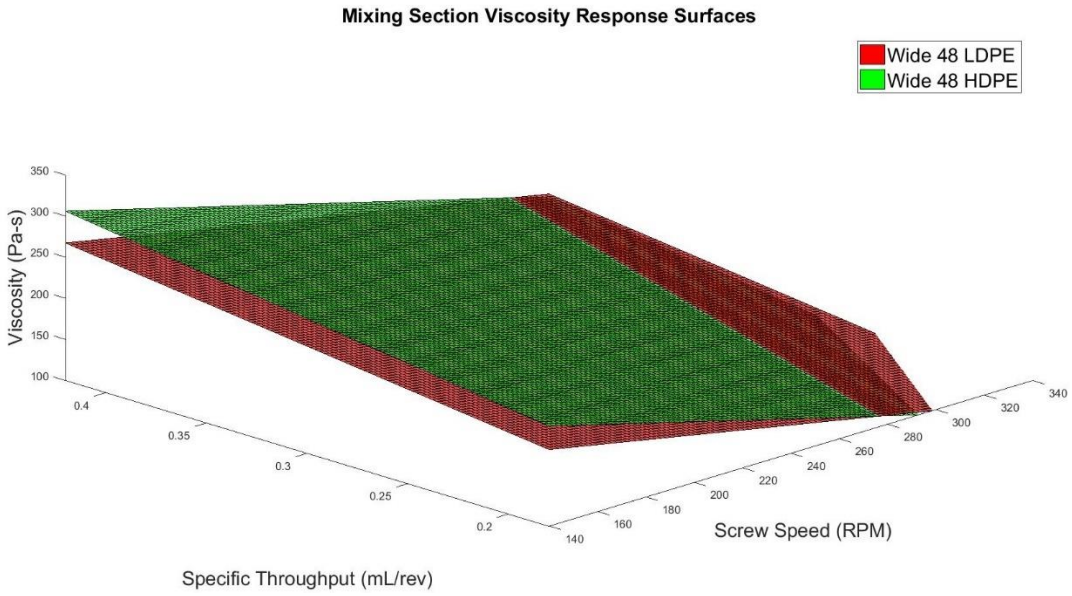


Figure 5.49: Surface Plot Comparison between Viscosity for 48mm Wide Mixing Section

Figure 5.42-5.49 reveal the data on viscosity of the polymer melt when subjected to a maximum shear rate within the Twin Screw Extruder. In the previous section, shear rate

was observed to be slightly lower for HDPE compared to LDPE, while the temperature of HDPE melt in the mixing section was found to be higher at most of the CCD grid points for the screw configurations. As per polymer rheology [42] viscosity varies inversely with temperature. The relationship between viscosity, shear rate and temperature from Eq. 3.3 and 3.4 suggest that viscosity is dependent on both the shear as well the temperature. In this situation, K is dependent on the consistency index $K_0$, Activation energy E and temperature of the polymer melt T. Despite a lower shear rate, the viscosity of HDPE is higher at most CCD grid points due to the fact that the activation energy of HDPE is higher compared to LDPE **[**43]. The consistency index of HDPE is also higher compared to LDPE **[**44**]** which leads to the overall increase of the K term. Despite a higher temperature and lower shear rate, the viscosity is higher for HDPE at most points due to the characteristics of HDPE. Considering Fig 5.42-5.49, a common trend observed across the MATLAB plots is that the difference in the viscosity values of HDPE and LDPE decreases at high screw speeds (N) and specific throughputs (Q/N). The plots also merge towards this region due to the very small difference in the viscosity values between HDPE and LDPE. The influence of the operating conditions on viscosity decreases as the mixing section length is doubled and when the narrow kneading block is replaced with a wide kneading block as the shear rate is higher as explained in section 5.1.2.

### 5.2.5 Shear Stress in the Mixing Section

This section provides the comparison between experimental results obtained from calculation of shear stress values (explained in Sec 5.1.5) for HDPE and LDPE across all the 9 CCD grid points for all the four screw configurations for the mixing section.

Screw Configuration – 24mm Mixing Section (Narrow)

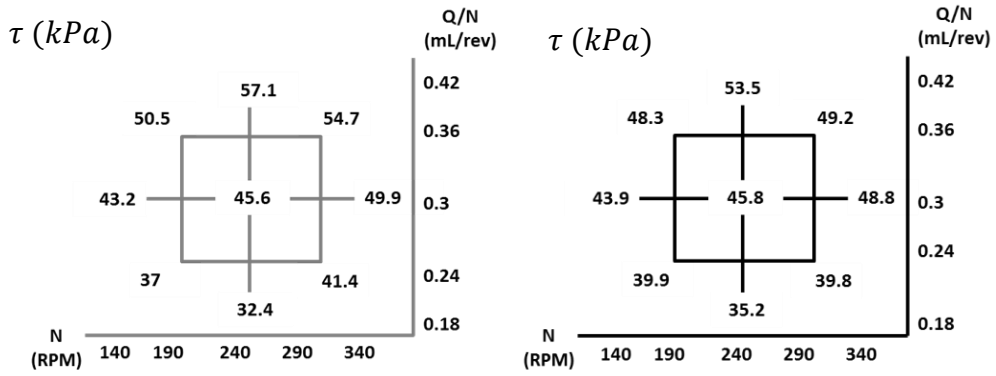


Figure 5.50: Shear Stress for 24mm Narrow Mixing Section LDPE (left) vs HDPE (right)

$$\tau_{LDPE} = 45.8 + 1.83\,N + 6.35\,\frac{Q}{N} \tag{5.37}$$

$$\tau_{HDPE} = 44.7 + 0.9\,N + 4.53\,\frac{Q}{N} \tag{5.38}$$

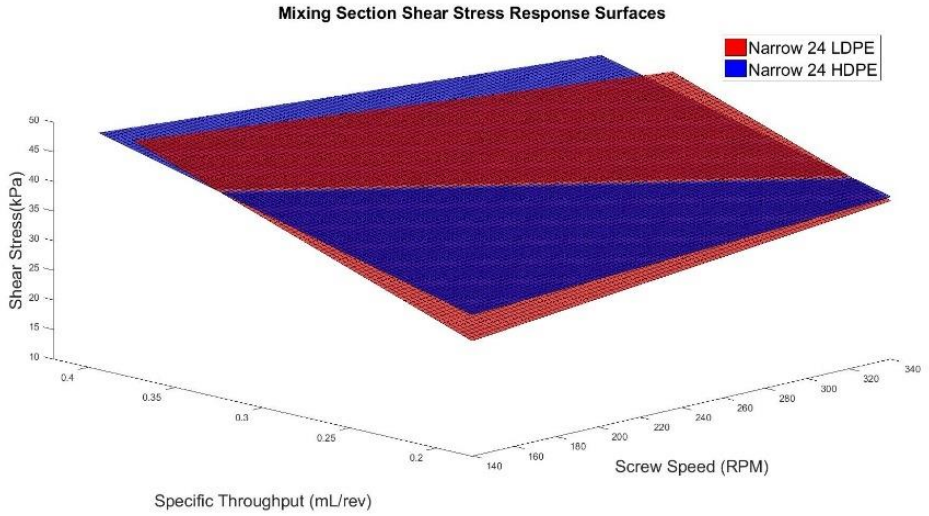


Figure 5.51: Surface Plot Comparison between Shear Stress for 24mm Narrow Mixing Section

Screw Configuration – 24mm Mixing Section (Wide)

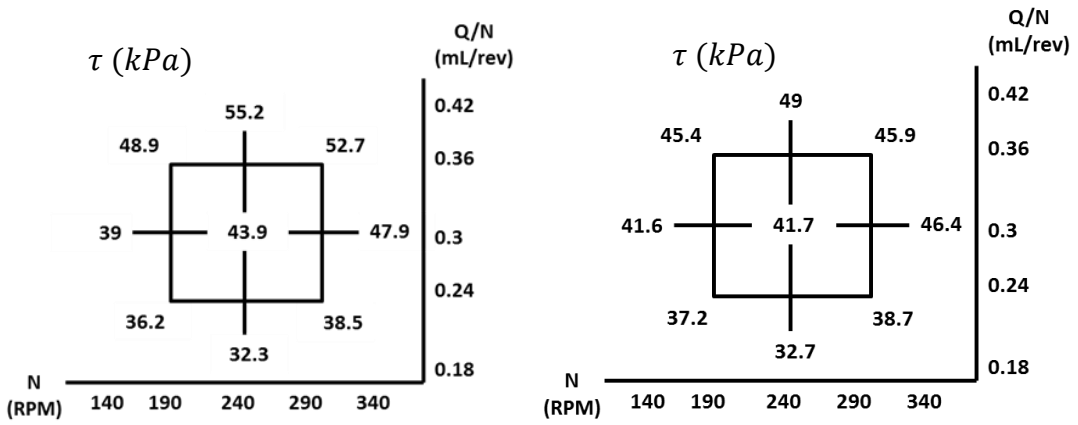


Figure 5.52: Shear Stress for 24mm Wide Mixing Section LDPE (left) vs HDPE (right)

$$\tau_{LDPE} = 44.2 + 1.99\,N + 6.05\,\frac{Q}{N} \tag{5.39}$$

$$\tau_{HDPE} = 41.5 + 1\,N + 4\,\frac{Q}{N} \tag{5.40}$$

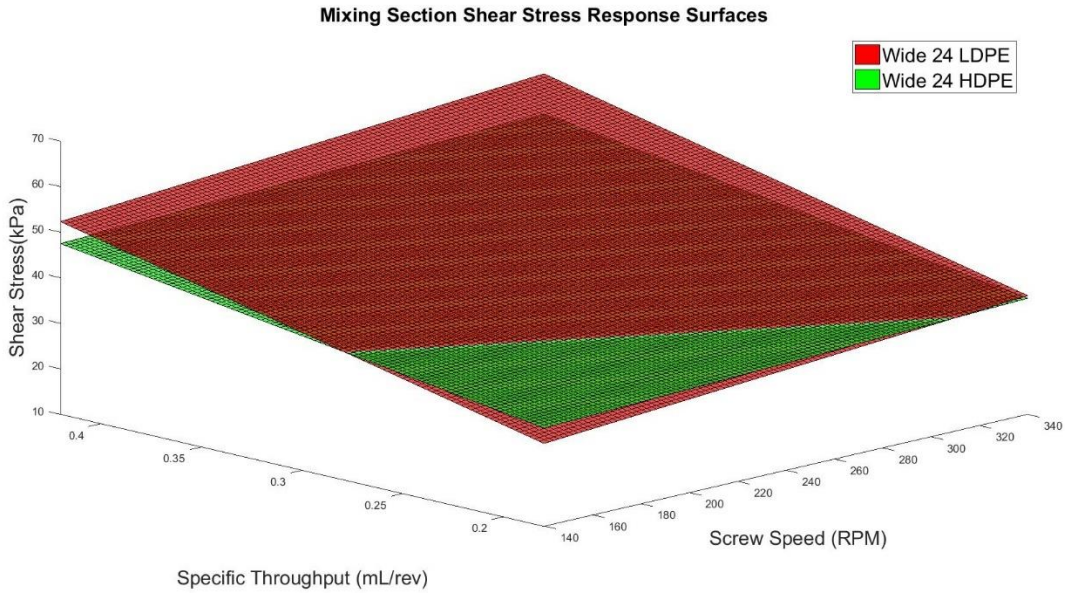


Figure 5.53: Surface Plot Comparison between Shear Stress for 24mm Wide Mixing Section

Screw Configuration – 48mm Mixing Section (Narrow)

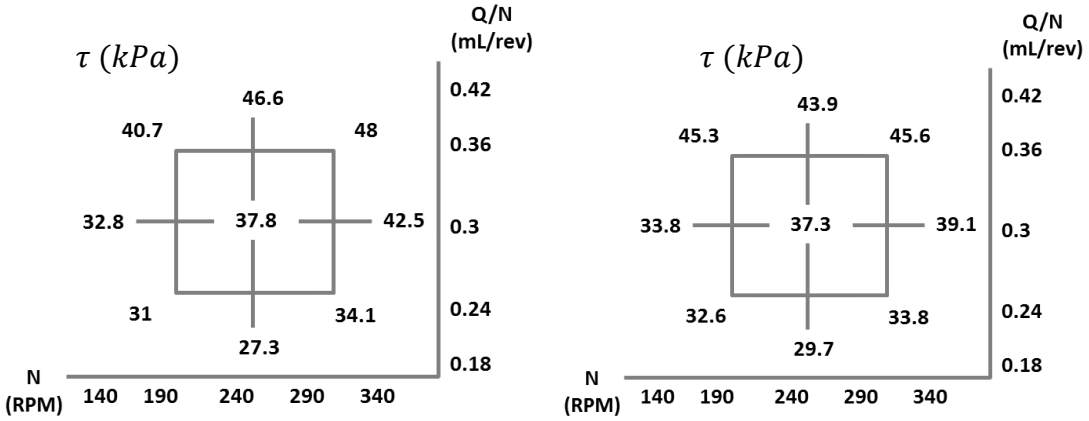


Figure 5.54: Shear Stress for 48mm Narrow Mixing Section LDPE (left) vs HDPE (right)

$$\tau_{LDPE} = 38.6 + 2.5\,N + 5.2\,\frac{Q}{N} \tag{5.41}$$

$$\tau_{HDPE} = 39.4 + 1.05\,N + 4.43\,\frac{Q}{N} \tag{5.42}$$

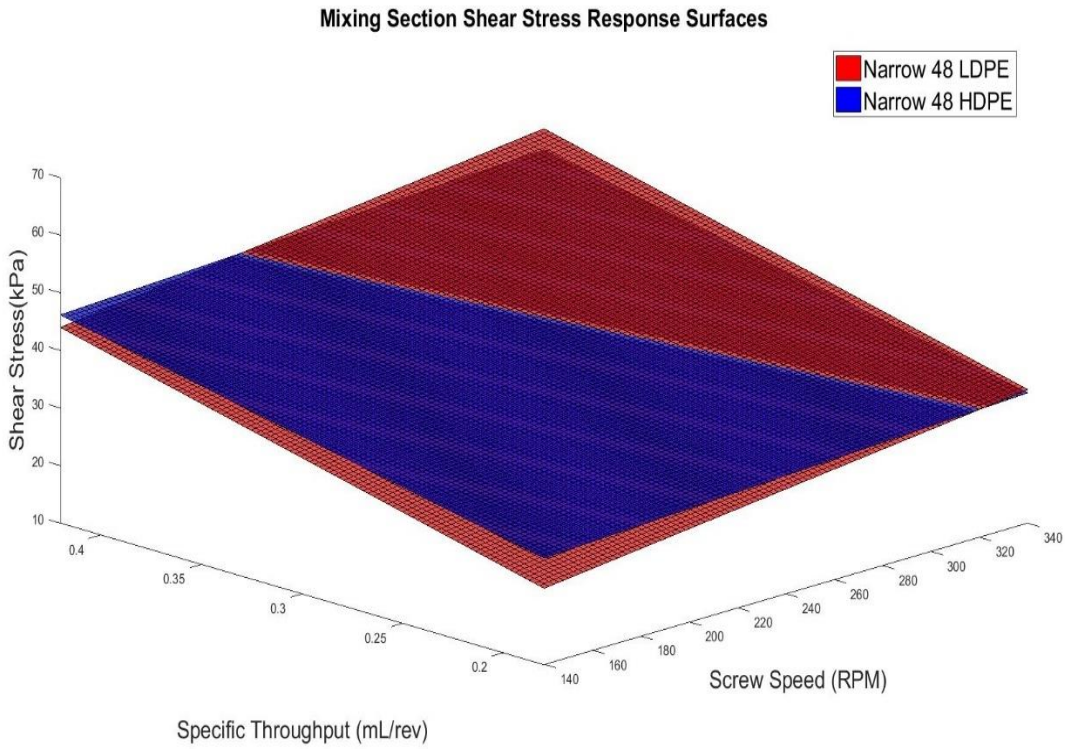


Figure 5.55: Surface Plot Comparison between Shear Stress for 48mm Narrow Mixing Section

Screw Configuration – 48mm Mixing Section (Wide)

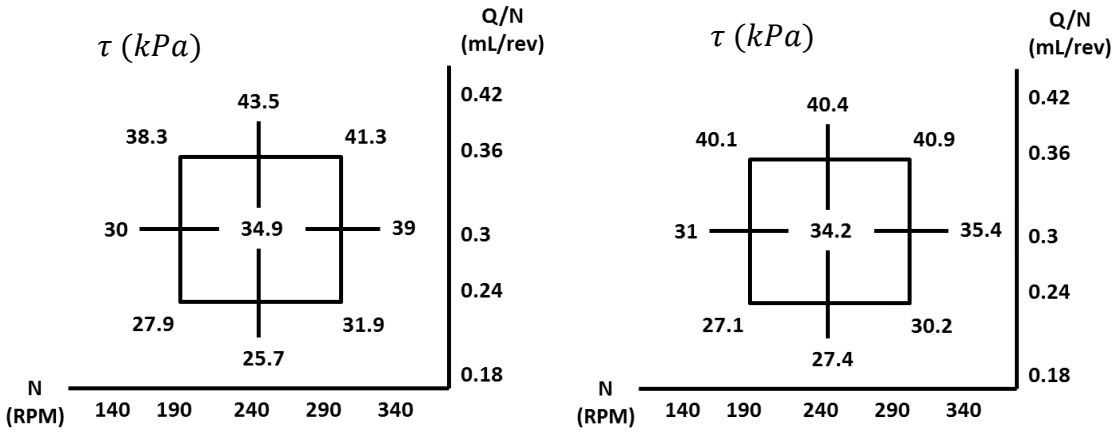


Figure 5.56: Shear Stress for 48mm Wide Mixing Section LDPE (left) vs HDPE (right)

$$\tau_{LDPE} = 35 + 2.1\,N + 4.6\,\frac{Q}{N} \tag{5.43}$$

$$\tau_{HDPE} = 34.8 + 1.1\,N + 4.1\,\frac{Q}{N} \tag{5.44}$$

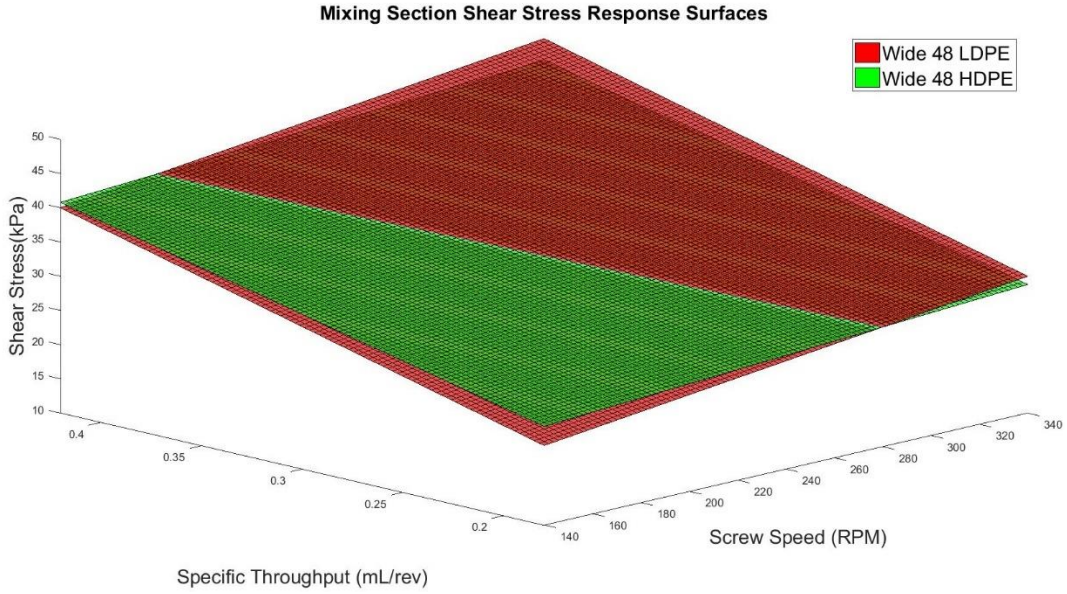


Figure 5.57: Surface Plot Comparison between Shear Stress for 48mm Wide Mixing Section

Fig 5.50-5.57 provides the experimental results obtained for shear stress developed in the mixing section of the TSE for HDPE and LDPE at four different screw configurations. The

shear stress values for HDPE is higher compared to LDPE at lower screw speed (N) and lower specific throughput (Q/N) but when the screw speed and specific throughput increases the shear stress for HDPE is higher compared to LDPE. The influence of screw speed and specific throughput is higher for LDPE compared to HDPE due to the larger magnitudes of the coefficient of N and Q/N. As the narrow kneading blocks in the mixing section are replaced by the wider kneading blocks, the coefficient of N increases while the coefficient of Q/N decreases for both LDPE and HDPE. The results provided based on the comparison between HDPE and LDPE for shear stress are not consistent with the Percent Break-Up results. The percent break-up for LDPE is higher when the mixing section is 24mm long, however, when the length of the mixing section is doubled the percent break-up of HDPE is slightly higher than HDPE. There are two types of stress – shear stress and extensional stress. Since the shear stress values are not consistent with all the %BU trends, there is a need to evaluate the extensional stress component to infer about the %BU trends.

### 5.2.6 Maximum Pressure in the Mixing Section

This section compares the pressure (in psi) developed in the mixing section for HDPE and LDPE. The comparisons have been made for each screw configuration in the form of CCD grids and based on the predictive equations developed post statistical analysis using JMP, the MATLAB surface plots have been created to provide a better understanding of the trends in the results generated.

Screw Configuration – 24mm Mixing Section (Narrow)

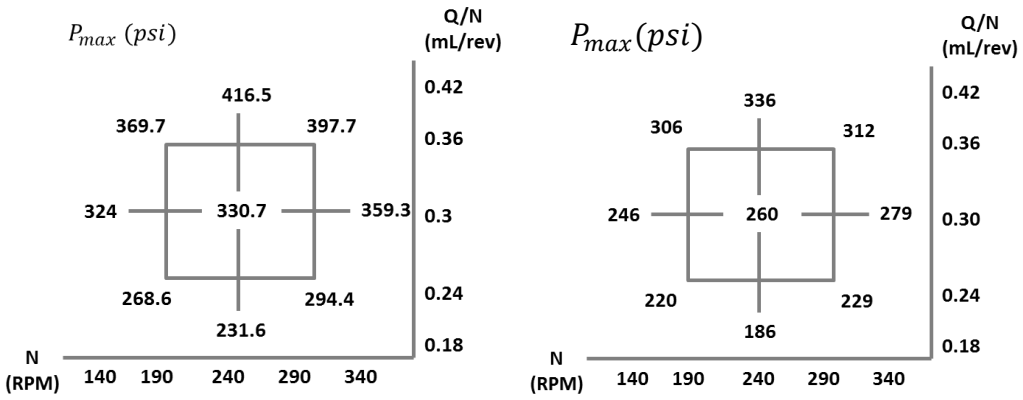


Figure 5.58: Maximum Pressure in the Mixing Section 24mm LDPE - Left and HDPE – Right

$$P_{max_{LDPE}} = 331.4 + 10.3N + 47.8\frac{Q}{N} \quad (5.45)$$

$$P_{max_{HDPE}} = 265.3 + 6.82\,N + 39\frac{Q}{N} \quad (5.46)$$

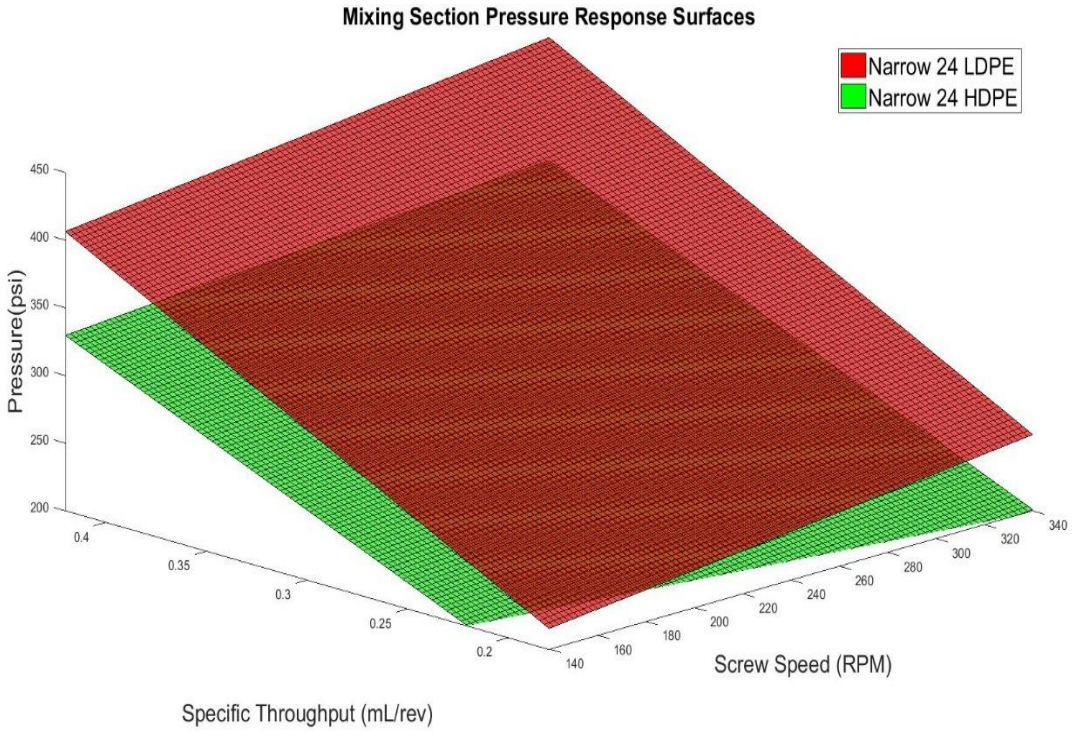


Figure 5.59: Surface Plot Comparison between Pressure for 24mm Narrow Mixing Section

Screw Configuration – 24mm Mixing Section (Wide)

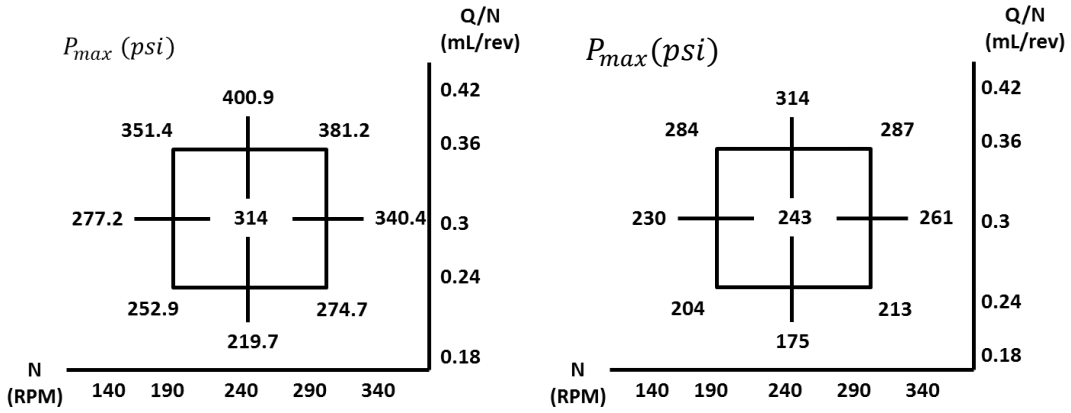


Figure 5.60: Maximum Pressure in the Mixing Section 24mm LDPE - Left and HDPE – Right

$$P_{max_{LDPE}} = 316.9 + 14.8N + 47.2\frac{Q}{N} \quad (5.47)$$

$$P_{max_{HDPE}} = 251.7 + 3.9\,N + 33.9\frac{Q}{N} \quad (5.48)$$

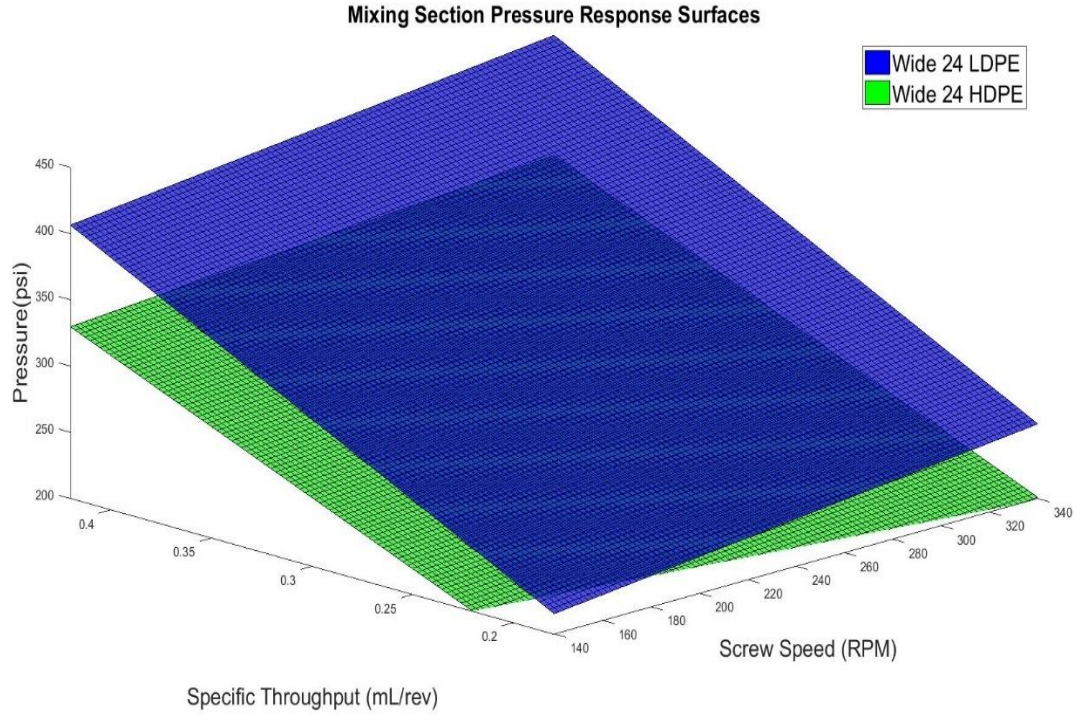


Figure 5.61: Surface Plot Comparison between Pressure for 24mm Wide Mixing Section

Screw Configuration – 48mm Mixing Section (Narrow)

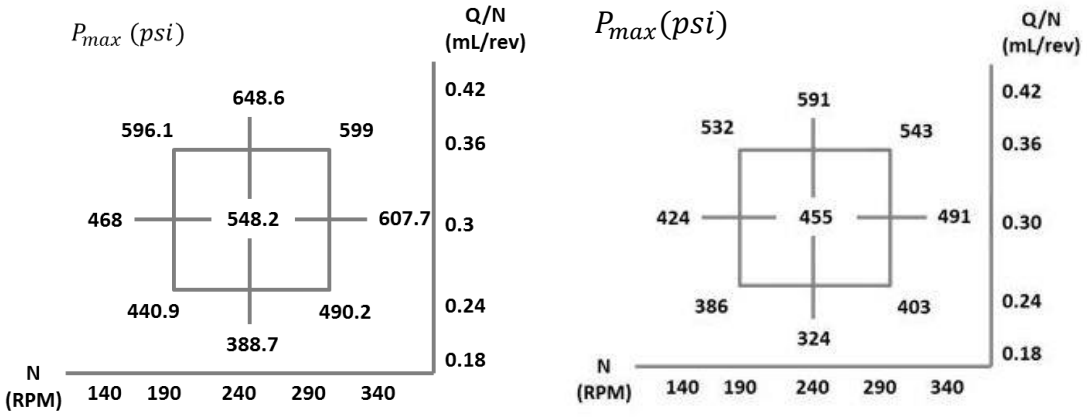


Figure 5.62: Maximum Pressure in the Mixing Section LDPE - Left and HDPE – Right

$$P_{max_{LDPE}} = 542.3 + 27.6N + 65.3\frac{Q}{N} \quad (5.49)$$

$$P_{max_{HDPE}} = 463.6 + 13.5\,N + 68.3\frac{Q}{N} \quad (5.50)$$

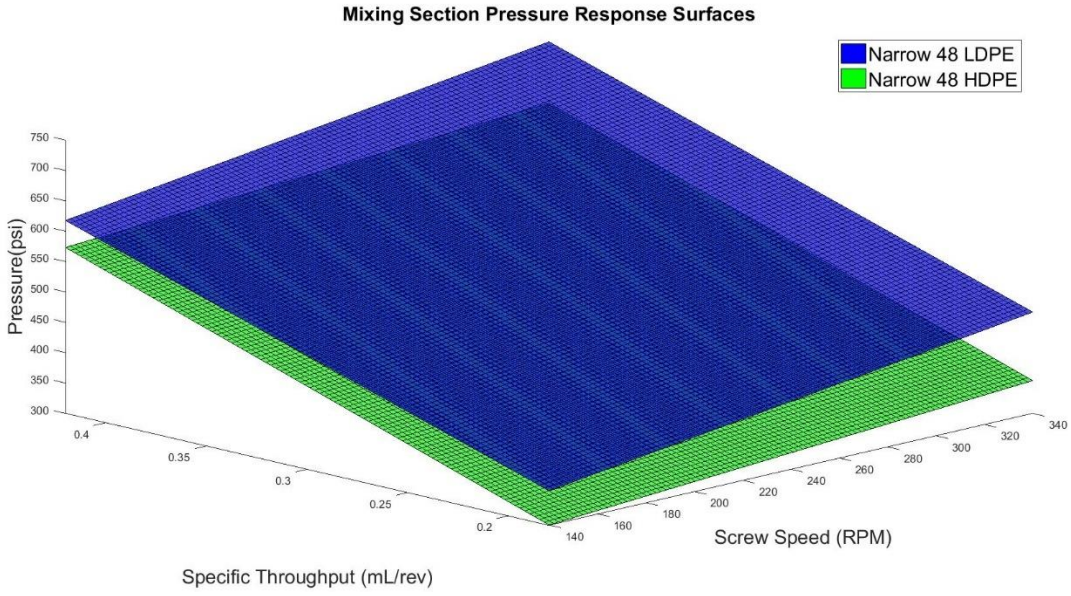


Figure 5.63: Surface Plot Comparison between Pressure for 48mm Narrow Mixing Section

Screw Configuration – 48mm Mixing Section (Wide)

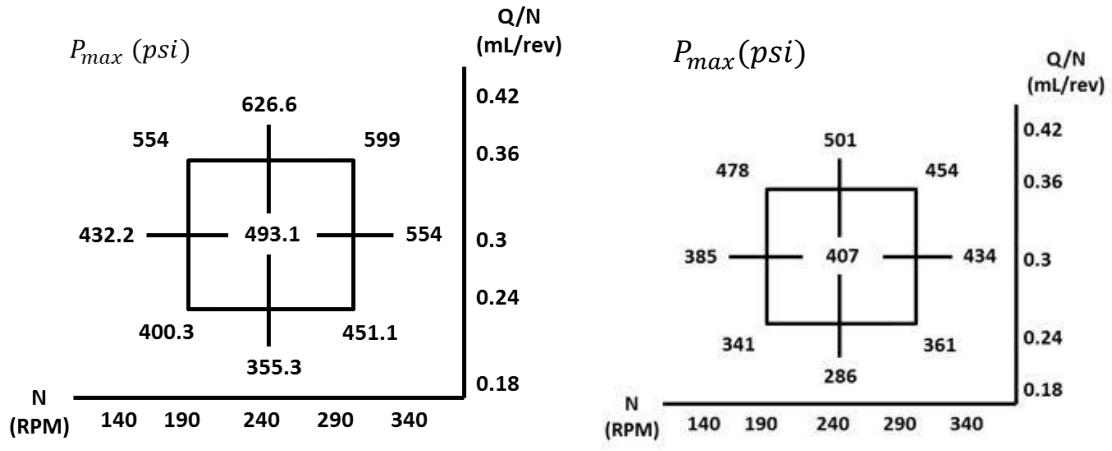


Figure 5.64: Maximum Pressure in the Mixing Section LDPE - Left and HDPE – Right

$$P_{max_{LDPE}} = 500.6 + 28.3N + 70.2\frac{Q}{N} \quad (5.51)$$

$$P_{max_{HDPE}} = 410.7 + 7.9\,N + 55.1\frac{Q}{N} \quad (5.52)$$

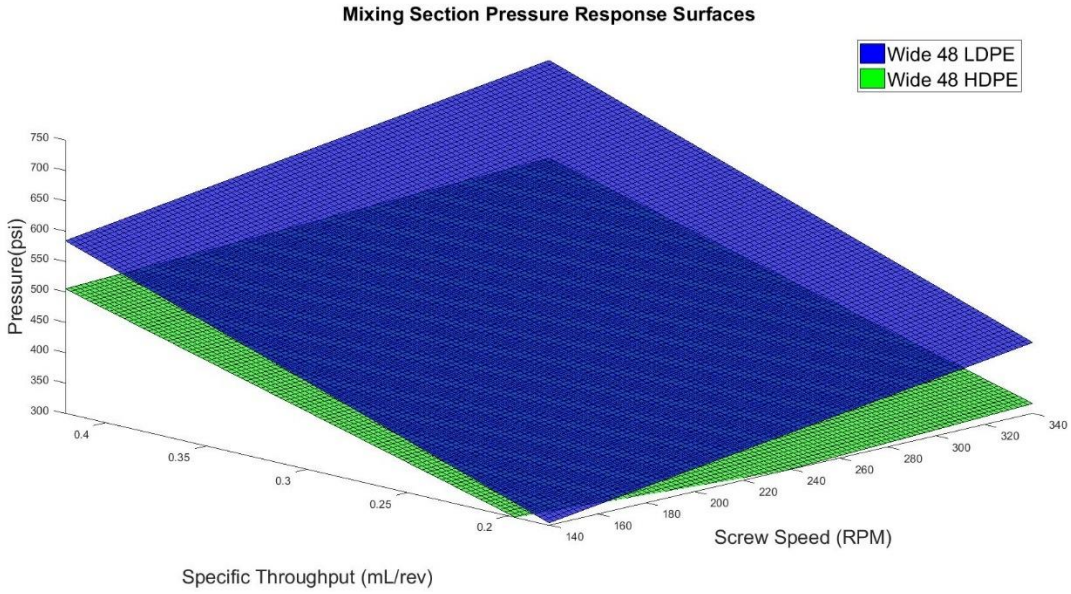


Figure 5.65: Surface Plot Comparison between Pressure for 48mm Narrow Mixing Section

Fig 5.58 - 5.65 provides a comparison between the maximum values of pressure generated when processing LDPE and HDPE in the twin screw extruder. Across all the screw configurations, it is observed that the pressure in the mixing section is higher for LDPE compared to HDPE. The intercept values of pressure are higher for LDPE compared to HDPE. Similarly, the coefficient of N and Q/N is higher for LDPE compared to HDPE implying that change in operating conditions has a greater influence on the pressure generated in the mixing section for LDPE compared to HDPE. The intercept values and coefficients of N and Q/N increases when the mixing section length is doubled. However, when the narrow kneading blocks in the mixing section is replaced by wide kneading blocks, the pressure term decreases. The pressure generated in LDPE is higher compared to HDPE because of the fill length (discussed in Chapter 6) of the screw channel. The degree of fill was simulated by Ludovic and based on the length of the fully filled zone in the screw channel, which was calculated using the graph plotted by Ludovic; it was observed that for LDPE, the channel is fully filled (100%) for a longer portion of the mixing section compared to HDPE. This requires higher pressure to push the polymer melt towards the die.

### 5.2.7 Residence Time in the Mixing Section

This section discusses the comparison between the residence time of HDPE and LDPE in the mixing section of the extruder. The results are displayed in the form of CCD grids for all the four screw configurations. MATLAB surface plots are displayed based on the predictive equations generated by statistically analyzing the data using JMP 12.2.

Screw Configuration – 24mm Narrow Mixing Section

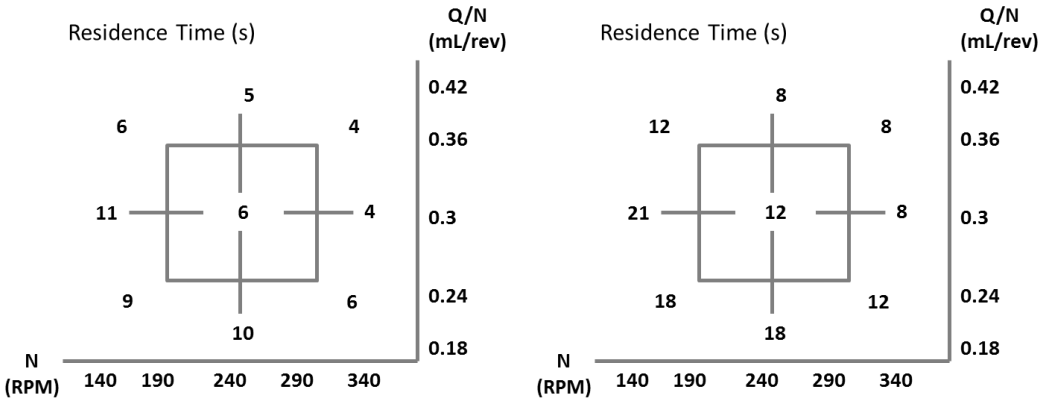


Figure 5.66: Residence Time in the Mixing Section LDPE - Left and HDPE – Right

$$t_{mix_{LDPE}} = 5.5 - 1.6\,N - 1.25\,\frac{Q}{N} \tag{5.53}$$

$$t_{mix_{HDPE}} = 11.7 - 3\,N - 2.5\,\frac{Q}{N} \tag{5.54}$$

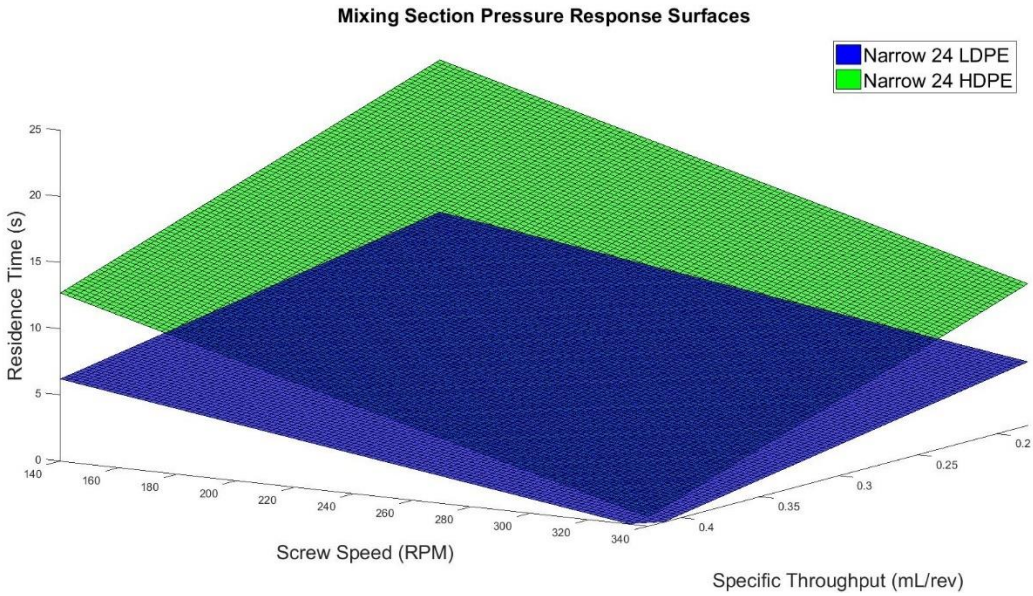


Figure 5.67: Surface Plot Comparison between Residence Time for 24mm Narrow Mixing Section

Screw Configuration – 24mm Wide Mixing Section

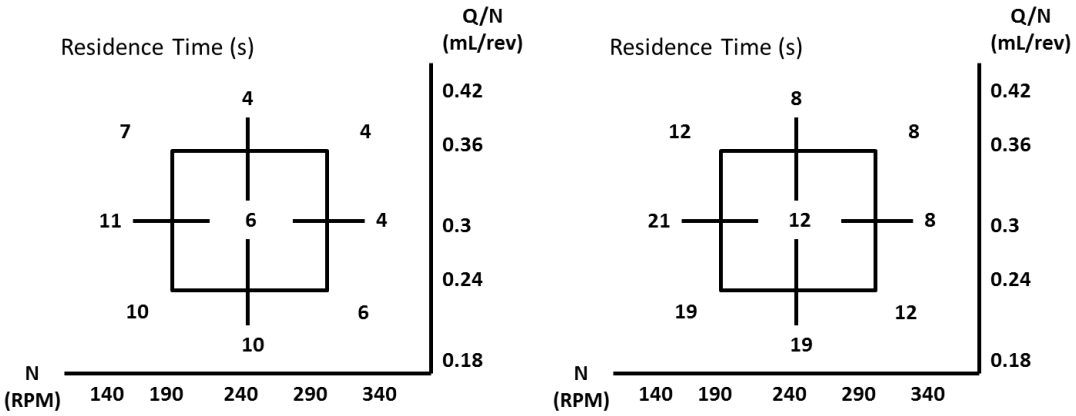


Figure 5.68: Residence Time in the Mixing Section LDPE - Left and HDPE – Right

$$t_{mix_{LDPE}} = 6.1 - 1.75\,N - 1.42\,\frac{Q}{N} \tag{5.55}$$

$$t_{mix_{HDPE}} = 11.8 - 3.1\,N - 2.75\,\frac{Q}{N} \tag{5.56}$$

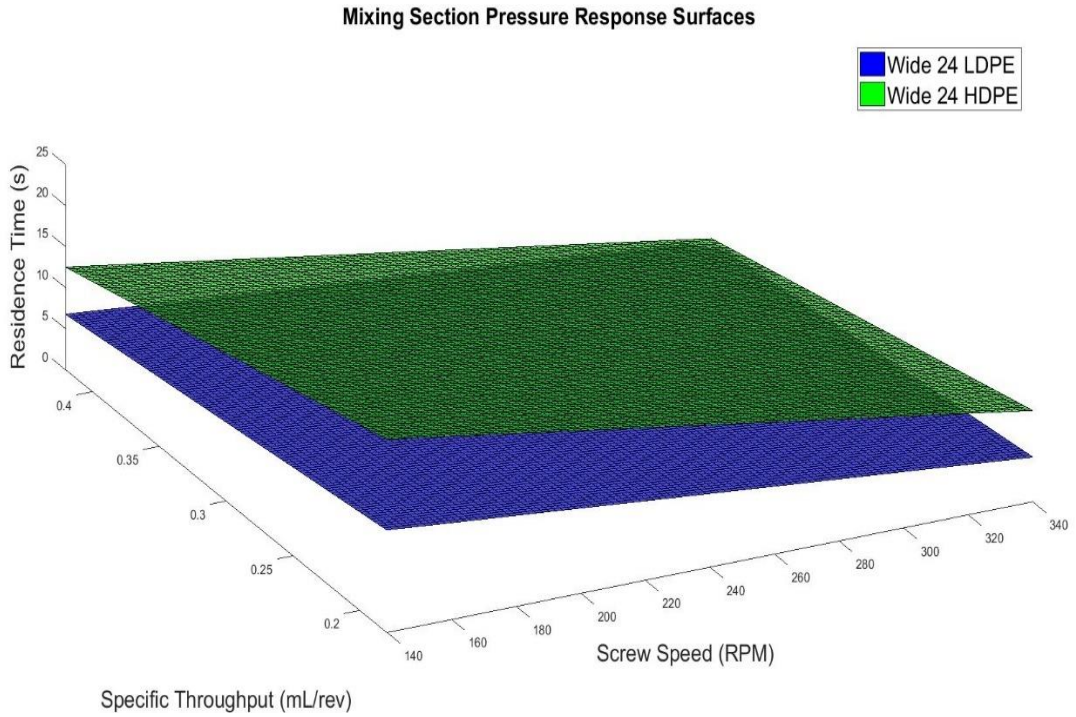


Figure 5.69: Surface Plot Comparison between Residence Time for 24mm Wide Mixing Section

Screw Configuration – 48mm Narrow Mixing Section

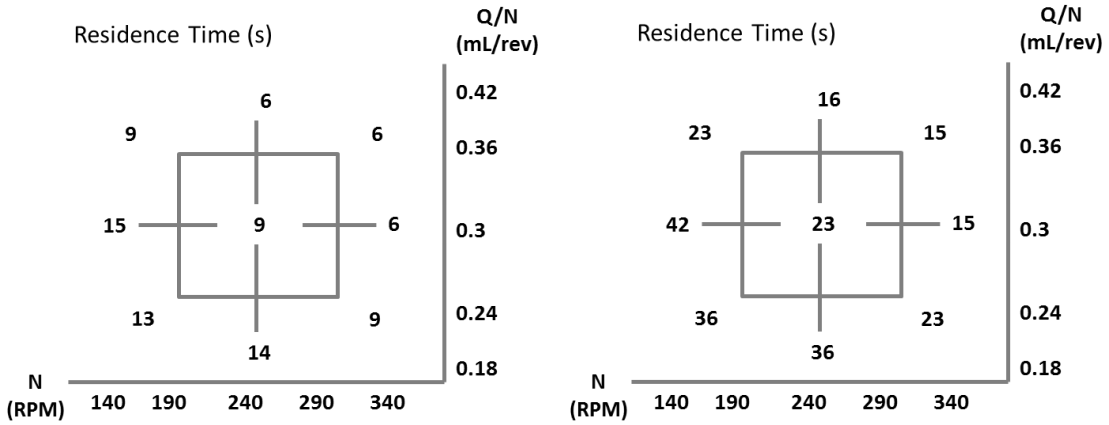


Figure 5.70: Residence Time in the Mixing Section LDPE - Left and HDPE – Right

$$t_{mix_{LDPE}} = 8.7 - 2.1\,N - 1.9\,\frac{Q}{N} \tag{5.57}$$

$$t_{mix_{HDPE}} = 22.2 - 6.25\,N - 5.1\,\frac{Q}{N} \tag{5.58}$$

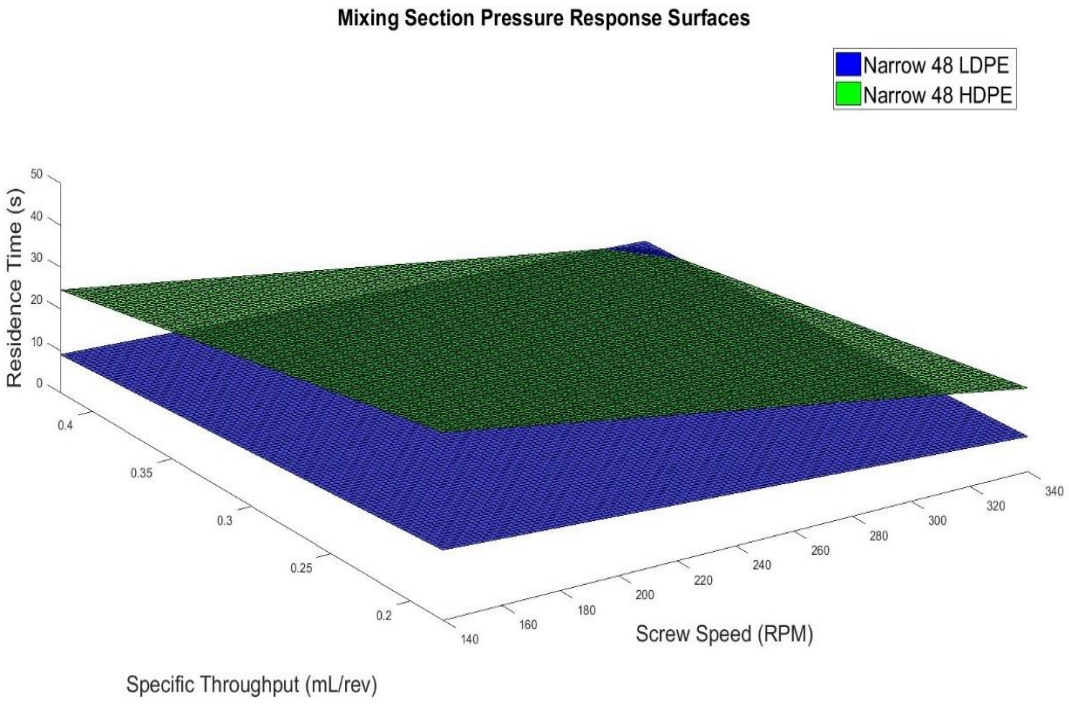


Figure 5.71: Surface Plot Comparison between Residence Time for 48mm Narrow Mixing Section

Screw Configuration – 48mm Wide Mixing Section

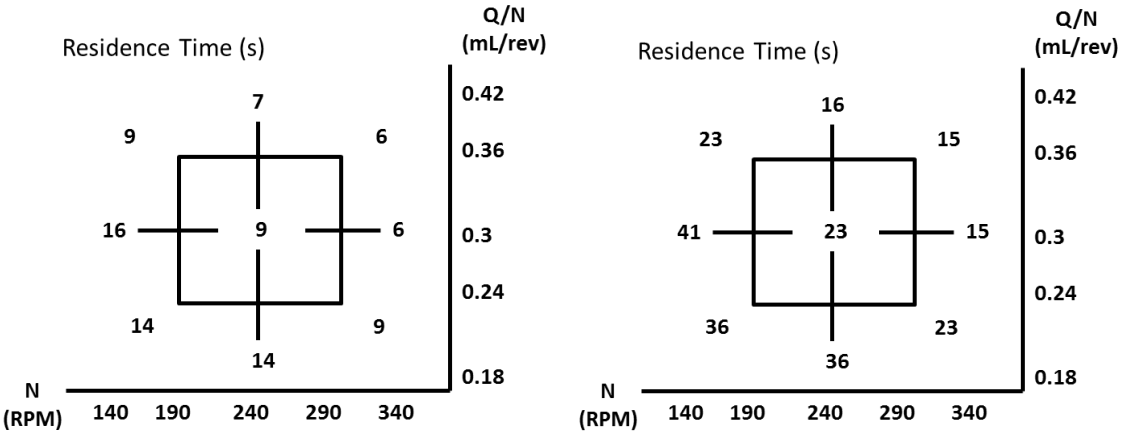


Figure 5.72: Residence Time in the Mixing Section LDPE - Left and HDPE – Right

$$t_{mix_{LDPE}} = 8.7 - 2.3\,N - 1.85\,\frac{Q}{N} \quad (5.59)$$

$$t_{mix_{HDPE}} = 22.2 - 6.1\,N - 5.1\,\frac{Q}{N} \quad (5.60)$$

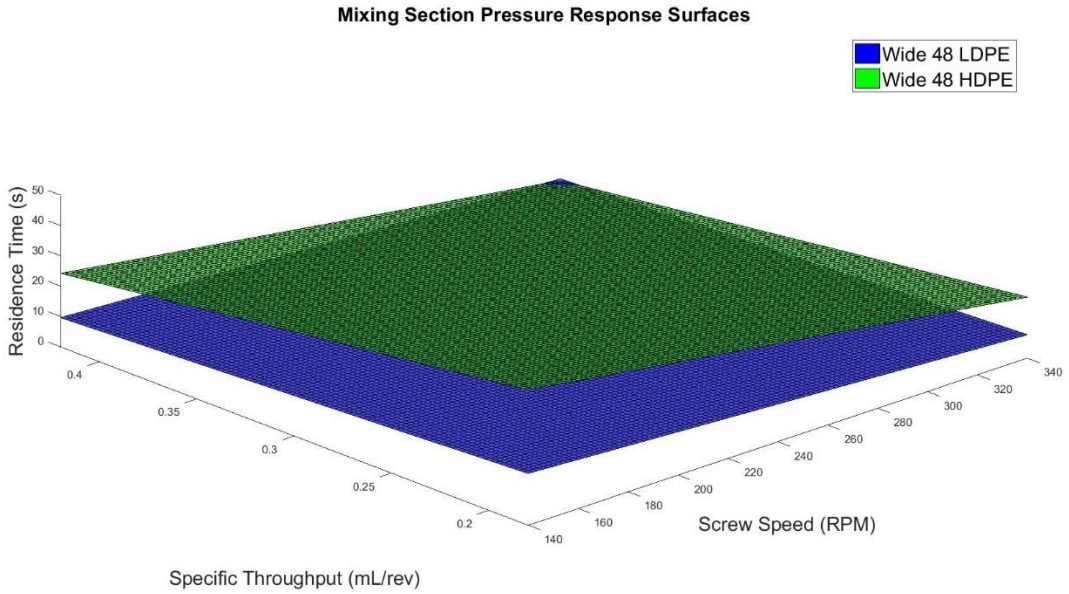


Figure 5.73: Surface Plot Comparison between Residence Time for 48mm Wide Mixing Section

Fig 5.66 - 5.73 provides a comparison between the residence time spent by LDPE and HDPE in the mixing section of the extruder. From the results, it can be seen that HDPE has a higher residence time in the mixing section compared to the LDPE. As the length of the mixing section is doubled, the residence time increases for both HDPE and LDPE but the magnitude of increase is higher for HDPE compared to LDPE. When the narrow kneading blocks in the mixing section are replaced by wider kneading blocks, there is a slight increase in the residence time for both LDPE and HDPE. The influence of the operating conditions on the residence time is higher for HDPE compared to LDPE due to the higher coefficient values of N and Q/N. The intercepts of residence time (obtained by computing the average of the residence time across all the 9 CCD grid points) are higher for HDPE compared to LDPE. This can be related to the degree of fill because LDPE has a higher fill length (100% fill) in the mixing section compared to HDPE. The higher the degree of fill; the lesser the residence time in the mixing section.

### 5.2.8 Maximum Number of revolutions in the mixing section

This section compares the number of revolutions taken by LDPE and HDPE to travel along the mixing section towards the die. The number of revolutions were calculated using Eq. 5.4 for all the screw configurations for both HDPE and LDPE using a CCD grid. The predictive equations generated based on the statistical analysis performed using JMP have been surface plotted using MATLAB to understand the differences in the results generated by HDPE and LDPE.

Screw Configuration – 24mm Narrow Mixing Section

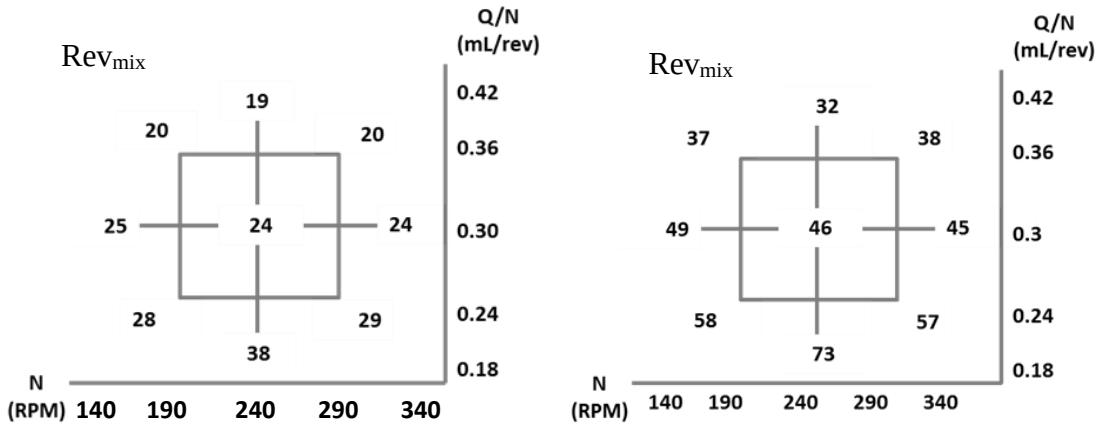


Figure 5.74: Number of Revolutions in the Mixing Section LDPE - Left and HDPE – Right

$$Rev_{mix_{LDPE}} = 23.1 - 4.58\ Q/N \tag{5.61}$$

$$Rev_{mix_{HDPE}} = 45.7 - 10.2\ Q/N \tag{5.62}$$

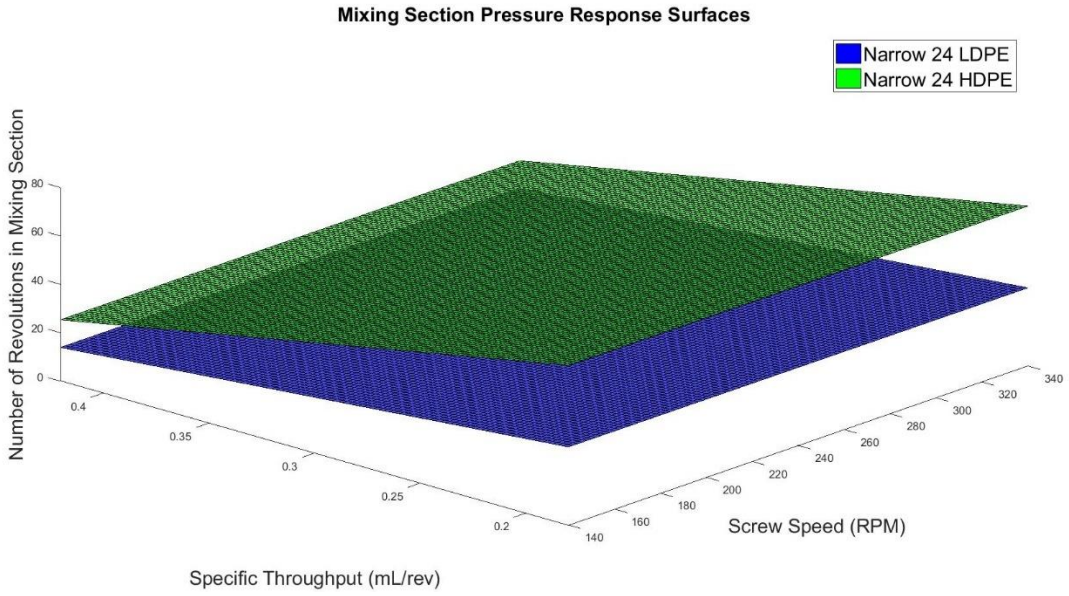


Figure 5.75: Surface Plot Comparison between Rev$_{mix}$ for 24mm Narrow Mixing Section

Screw Configuration – 24mm Wide Mixing Section

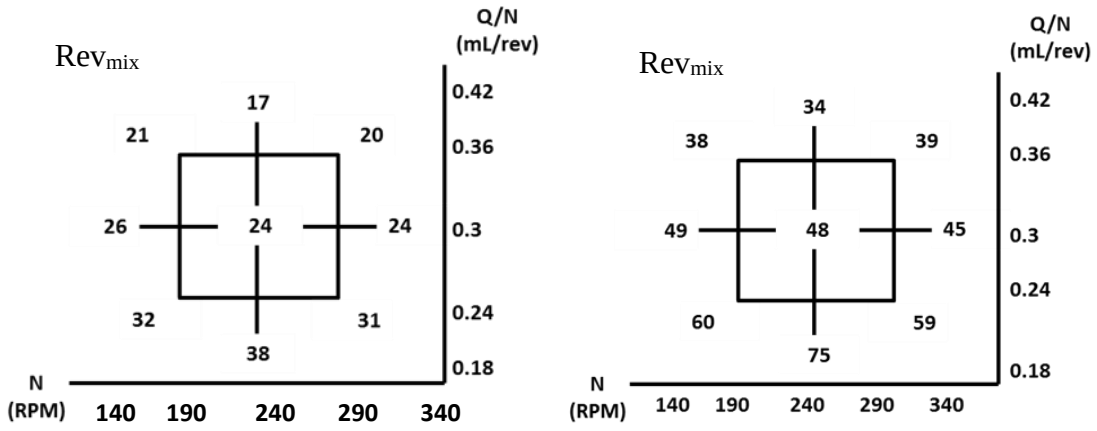


Figure 5.76: Number of Revolutions in the Mixing Section LDPE - Left and HDPE – Right

$$Rev_{mix_{LDPE}} = 24.8 - 5.33\ Q/N \tag{5.63}$$

$$Rev_{mix_{HDPE}} = 47.7 - 10.3\ Q/N \tag{5.64}$$

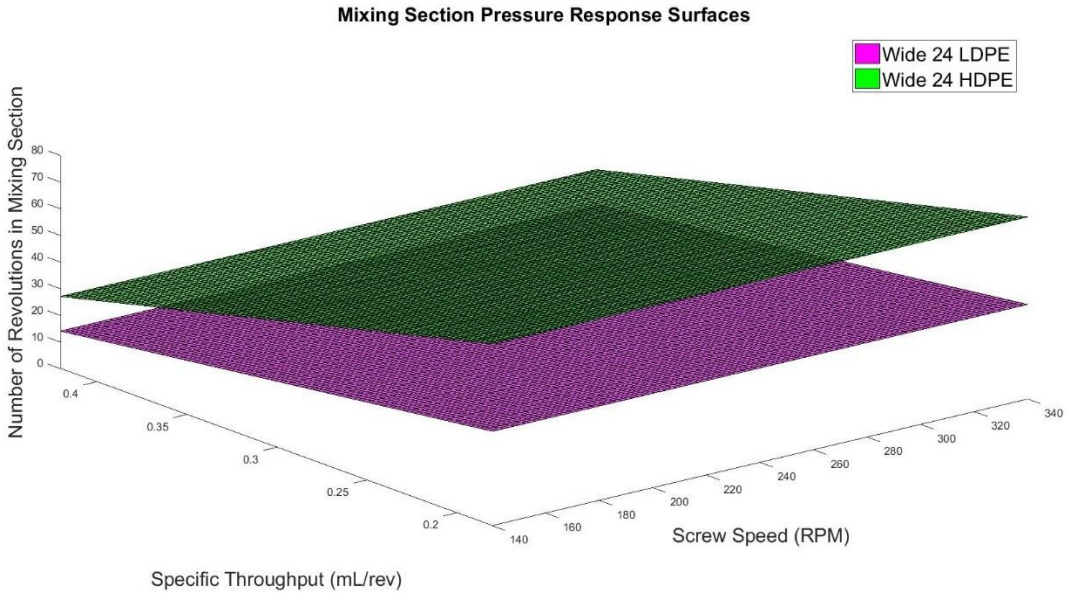


Figure 5.77: Surface Plot Comparison between $Rev_{mix}$ for 24mm Wide Mixing Section

Screw Configuration – 48mm Narrow Mixing Section

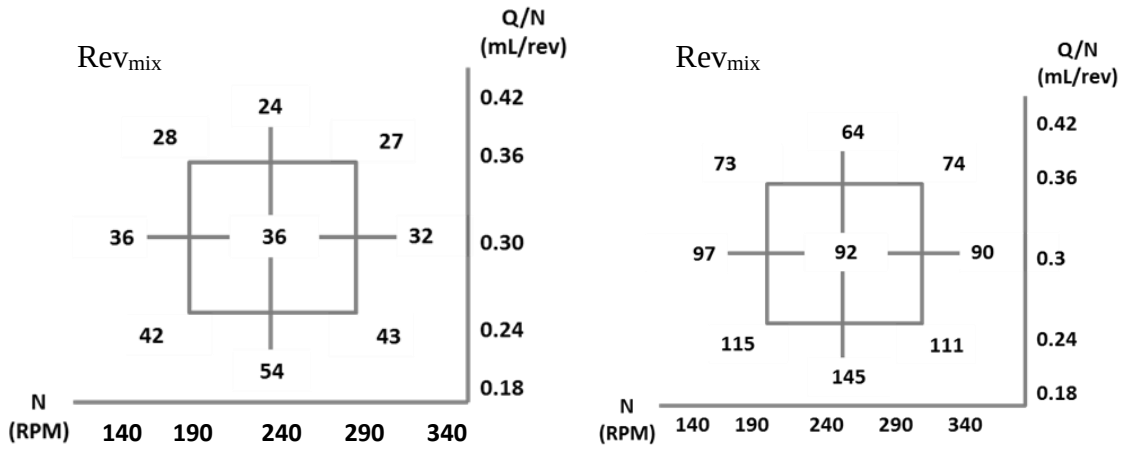


Figure 5.78: Number of Revolutions in the Mixing Section LDPE - Left and HDPE – Right

$$Rev_{mix_{LDPE}} = 34.9 - 7.5\ Q/N \tag{5.65}$$

$$Rev_{mix_{HDPE}} = 90 - 20.1\ Q/N \tag{5.66}$$

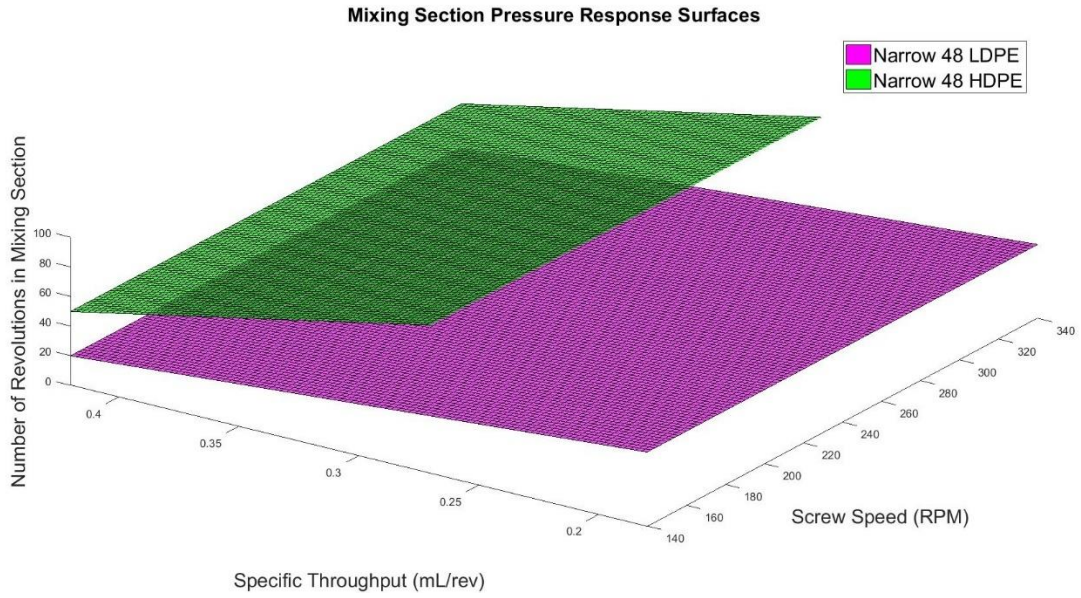


Figure 5.79: Surface Plot Comparison between $Rev_{mix}$ for 48mm Narrow Mixing Section

Screw Configuration – 48mm Wide Mixing Section

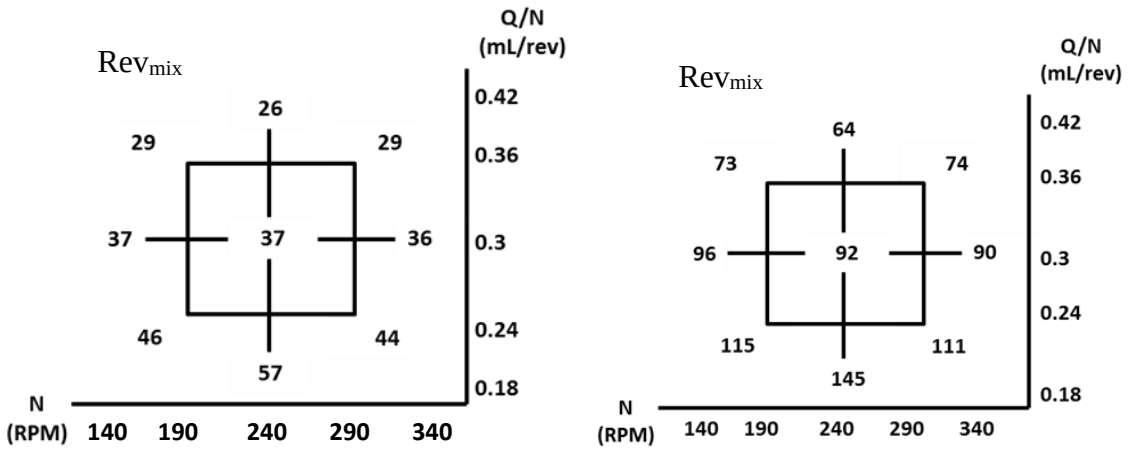


Figure 5.80: Number of Revolutions in the Mixing Section LDPE - Left and HDPE – Right

$$Rev_{mix_{LDPE}} = 36.1 - 7.8\ Q/N \tag{5.67}$$

$$Rev_{mix_{HDPE}} = 90 - 20.1\ Q/N \tag{5.68}$$

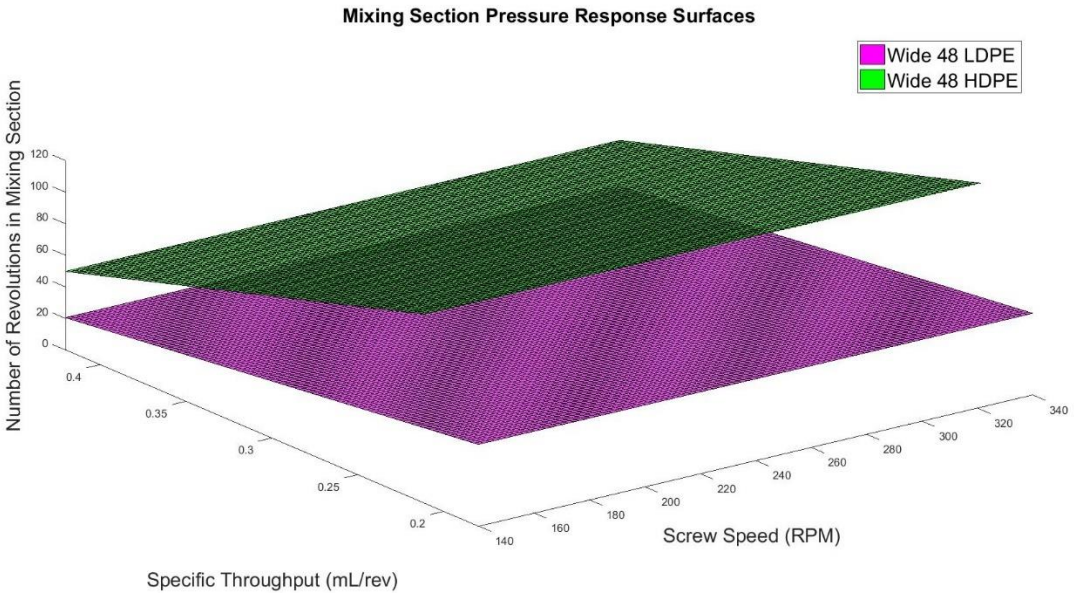


Figure 5.81: Surface Plot Comparison between Rev$_{mix}$ for 48mm Wide Mixing Section

Fig 5.74 - 5.81 displays the comparison between the number of revolutions taken by LDPE to pass through the mixing section with HDPE. The number of revolutions taken by the polymer melt is strongly dependent on Q/N (specific throughput); it is almost a constant at

a fixed Q/N when the screw speed (N) is changed. The number of revolutions taken by HDPE to pass the mixing section is larger than the number of revolutions taken by LDPE. LDPE has a longer fill length (100% fill) in the mixing section compared to HDPE, which is a major contributor in pushing the material towards the die in a shorter number of revolutions of the screw. The number of revolutions increases when the length of the mixing section is doubled for both LDPE and HDPE; the magnitude of change for HDPE is greater compared to LDPE. The intercept values of $Rev_{mix}$ increase as the screw configuration is replaced by wider kneading block and when the length of the mixing section is doubled. Similarly, the coefficients of Q/N increases from Fig 5.74 – Fig 5.81 i.e. with change in screw configuration for both the polymer melts. The degree of fill / fill length is an important factor that contributes towards the changes in the results. This will be discussed in Chapter 6**.**

Section 5.2 provided a detailed comparison between the behaviors exhibited by two base polymers i.e. HDPE and LDPE for the same screw configuration (4 screw geometries of 18mm TSE). The results indicate that the morphology of the polymer plays an important role in influencing the mixing behavior observed as a result of the percent break-up results. Shear stress is not the only factor that contributes towards the break-up of the CAMES beads, even though the shear stress results for a particular screw configuration comply with %BU results. (Extensional stress, which is another component of stress could be a contributing factor which could provide further insight into the observed results.**)** HDPE has a lesser fill length compared to LDPE and is a driving factor behind the results observed for pressure, residence time and number of revolutions.

## 5.3 Scale – Up Results – Comparison of 18mm vs 26mm TSE using HDPE

The main purpose of scale-up is to accurately replicate the processes performed on small scale laboratory equipment to large scale industrial operations. In this case, scale-up is used to main a particular level of dispersive mixing behavior when operating across various sizes of extruders. Volumetric scale -up is a method used to a great extent by industries; the ideology behind volumetric scale-up was to geometrically scale-up from a small scale to a large-scale extruder. Eq. 5.69 shows the scaling factor relationship with the operating conditions. The second scale-up methodology is based on establishing a relationship between the operating conditions of the different sizes of extruders by maintaining the same percent drag flow [45]. Percent drag-flow is an effective tool to study the dispersive mixing behavior; the focus of percent-drag scale up approach is to achieve a similar flow path along the screw channel by maintaining the same percent drag flow. The scale-up factor for each of these methods is established using the following relationship:

Volumetric Scale-Up

$$\frac{Q_{26\,mm}}{Q_{18\,mm}} \propto \left(\frac{D_{26\,mm}}{D_{18\,mm}}\right)^3 \rightarrow scaling\ factor \tag{5.69}$$

Where D is the base diameter, Q/N is the specific throughput (mL/rev)

Percent Drag Flow Scale-Up

$$\frac{\frac{Q}{N}_{18mm}}{\frac{Q}{N}_{100\%\ 18mm}} = \frac{\frac{Q}{N}_{26mm}}{\frac{Q}{N}_{100\%\ 26mm}} = (\%DF)$$

$$\frac{\frac{Q}{N}_{26\,mm}}{\frac{Q}{N}_{18\,mm}} \rightarrow scaling\ factor \tag{5.70}$$

The accuracy of the two scale-up methods can be proved by comparing the stress histories developed in the extruders. This was done by performing the RSD methodology to compute the percent break-up values. The base polymer used for the scale-up experiments is HDPE. The obtained percent break-up values are validated using Ludovic simulations for both 18mm and 26mm Twin Screw Extruders by comparing the scale-up approaches and how the relationship between the properties (shear rate, viscosity, temperature) varies. The screw geometry discussed in this section is the 48mm long mixing section with Narrow Kneading Blocks for both 18mm and 26mm TSE. The operating conditions have already been discussed in Chapter 4. The results will be provided in the same order as the previous two sections. The obtained datasets will be statistically analyzed using JMP 12.2 to obtain prediction equations relating the results with the operating conditions.

### 5.3.1 Percent Break-Up

This section compares the percent break-up values obtained by performing the RSD experiments on the 18mm and 26mm TSE (Narrow 48mm Mixing Section). The %BU values have been obtained for the TSE based on the two scale-up methods explained in the above section. The obtained data has been statistically analyzed using JMP 12.2 and the intercept and coefficient values for the operating conditions have been listed in Table 5.10.

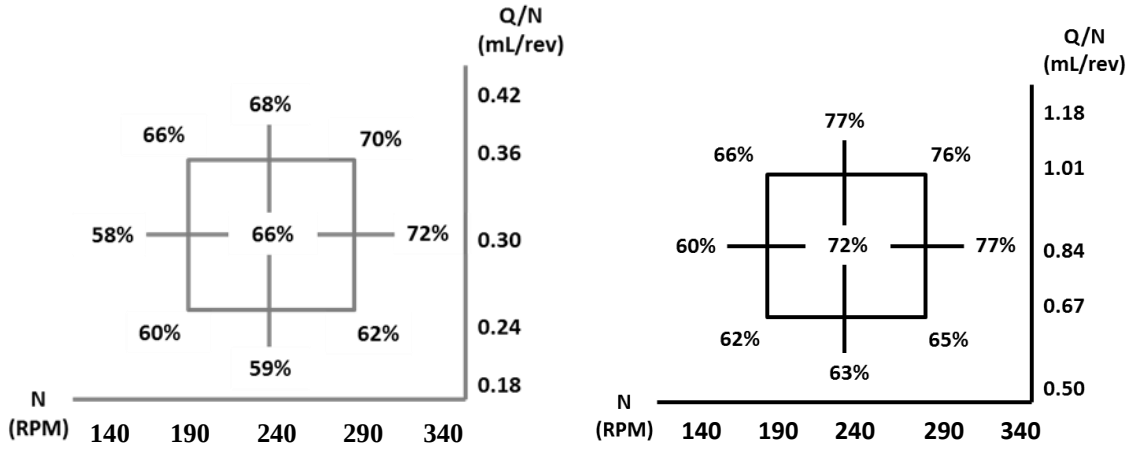


Figure 5.82: % BU comparison for 18mm (left) and 26mm (Volumetric - right)

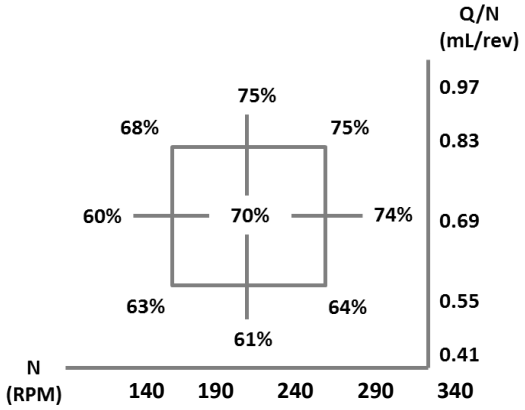


Figure 5.83: %BU comparison for 26mm (% Drag)

Fig 5.82-5.83 reveals the data on the %BU results obtained using RSD Methodology. The three CCD grids seen in Fig 5.88-5.89 compare the %BU results for a 48mm long mixing section with Narrow Kneading blocks when an 18mm and 26mm Twin Screw Extruder is used. %BU increases with screw speed at constant specific throughput (Q/N) as well as increases with specific throughput at constant screw speed (N) in each of the cases. The %BU results obtained from the scaled-up 26mm TSE shows that the scale method using %Drag Flow is comparatively closer to the %BU results obtained from 18mm TSE as compared to the volumetric scale-up approach. To understand the influence of the

operating conditions on the %BU values, the data is statistically analyzed using JMP as seen in Table 5.10.

Table 5.10: Predictive Coefficient for Percent Break-Up

| Extruder Size | COEFFICIENTS | | | |
|---|---|---|---|---|
| | Scale – Up Method | Intercept | $X_N$ | $X_{Q/N}$ |
| 18mm | | 65.4 | 2.83 | 3.86 |
| 26mm | Volumetric | 69 | 3.92 | 3.60 |
| | %Drag Flow | 68.9 | 3 | 3.70 |

Table 5.10 reveals the intercept and coefficient of operating conditions (N, Q/N) for 18mm and 26mm TSE. The intercept values of %BU are higher for 26mm TSE compared to 18mm TSE which implies that average of %BU values across all the CCD grid points is higher for 26mm TSE (using both %Drag Flow and Volumetric scale-up method) compared to the 18mm TSE. Comparing the coefficients of operating conditions; %Drag Scale-Up method reflects values of coefficients of N and Q/N which are closer to the coefficients of N and Q/N for the 18mm TSE implying that the effect of N and Q/N on the %BU values is comparable. The Volumetric Scale-Up using 26mm TSE has a higher coefficient for N and Q/N as well as intercept values for %BU which is due to the fact that the Q/N range is higher for volumetric scale-up CCD grid compared to % drag CCD grid (discussed in Chapter 4). The %BU increases with increase in Q/N at a constant screw speed which explains the higher %BU obtained when using the Volumetric Scale-Up approach compared to %Drag Flow approach.

**Ludovic Results**

## 5.3.2 Maximum Shear Rate in Mixing Section

This section provides a comparison between the shear rate generated in the mixing section for 18mm TSE and 26mm TSE (%Drag Flow and Volumetric Scale-Up). The same screw geometry is used for both 18mm and 26mm i.e. 48mm long mixing section with Narrow Kneading blocks.

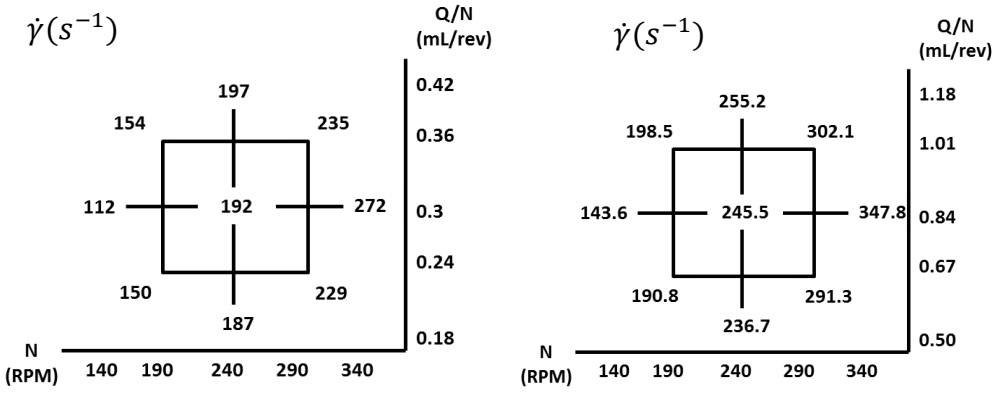


Figure 5.84: Shear Rate comparison for 18mm (left) and 26mm (Volumetric Scale-Up - right)

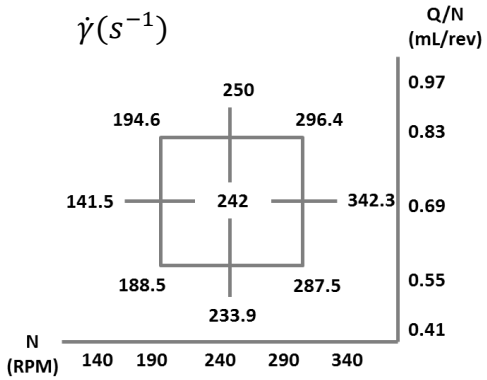


Figure 5.85: Shear rate comparison for 26mm (% Drag Flow Scale-Up)

Figure 5.84-5.85 provide a comparison between the shear rate values obtained for 18mm and 26mm TSE (Volumetric and % Drag Flow Scale-Up). The shear rate values obtained for 18mm TSE is lesser compared to the 26mm TSE; this is due to the fact that shear rate

is highly dependent on the base diameter of the TSE apart from the screw speed and specific throughput. Shear rate increases with increase in the size of the extruder. In the case of 26mm TSE, volumetric scale-up approach has a higher shear rate compared to %drag flow scale-up; this is due to the fact that the specific throughput range is higher for the volumetric CCD grid compared to % Drag Flow CCD grid. Shear rate being slightly dependent on the specific throughput increases with Q/N which leads to a higher shear rate generated when volumetric scale-up approach is used.

Table 5.11: Prediction coefficient for Shear Rate

| Extruder Size | COEFFICIENTS | | | |
|---|---|---|---|---|
| | Scale – Up Method | Intercept | $X_N$ | $X_{Q/N}$ |
| 18mm | | 192 | 40 | 2.5 |
| 26mm | Volumetric | 245.5 | 51 | 4.6 |
| | %Drag Flow | 241 | 50.2 | 3.9 |

Table 5.11 reveals the intercept and coefficient values for shear rate and provides a comparison between the trends observed from the data. The intercept value increases when the extruder size is scaled up from 18mm to 26mm. Similarly, the coefficient of N and Q/N also increases when extruder is scaled up implying that for the 26mm TSE, change in operating conditions leads to a greater change in the shear rate compared to the 18mm TSE. Volumetric Scale-Up approach has a higher intercept value for shear rate compared to % Drag Flow Scale-Up; however, the coefficients of N and Q/N does not differ by a great magnitude.

### 5.3.3 Maximum Temperature in the Mixing Section

This section provides a comparison between the maximum temperature attained by the polymer melt in the mixing section when scaled up from 18mm to 26mm using Volumetric Scale-Up approach and %Drag-Flow Scale-Up approach.

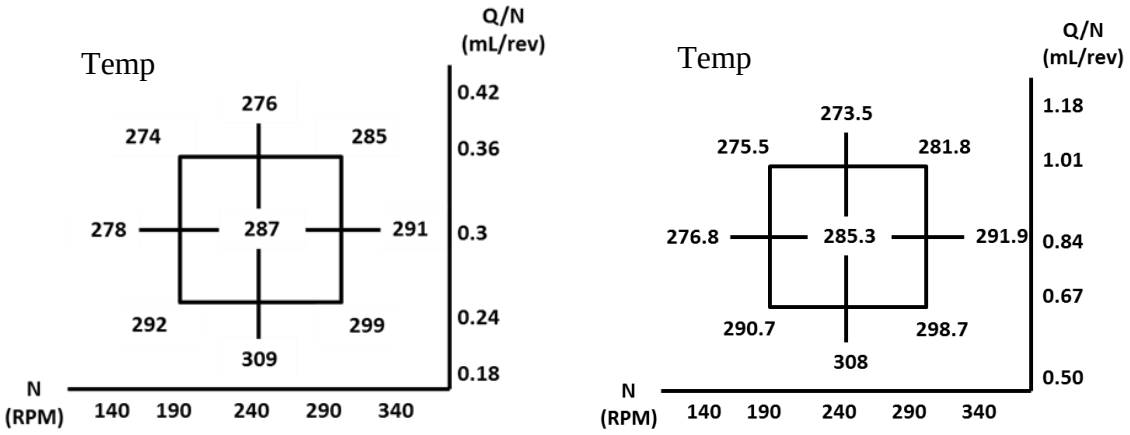


Figure 5.86: Max. Temp comparison for 18mm (left) and 26mm (Volumetric Scale-Up - right)

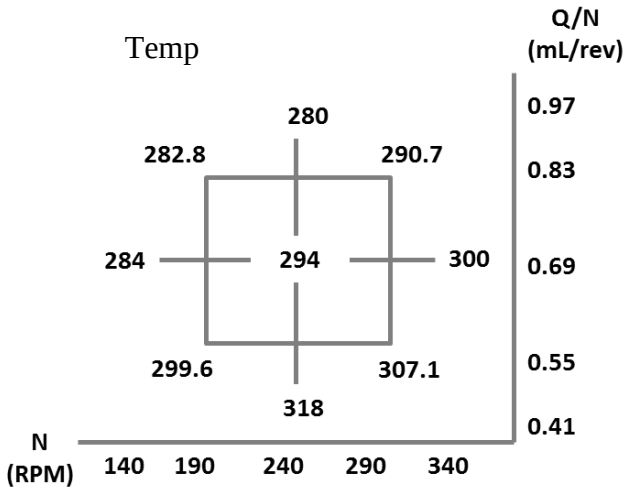


Figure 5.87: Max. Temp comparison for 26mm (% Drag Flow Scale-Up)

Upon Scale-up, the temperature is seen is seen to be higher for the 26mm TSE compared to 18mm TSE. This is due to the fact that when the diameter of the extruder increases, the heat transfer coefficient decreases, which leads to lesser heat being dissipated and the temperature of the melt increases. However, the idea of scale-up is to reduce the variation in the differences in the results, with increase in the size of the extruder. Based on both the

Volumetric and % Drag Flow Scale-Up method, Volumetric scale-up seems to display results that are closer to the results generated by 18mm TSE compared to the Volumetric Grid Scale-Up. Based on observations from the temperature results (Sec 5.2.3) it was seen that temperature of the polymer melt decreases as the mass flow rate increases; Volumetric Scale-Up has a higher specific throughput range compared to % Drag Flow Scale-Up. The common trend observed in each of the grids is that the temperature of the polymer melt increases with increase in screw speed (N). This is due to the fact that as the temperature increases, the shear rate increases leading to more viscous dissipation heating. A melt film is formed in between the barrel wall and the polymer as a result of heat conduction from barrel wall. The melt film is stretched as the screw speed increases, as a result of which the torque required to rotate the screw, is converted as heat which is stored in the polymer melt. This leads to the increase in the temperature of the polymer melt. On the other hand, temperature of the polymer decreases as the specific throughput is increased at a constant screw speed.

Table 5.11: Prediction coefficient for Maximum Temperature in the Mixing Section

| Extruder Size | COEFFICIENTS | | | |
|---|---|---|---|---|
| | Scale – Up Method | Intercept | $X_N$ | $X_{Q/N}$ |
| 18mm | | 279.2 | 3 | -8.8 |
| 26mm | Volumetric | 285.5 | 3.71 | -8.42 |
| | %Drag Flow | 294.3 | 3.95 | -9.1 |

Table 5.11 reveals the intercept and coefficients of operating conditions for temperature of polymer melt in the mixing section for both 18mm and 26mm TSE. The intercept value for temperature is the least of 18mm TSE and it increases for 26mm TSE. Similarly, the coefficient of N is higher for 26mm TSE compared to 18mm implying that change in screw

speed has a higher impact on temperature of the mixing section for the 26mm TSE. However, the coefficient of Q/N is higher for 18mm TSE compared to 26mm Volumetric Scale-Up TSE but lower compared to 26mm % Drag Flow Scale-Up TSE. Based on Table 5.11 it can be seen that % Drag- Flow Scale-Up approach leads to a higher temperature of the polymer melt compared to Volumetric Scale-Up approach.

### 5.3.4 Viscosity in the Mixing Section

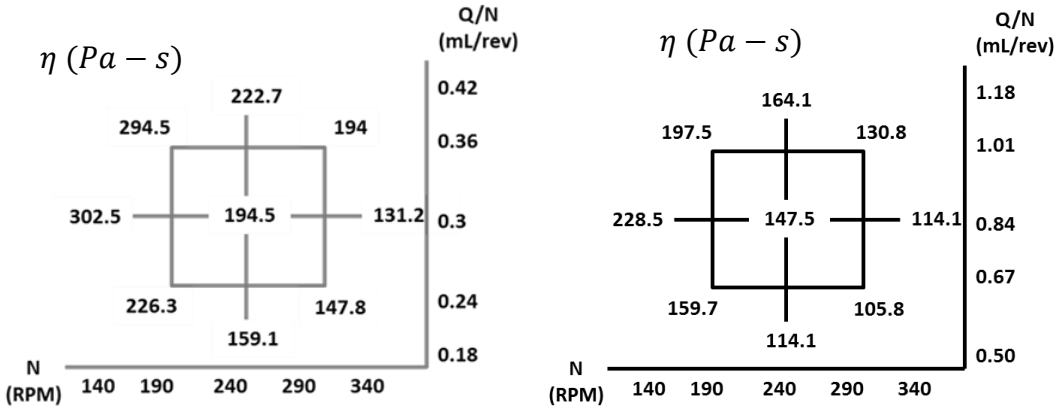


Figure 5.88: Viscosity comparison for 18mm (left) and 26mm (Volumetric Scale-Up - right)

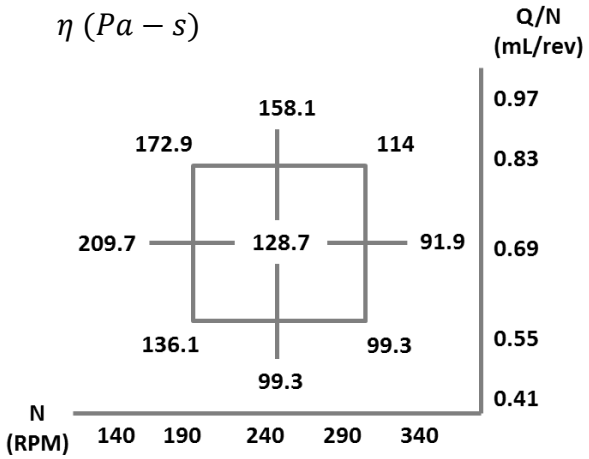


Figure 5.89: Viscosity comparison for 26mm (% Drag Flow Scale-Up)

Fig 5.88 – 5.89 provide comparison on the viscosity data obtained for the Narrow 48mm long Mixing Section screw configuration for 18mm and 26mm TSE. The viscosity trends

for each CCD grid display similar behavior; viscosity increases with increase in specific throughput at constant screw speed and decreases with increase in screw speed at constant specific throughput. However, when comparing the viscosity data between the scale-up geometries, it is observed that viscosity values are higher for 18mm screw configuration compared to 26mm screw configuration. This is due to the fact that the shear rate in the 18mm TSE is lower compared to the 26mm TSE. Similarly, the temperature of the mixing section is lower for the 18mm TSE compared to 26mm TSE. As a result, the lower shear rate and temperature leads to a higher viscosity for the 18mm TSE. In the case of the 26mm TSE, the volumetric scale-up approach gives rise to a higher viscosity compared to the % Drag Flow scale-up approach. Higher mass flow due to higher specific throughput range in case of volumetric scale-up is a factor that results in the higher viscosity values as both the scale-up approaches operate on the same screw speed range.

Table 5.12: Prediction coefficient for Viscosity in the Mixing Section

| Extruder Size | COEFFICIENTS | | | |
|---|---|---|---|---|
| | Scale – Up Method | Intercept | $X_N$ | $X_{Q/N}$ |
| 18mm | | 209.1 | - 43.4 | 19.4 |
| 26mm | Volumetric | 144.9 | - 29.1 | 13.6 |
| | %Drag Flow | 125.4 | - 27.6 | 14.1 |

Table 5.12 compares the intercept and coefficient values for the operating conditions for 18mm and 26mm TSE. As seen from the viscosity data in Fig 5.88-5.89, the intercept values for 18mm TSE is the higher compared to 26mm TSE. The coefficient of screw speed and specific throughput is higher for 18mm screw configuration compared to 26mm screw configuration implying that corresponding change in operating conditions has a greater effect on the viscosity values for the 18mm TSE. Comparing the scale-up approaches, %

Drag Flow method has a lower intercept and coefficient value for screw speed compared to volumetric scale-up. The coefficient values for specific throughput vary by a small margin for both the scale-up approaches.

### 5.3.5 Shear Stress in the Mixing Section

This section provides a comparison between the shear stress generated in the mixing section for the 18mm and 26mm TSE. The shear stress calculations have been explained in Sec 5.2.5; based on the viscosity and the shear rate values obtained from Ludovic simulations, the shear stress values have been calculated as per Eq. 30. The screw configuration used for both the 26mm and 18mm TSE include a mixing section of length 48mm with narrow kneading blocks. The shear stress values have been calculated in kPa.

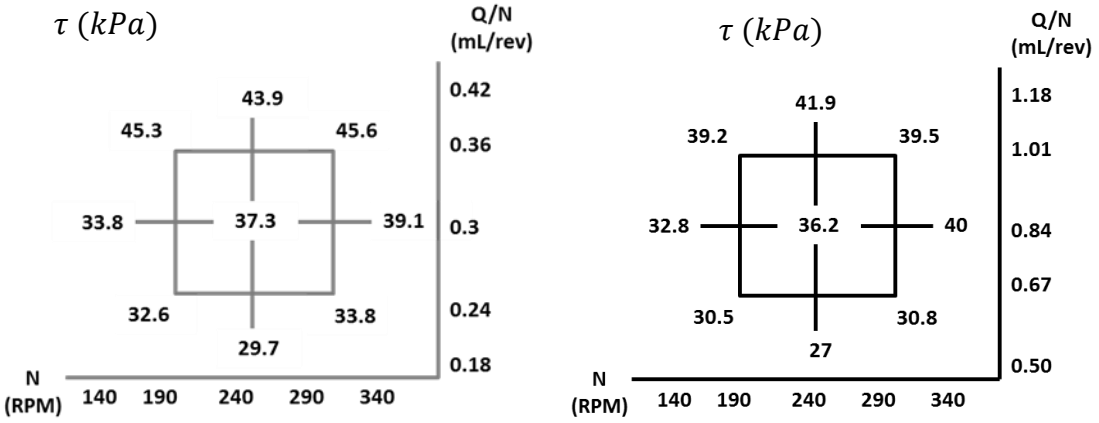


Figure 5.90: Shear Stress comparison for 18mm (left) and 26mm (Volumetric Scale-Up - right)

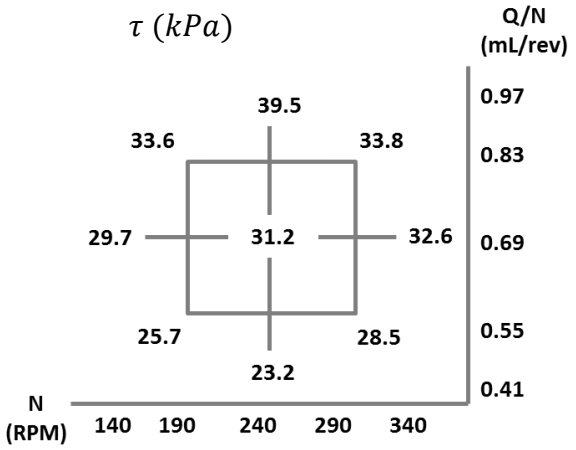


Figure 5.91: Shear Stress comparison for 26mm (% Drag Flow Scale-Up)

Fig 5.90-5.91 provides the shear stress values in terms of a CCD grid for the 18mm TSE and 26mm TSE using Volumetric Scale-Up approach and %Drag Flow approach. As explained in Sec 5.2.5, shear stress increases with screw speed and specific throughput. In this case, 18mm TSE has a higher shear stress value for each corresponding CCD grid point compared to the 26mm TSE. Despite exhibiting a lower shear rate (Sec 5.3.2), the 18mm TSE screw configuration exhibits higher viscosity, which leads to an overall increase in shear stress. For the 26mm TSE, shear stress value does not differ much from the 18mm shear stress values; the lower magnitude of shear stress is due to the lesser viscosity range despite exhibiting a higher shear rate. The larger the size of the extruder, the higher is the shear rate, which plays a major role in the reduction of the viscosity of the polymer melt.

Table 5.13: Prediction coefficient for Shear Stress in the Mixing Section

| Extruder Size | COEFFICIENTS | | | |
|---|---|---|---|---|
| | Scale – Up Method | Intercept | $X_N$ | $X_{Q/N}$ |
| 18mm | | 39.4 | 1.05 | 4.43 |
| 26mm | Volumetric | 35.5 | 1.25 | 3.93 |
| | %Drag Flow | 30.5 | 0.95 | 3.81 |

Table 5.13 provides the intercept and coefficients for operating conditions based on statistical analysis of shear stress data for the 18mm and 26mm TSE. The intercept values for shear stress decreases as the extruder size is scaled up. For the 26mm TSE, the intercept values are higher for volumetric scale-up method compared to % Drag Flow Scale-up method. The coefficient for specific throughput (Q/N) decreases as the extruder size is scaled up. However, in the case of screw speed, the coefficient value increases when scaled up from 18mm to 26mm using volumetric scale-up approach as opposed to % Drag flow scale-up approach where, the coefficient of screw speed is seen to decrease. Based on the % BU results, the % Drag Flow scale-up approach has a closer correspondence with the 18mm TSE screw configuration as compared to volumetric scale-up; the same trend is not observed with shear stress results. As mentioned in Sec 5.2.5, the extensional stress need to be calculated in order to have an accurate understanding of the %Break-Up trends as the magnitude of shear stress is less to result in the break-up of the CAMES beads used in the RSD experiments.

### 5.3.6 Maximum Pressure in the Mixing Section

This section deals with the maximum pressure generated in the mixing section and provides a comparison to understand the variance in the pressure values as the size of the extruder is scaled-up. The pressure values are simulated using Ludovic based on the input specified i.e. the screw configuration and operating conditions. The results are presented in the form of CCD grids to show the visualize the relationship between the result and the operating conditions.

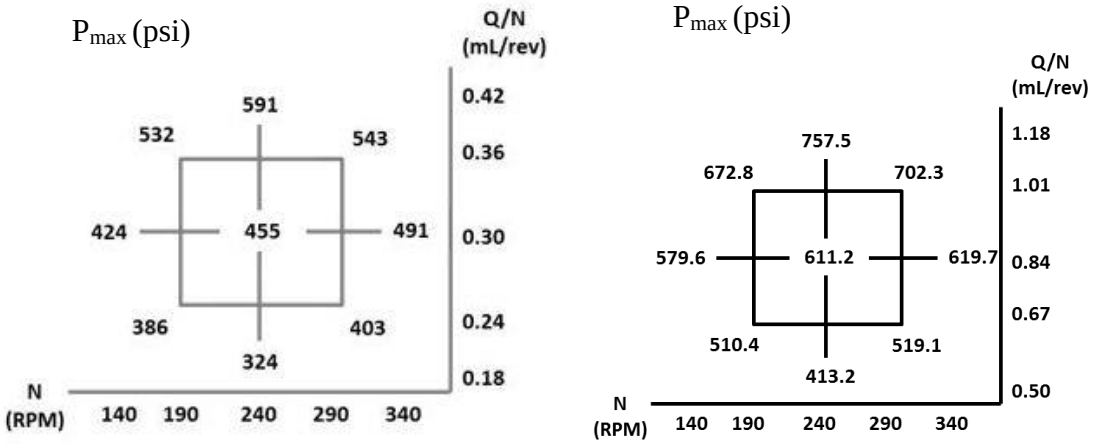


Figure 5.92: Pressure comparison for 18mm (left) and 26mm (Volumetric Scale-Up - right)

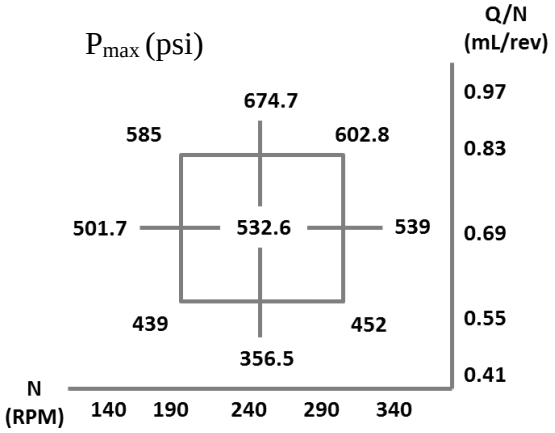


Figure 5.93: Pressure comparison for 26mm (% Drag Flow Scale-Up)

Fig 5.92-5.93 provide a comparison between the pressure values simulated using Ludovic across all the CCD grid points for the 18mm and 26mm TSE. The pressure trends across all the 9 CCD grid points have been explained in Sec 5.2.6. Based on the results obtained, it can be observed that pressure increases as the extruder size is scaled up. The pressure values are dependent on the screw geometry as well as the operating conditions. In the case of 26mm TSE, volumetric scale-up approach results in higher pressure generation in the mixing section as compared to % drag flow scale-up approach. The pressure data obtained

using Ludovic simulations were statistically analyzed using JMP 12.2, to understand the influence of operating conditions on the pressure values generated in the mixing section.

Table 5.14: Prediction coefficient for Pressure in the Mixing Section

| Extruder Size | COEFFICIENTS | | | |
|---|---|---|---|---|
| | Scale – Up Method | Intercept | $X_N$ | $X_{Q/N}$ |
| 18mm | | 463.6 | 13.5 | 68.3 |
| 26mm | Volumetric | 610.6 | 6.82 | 86.2 |
| | %Drag Flow | 527.6 | 8.78 | 77.7 |

Table 5.14 provides the values for the intercept and coefficient for operating conditions post statistical analysis using JMP 12.2. From Table 5.14, it can be seen that intercept values for pressure increases with scale-up and the volumetric scale-up method has the highest intercept for pressure generated in the mixing section. The coefficient of screw speed decreases as the extruder size is scaled-up implying that the influence of screw speed on pressure decreases as the extruder size increases. However, the coefficient of specific throughput increases as the extruder size is scaled-up. The purpose of using scale-up is to replicate the results obtained from small scale to large scale. % Drag Scale-Up approach gives results that are closer to the 18mm TSE results as compared to the Volumetric Scale-Up approach.

### 5.3.7 Residence Time in the Mixing Section

This section provides a comparison between the residence time values in the mixing section for the 18mm and 26mm TSE screw configuration. Ludovic simulates the residence time (in seconds) results based on the input specified. The residence time values are provided in terms of the CCD grids for both 18mm and 26mm TSE.

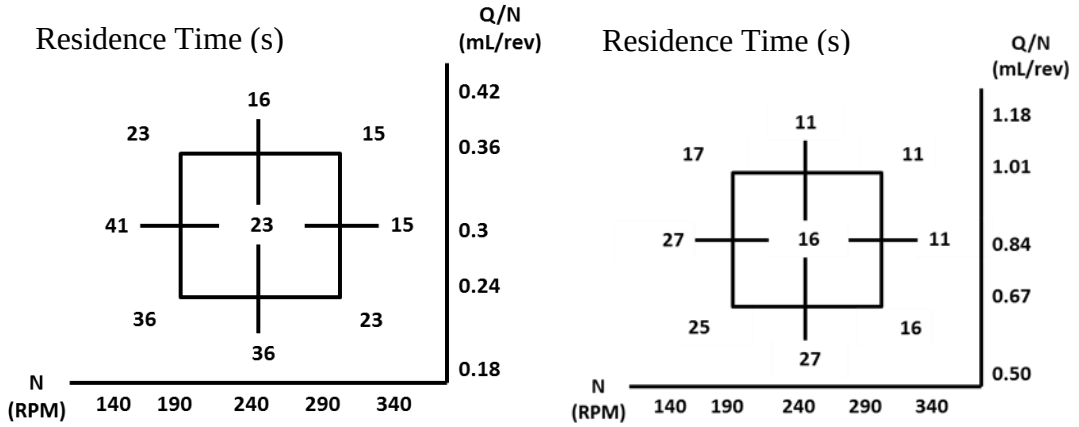


Figure 5.94: Residence Time comparison for 18mm (left) and 26mm (Volumetric Scale-Up - right)

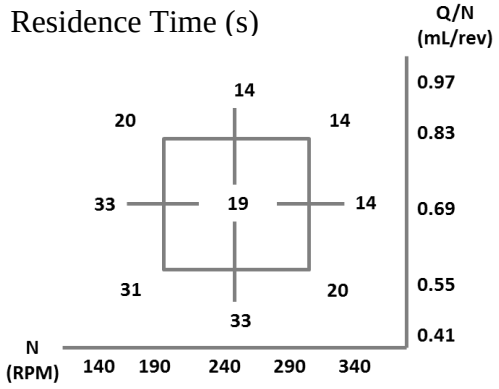


Figure 5.95: Residence Time comparison for 26mm (% Drag Flow Scale-Up)

Fig 5.94-5.95 provide the comparison between residence time results when scaled-up from 18mm to 26mm. The general trend observed across the CCD grid points for residence time **(**Sec 5.1.7 and 5.2.7**)** holds true for scale-up results as well; residence time decreases as screw speed and specific throughput increases. When scaled-up from 18mm TSE to 26mm TSE, residence time is seen to decrease. Despite operating on the same screw speed, specific throughput ranges vary which is a contributing factor towards the decrease in residence time. Comparing the volumetric scale-up and % drag flow scale-up method for the 26mm TSE, residence time is lower for the former method due to the higher range of specific throughput. To precisely understand the influence of operating conditions on

residence time, the obtained data is statistically analyzed using JMP 12.2 as seen in Table 5.15.

Table 5.15: Prediction coefficient for Residence Time in the Mixing Section

| Extruder Size | COEFFICIENTS | | | |
|---|---|---|---|---|
| | Scale – Up Method | Intercept | $X_N$ | $X_{Q/N}$ |
| 18mm | | 22.2 | - 6.25 | - 5.1 |
| 26mm | Volumetric | 15.8 | - 3.92 | 3.75 |
| | %Drag Flow | 19 | - 4.58 | - 4.58 |

Based on Table 5.15, it can be seen that the intercept value for residence time i.e. the average of the residence time values obtained across all the 9 CCD grid points, decreases as the size of the extruder is reduced. Volumetric Scale-Up approach results in a reduced residence time as compared to %Drag Flow Scale-Up approach. The coefficient of N and Q/N decreases as well when scaled-up from 18mm to 26mm. The Volumetric scale-up CCD grid has the lowest coefficient of N and Q/N implying that the effect of change in operating conditions will have a minimal effect on the change of residence time results. In this situation, % Drag Flow Scale-Up approach provides the results that are closest to the 18mm TSE as compared to Volumetric Scale-Up approach.

### 5.3.8 Maximum Number of Revolutions in the Mixing Section

This section provides the comparison between 18mm and 26mm TSE for the maximum number of revolutions taken by the polymer melt to move across the mixing section. The number of revolutions can be calculated using Eq. 33 based on the residence time results provided by Ludovic. The screw configuration for the 18mm and 26mm TSE involves a longer mixing section with narrow kneading blocks (explained in Chapter 4).

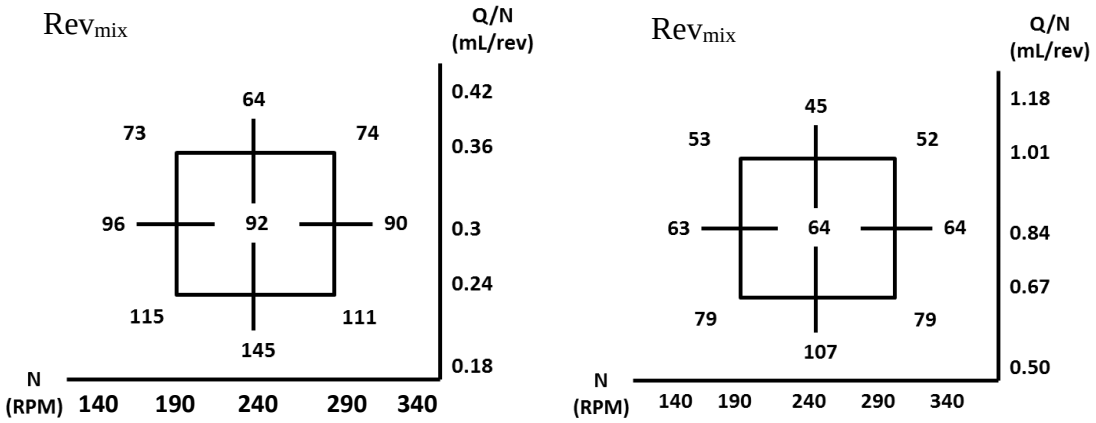


Figure 5.96: $Rev_{mix}$ comparison for 18mm (left) and 26mm (Volumetric Scale-Up - right)

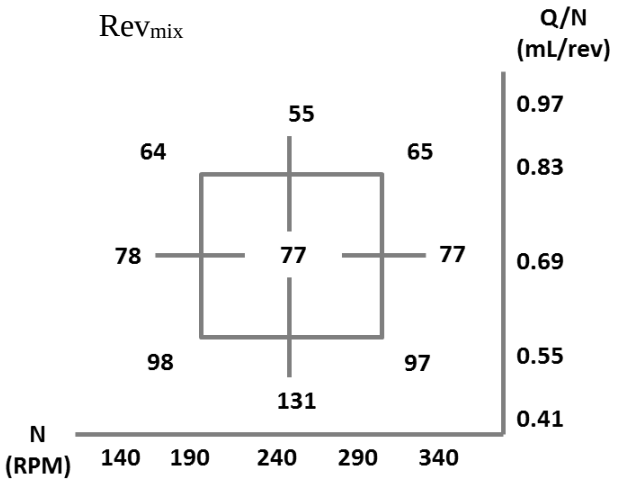


Figure 5.97: $Rev_{mix}$ comparison for 26mm (% Drag Flow Scale-Up)

Based on the data displayed in Fig 5.96-5.97 regarding the maximum number of revolutions taken by the polymer melt to get past the mixing section, it can be seen that $Rev_{mix}$ decreases as the size of the extruder is scaled up. $Rev_{mix}$ being a function of specific throughput (Q/N) varies for the 18mm and 26mm due to the different ranges of specific throughput used. $Rev_{mix}$ decreases as the specific throughput increases. In order to get a quantitative estimate of the influence of the operating conditions on $Rev_{mix}$, the data obtained has been statistically analyzed using JMP 12.2.

Table 5.16: Prediction coefficient for Number of Revolutions in the Mixing Section

| Extruder Size | COEFFICIENTS | | | |
|---|---|---|---|---|
| | Scale – Up Method | Intercept | $X_N$ | $X_{Q/N}$ |
| 18mm | | 90 | NS | - 20.1 |
| 26mm | Volumetric | 63 | NS | - 14.75 |
| | %Drag Flow | 76.9 | NS | - 18.2 |

Table 5.16 reveals the intercept and the coefficient values to understand the influence of the operating conditions on $Rev_{mix}$. The intercept values decrease as the size of the extruder is scaled-up implying that the number of revolutions taken by polymer melt to get across the mixing section decreases as the extruder size increases. The volumetric scale-up method gives rise the lowest $Rev_{mix}$ value as it has the highest operating specific throughput range compared to % Drag Flow Scale-Up method. As seen in section 5.1.8 and 5.2.8, $Rev_{mix}$ is a function of specific throughput and is not influenced by the screw speed. The specific throughput coefficient decreases as the extruder size is scaled up. The % Drag Flow scale-up approach provides the results that have the closest resemblance to the 18mm TSE results.

Section 5.3 discusses in brief the comparison between the results obtained when the extruder is scaled-up and provides a detailed analysis on the results obtained using two different types of scale-up approaches. Based on the % BU results obtained by conducting the RSD experiments, it was observed that % Drag Flow Scale-Up approach is accurate in replicating the 18mm TSE %BU results. The results provided by Ludovic also imply that %Drag Flow provides values that are closer to replicating the 18mm TSE results. However, the shear stress values provided based on Ludovic calculations show that Volumetric scale-up approach has the closest approximation to the 18mm TSE. The extensional stress

component needs to be evaluated as well based on the Ludovic results provided in order to have a better insight on the accuracy of the scale-up method.

## 5.4 Study on Kollidon VA-64

The final section of Chapter 5 discusses the influence of Barrel Temperature on the % Break-Up results as well as the thermomechanical properties provided based on Ludovic simulations. The RSD experiment was performed on a 16mm Thermo Extruder by Ben et al [24]. The experimental setup has been discussed in Chapter 4. The base polymer used to perform this experiment was Kollidon VA-64 (discussed in Chapter 4). The operating conditions for the experiment have been discussed in Chapter 4 (Sec 4.5) and the experiment was performed for the same screw configuration at the same set of screw speed (N) and specific throughput (Q/N) for three different barrel temperatures ($170^0$C, $190^0$C and $220^0$C) in order to understand the impact of changing the barrel temperatures on the extrudate properties. The results that had been discussed in the previous three sections would be focused on in this section.

### 5.4.1 Percent Break-Up Results

% BU values had been calculated based on the RSD experiments conducted on the 16mm TSE. % BU results are presented in the form of CCD grids to visualize the relationship between %BU and the operating conditions (N, Q/N). The same experimental operating conditions and screw geometry were tested on different barrel temperatures ($170^0$C, $190^0$C and $220^0$C) as seen in Fig 5.100.

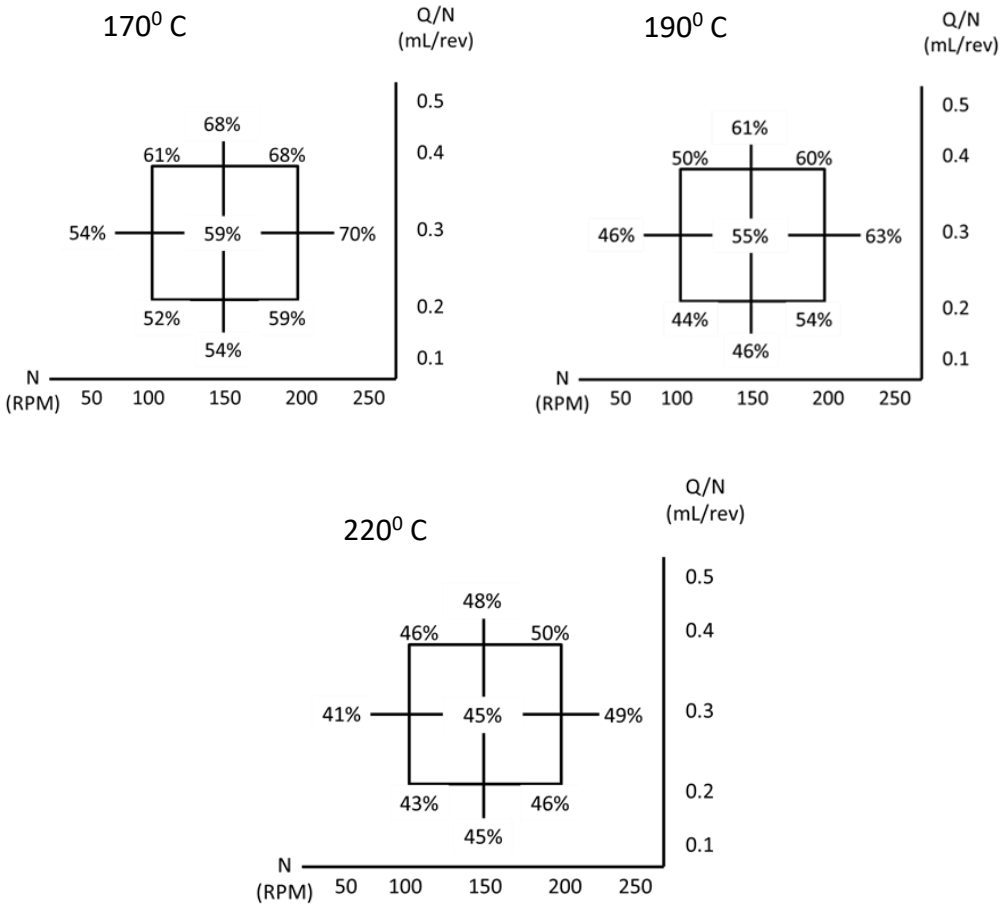


Figure 5.98: %BU comparison for 16mm TSE across different barrel temperatures

Figure 5.98 compares the %BU results across different barrel temperatures. %BU trends across CCD grid points for a screw configuration had already been discussed in Sec 5.1.1. Based on the data obtained across the 3 CCD grids, it can be seen that %BU decreases as the barrel temperature increases. The increase in barrel temperature leads to a higher temperature attained by the polymer melt causing a reduction in the viscosity. The reduction in viscosity leads to a decrease in the stress that the polymer melt is being subjected to, leading to a decrease in the %BU results. This behavior can be explained accurately using Ludovic results (explained in the subsequent sections of 5.4). The

predictive equations for %BU across different barrel temperatures have been calculated based on statistical analysis performed using JMP 12.2.

Table 5.17: Predictive Coefficient for %BU

| Extruder Size | COEFFICIENTS | | | |
|---|---|---|---|---|
| | Barrel Temperatures ($^0$C) | Intercept | $X_N$ | $X_{Q/N}$ |
| 16mm | 170 | 58.8 | 3.4 | 3.43 |
| | 190 | 52.8 | 3.5 | 4.5 |
| | 220 | 45.8 | 1.9 | 1.1 |

Based on statistical analysis performed on the %BU data, 5.17 displays the intercept and coefficient values for the operating conditions. The table shows the variation in the intercept and coefficient values as the barrel temperature increases. The intercept value of %BU i.e. average %BU across all the CCD grid points decreases with increase in barrel temperature. However, the coefficient value of specific throughput initially increases when barrel temperature is increased to 190$^0$C and decreases rapidly as the barrel temperature is increased to 220$^0$C. The coefficient value of screw speed almost remains the same as barrel temperature increases from 170$^0$C to 190$^0$C but decreases as the barrel temperature increases to 220$^0$C.

**Ludovic Results**

### 5.4.2 Maximum Shear Rate in the Mixing Section

The maximum shear rate in the mixing section for the 16mm TSE has been simulated using Ludovic based on the operating conditions and input screw geometry specified. The

maximum shear rate generated in the mixing section across different barrel temperatures can be seen across the CCD grids in Fig 5.101

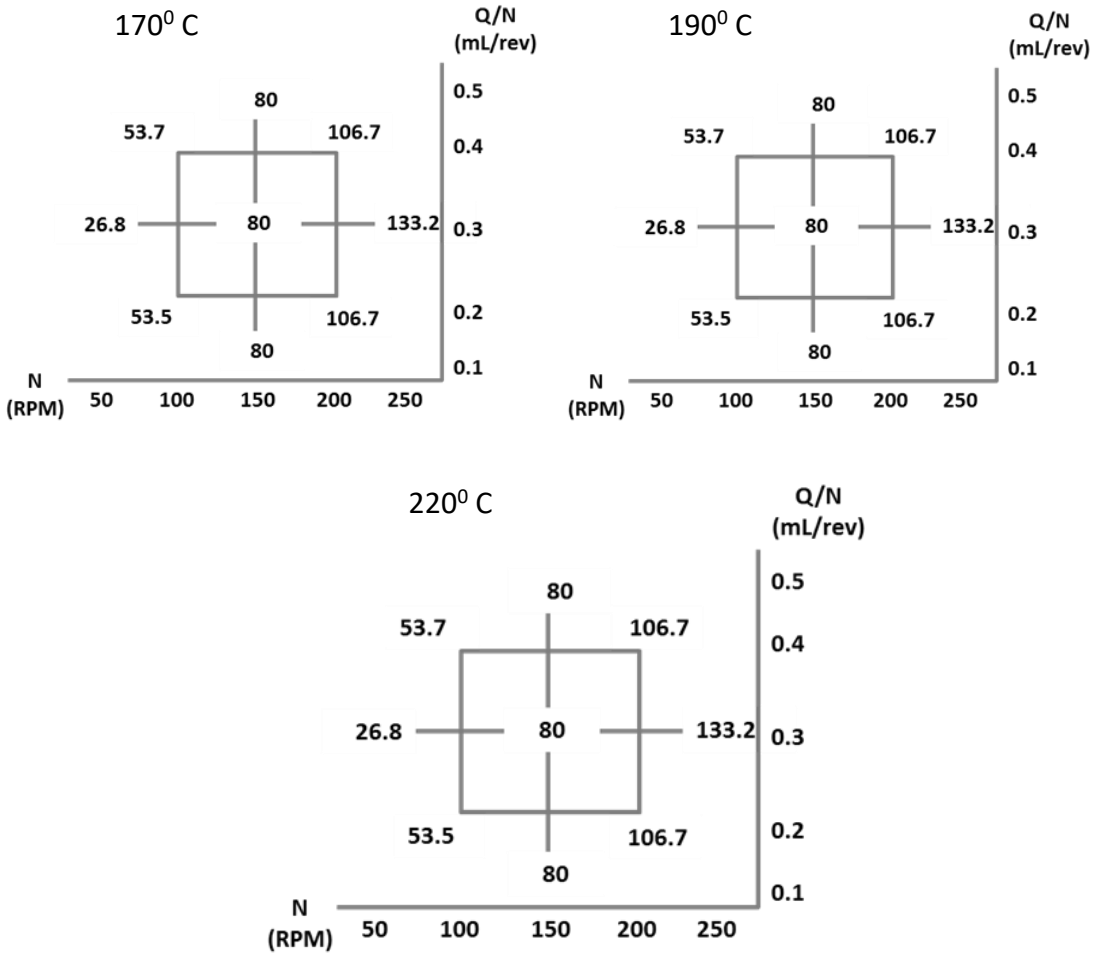


Figure 5.99: Shear Rate comparison for 16mm TSE across different barrel temperatures

Figure 5.99 displays the maximum shear rate generated in the mixing section across different barrel temperatures. General trend observed across the CCD grids; shear rate increases with increase in screw speed at constant Q/N. However, at constant N, shear rate remains constant as specific throughput increases. This is due to the fact that the specific throughput is in the range of 0.1 mL/rev which might cause a small change in the shear rate values, which could not be interpreted from the simulations. Across the 3 CCD grids, it is observed that shear rate at the 9 CCD grid points remains constant at different barrel

temperatures which implies that shear rate is not dependent on the barrel temperature as it is a function of screw speed, specific throughput and screw geometry. To get a further insight into the influence of the operating conditions on the shear rate values, the data has been statistically analyzed using JMP 12.2.

Table 5.18: Predictive Coefficient for Maximum Shear Rate in Mixing Section

| Extruder Size | COEFFICIENTS | | | |
|---|---|---|---|---|
| | Barrel Temperatures ($^0$C) | Intercept | $X_N$ | $X_{Q/N}$ |
| 16mm | 170 | 80.1 | 26.6 | - |
| | 190 | 80.1 | 26.6 | - |
| | 220 | 80.1 | 26.6 | - |

From Table 5.18, it can be seen that the intercept of shear rate in mixing section i.e. the average of the shear rate values across all the CCD grid points remains constant across the different barrel temperatures. The coefficient of screw speed remains constant across the three barrel temperatures implying that the influence of screw speed on the shear rate generated in the mixing section remains unaffected by the change in barrel temperature. The coefficient of specific throughput is not included in the table; the data obtained from Ludovic does not show any significant change in the shear rate values when the specific throughput (Q/N) is varied at a constant screw speed.

### 5.4.3 Maximum Temperature of polymer melt in Mixing Section

This section provides a comparison of the maximum temperature attained by the polymer melt in the mixing section when a specific screw geometry is subjected to three different

barrel temperatures. The operating conditions (N, Q/N) seen in Fig 5.102 remain constant across the 3 CCD grids as the barrel temperature is varied.

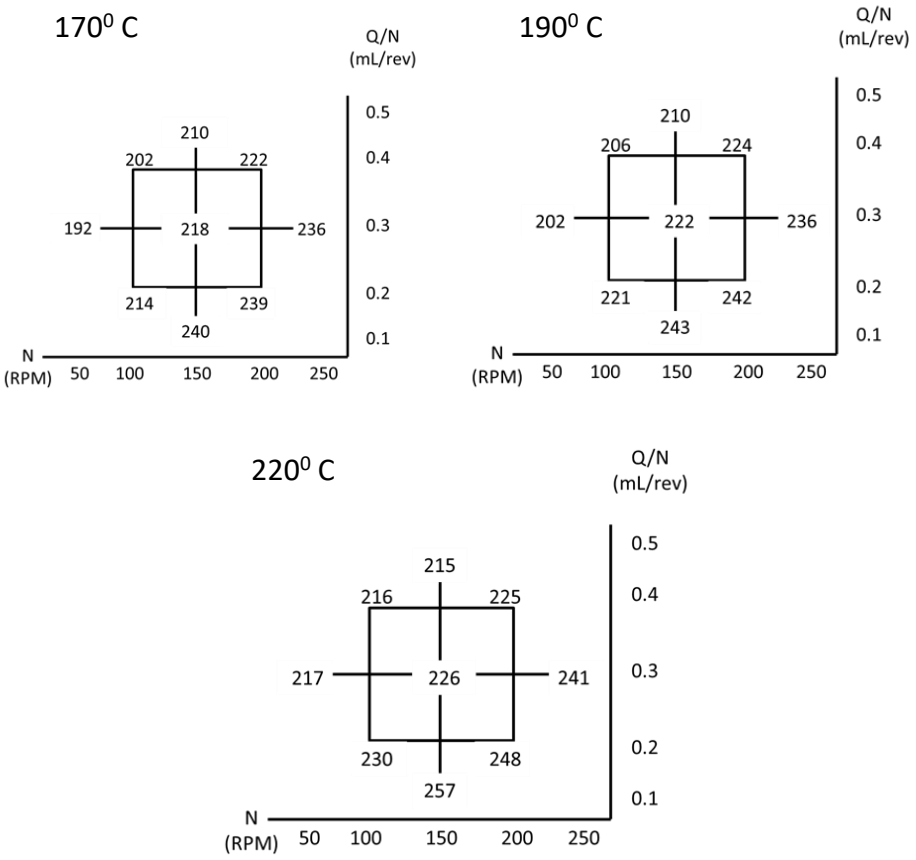


Figure 5.100: Max. Temperature comparison for 16mm TSE across different barrel temperatures

Fig 5.100 reveal the data on the maximum temperature attained by the polymer melt in the mixing section. The temperature trends have been discussed in Sec 5.1.**3** so the focus will be on understanding the impact of change in barrel temperature on the temperature of the polymer melt in the mixing section. The temperature of the polymer melt increases with increase in barrel temperature; increase in barrel temperature implies the conduction of heat from the barrel towards the polymer melt which is already being subjected to shear as a result of the screw rotation. This results in an increase in temperature of the polymer melt.

Table 5.20: Predictive Coefficient for Maximum Temperature in Mixing Section

| Extruder Size | COEFFICIENTS | | | |
|---|---|---|---|---|
| | Barrel Temperatures ($^0$C) | Intercept | $X_N$ | $X_{Q/N}$ |
| 16mm | 170 | 218.4 | 11.1 | - 7.4 |
| | 190 | 222.8 | 8.9 | - 8.2 |
| | 220 | 226.4 | 6.2 | - 10.1 |

Statistical analysis performed on the obtained data using JMP gives rise to prediction coefficient values for operating conditions which helps get a better understanding of the results. Based on Table 5.20, it can be seen that the intercept of temperature of the polymer melt in mixing section increases with increase in barrel temperature; this implies that temperature of polymer melt is influenced by the temperature of the barrel. The coefficient of screw speed N decreases as $T_b$ increases, implying that the impact of screw speed on the temperature of polymer melt decreases as $T_b$ increases. However, the coefficient of specific throughput increases with increase in $T_b$. The increase in temperature of the polymer melt plays a vital role in the decrease in %BU results.

### 5.4.4 Viscosity in Mixing Section

This section discusses the viscosity of the polymer melt in the mixing section. Viscosity plays a vital role in determining the stress that the polymer melt is being subjected to in the mixing section. The influence of the barrel temperature on the viscosity of the polymer melt can be understood from the results provided by Ludovic. The results are provided in the form of CCD grids to help visualize the relationship between viscosity and the operating conditions.

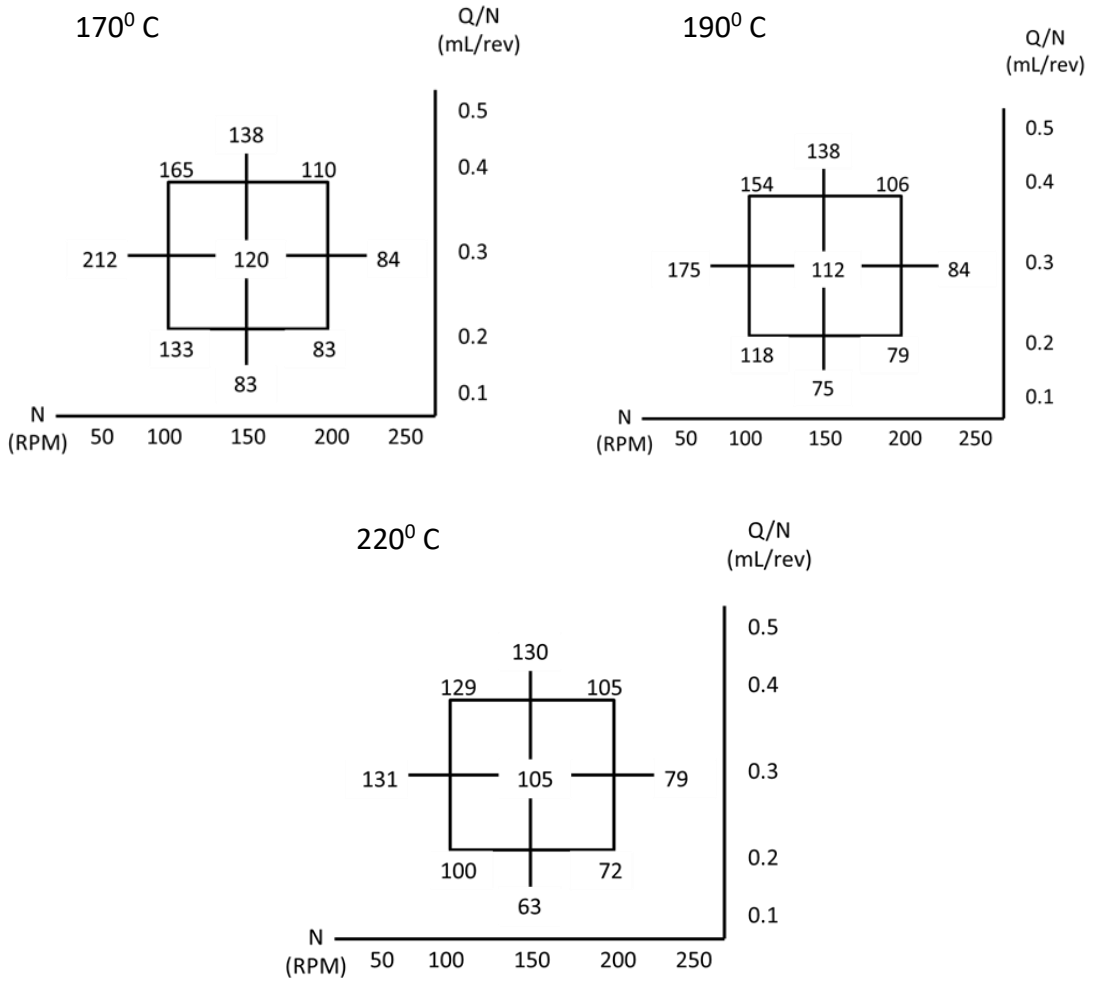


Figure 5.101: Viscosity comparison for 16mm TSE across different barrel temperatures

Fig 5.101 reveals the data on viscosity of the polymer melt in the mixing section and provides a comparison between the results obtained across different barrel temperatures. The general trend for viscosity is observed in Fig 5.101 across the CCD grids; viscosity decreases with increase in screw speed and increases with increase in specific throughput (Sec 5.1.4). As the barrel temperature increases the viscosity of the polymer melt decreases which is due to the higher temperature of the polymer melt despite the fact that shear rate remains constant across the different barrel temperatures. To get a better insight into the

influence of operating conditions on the viscosity of the polymer melt, the results were statistically analyzed using JMP 12.2.

Table 5.21: Predictive Coefficient for Viscosity in Mixing Section

| Extruder Size | COEFFICIENTS | | | |
|---|---|---|---|---|
| | Barrel Temperatures ($^0$C) | Intercept | $X_N$ | $X_{Q/N}$ |
| 16mm | 170 | 118.3 | - 30.1 | 10.1 |
| | 190 | 111.3 | - 22.4 | 15.7 |
| | 220 | 103.8 | - 13 | 16.3 |

Table 5.21 provides a comparison between the intercept and coefficient values for the operating conditions between different barrel temperatures. The intercept value of viscosity decreases as the barrel temperature increases from 170 to 220$^0$C. The coefficient of screw sped (N) decreases as the barrel temperature increases, while the coefficient of specific throughput increases with barrel temperature. This behavior is similar to the trends observed in Sec 5.1.3, which implies that increase in the temperature of polymer melt leads to a reduction in the viscosity values.

### 5.4.5 Shear Stress in Mixing Section

Shear stress generated in the mixing section is an important parameter in understanding the %BU values. Shear Stress values are calculated as per Eq. 30 based on the shear rate and viscosity values generated using Ludovic. The shear stress values obtained across different barrel temperatures have been displayed as CCD grids to get a better understanding of the relationship between shear stress and the operating conditions (N, Q/N) as well as barrel temperature ($T_b$).

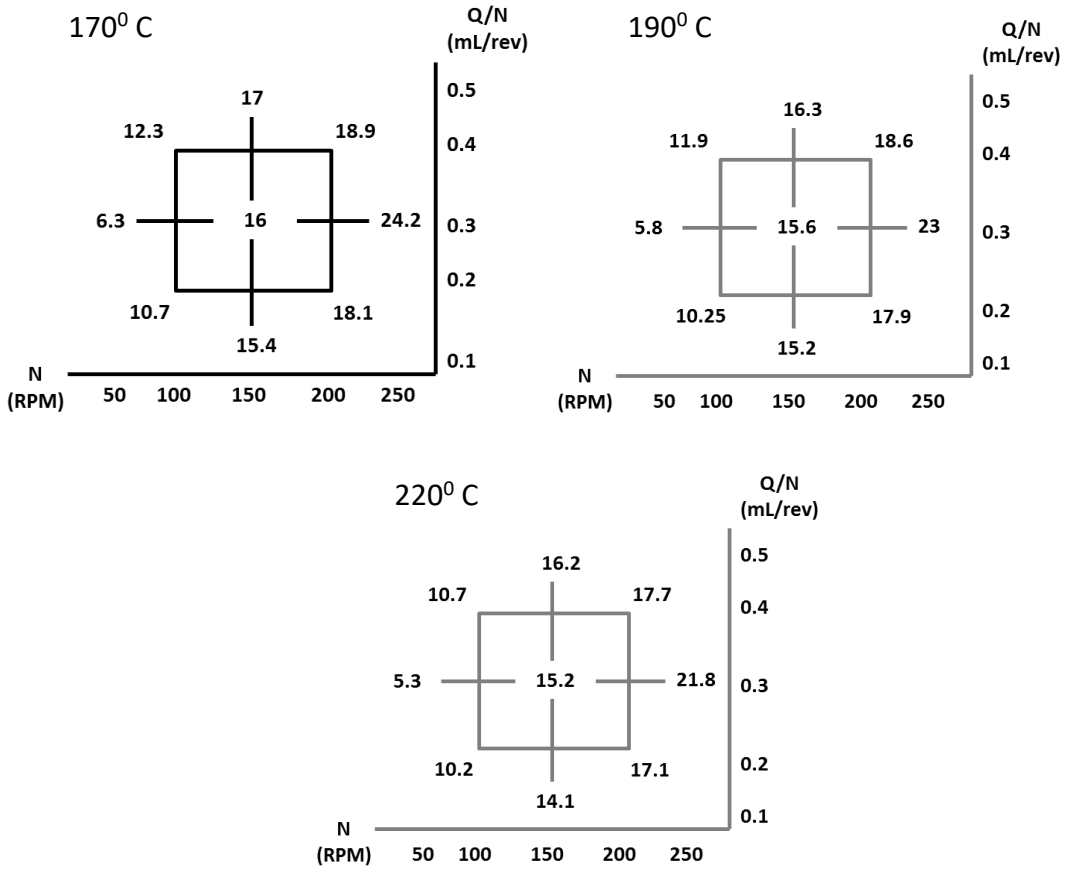


Figure 5.102: Shear Stress comparison for 16mm TSE across different barrel temperatures

Fig 5.102 provides a comparison between the shear stress values obtained across different barrel temperatures. Across a particular CCD grid, shear stress increases with increase in screw speed (N) and specific throughput (Q/N) (discussed in Sec 5.1.5). However, when the same screw configuration is subjected to different barrel temperatures, the shear stress values decrease which is due to the reduction in the viscosity values **(Sec** 5.4.4**)**. The higher temperature of polymer melt leads to a decrease in the viscosity values which affects the shear stress results. Given that shear rate was a constant across different barrel temperatures (Sec 5.4.2), the shear stress is impacted by the viscosity of the polymer melt. The obtained data are statistically analyzed using JMP 12.2.

Table 5.22: Predictive Coefficient for Shear Stress in Mixing Section

| Extruder Size | COEFFICIENTS | | | |
|---|---|---|---|---|
| | Barrel Temperatures ($^0$C) | Intercept | $X_N$ | $X_{Q/N}$ |
| 16mm | 170 | 15.23 | 4.15 | 0.5 |
| | 190 | 15 | 4.06 | 0.4 |
| | 220 | 14.4 | 3.9 | 0.37 |

As seen in Fig 5.102, the intercept values of shear stress provided based on statistical analysis decrease as the barrel temperature increases. The coefficient of screw speed (N) and specific throughput (Q/N) decreases with increase in barrel temperature, implying that shear stress values are less likely to be influenced by the change in operating conditions as the barrel temperature increases. Shear Stress, despite having a lower magnitude provides similar trends as compared to %BU results (Sec 5.4.1). The pattern of results obtained for shear stress are consistent with the %BU results. The decrease of % BU with barrel temperature is the consequence of the reduction of viscosity values (seen in Fig 5.4.4).

### 5.4.6 Residence Time in Mixing Section

Residence Time is an important parameter to understand the mixing performance in the extruder. This section discusses the influence of change in barrel temperature on the residence time of the polymer melt in the mixing section. The CCD grids visualize the relationship between residence time and the operating conditions across different barrel temperatures.

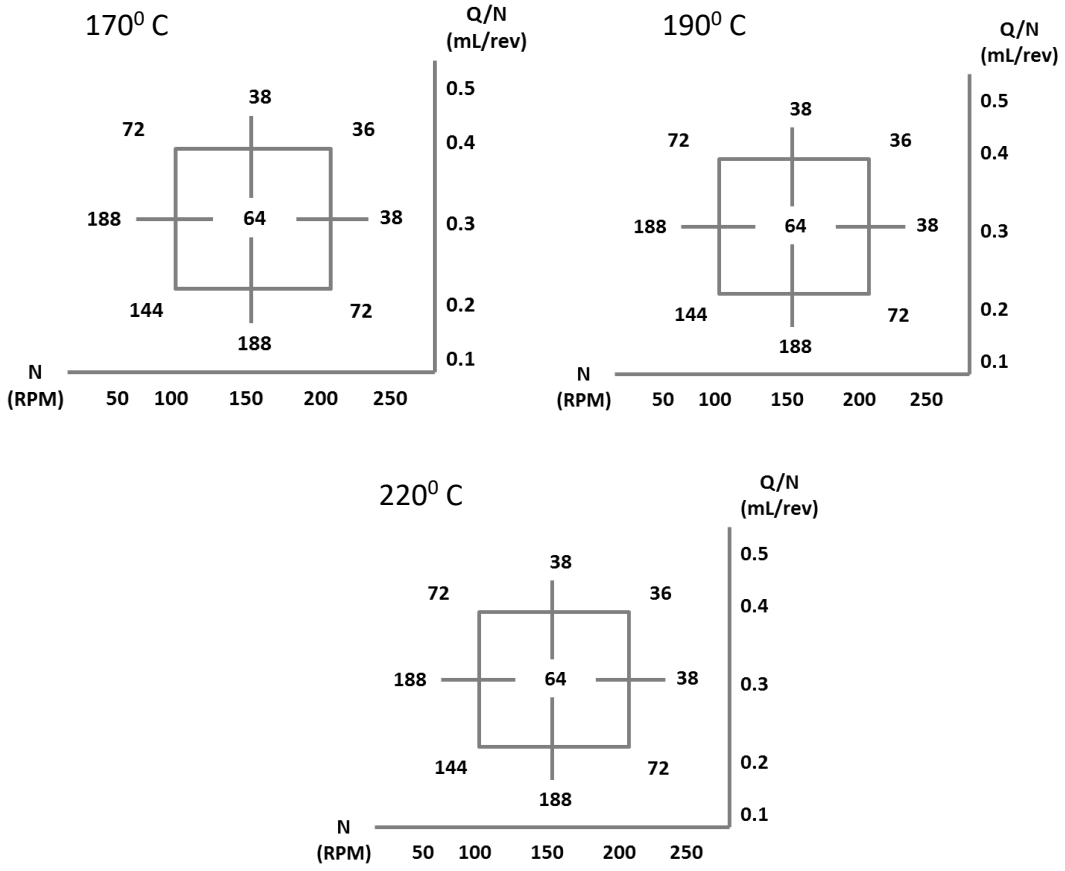


Figure 5.103: Residence Time comparison for 16mm TSE across different barrel temperatures

Fig 5.103 provides the comparison between residence time of polymer melt in the mixing section across different barrel temperatures. The residence time decreases with increase in screw speed as well as with increase in specific throughput (Sec 5.1.7). Residence time remains the same at CCD grid points that have the same feed rate (Chapter 4). Across the different barrel temperatures, it is seen that residence time remains unchanged; this implies that barrel temperature does not affect the residence time of the polymer melt in the mixing section. Despite the decrease in the %BU values, the residence time remains unchanged when the barrel temperature changes. The influence of operating conditions on the

residence time have been summarized in Table 5.23 based on statistical analysis of obtained data.

Table 5.23: Predictive Coefficient for Residence Time in Mixing Section

| Extruder Size | COEFFICIENTS | | | |
|---|---|---|---|---|
| | Barrel Temperatures ($^0$C) | Intercept | $X_N$ | $X_{Q/N}$ |
| 16mm | 170 | 57.33 | -34 | -34 |
| | 190 | 57.33 | -34 | -34 |
| | 220 | 57.33 | -34 | -34 |

Table 5.23 provides summary of the prediction coefficients for residence time along with intercept values based on statistical analysis using JMP 12.2. The intercept values and predictive coefficient of operating conditions remain constant across the barrel temperature implying that barrel temperature is not a function of residence time. Screw Speed and specific throughput exert equal influence on the residence time of polymer melt in mixing section. Residence time decreases as the specific throughput and screw speed increases.

### 5.4.7 Maximum Number of Revolutions in the Mixing Section

Maximum Number of Revolutions in the mixing section is an indicator of the path travelled by the polymer melt along the mixing section. As seen in previous section (Sec 5.1.8), $Rev_{mix}$ is a function of the specific throughput which is a function of the degree of fill in the screw channel. This section discusses the influence of barrel temperature on $Rev_{mix}$ on a particular screw configuration of the 16mm TSE. The results have been displayed in the form of CCD grids as seen in Fig 5.106.

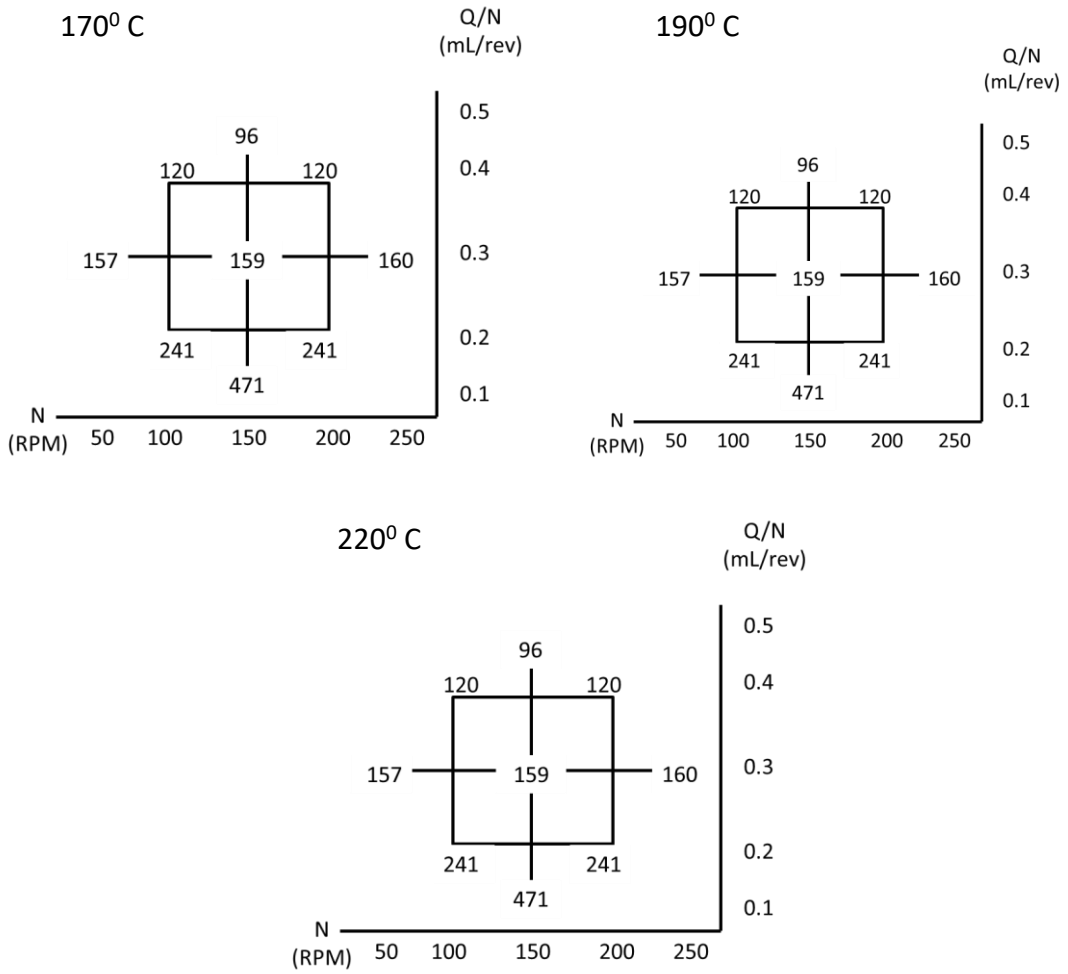


Figure 5.104: $Rev_{mix}$ comparison for 16mm TSE across different barrel temperatures

Fig 5.104 compares the $Rev_{mix}$ obtained for a particular screw geometry when the barrel temperature is varied. As seen in Sec 5.1.8, 5.2.8 and 5.3.8, $Rev_{mix}$ is a function of specific throughput and does not vary when the screw speed changes at a constant Q/N. When the screw configuration is subjected to different barrel temperatures, $Rev_{mix}$ remains constant and does not vary with $T_b$. This implies that the barrel temperature does not influence the path of travel of the polymer melt in the mixing section as irrespective of the barrel temperature changes, the polymer melt travels along the same path when operated under

the same Q/N. The predictive equations for $Rev_{mix}$ can be obtained based on performing statistical analysis of data using JMP 12.2.

Table 5.24: Predictive Coefficient for Number of Revolutions in Mixing Section

| Barrel Temperature ($T_b$) | COEFFICIENTS | | |
|---|---|---|---|
| | Intercept | $X_N$ | $X_{Q/N}$ |
| $170^0$C | 150.5 | NS | -82.7 |
| $190^0$C | 150.5 | NS | -82.7 |
| $220^0$C | 150.5 | NS | -82.7 |

As seen in Fig 5.104, Table 5.24 affirms that maximum number of revolutions in the mixing section of the Twin Screw Extruder is not dependent on the barrel temperature. As discussed in Sec 5.1, 5.2 and 5.3, maximum number of revolutions is dependent on the specific throughput and is not influenced by screw speed. The intercept values i.e. average of $Rev_{mix}$ across the CCD grid points remains constant as temperature increases; this was observed in Fig 5.104. The specific throughput which is an indicator of the degree of fill in the screw channel influences the path that the polymer melt travels along. The RRD assumptions (Chapter 1) are validated by the $Rev_{mix}$ results provided using Ludovic.

Chapter 5 provides an in-depth analysis of the internal behavior of the Twin Screw Extruder and uses the Ludovic results to understand the results provided by RSD experimental methods. The data provided in each of Sec 5.1, 5.2, 5.3 and 5.4 help understand the thermomechanical behavior of polymer melts inside the extruder and help distinguish the results obtained based on screw configuration, polymer rheology, scale-up as well as influence of other properties apart from the operating conditions.

# Chapter 6 – Insights from RSD and RRD Methodology

This chapter summarizes the findings from the results obtained using the RSD Methodology and Ludovic Simulations. The ideology behind using Residence Stress Distribution as a tool to comprehend the mixing efficiency of the Twin Screw Extruder has been explained briefly. It is used as a metric to understand the differences in the mixing performance of the TSE based on changes to the screw configuration, base polymer, and scale-up method. Ludovic is a computer simulation software used to validate the findings of RSD Methodology as well as understand the internal behavior of the extruder. Similarly, the assumptions put forth by RRD were ratified using Ludovic. Each of these topics will be summarized in the following sections of Chapter 6.

## 6.1 Internal Behavior inside TSE

The efficiency of the extrusion process is determined by the quality of the extrudate obtained. To improvise the product quality, it is vital to understand the internal behavior (mixing section) within the twin screw extruder. This purpose was accomplished using Ludovic as it gives the flexibility to simulate various operating conditions, screw geometries and choice of polymers. The results obtained from the Ludovic simulations can be used as a tool towards understanding the implications of changing operating conditions, screw geometries on the quality of the extrudate obtained. Twin Screw Extruder, being a primary compounding device, has been used in the industry to improve the quality of plastics, pharmaceutical products by efficiently mixing existing base polymers with additives/fillers. Improving the properties of the final extrudate requires superior understanding of the mixing process – dispersive and distributive mixing (Sec 1.6 and 1.7).

The trends observed for thermo-mechanical properties such as temperature, pressure, shear rate, viscosity need to be analyzed so that the corresponding screw configuration and operating conditions could be controlled to generate the desired output. Ludovic is a global model which helps quantify these properties at specific points along the length of the extruder and gives the flexibility to vary the input conditions until the desired output is obtained. Chapter 5 discusses each of the properties in detail and explains the variations obtained when the changes are made to the screw configuration, choice of base polymer and scale-up. These properties are inter-related; for instance, increase in screw speed at constant Q/N increases the shear rate which causes the temperature of the polymer melt to increase and viscosity of the polymer melt to decrease. Based on the amount of increase in shear rate compared to the decrease in viscosity, the shear stress values vary accordingly. In this manner, each of the properties is dependent on one another and can be used to improve the efficiency of the mixing process, provided the relationship between the operating conditions and the properties are clearly understood.

## 6.2 Validation of Residence Stress Distribution Methodology

As discussed in the above section, the process of mixing in the twin screw extruder needs to be understood to improve the quality of the final extruder. Residence Stress Distribution (RSD) was a methodology that was designed to quantify the amount of polymer melt being exposed to a particular amount of stress as it is processed within the TSE using CAMES beads, due to certain disadvantages in using Residence Time Distribution as a tool to estimate the quality of mixing (explained in detail in Chapter 2). Percent Break-Up (%BU) is a metric that was used to quantify the stress experienced by the polymer melt in the mixing section. The %BU values were calculated for a range of operating conditions, for

various screw configurations, different base polymers, and scaling-up. The trends for %BU have been analyzed in Chapter 5. The results predicted using RSD methodology were ratified using Ludovic software simulations. This was performed by correlating the results (thermo-mechanical properties) obtained using Ludovic to understand the %BU trends obtained using RSD methodology and serve as a validation tool.

RSD experiments showed that % BU increases when screw speed is increased at constant specific throughput; similarly, %BU increases when specific throughput is increased at constant speed. When specific throughput is increased at constant screw speed, the degree of fill increases (explained further in Sec 6.4), as well as the velocity profile of the polymer melt increases leading to extensional stress, as more material is squeezed between the kneading disks. When screw speed increases at constant specific throughput, the shear rate (Sec 5.1.2) and extensional stress increase leading to higher %BU. To understand the variation of %BU w.r.t screw geometry, narrow and wide kneading blocks were used in the mixing section and the obtained results show that wider kneading blocks cause rupture of a greater percentage of CAMES beads. In the case of wide kneading blocks, the width of the paddles is larger and the polymer melt that flows in between the paddles get squeezed to a greater extent compared to the narrow kneading blocks.

In order to understand the behavior exhibited by the %BU results for the different experimental setups (Chapter 4), Ludovic simulation results were used. The Ludovic simulation results that were focused on for this thesis include the shear rate, temperature, viscosity, shear stress, pressure, residence time and the maximum number of revolutions in the mixing section. The operating conditions were similar to the RSD experiments. When specific throughput is increased at constant screw speed, the shear rate increases;

similarly, when screw speed is increased at constant specific throughput, the shear rate increases (Sec 5.1.2, 5.2.2, 5.3.2, 5.4.2). Shear rate is a function of screw speed and increases with increase in screw speed. When specific throughput is increased at constant screw speed, shear rate increases by a smaller magnitude. In the case of temperature profile of the polymer melt in the mixing section, temperature increases with increase in screw speed at constant specific throughput due to viscous dissipation. However, when the screw speed is kept constant and when the specific throughput increases, temperature decreases as the mass flow rate of the polymer melt is increased and heat conduction across the barrel towards the polymer melt is decreased. Viscosity can be related to the temperature and shear rate trends observed when the operating conditions are varied. When specific throughput is increased at constant screw speed, viscosity of the polymer melt increases due to the higher mass flow rate of the feed at the same screw speed. However, when screw speed is increased at constant specific throughput, due to higher shear rate and temperature increase, the viscosity of the polymer melt decreases. Shear stress increases with screw speed when specific throughput is kept constant; the increase in shear rate is higher compared to the decrease in viscosity of the polymer melt in the mixing section resulting in an overall increase of the shear stress values. Similarly, shear stress is seen to increase when specific throughput is increased at a constant screw speed; this is due to the increase in viscosity of the polymer melt. The magnitude of shear stress is lower compared to the critical stress value of the CAMES beads which implies that there is the extensional stress component which dominates the shear stress values and the combined stress results in the break-up of the CAMES beads. Extensional stress has to be modeled in order to validate this theory since the shear stress component could only be calculated using the computer

simulations. The trends observed for each of the above-mentioned properties align with the RSD experimental observations. When comparing the screw geometries, shear stress is seen to decrease when narrow kneading blocks are replaced by wide kneading blocks; however, the % Break-Up increases for wide kneading blocks compared to narrow kneading blocks. The extensional stress component needs to be calculated, so that the overall magnitude of stress can be computed and can be used to ratify the observations of RSD experiments.

## 6.3 Insights on N and Q/N

RSD Methodology was used to quantify the stress experienced along the mixing section of the extruder in order to understand the mixing behavior. The experiments performed using RSD methodology revealed % BU as a function of N and Q/N. Using Ludovic, screw speed and specific throughput were identified as key parameters in influencing the thermos-mechanical properties of the polymer melt such as shear rate, temperature, pressure, residence time. The influence of N and Q/N was quantified based on the statistical analysis performed using JMP 12.2. The influence of specific throughput was understood using Ludovic simulations as it validated the findings of the RSD methodology regarding the significance of specific throughput. Each of the properties that were focused using Ludovic was influenced greatly by the specific throughput.

### 6.3.1 Relationship between Specific Throughput and Degree of Fill

Specific throughput influences the degree of fill within the screw channels; this could be proved mathematically from Eq. 3.23. To verify the effects of specific throughput on the degree of fill, Ludovic simulations were used. For this purpose, the 48mm long Mixing

Section with wide kneading blocks geometry was simulated using LDPE as the base polymer. Fig 6.1 shown below provides a graphical display of the Ludovic simulation providing degree of fill comparison between two CCD grid points from Fig 4.7, where the specific throughput is maintained as a constant while the screw speed changes. Similarly, Fig 6.2 provides a comparison between degree of fill when the specific throughput is increased at constant screw speed. This would help understand the relationship between degree of fill and specific throughput.

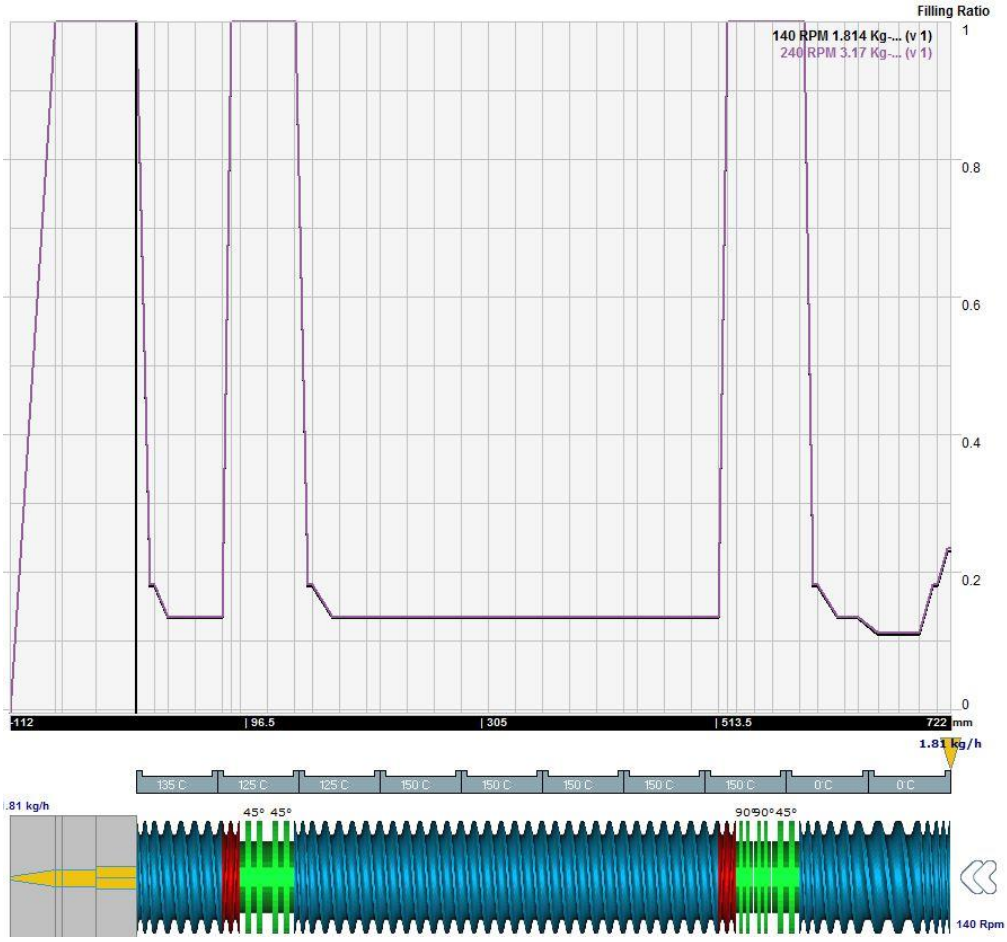


Figure 6.1: Comparison of Degree of Fill at Constant Specific Throughput

Fig 6.1 shows the Ludovic simulations for a 48mm long mixing section with wide kneading blocks. The CCD grid points chosen for this purpose have a constant specific throughput

(0.3 mL/rev) while the screw speed is increased from 140 RPM to 240 RPM. Ludovic simulates the input geometry and provides a comparison for the corresponding geometry for the given set of operating conditions. The graphical plots can be seen from the right (feed section) to the left (die section). Based on the obtained result, it can be seen that degree of fill remains constant throughout the length of the extruder, as the specific throughput is maintained constantly. This proves that degree of fill within the screw channel is a function of Q/N.

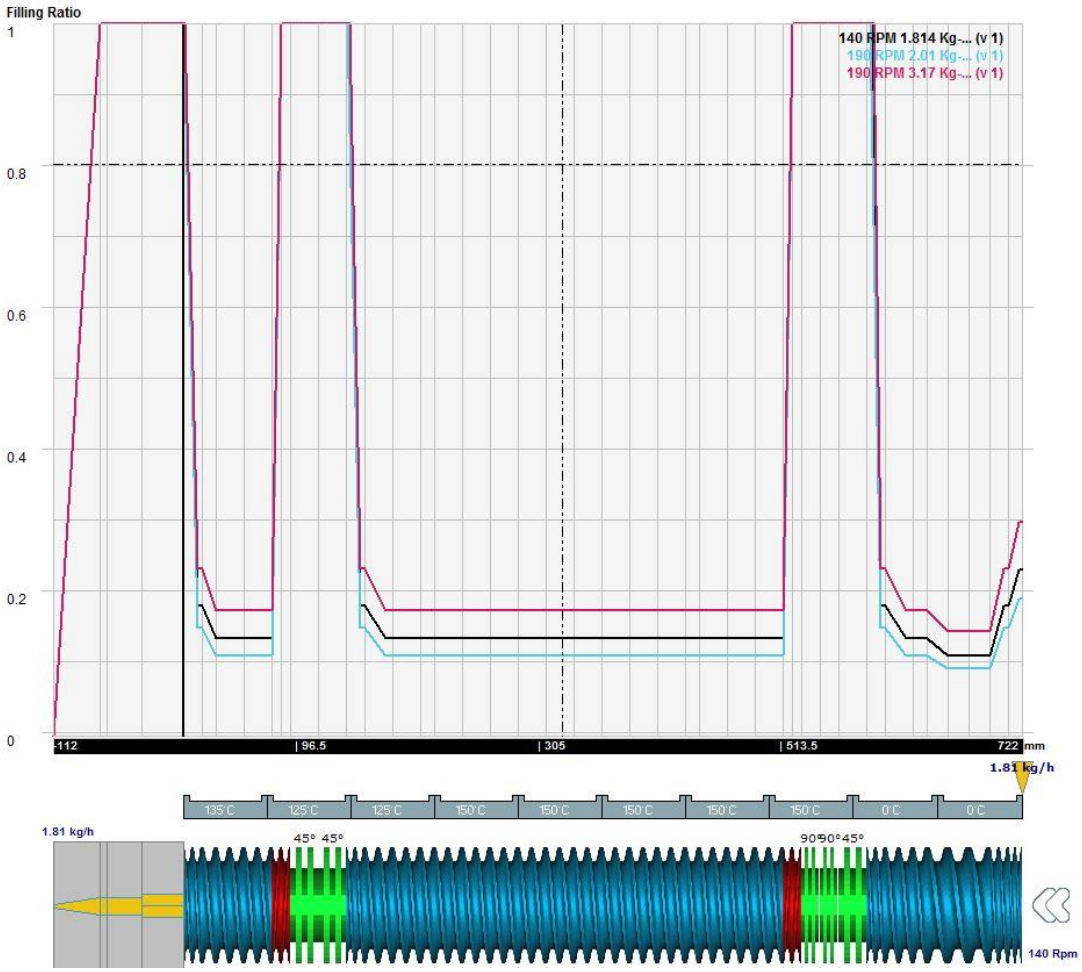


Figure 6.2: Comparison between degree of fill when specific throughput is varied

Fig 6.2 provides the comparison between the degree of fill values obtained for a specific screw geometry (48mm Mixing Section with Wide Kneading Blocks). The CCD grid

points chosen for this comparison include operating conditions when specific throughput increases. As the specific throughput increases, the degree of fill is seen to increase. From Fig 6.1 and 6.2, it can be seen that degree of fill is a function with specific throughput.

## 6.4 Influence of Degree of Fill on Properties of Polymer Melt

### 6.4.1 Influence on Viscosity of Polymer Melt

The viscosity of the polymer melt is an important property in determining the stress that the melt is being subjected to when processed in the extruder. Having discussed the viscosity trends for the different experimental setups in Chapter 5, this section discusses the influence of the degree of fill on the viscosity of the polymer melt. For this purpose, the screw geometry considered in Sec 6.3.1 would be simulated by Ludovic using LDPE as the base polymer matrix. Similar to the graphical plot displayed in Fig 6.1 and 6.2, Fig 6.3 displays the degree of fill along with the viscosity of the polymer melt in order to understand the relationship between degree of fill and viscosity of the polymer melt. The results compared by Ludovic include the viscosity and the degree of fill along the length of the extruder.

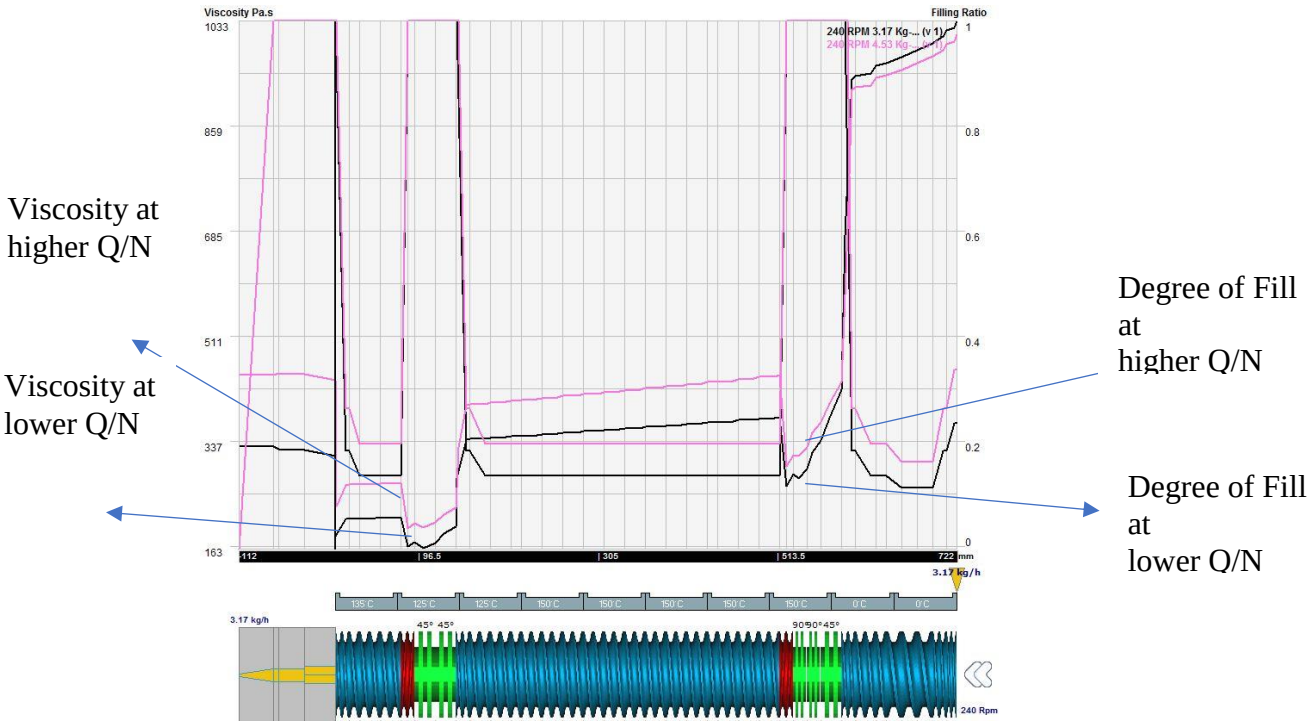


Figure 6.3: Relationship between viscosity and degree of fill

From Fig 6.3, the graphical plots simulated by Ludovic for a specific geometry can be seen. In order to understand the plots, the corresponding plots for degree of fill and viscosity at higher specific throughput and lower specific throughput have been labelled as seen in Fig 6.3. It can be seen that when the degree of fill in the screw channel is high; the viscosity of the polymer melt increases. Higher specific throughput increases the viscosity of the polymer melt (Chapter 5) and from the previous section, it was observed that the degree of fill in the screw channel is dependent on the specific throughput. Hence, it can be seen that viscosity of the polymer melt and degree of fill have a positive relationship i.e. at higher degree of fill, the viscosity of the polymer melt increases. The viscosity of the polymer melt is higher before the melting section because the polymer fed into the hopper (Chapter 1) is in the form of pellets which gets melted upon reaching the melting section of the extruder. The degree of fill reaches 100% upon encountering restrictive elements. The

longer the length of the section with restrictive elements, the longer the 100% fill within the screw channel. This behavior can be noticed from each of Fig 6.1, 6.2 and 6.3.

### 6.4.2 Relationship between degree of fill and pressure

Pressure trends had already been discussed in Chapter 5 for different experimental setups. This section focusses on the relationship between degree of fill and pressure along the length of the extruder. The screw configuration chosen is similar to those specified in the above sections – 48mm long mixing section with wide kneading blocks. Fig 6.4 provides a detailed graphical plot including the pressure and degree of fill values along the length of the extruder. The screw configuration is simulated using LDPE as the base polymer material. The graphical plot consists of two operating conditions i.e. when screw speed is kept constant and pressure increases.

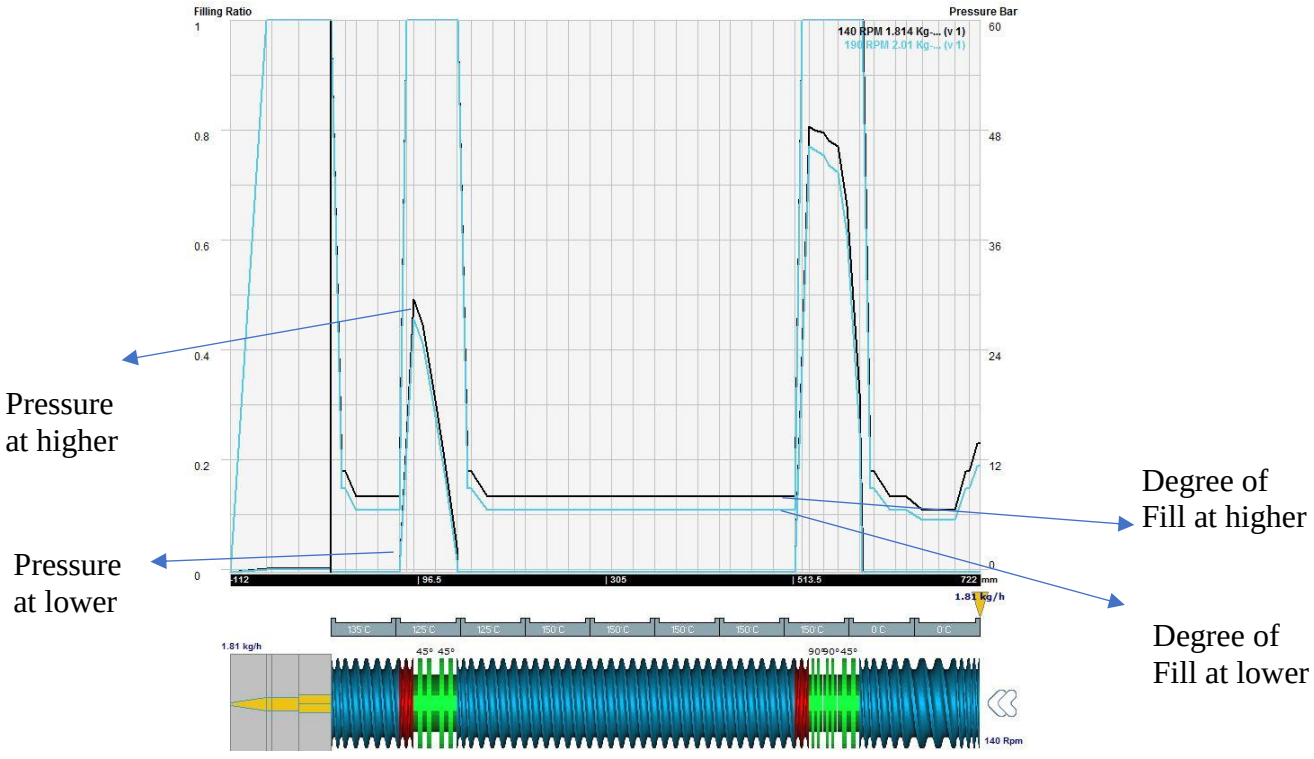


Figure 6.4: Relationship between pressure and degree of fill along the extruder length

The pressure trends in the mixing section had already been discussed in the previous chapter. From Fig 6.4, the graphical plots for pressure and degree of fill can be seen along the extruder length from the feeder (right) to the die section (left). As expected, the pressure increases in sections where restrictive elements are used. The degree of fill increases to 100% in the mixing section as well as the melting section due to the presence of restrictive elements. It is observed that degree of fill is higher when the specific throughput is higher similar to pressure rise when the specific throughput increases. When a channel is fully filled, higher pressure would be required to push forward the material because in the case of reverse conveying elements the drag flow is in the opposite direction to the flow of polymer melt from feed to die. To overcome the reverse flow, higher pressure is required. Fig 6.4 shows that degree of fill and pressure are inter-related as when the degree of fill increases the pressure increases accordingly.

### 6.4.3 Relationship between degree of fill and residence time

This section discusses the relationship between degree of fill and residence time. In chapter 5, it was observed that residence time decreases with increase in screw speed and specific throughput. However, it was observed that at CCD grid points where the feed rate is kept constant (Q), the residence time remains constant. In this case, the relationship between degree of fill and residence time is observed, when the operating conditions for the Narrow 48mm long mixing section with Wide Kneading Block geometry is simulated for LDPE. The two operating conditions considered in this situation is when the specific throughput is kept constant when the screw speed is increased. From Sec 6.3.1, it can be seen that degree of fill remains constant when specific throughput remains constant. However, it is observed that residence time decreases when the specific throughput remains constant but

screw speed is increased. When Q/N is kept constant, increase in N implies that Q increases, which accounts for the decrease in the residence time results. The slope of the residence time plot decreases for the higher N CCD grid point, as it implies that the polymer melt is pushed across the mixing section when N increases at constant Q/N. The relationship between degree of fill and residence time cannot be clearly stated as degree of fill is predominantly dependent on specific throughput but residence time depends on Q and N.

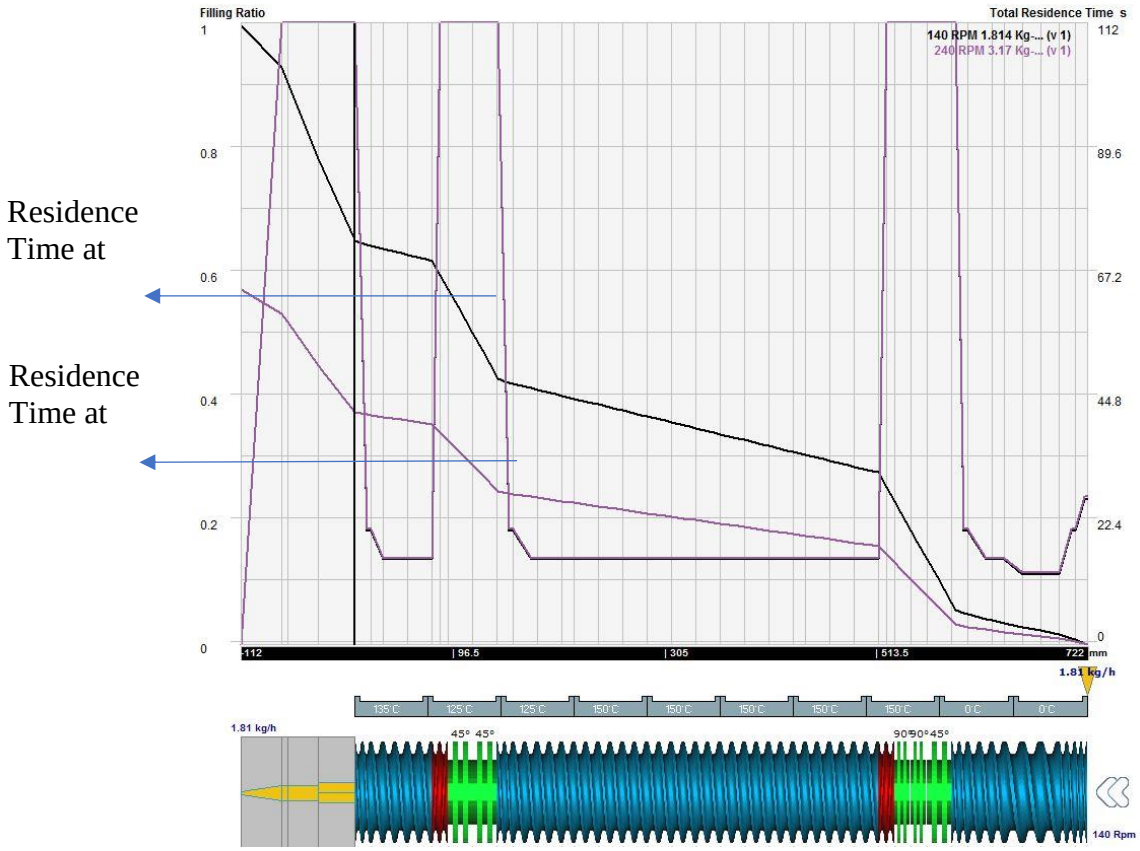


Figure 6.5: Relationship between degree of fill and residence time along extruder length

The relationship between degree of fill and properties of the polymer melt in the extruder have been discussed in Section 6.4. This discussion helps understand the importance of specific throughput (Q/N) in understanding the mixing behavior experienced in the

extruders. The results declared using RSD methodology that the amount of stress experienced in the extruder (factor affecting mixing behavior) is a function of screw speed (N) and specific throughput (Q/N). This has been justified in this section in understanding the influence of Q/N on degree of fill and its effect on other properties such as viscosity, pressure and residence time.

### 6.4.4 Influence of % Drag Flow on the Fill Length

This section discusses the relationship between % Drag Flow and the fill length within the extruder channel.

$$\%DF = \left(\frac{Q_{actual}}{Q_{100\%\ drag}}\right) * 100 \quad (6.1)$$

Where, %DF is the % Drag Flow, $Q_{actual}$ is the actual flow rate in the extruder channel, $Q_{100\%\ drag}$ is the flow rate when a polymer melt is conveyed by pure drag.

As seen in Chapter 3, the actual throughput in the screw channel is the sum of drag flow and the pressure flow. However, when a material is conveyed by pure drag flow i.e. no pressure flow, the total throughput is equal to $Q_{drag}$.

In order to understand the variation in the fill length values when the %Drag Flow is altered, Ludovic simulations were used. A particular screw geometry was chosen (48mm Wide Mixing Section) and LDPE was chosen as the base polymer. % Drag Flow was varied from 30% to 75% in order to find the relation between fill length and % Drag Flow. Using Ludovic, the fill length in the mixing section was calculated. The results are summarized in Table 6.1. Based on the required %drag flow, the operating conditions were calculated accordingly and input into Ludovic.

Table 6.1: Effect of % Drag Flow Variation in Fill Length

| % DF | N (RPM) | Feed Rate (g/min) | Fill Length | Res. Time (Mixing) | Revolutions (Mixing) |
|---|---|---|---|---|---|
| 30% | 140 | 30.2 | 49 | 16 | 37 |
| 50% | 140 | 49 | 61 | 13 | 30 |
| 60% | 140 | 58.8 | 64 | 10.9 | 25 |
| 75% | 140 | 73.6 | 66 | 8.7 | 20 |

Table 6.1 provides data on the effect of change in %Drag Flow on Fill Length, Residence Time and Number of Revolutions in the Mixing Section. From the data obtained, it can be seen that as the % Drag Flow increases, the fill length of the screw element increases. When % Drag Flow increases from 30% to 50%, the fill length increases from 49mm to 61mm; however, when %DF increases from 50% to 60%, the magnitude of change in fill length is lesser. Similarly, the residence time and the number of revolutions taken by polymer melt in the mixing section decreases with increase in % Drag Flow. To get a better understanding of the result, the graphical plots generated using Ludovic can be seen in Fig 6.6.

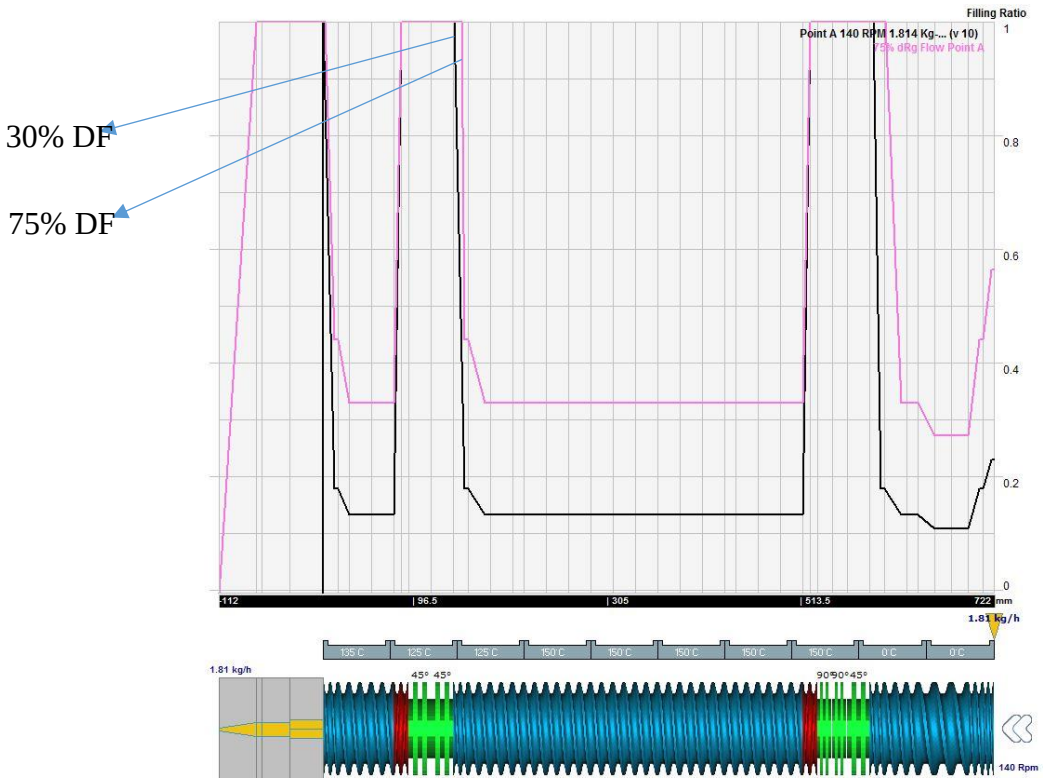


Figure 6.6: Fill Length comparison between 30% and 75% Drag Flow

Fig 6.6 provides a comparison between the fill length trends observed when % Drag Flow is varied from 30% to 75%. The fill length is calibrated based on the extruder length for which the screw channel is 100% filled. Based on individually calibrating each of the fill length values for the % Drag Flow changes, Table 6.1 was summarized.

## 6.5 Validation of Residence Revolution Distribution Assumption using Ludovic Results

Residence Time Distribution (RTD) was discussed in brief in Chapter 1 along with Residence Revolution Distribution (RRD) and Residence Volume Distribution (RVD). Gao's work on developing an RRD and RVD model from the Residence Time Distribution model has concluded that both RRD and RVD are functions of specific throughput. Based on experiments conducted for a specific screw geometry, it was observed that axial mixing

of the polymer matrix within the TSE was similar for all conditions when the specific throughput was held uniform across the operating conditions [14]. Residence Revolution Distribution (RRD) was useful in understanding the material transport through the extruder. It was inferred that the polymer melt travels along the same path in an extruder, when the specific throughput is held constant, based on the equal number of revolutions taken by the polymer melt for every screw configuration. To validate this theory, Ludovic was used as a tool to compute the residence time for each screw configuration and choice of base polymer. The experimental setup was already mentioned in Chapter 4. The results were observed in Chapter 5 (Sec 5.1.8, 5.2.8, 5.3.8 and 5.4.7) based on the calculations performed for the maximum number of revolutions in the mixing section. From the calculations performed, it was observed that the maximum number of revolutions in the mixing section remain constant when the specific throughput remains constant. Since the calculations were explained in detail in Chapter 5 (Sec 5.1.8, 5.2.8, 5.3.8 and 5.4.7), this section will discuss the insights obtained from the performed calculations. The calculated results were statistically analyzed using JMP 12.2, which suggested that the number of revolutions in the mixing section is a function of the specific throughput and is not significantly affected by the screw speed. The number of revolutions in the mixing section decrease as the specific throughput increases which implies that when the degree of fill in the screw channel increases, the polymer melt is pushed across the mixing section in a lesser number of revolutions. Another inference from RTD model developed by Gao suggested that throughput is the dominant factor that affects the residence time distribution of the polymer melt in the extruder. In order to validate this observation, Ludovic simulations were used to calculate the residence time in the mixing section of the extruder

(Sec 5.1.7, 5.2.7, 5.3.7, 5.4.6). The results obtained from the simulations suggested that N and Q/N influenced the residence time values as the residence time decreases when the screw speed and specific throughput is increased. However, it was observed that when the throughput (Q) is kept constant (Can be found in the CCD grid for operating conditions specified in Chapter 4), the residence time results are constant. This confirms the theory that residence time is dependent on the throughput. The assumptions based on the RTD model were ratified using Ludovic and it helps understand the significance of operating conditions such as specific throughput (Q/N), throughput (Q) and screw speed in the mixing behavior of the polymer melt when processed in the extruder.

# Chapter 7 – Conclusion and Future Scope

## 7.1 Conclusion

The purpose of this thesis was to demonstrate the role of computer simulations in understanding the internal behavior within the Twin Screw Extruder. Residence Stress Distribution (RSD) Methodology was used to quantify the stress history within the mixing section of the extruder for different screw configurations and different operating conditions. Ludovic, a 1- Dimensional Twin Screw Extrusion software, is a global model developed based on modeling the flow behavior within the extruder. Quantification of thermo-mechanical properties along the extruder length is a feature of Ludovic, which helps understand the variation of such properties for different operating conditions. Using different experimental setup (Chapter 4), Ludovic simulations were useful in understanding the trends of thermo-mechanical properties (Temperature, Pressure, Residence Time, Viscosity, Shear Rate, Degree of Fill) and the relationship with operating conditions (specific throughput (Q/N) and screw speed). The %BU results obtained via the RSD methodology is seen to increase with screw speed (N) as well as specific throughput. % BU changes as the screw configuration changes; replacing narrow kneading blocks with wider kneading blocks leads to a higher percentage of ruptured CAMES beads. Similarly, doubling the length of the mixing section results in an increase in the %BU values. Using Ludovic as a tool to get an insight into the %BU trends was useful in understanding the internal behavior of the polymer melt within the extruder. Each of the thermo-mechanical properties was explained in Chapter 5 for the different experimental conditions. Shear Rate increases with N and slightly increases with Q/N. For a specific extruder size, maximum

shear rate values are unaffected by changes in the configuration of the mixing section i.e. replacing narrow kneading blocks with wide kneading blocks. The cumulative shear rate is higher for wider kneading blocks compared to narrow kneading blocks as polymer melt is subjected to a maximum shear rate for a longer portion of the mixing section. As seen with the experiment performed with Kollidon VA-64, for different barrel temperatures shear rate is unaffected for a single screw geometry. The temperature of the polymer melt increases with increase in screw speed (N) at constant specific throughput (Q/N). However, the temperature decreases with increase in specific throughput (Q/N) at constant screw speed. The temperature of the polymer melt changes with screw configuration; maximum of temperature increases when narrow kneading block is replaced with wide kneading blocks. When the barrel temperature is increased for a specific screw geometry, the temperature of the polymer melt increases. The viscosity of the polymer melt decreases with increase in screw speed at constant Q/N; viscosity increases with specific throughput at constant screw speed (N). The viscosity of the polymer melt changes with screw configuration; viscosity decreases when the narrow kneading blocks in the mixing section are replaced by wider kneading block. When the barrel temperature is increased, the viscosity of the polymer melt decreases. Shear stress is seen to increase with screw speed as well as specific throughput. The shear stress values obtained based on the performed calculations are of lower magnitude compared to the critical stress values to rupture the CAMES beads. This implies that apart from the shear component of stress, the contributing factor to the break-up of CAMES beads involves extensional stress. The contribution of both extensional stress and shear stress result in the break-up of CAMES beads. The pressure generated in the mixing section increases with screw speed (N) and specific

throughput (Q/N). When the length of the mixing section is doubled, the pressure generated in the mixing section increases. Residence Time decreases with increase in screw speed and specific throughput. Residence Time increases marginally when the narrow kneading block in the mixing section are replaced by wide kneading blocks. Similarly, when the length of mixing section is doubled, the residence time increases. Change in barrel temperature does not have an impact on residence time. Finally, the number of revolutions taken by the polymer melt in the mixing section is dependent on specific throughput. At constant specific throughput, $Rev_{mix}$ remains constant when the screw speed increases. However, at constant screw speed, $Rev_{mix}$ decreases with increase in screw speed. As screw geometry changes, $Rev_{mix}$ increases marginally when the narrow kneading blocks in the mixing section are replaced by wide kneading blocks. Each of the results has been discussed in brief in Chapter 5 for different experimental setup. Ludovic results provided insight into the behavior of RSD methodology for different operating conditions and screw configurations. Screw Speed and Specific Throughput are predominant factors in determining the stress history within the twin screw extruder; the results provided by Ludovic imply that N and Q/N are factors that influence the mixing behavior. The conclusions arrived at using the Residence Time Distribution (RTD) and Residence Revolution Distribution (RRD) model was ratified using Ludovic simulations.

## 7.2 Future Scope

Using computer simulations are extremely useful in understanding the behavior of a twin screw extruder as demonstrated from this thesis. Apart from using computer simulations to understand the internal behavior of the twin screw extruder for different operating

conditions; these could be used to arrive at the optimal conditions to process the polymer melt. The thesis focused on understanding the behavior of RSD experimental results. The observed behavior was explained using the Ludovic simulation results. Shear stress was the only stress component that was computed using the Ludovic simulations. The extensional stress component which was a major contributor towards the stress rates experienced by the polymer melt could be modeled and implemented in order to provide the total magnitude of stress. This could help provide a better understanding of the %BU results for the different screw configurations. Similarly, computer simulations could be used in the field of pharmaceutical study to understand the properties of polymers and relate them to critical parameters that govern the external behavior. For instance, crystallinity, the water content in the active pharmaceutical ingredients (API) are vital characteristics that need to be understood in order to produce good quality extrudate.

# Appendix A: MATLAB Code

```
% Code to generate surface plot for given operating conditions and
result
%Input range for screw speed and specific throughput
n = linspace(140,340);
q_n = linspace(.18,.42);
[N,Q_N] = meshgrid(n,q_n);

%Conversion to coordinate grid point value
N_scale = (N-240)/50;           % Transforming N to Coordinate Value
Q_N_scale = (Q_N-.3)/.06;       % Transforming Q/N to Coordinate Value

%Based on the predictive equation generated by JMP
Shearrate_LDPENarrow24mm = 203.2 + 42.75*N_scale + 5.1*Q_N_scale;

Shearrate_LDPEWide24mm = 192 + 40*N_scale + 2.5*Q_N_scale;

%Plotting surface plot based on the given equation
G = figure(1);
hold on
a = surf(N,Q_N,Shearrate_LDPENarrow24mm);
b = surf(N,Q_N,Shearrate_LDPEWide24mm);
alpha(1)                        % Set plot transparency
set(a,'FaceColor',[1 0 0]);     % Set surface color
set(b,'FaceColor',[0 1 0]);     % Set surface color

% set(a,'edgecolor',[0 0 1]);     % Set gridline color
% set(a,'FaceColor','none');    % Remove face color

title('Mixing Section Shear Rate Response','FontSize',18)
xlabel('Screw Speed (RPM)','FontSize',18)
ylabel('Specific Throughput (mL/rev)','FontSize',18)
zlabel('Shear Rate (s^-1)','FontSize',18)
h = legend('Narrow 24 LDPE','Wide 24 HDPE');
set(h,'FontSize',18);
%[-45,30] provides an all view angle
view([-45 30]);
%define axis as CCD grid axis
axis([140 340 .18 .42 100 250])
grid off
hold off
```

# Bibliography


[1] S. Levy and J. Carley, *Plastics Extrusion Technology Handbook*, 2nd Edition. Industrial Press Inc., 1989.

[2] C. Rauwendaal, *Polymer Extrusion*, 1st Edition. Hanser Publishers, 1986.

[3] Z. Tadmor and C.G. Gogos, *Principles of Polymer Processing*, 1st Edition. Wiley-Interscience Publication, 1979.

[4] I. Ghebre-Selassie and C. Martin, *Pharmaceutical Extrusion Technology*. CRC Press, 2003.

[5] L. Incarnato and L. Di Maio, "Polymeric Extrusion", *Wiley Encyclopedia of Composites*. John Wiley & Sons Inc., 2012.

[6] C.I. Chung, *Extrusion of Polymers: Theory and Practice*, 2nd Edition. Hanser Publishers, 2000.

[7] J.L. White, Twin Screw Extrusion: Technology and Principles. Munich Vienna New York: Hanser Publishers, 1990.

[8] CPM Extricom Extrusion, accessed 9th April 2017, <http://www.extricom.de/index.php?option=com_content&view=article&id=8&Itemid=35&lang=en>

[9] C. Rauwendaal, *Mixing in Polymer Processing*, Marcel Dekker Inc., 1991.

[10] L. Erwin, *Theory of Laminar Mixing*, Polym Eng Sci, vol. 18: 1044-1048., 1978

[11] N.P. Cheremisinoff, *Polymer Mixing and Extrusion Technology*. CRC Press, 1987

[12] K. Kohlgruber, *Co-Rotating Twin Screw Extruder: Fundamentals, Technology and Applications*, Carl Hanser Verlag GmbH & Company KG, 2008.

[13] XM. Zhang, LF. Feng, S. Hoppe and GH. Hu, "*Local residence time, residence revolution, and residence volume distributions in twin-screw extruders*". Polymer Engineering & Science, vol. 48, pp. 19–28, 2008.

[14] J Gao, G.C. Walsh, D. Bigio, R.M. Briber and M.D. Wetzel, "*Residence-time distribution model for twin-screw extruders*". AIChE, vol. 45. pp. 2541–2549, 1999.

[15] G. Shearer and C. Tzoganakis, "*The effects of kneading block design and operating conditions on distributive mixing in twin screw extruders*", Polymer Engineering & Science, vol. 40, no. 5, pp. 1095-1106, May 2000

[16] G. Shearer and C. Tzoganakis, "*Relationship between local residence time and distributive mixing in sections of a twin-screw extruder*", Polymer Engineering & Science, vol. 41, no. 12, pp. 2206-2215, Dec. 2001

[17] D. B. Todd, "*Residence time distribution in twin-screw extruders*", Polymer Engineering & Science, vol. 15, no. 6, pp. 437-443, Jun. 1975

[18] Z. Tadmor and C.G. Gogos, *Principles of Polymer Processing*, 2nd Edition, pp. 648-650, Wiley-Interscience Publication, 2006.

[19] J. Cheng, Y. Xie and D. Bigio, "*Characterization of Kneading Block Performance in Co-Rotating Twin Screw Extruders*", in SPE-ANTEC Tech. Papers, pp. 198-202, 1998.

[20] J. Curry and A. Kiani, "*Measurement of Stress Level in Continuous Melt Compounders*", in SPE-ANTEC Tech. Papers, vol. 36, pp. 1599-1602, 1990.

[21] D. Bigio, W. Pappas, H. Brown II "*Residence Stress Distributions in a Twin Screw Extruder*", in SPE-ANTEC Tech. Papers, 2011.

[22] W. Pappas, H. Brown II, G. Fukuda, R. Andrew and D. Bigio, "*Variable strength stress bead analysis in a Twin-screw extruder*", in SPE-ANTEC Tech. Papers, 2012.
[23] D. Bigio, G. Fukuda, R. Andrew, J. Kim, B. Bhatia and M. Wetzel, "*Residence Stress Distribution Study Using a Robust Design of Experiment Approach*", in SPE-ANTEC Proceedings, 2013.
[24] B. Dryer, J. Webb, C. Brown, F. Flanagan and F. Yang, "*Modeling of Dispersive Mixing in a Twin Screw Extruder with Three Parameter Residence Stress Distribution",* in SPE-ANTEC Proceedings, 2016.
[25] M. L. Booy, "*Isothermal flow of viscous liquids in corotating twin screw devices*", Polymer Engineering & Science, vol. 20, pp. 1220–1228, 1980.
[26] H. E. H. Meijer and P. H. M. Elemans, "*The modeling of continuous mixers. Part I: The corotating twin-screw extruder*", Polymer Engineering & Science, vol. 28, pp. 275 – 290, 1988.
[27] J. Tayeb, B. Vergnes and G. Della Valle, "*A Basic Model for a Twin-Screw Extruder*", Journal of Food Science, vol. 54, pp. 1047 – 1056, 1989.
[28] C. D. Denson and B. K. Hwang, "*The influence of the axial pressure gradient on flow rate for Newtonian liquids in a self wiping, co-rotating twin screw extruder*" Polymer Engineering & Science, vol. 20. pp. 965 – 971, 1980.
[29] O.C. Zienkiewicz, "The Finite Element Method", 3rd Edition. McGraw-Hill (UK), 1977.
[30] Y. Wang, J. L. White, and W. Szydlowski, "*Flow in a Modular Intermeshing Co-Rotating Twin Screw Extruder*", International Polymer Processing, vol. 4, pp. 262-269, 1989.
[31] Z. Tadmor, E. Broyer, C. Gutfinge, "*Flow Analysis Network - A Method for solving flow problems in polymer processing*", Polymer Engineering & Science, vol. 14, pp. 660 – 650, 1974.
[32] D. Goffart, D. J. Van der Wal, E. M. Klomp, H. W. Hoogstraten, L. P. B. M. Janssen, L. Breysse, and Y. Trolez, "*Three-dimensional flow modeling of a self-wiping corotating twin-screw extruder. Part I: The transporting section*", Polymer Engineering & Science, vol. 36, pp. 901–911, 1996.
[33] R. V. Chiruvella, Y. Jaluria, M. V. Karwe and V. Semas, "*Transport in a twin-screw extruder for the processing of polymers*", Polymer Engineering & Science, vol. 36, pp. 1531 – 1540, 1996.
[34] Z. Chen and J. L. White, "*Simulation of Non-isothermal Flow in Twin Screw Extrusion*", International Polymer Processing, vol. 9, No. 4, pp. 310-318, 1994.
[35] W. Szydlowski, R. Brzoskowski, and J. L. White, "*Modelling Flow in an Intermeshing Co-rotating Twin Screw Extruder: Flow in Kneading Discs*" International Polymer Processing, vol. 1, No. 4, pp. 207-214, 1987.
[36] "*Twin Screw Extrusion simulation programs and what can they offer?*", Plastics Additives and Compounding, Feb 2002.
[37] B. Vergnes, G. Della Valle, L. Delamare, "*A global computer software for polymer flows in corotating twin screw extruders*", Polymer Engineering & Science, vol. 38, pp. 1781–1792, 1998.
[38] M.L. Booy, "*Geometry of fully wiped twin-screw equipment*". Polymer Engineering & Science, vol. 18, pp. 973–984, 1978.

[39] H. Werner, Dr. Ing. dissertation, University of Munich, 1976.
[40] L. Delamare, PhD dissertation, Ecole des Mines de Paris, 1995.
[41] D.B. Todd, "*Heat Transfer in Twin Screw Extruders*", in SPE ANTEC Tech. Papers, pp. 54–58, 1988.
[42] J. Vlachopoulos and N. Polychronopoulos, "*Basic Concepts in Polymer Melt Rheology and Their Importance in Processing*", John Wiley & Sons Inc., 2011
[43] I. Kayacan & O.M. Dogan, "*Pyrolysis of Low and High Density Polyethylene. Part I: Non-isothermal Pyrolysis Kinetics*", Energy Sources, Part A: Recovery, Utliziation and Environmental Effects, pp. 385 – 391, 2008.
[44] J. Frankland, "*The Power-Law Coefficient*." Plastics Technology, 27 Aug. 2012. Web. 11 Apr. 2017
[45] G. Fukuda, D. Chavez, D. Bigio. P. Andersen and M. Wetzel, "*Investigation of Scale-Up Methodologies in Twin Screw Compounding*", in SPE-ANTEC Proceedings, 2014.